

Some pages of this thesis may have been removed for copyright restrictions.

If you have discovered material in AURA which is unlawful e.g. breaches copyright, (either yours or that of a third party) or any other law, including but not limited to those relating to patent, trademark, confidentiality, data protection, obscenity, defamation, libel, then please read our [Takedown Policy](#) and [contact the service](#) immediately

PARAMETRIC STUDY OF THE BEHAVIOUR OF
REINFORCED CONCRETE COLUMNS IN FIRE

KAMAL NASHARUDDIN MUSTAPHA

Doctor of Philosophy

THE UNIVERSITY OF ASTON IN BIRMINGHAM

September 1994

This copy of the thesis has been supplied on condition that anyone who consults it is understood to recognise that its copyright rests with its author and that no quotation from the thesis and no information derived from it may be published without proper acknowledgement.

THE UNIVERSITY OF ASTON IN BIRMINGHAM

PARAMETRIC STUDY OF THE BEHAVIOUR OF
REINFORCED CONCRETE COLUMNS IN FIRE

KAMAL NASHARUDDIN MUSTAPHA

Doctor of Philosophy

September 1994

SUMMARY

The research is concerned with the application of the computer simulation technique to study the performance of reinforced concrete columns in a fire environment. The effect of three different concrete constitutive models incorporated in the computer simulation on the structural response of reinforced concrete columns exposed to fire is investigated. The material models differed mainly in respect to the formulation of the mechanical properties of concrete. The results from the simulation have clearly illustrated that a more realistic response of a reinforced concrete column exposed to fire is given by a constitutive model with transient creep or appropriate strain effect.

The assessment of the relative effect of the three concrete material models is considered from the analysis by adopting the approach of a parametric study, carried out using the results from a series of analyses on columns heated on three sides which produce substantial thermal gradients. Three different loading conditions were used on the column; axial loading and eccentric loading both to induce moments in the same sense and opposite sense to those induced by the thermal gradient. An axially loaded column heated on four sides was also considered.

The computer modelling technique adopted separated the thermal and structural responses into two distinct computer programs. A finite element heat transfer analysis was used to determine the thermal response of the reinforced concrete columns when exposed to the ISO 834 furnace environment. The temperature distribution histories obtained were then used in conjunction with a structural response program.

The effect of the occurrence of spalling on the structural behaviour of reinforced concrete column is also investigated. There is general recognition of the potential problems of spalling but no real investigation into what effect spalling has on the fire resistance of reinforced concrete members. In an attempt to address the situation, a method has been developed to model concrete columns exposed to fire which incorporates the effect of spalling. A total of 224 computer simulations were undertaken by varying the amounts of concrete lost during a specified period of exposure to fire. An array of six percentages of spalling were chosen for one range of simulation while a two stage progressive spalling regime was used for a second range. The quantification of the reduction in fire resistance of the columns against the amount of spalling, heating and loading patterns, and the time at which the concrete spalls appears to indicate that it is the amount of spalling which is the most significant variable in the reduction of fire resistance.

Key words: Computer, Column, Fire, Material Models, Spalling

To our children:

Tawfi *ijahid, Hidayah and Safwan*

ACKNOWLEDGEMENTS

First and foremost, I would like to express my deepest gratitude to my supervisor Dr. J.A. Purkiss for his time, constant help and guidance throughout the duration of my research. I shall always remember his excellent supervision, advice and invaluable support with all aspects of the work.

I would also like to thank Mr. R. H. Poole of the Department of Civil Engineering and the technical staff of the Information System, in particular Mr. F. Parkar, for their assistance with the computational work. I express my gratitude to Messrs J. Hollins, M. Lyons and J. Atkins of the Department of Civil Engineering for their help. Thanks are also due to Dr. P. Edmunds, Dr. D. P Greene and Messrs M.K Salbin, K.A Mohd Nasir and K. Al-Gasous for being a constant source of help and friendship. I must also extend my thanks to Mr. Z. Jusoh for his interest during the preparation of the text.

I am very grateful to the Universiti Kebangsaan Malaysia (U.K.M) and Public Services Department, Malaysia (J.P.A) for their financial support and for giving me the opportunity to undertake the present work.

I am greatly indebted to my wife, Elis for her companionship and understanding throughout the period of my studies. I would also like to express my deepest gratitude to my children, parents and parents in-law for their unfailing moral support during the course of my research. They have all been a source of encouragement and strength.

Finally, let me thank all those who have helped me in some way but who have not been mentioned by name. May God bless all of you.

LIST OF CONTENTS

	<u>PAGE</u>
TITLE PAGE	1
SUMMARY	2
DEDICATION	3
ACKNOWLEDGEMENTS	4
LIST OF CONTENTS	5
LIST OF FIGURES	10
LIST OF TABLES	18
NOTATION	19
CHAPTER 1 INTRODUCTION	25
CHAPTER 2 GENERAL DISCUSSION AND REVIEW OF PREVIOUS WORK	31
2.1 Introduction	31
2.2 Standard Furnace Test	32
2.3 Column Testing	36
2.4 Structural Behaviour of a Heated Column	48
2.5 Spalling	59
2.6 Computer Modelling	67
CHAPTER 3 PROPERTIES OF MATERIALS AT ELEVATED TEMPERATURES	77
3.1 Introduction	77
3.2 Thermal Properties	78
3.2.1 Concrete	79

3.2.1.1	Thermal Conductivity	81
3.2.1.2	Specific Heat	82
3.2.1.3	Thermal Diffusivity	84
3.2.1.4	Density	84
3.2.2	Steel	85
3.2.2.1	Thermal Conductivity	85
3.2.2.2	Specific Heat	88
3.2.2.3	Thermal Diffusivity	89
3.2.2.4	Density	89
3.3	Mechanical Properties	89
3.3.1	Concrete	90
3.3.1.1	Compressive Strength	90
3.3.1.2	Modulus of Elasticity	91
3.3.1.3	Stress-Strain Characteristics	96
3.3.1.4	Creep	97
3.3.1.5	Thermal Expansion	101
3.3.1.6	Transient Strain	105
3.3.1.7	Bond Strength	107
3.3.2	Steel	107
3.3.2.1	Strength Characteristics	108
3.3.2.2	Modulus of Elasticity	110
3.3.2.3	Creep	110
3.3.2.4	Thermal Expansion	114
CHAPTER 4	MATERIAL BEHAVIOUR MODELS	117
4.1	Introduction	117
4.2	Constitutive Model for Concrete	118
4.2.1	Instantaneous Stress-Related Strain	120
4.2.1.1	Anderberg and Thelandersson's Model	121
4.2.1.2	Schneider's Model	125
4.2.1.3	Khennane and Baker's Model	127
4.2.1.4	Baldwin and North on Furumura	131
4.2.2	Transient Strain	133
4.2.2.1	Anderberg and Thelandersson's Model	134
4.2.2.2	Schneider's Model	136

4.2.3	Thermal Strain	138
4.2.4	Creep Strain	139
4.2.5	Shrinkage Strain	142
4.3	Constitutive Model for Steel	144
4.3.1	Stress-Strain Model	144
4.3.2	Thermal Strain Model	146
4.3.3	Creep Model	148
CHAPTER 5	DESCRIPTION OF COMPUTER PROGRAMS	153
5.1	Introduction	153
5.2	Thermal Response Program: FIRES-T	154
5.2.1	Thermal Model and Solution Procedure	155
5.2.2	Conductivity Matrix \underline{K}	157
5.2.3	Capacity Matrix \underline{C}	160
5.2.4	External Heat Flow Vector \underline{Q}	162
5.2.4.1	Linear Heat Transfer	163
5.2.4.2	Non-Linear Heat Transfer	164
5.2.5	Numerical Scheme	165
5.2.6	Commentary on the Use of FIRES-T	167
5.3	Structural Response Program: SAFE-RCC	172
5.3.1	SAFERCC - The Primary Solution Executor	173
5.3.2	Data Input	176
5.3.2.1	Subroutine PARAM	176
5.3.3	System Initialisation	176
5.3.3.1	Calculation of Proposed End Moments	177
5.3.3.2	Calculation of Proposed End Slopes	177
5.3.3.3	Calculation of Proposed Division Point Deflections	179
5.3.3.4	Calculation of Proposed Curvatures	179
5.3.3.5	Direct Strain at the Column Axis	179
5.3.3.6	Calculation of Second Moment of Area	180
5.3.4	Calculations of Strains Due to Fire	181
5.3.4.1	Subroutine THERM	181
5.3.4.2	Subroutine TRANS	182

5.3.4.3	Subroutine CREEP	184
5.3.4.4	Subroutine SHRINK	184
5.3.4.5	Subroutine STREEP	185
5.3.5	Calculation of Internal Moments and Axial Force	185
5.3.6	Calculation of Curvatures	186
5.3.6.1	Subroutine STRESIN	187
5.3.7	Temperature Dependence of Material Parameters	189
5.3.8	Calculation of Deflections	189
5.3.9	Output of Results	192
CHAPTER 6	DESCRIPTION OF MODELLING PROCEDURE	193
6.1	Introduction	193
6.2	Procedure for Modelling Material Behaviour Models	195
6.3	Procedure for Modelling Spalling of Concrete	197
6.3.1	First Range of Spalling	197
6.3.1.1	Simulation of Spalling After 15 Minutes	199
6.3.1.2	Simulation of Spalling After 30 Minutes	203
6.3.2	Second Range of Spalling	203
CHAPTER 7	EFFECT OF VARIATION IN MODELLING PARAMETERS ON COLUMN BEHAVIOUR	207
7.1	Introduction	207
7.2	Effect of Mesh Designs on the Temperature Distribution Histories	213
7.3	Effect of Boundary Conditions on the Temperature Distribution Histories	216
7.4	Comparisons Between the Effect of Different Concrete Material Models on the Structural Response	219
7.5	Conclusion	228

CHAPTER 8	THE EFFECT OF SPALLING ON COLUMN BEHAVIOUR	231
	8.1 Introduction	231
	8.2 Discussion of Results	232
	8.3 Conclusion	269
CHAPTER 9	CONCLUSIONS AND RECOMMENDATIONS FOR FUTURE WORK	271
	9.1 Introduction	271
	9.2 The Application of the Computer Simulation Technique	272
	9.3 Assessment of the Effect of Concrete Material Models	273
	9.4 The Effect of Spalling on Column Behaviour	274
	9.5 Quantification of the Reduction in Fire Resistance	275
	9.6 Recommendations for Future Work	275
	LIST OF REFERENCES	277
APPENDIX A	MODELLING THE EFFECT OF SPALLING ON THE FAILURE MODES OF CONCRETE COLUMNS IN A FIRE	290

<u>LIST OF FIGURES</u>	<u>PAGE</u>
2.1 Standard time-temperature curve.	35
2.2 Gas temperature for various fire load densities and ventilation system.	35
2.3 Tentative relationships between the values of α_t and the time of exposure to fire for various column sizes.	40
2.4 Structural arrangement of building frame and heated column.	51
2.5 Loads and strains at failure of a column in a flexible structure.	52
2.6 Loads and strains at failure of a column in a stiff structure.	52
2.7 A possible structural arrangement that provides a combination of flexural restraint and axial load in a panel subject to heating.	54
2.8 The effect of axial load on the behaviour of panels heated under full flexural restraint with $\beta=1$.	54
2.9 Expansion of panels heated under different degrees of flexural restraint and constant axial load of 11 N/mm^2 and with $\beta=3$.	55
2.10 The effect of strain softening upon the performance of flexurally restrained panels.	55
2.11 Practically effective temperatures for RC elements (for a given actual temperature on the exposed face e.g. according to the standard fire).	58
2.12 Different heating regimes.	65
2.13 Approximate boundary between explosive and non-explosive spalling.	65

2.14	Summary of spalling test results of Meyer-Ottens.	66
2.15	Safe spalling envelope.	66
3.1	Different testing regimes for determining mechanical properties.	80
3.2	Thermal conductivity of normal weight and lightweight concretes as a function of temperature.	83
3.3	Ranges of volumetric specific heats of normal weight and lightweight concretes.	83
3.4	Specific heat for different types of concrete.	86
3.5	Effect of temperature on thermal diffusivity of concrete.	86
3.6	Density of structural concretes at high temperatures.	87
3.7	Thermal conductivity of steel at elevated temperatures.	87
3.8	Volumetric specific heat for steel at elevated temperatures.	92
3.9	Thermal diffusivity of steel.	92
3.10	Compressive strength of concrete.	93
3.11	Influence of the aggregate on the compressive strength of concrete at elevated temperatures.	93
3.12	Influence of cement-aggregate ratio and load conditions on the concrete strength.	94
3.13	Modulus of elasticity of concrete.	94
3.14	Variations in modulus of elasticity with different concrete strength.	95

3.15	Stress-strain relationships for dense concrete (no preload).	99
3.16	Creep of a carbonated aggregate concrete at various temperatures.	99
3.17	Effect of temperature and stress level on creep.	102
3.18	Expansion with temperature of concretes made with various aggregates.	102
3.19	Thermal expansion of concretes made with different aggregates.	103
3.20	Expansion with temperature of a material mainly quartz. (Heating rate: 5 ⁰ C per minute).	103
3.21	Effect of load levels on concrete deformation.	106
3.22	Different components of thermal strain.	106
3.23	Reduction of bond strength for different steels.	109
3.24	Stress-strain curves for a mild steel (ASTM A36) at various temperatures.	109
3.25	Strength of some steels at high temperature.	112
3.26	Modulus of elasticity of steel at elevated temperatures.	112
3.27	Typical creep curve.	113
3.28	Creep rate for prestressing (ASTM A421) and mild steel (ASTM A36) - stressed.	113
3.29	Harmathy's formulation of creep model.	115
3.30	Thermal expansion of steel.	115

4.1	General description of the stress-strain relation used in the material model.	124
4.2	Theoretical model of stress history dependence of concrete maximum strain.	124
4.3	Elliptical idealisation of the non-linear parts of the uniaxial stress strain curves.	129
4.4	Idealised stress-strain relation showing tensile zone and unloading characteristics.	135
4.5	$\frac{\epsilon_{tr}}{\left(\frac{\sigma}{\sigma_{maxp}}\right)}$ plotted against thermal strain ϵ_{th} .	135
4.6	Thermal expansion of quartz aggregate concrete.	141
4.7	Strain hardening principle for temperature dependent concrete creep strain.	141
4.8	Simplified model of the stress-strain curve for steel (used in CONFIRE).	147
4.9	Refined model of stress-strain curve for steel.	147
4.10	Steel stress-strain envelope.	149
4.11	Harmathy's formulation of creep model.	149
5.1	Main composition of the computer analysis.	156
5.2	Quadrilateral finite element.	159
5.3	Heat capacity idealisation.	161

5.4	Flow chart for program FIRES-T.	169
5.5	Origin of co-ordinate axis with respect to finite element mesh for tension and compression sign convention incorporated in SAFE-RCC for column cross sections.	170
5.6	Macro flow diagram showing the structure of the computer program SAFE-RCC.	174
5.7	Hierarchical structure of SAFE-RCC.	175
5.8	System analysed for pinned rotational restraint at both ends of the column exposed to fire.	178
5.9	Calculation of steel thermal strain (subroutine THERM).	183
5.10	Examples of stress-strain path.	191
6.1	Example of finite element mesh for column cross section with 132-elements (8 x 32 mm diameter bars).	198
6.2	Example of finite element mesh for spalling condition representing 3% of total area.	200
6.3	Example of finite element mesh for spalling condition representing 7.2% of total area.	201
6.4	Example of finite element mesh for spalling condition representing 29.5% of total area.	202
6.5	Example of finite element mesh for spalling condition representing 14.5% of total area.	205
6.6	Example of finite element mesh for spalling condition representing 28% of total area.	206

7.1	Illustration of testing arrangement.	209
7.2	Schematic diagram indicating the boundary conditions used in the FIRES-T run for the test column.	211
7.3	Schematic diagram indicating the material types used in the FIRES-T run for the test column.	212
7.4	Temperature at 100 mm depth in a reinforced concrete column as a function of time (fire exposure time: 2 hours).	214
7.5	Temperature at 160 mm depth in a reinforced concrete column as a function of time (fire exposure time: 2 hours).	214
7.6	Temperature at 200 mm depth in a reinforced concrete column as a function of time (fire exposure time: 2 hours).	215
7.7	Temperature at 100 mm depth in a reinforced concrete column as a function of time (fire exposure time: 2 hours).	217
7.8	Temperature at 160 mm depth in a reinforced concrete column as a function of time (fire exposure time: 2 hours).	218
7.9	Temperature at 200 mm depth in a reinforced concrete column as a function of time (fire exposure time: 2 hours).	218
7.10	Measured and calculated behaviour of column C1.	225
7.11	Measured and calculated behaviour of column C2.	226
7.12	Measured and calculated behaviour of column C3.	227
8.1	Temperature history for element 102 (steel) in columns C1, C2 and C3.	236

8.2	Temperature history for element 29 (steel) in columns C1, C2 and C3.	236
8.3	Temperature history for element 15 (concrete) in columns C1, C2 and C3.	237
8.4	Temperature history for element 119 (concrete) in columns C1, C2 and C3.	237
8.5	Temperature history for element 60 (concrete) in columns C1, C2 and C3.	238
8.6	Temperature history for element 64 (concrete) in columns C1, C2 and C3.	238
8.7	Temperature history for element 102 (steel) in column C4.	239
8.8	Temperature history for element 28 (steel) in column C4.	239
8.9	Temperature history for element 60 (concrete) in column C4.	240
8.10	Temperature history for element 64 (concrete) in column C4.	240
8.11	Temperature history for element 1 (concrete) in column C4.	241
8.12	Calculated behaviour of column C1 for Model M1.	244
8.13	Calculated behaviour of column C1 for Model M2.	245
8.14	Calculated behaviour of column C1 for Model M3.	246
8.15	Calculated behaviour of column C3 for Model M1.	247
8.16	Calculated behaviour of column C3 for Model M2.	248
8.17	Calculated behaviour of column C3 for Model M3.	249

8.18	Calculated behaviour of column C2 for Model M1.	250
8.19	Calculated behaviour of column C2 for Model M2.	251
8.20	Calculated behaviour of column C2 for Model M3.	252
8.21	Calculated behaviour of column C4 for Model M1.	253
8.22	Calculated behaviour of column C4 for Model M2.	254
8.23	Calculated behaviour of column C4 for Model M3.	255
8.24	Mid-height deflection versus percentage spalling for column C1.	258
8.25	Mid-height deflection versus percentage spalling for column C2.	259
8.26	Mid-height deflection versus percentage spalling for column C3.	260
8.27	Fire Resistance versus percentage spalling for column C1.	261
8.28	Fire Resistance versus percentage spalling for column C2.	262
8.29	Fire Resistance versus percentage spalling for column C3.	263
8.30	Fire Resistance versus percentage spalling for column C4.	264

	<u>LIST OF TABLES</u>	<u>PAGE</u>
4.1	Parameters for transient creep functions of structural concretes.	138
5.1	Values of concrete parameters for non-linear heat flow equation.	171
7.1	Values of thermal conductivity for quartzite concrete used in calculation.	210
7.2	Values of specific heat for quartzite concrete used in calculation.	210
7.3	Values of thermal conductivity for steel used in calculation.	211
7.4	Values of specific heat for steel used in calculation.	211
7.5	Boundary conditions for simulating cool face.	217
7.6	Types of column and loading conditions.	222
7.7	Variation of maximum concrete stress with temperature.	222
7.8	Variation on the concrete strain at maximum stress with temperature.	223
7.9.	Variation of steel proof strength with temperature.	223
7.10	Variation of steel initial tangent modulus with temperature.	224
7.11	Calculated and measured fire resistances of the columns.	224
8.1	Description of the amount and time of spalling for the two stage progressive spalling regimes.	235
8.2	Description of the number of computer runs performed.	235

NOTATION

A	convection coefficient
A_c	area of concrete
A_j, A_k	areas of triangles in elements adjacent to node i
A_s	area of steel
A_{sc}	area of compression steel
A_{st}	area of tension steel
A_{s1}	area of steel corner bars
A_{s2}	area of steel side bars
a	surface absorption
b	breadth of column
C	compressive force
\underline{C}	capacity matrix
C_e	elastic compliance parameter
C_p	plastic compliance parameter
C_p	specific heat
C_1, C_2, C_3	parameters for transient creep function
d_2	distance between centroid of section and centroid of steel
E_c	modulus of elasticity of concrete
E_0	initial tangent modulus of elasticity
E_s	modulus of elasticity of steel
E^*	slope of descending branch
E_s^*	strain hardening modulus for steel
e	eccentricity of the application of the axial force
F	external heat source
f_c	concrete effective strength

f_{cu}	concrete cube strength
$f_{c,j}$	concrete compressive strength in element j
f_s	steel effective strength
f_y	steel yield strength
g	elasticity function
g_A, g_B	rigid gusset lengths at end A, B
H	plastic hardening parameter
h	overall depth of section
h	coefficient of heat transfer
I_c	second moment of area of concrete
I_s	second moment of area of steel
$I_{uncracked}$	second moment of area of uncracked section
J	compliance function
\underline{K}	conductivity matrix
k_1	concrete creep factor
k_2	transient strain factor
L	length of structural member
M	bending moment
M_A, M_B	end moments acting at A,B
M_r	division points bending moments
N	convective power factor
N_{fl}	number of floors above
P	axial load
P_a	axial strength of column cross section
P_c	Euler buckling load of slender column
P_t	total axial load supported at time t
P_u	ultimate load at failure

P	concrete creep factor
Q	external heat flow
\underline{Q}	external heat flow vector
q	rate of heat flow
R	gas constant
R	radius of curvature
R	relative stiffness of surrounding structure
T	temperature
\underline{T}	temperature vector
$\dot{\underline{T}}$	temperature time rate of change vector
T_c	concrete temperature
T_g	parameter for transient creep function
T_s	steel temperature
t	time
t_d	fire duration
t_r	reference time
U_a	activation energy
u_s	distance from centroid of cross section to centre of steel bar
$u_{1r}, \dots, u_{jr}, \dots, u_{kr}$	distances of element centres from column axis
V	radiation view factor
V	volume
x, y	local Cartesian co-ordinates
y	deflection
$y_0, \dots, y_r, \dots, y_n$	division point deflections
Z	Zener-Holloman constant
α	eccentricity factor

α	coefficient of thermal expansion
α_e	ratio of initial tangent modulus of steel to the initial tangent modulus of concrete
α_t	strength reduction parameter for concrete
β	overconvergence factor
β_o	concrete creep factor
β_t	strength reduction parameter for steel
β_t'	strength reduction constant for steel corner bars
ΔH	activation energy of creep
Δj	width of square element j
Δp	horizontal offset of peak stress from initial elastic tangent
δ	column shortening
δ_o	initial column shortening
ϵ	strain
ϵ_{cr}	creep strain
ϵ_{axial}	axial strain
$\epsilon_{bending}$	bending strain
$\bar{\epsilon}_{cr}$	accumulated increment creep strain
ϵ_{cro}	y axis intercept of secondary creep phase
ϵ_e	elastic strain
ϵ_f	emissivity of radiation source
ϵ_{max}	value of strain at the point of maximum stress
$\epsilon_{max,0}$	value of strain at the point of maximum stress at ambient conditions
$\bar{\epsilon}_{max}$	value of strain at the point of maximum stress for unloaded specimens
ϵ_p	plastic steel strain

ϵ_r	resultant emissivity
ϵ_s	surface emissivity
ϵ_{shr}	shrinkage strain
ϵ_{th}	thermal strain
ϵ_{tr}	transient strain
$\epsilon_{tr,cr}$	transient creep strain
ϵ_{tot}	total strain
ϵ_y	steel yield strain
ϵ_σ	instantaneous stress related strain
ϵ_∞	total potential shrinkage strain
ϵ_1	strain at transient between parabolic branch and linear descending branch
Φ	transient creep function
ϕ	curvature
γ	thermal diffusivity
γ_o, γ_w	parameters for transient creep function
κ	parameter allowing for non-linear stress-strain behaviour
λ	thermal conductivity
θ	absolute temperature
θ_A, θ_B	end slope
θ_r	absolute temperature of radiation source
θ_s	absolute temperature of surface
ρ	density
σ	Stefan-Boltzmann constant
σ	stress
$\bar{\sigma}$	stress history

σ_{\max}	the value of stress at the point of maximum stress or the concrete compressive strength
$\sigma_{\max,0}$	the value of stress at the point of maximum stress at ambient conditions

CHAPTER ONE

INTRODUCTION

The analysis of a building frame exposed to fire is complicated because of the many variables involved. These variables include the interaction between the building components, influence of loads on the structural system, fire growth and its duration, changes in the material properties and the temperature distribution in the structural elements.

The high temperatures that result from building fires have a significant effect on the strength and deformation characteristic of structural components such as columns, beams, walls and slabs. These effects are dependent on the thermal and mechanical properties of the materials comprising the structure. Amongst the various structural elements, columns form the most critical components as the failure of a column in a lower storey could lead to a partial or complete collapse of a structure. In addition, in a reinforced concrete column the compression zone and the steel near the face of the column may both be subjected to high temperatures whilst under the effect of compressive stresses. A good understanding of the structural behaviour and the overall response of a column exposed to fire is therefore important in an effort towards eliminating costly damage to the structure and saving human lives.

It should be noted that the long established method to determine the structural fire endurance of structural elements has been through the use of standardised laboratory tests conducted in a furnace. The standard furnace test provides a

method of quantifying the ability of an element to withstand exposure to high temperatures by setting criteria by which the load bearing capacity, the fire containment (integrity) and the thermal transmittance (insulation) functions can be adjudged. The requirements are expressed by a duration of exposure to a temperature-time curve during which the elements have to fulfil those specified criteria. The required fire resistance is defined as the time to which the specimen ceases through structural weaknesses or excessive heat transmission to be an effective bearer against the spread of fire. In the case of a column, the fire resistance is assessed against the criterion of loadbearing capacity where failure is deemed to have occurred when the specimen either fails to support the test loading or excessive deformations occur.

While the standard furnace test provides a reasonably simple solution to an otherwise complex problem, it does not furnish a designer with a clear demonstration of how an actual column will perform in a fire. The standard furnace test also fails to model satisfactorily the structural restraint and continuity experienced by a column in a real structure. In addition, evaluating the fire performance of a column exposed to a standard fire instead of an actual fire gives less accurate information on its performance. The standard furnace test is also cumbersome, requires large specialist apparatus and expensive to conduct.

It is thus necessary to develop alternative methods for assessing the fire performance of a column. A column in a continuous structure can now be studied by computer simulation using calculations based on heat transfer and the structural properties of materials at high temperatures. The development of computer techniques has enabled the determination of heat transfer from the heated surface to the inside of a heated column to be carried out and elaborate

calculations can also be made on simulation of structural response of a column in a fire environment. The developments in computer technology and the difficulties encountered when experimenting with the furnace test have contributed towards the surge of interest in computer simulation which is in evidence over the last two decades. In addition, computer simulation is far less expensive and time-consuming than conducting furnace tests which are usually performed on large scale test specimens.

However, the success of a computer simulation is likely to be highly dependent on the reliability of the material model used. Development of a reliable material model is a formidable task when the material in question experiences thermal expansion and contraction, elasto-plastic deformations, transient strain, cracking as well as degradation of material properties as the temperature rises. Concrete is such a material and, unlike steel, the development of concrete material models is subject to much debate.

Although it has been recognised that concrete subjected to transient temperatures behaves differently from concrete under steady thermal states there is disagreement as to whether the effects of transient strain ought to be included in the concrete material model used to predict the structural response. The varying approaches are clearly shown in the different constitutive models developed by Anderberg and Thelandersson (1976), Schneider (1986) and Lie and Chabot (1990). Anderberg and Thelandersson (1976) and Schneider (1986) both incorporated the effects of transient strain or the appropriate strain effect in their constitutive models whilst Lie and Chabot (1990) proposed a model that omitted the effect of transient strain component.

This investigation is concerned with the assessment of the relative effect of the three concrete material models mentioned above on the structural response of reinforced concrete columns. The assessment is considered from the analytical end by adopting the approach of a parametric study. The parametric studies are carried out using the results from a series of analyses on columns heated on three sides so as to produce substantial thermal gradients. Three different loading patterns are used on the columns; axial loading and eccentric loading both to induce moments in the same sense and opposite sense to those induced by the thermal gradient. In all cases the column geometry, the finite element mesh and the temperatures throughout the column are kept identical. Comparisons are then made between the calculated response using each model for the reinforced concrete columns.

In all the parametric studies, the computer modelling technique on the reinforced concrete columns separates the thermal and structural responses into two distinct computer programs. The thermal response for the structural cross sections of the column is calculated using a modified version of FIRES-T (Becker, Bizri and Bresler (1974)). The structural response is calculated using the modified version of SAFE-RCC (Weeks, 1985) which is an analytical tool developed to study the structural response of a reinforced concrete column. The temperature distribution histories generated by FIRES-T are used in conjunction with SAFE-RCC together providing an overall capability of predicting the structural response of a reinforced concrete column exposed to fire.

It should also be noted that presently little information is available to quantify the effect of spalling of concrete in structural members as a result of exposure to fire though spalling is generally recognised as a problem. Modelling capability is

limited in that no account is taken of the phenomenon of spalling either in the thermal or structural analysis. Spalling can effectively be represented by a loss of concrete which can be idealised as modifications to the finite element meshes used to discretise the cross sectional area of the column (Purkiss, 1990). It is felt that further research needs to be done in this respect to verify the effect of spalling on the fire resistance and the deformation of reinforced concrete columns at failure.

This investigation is also concerned with the development of a method to model concrete columns exposed to fire which incorporate the effect of spalling by varying the amounts of concrete lost during a specified period of exposure to fire. An array of three columns and six different percentages of spalling were considered for one range of simulations while a two stage progressive spalling regime conducted on similar columns was used for a second range of simulations. In both cases, sections of concrete material were deleted to simulate spalling of concrete after two periods of exposure of 15 and 30 minutes to the furnace environment. A similar procedure was also performed on a fourth column which was concentrically loaded and exposed to the heating regime on all four sides. The effect of the severity of fire resistance loss is then compared between the three concrete material models incorporated in the computer calculation, and an attempt made to quantify the reduction in fire resistance against the amount of spalling.

The versatility of computer simulation to an extensive parametric study to determine the structural response of a concrete element in a fire environment is shown through the simulation of the effect of the different mesh designs on the temperature distribution histories across the column cross section as well as the

possible alternative methods to simulate a boundary condition that defines the interaction of the column face with the surrounding fire environment.

The next chapter, Chapter 2 reviews the previous work on experimental investigation and computer simulation of reinforced concrete columns exposed to fire.

CHAPTER TWO

GENERAL DISCUSSION AND REVIEW OF PREVIOUS WORK

2.1 INTRODUCTION

The basic fire safety objectives are to protect life and property. In buildings, these objectives can be achieved in various ways. One of the most important is the prevention of the outbreak of fire, and if fire does occur the objective is to reduce its growth. Despite the preventive measures some fires however become large. At this stage, it is essential to confine the fire and to provide means that permit safe evacuation of people from the fire area.

The effectiveness and cost of all the preventive measures can be influenced by the building designer. Measures to retard or combat fire growth that are related to building design include the use of low fire hazard material and provision of fire detection and extinguishing systems. Measures to protect people against the hazards of the spread of fire are prevention of the spread of smoke and hot gases and the provision of adequate exits or safety areas. Other measures related to building design are those for the confinement of a fire that include provision of adequate fire barriers capable of delaying or preventing spread of fire from one room to another and adequate structural fire protection.

Over the years, there has been a considerable amount of research carried out in the area of structural fire protection. Much data on thermal and mechanical properties of various building materials at elevated temperatures have been

produced. Knowledge of these properties which are used as input data for the fire design of structures including computer programs is essential to be able to predict the behaviour of structural members during exposure to fire. The use of numerical techniques has also made it possible to develop mathematical models that simulate the behaviour of various structural members in fire. In addition, a large number of models that calculate the fire resistance of structural members now exist.

The following sections cover various aspects related to research work conducted on structural fire protection of reinforced concrete columns. Particular areas of research related to computer simulation of reinforced concrete columns will be discussed. A brief account of the historical development of research on fire behaviour of reinforced concrete columns will also be given.

2.2 STANDARD FURNACE TEST

The conventional method of assessing the performance of load-bearing structural elements under the action of fire is through the application of the standard furnace test. The concept of conducting tests to determine the fire resistance of structural elements started at the beginning of this century when the British Fire Prevention Committee (BFPC) under Edwin Sachs carried out investigations in specially built apparatus at Regents Park (Malhotra, 1982). The first International Congress was then held in London in 1903 under the auspices of BFPC when a standard time-temperature curve was first proposed. Based largely on this work and research undertaken in the United States, Germany and Sweden, British Standard BS 476 defining tests for fire resistance was published in 1932.

At present, tests are usually carried out according to specifications of the particular country concerned. In the United Kingdom the standard performance of a structural element is determined when subjected to a standard exposure condition following the procedure laid down in BS 476: Part 20 - 23: 1987. However, the major research organisations have collaborated through the International Organisation of Standardisation (ISO) to introduce an international specification for conducting fire resistance tests, namely ISO 834.

In a standard furnace test, an element of building construction is placed in a furnace with the fuel input controlled so that the temperature of thermocouples adjacent to the heated surface follows a standard temperature-time curve that describes a monotonically increasing temperature with respect to time, as shown in Figure 2.1 and represented by the formula:

$$T = 345 \log_{10} (8t + 1) + 20 \quad (2.1)$$

where t is time of test in minutes,
 T is furnace temperature in °C at time t .

The standard furnace test provides a means of quantifying the ability of an element to withstand exposure to high temperatures, by setting criteria from which the load bearing capacity, the fire containment (integrity) and the thermal transmittance (insulation) can be adjudged. The fire resistance of an element is expressed by a duration of exposure to the temperature-time curve during which the element has to fulfil the appropriate criteria. For a column, its performance is assessed against the criteria for load bearing capacity where failure is deemed to

have occurred when it fails to support the test loading or when excessive deformations occur.

Furnace tests have also been used to obtain relationships between performance and a number of design factors and it is the data from those exercises that form the basis of the information contained in the schedules and tables attached to Design Codes and regulations.

However, the standard furnace test suffers from several shortcomings. Although the temperatures attained in the standard furnace test are reasonably representative of those attained in most building fires, they do not represent the temperature-time relationship observed in real fires, in which temperatures may rise rapidly and reach higher values than in the standard temperature-time curve. Figure 2.2 shows a comparison between BS 476: Part 20 and the results of natural fire tests obtained from Hinkley (1984). The rate at which a fire develops and the temperatures reached are dependent upon the size and nature of the fire load i.e. the materials within the fire compartment, the oxygen supply available to feed the fire and the shape and size of the compartment. From this it can be seen that the standard furnace test does not simulate a real fire situation.

Dougill (1966) argued that the standard furnace test ignores the effects of continuity and that the structural element is tested as though it was unrestrained in service. This approach appears to be inappropriate to reinforced concrete with its capacity for large local deformations and the ability to redistribute forces and bending moments within a continuous structure. It is this property of reinforced concrete that suggest that it is necessary to examine the relevance of the standard furnace test to actual behaviour.

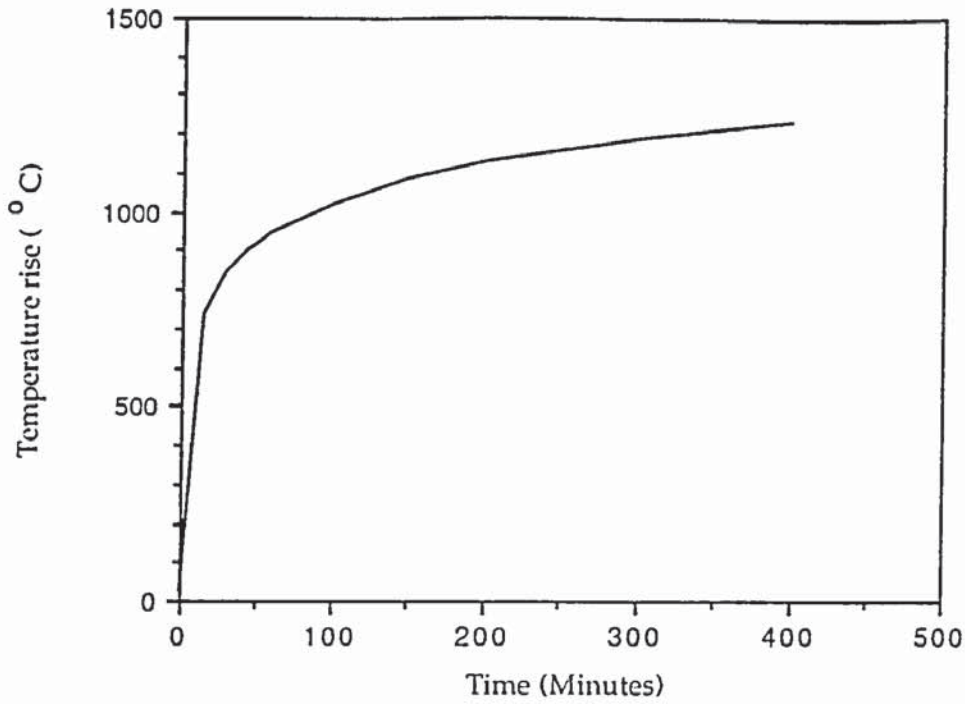


Figure 2.1: Standard time-temperature curve. (BS 476: Parts 20, 21 and 22).

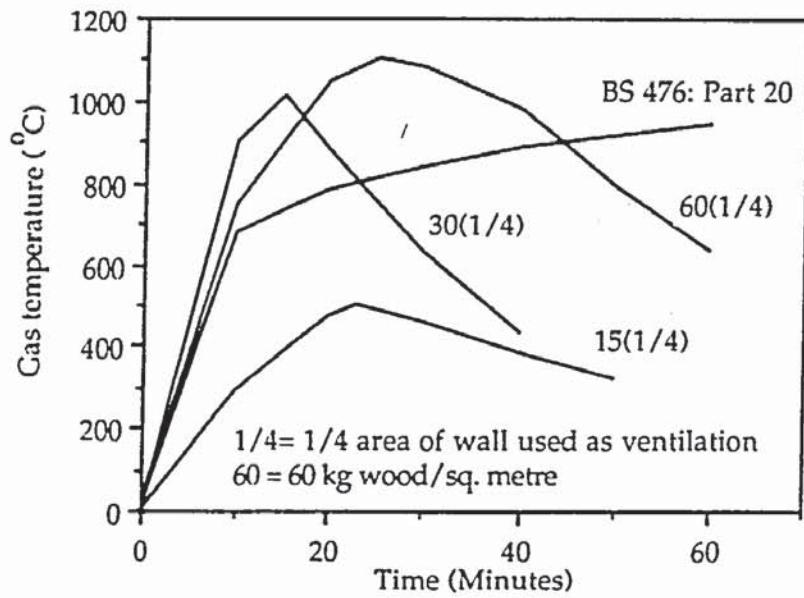


Figure 2.2: Gas temperature for various fire load densities and ventilation system. (Hinkley, 1984).

Weeks (1985) described the standard furnace test as expensive, cumbersome and requiring large specialist apparatus. More realistic conditions can now be studied by computer simulations using calculations based on heat transfer and the material properties at high temperatures.

2.3 COLUMN TESTING

The major historical work done on column testing in England was undertaken by Thomas and Webster (1953) where a programme of research was conducted according to the recommendations of the then, BS 476, to examine the influence of certain factors on the fire resistance of columns, namely:

- the effect of variation of the applied load to the column,
- the effect of variation in strength of the concrete in the column,
- the effect of variation in column size, with variations in concrete strength and reinforcement in accordance with the design procedure,
- the effect of using a very high percentage of longitudinal reinforcement.

In order to attempt to calculate the endurance of a column subject to fire, Thomas and Webster adopted the method that uses the usual ultimate load of a concrete column and then reduces the steel and concrete stresses by temperature dependent coefficients. The load bearing capacity of a column at any time during the furnace test was taken to be the sum of two quantities representing the strength contributions of the concrete and its reinforcement given by:

$$P_t = \Sigma [f_c (T_c) \delta A_c + f_s (T_s) A_s] \quad (2.2)$$

where: P_t is the total load that can be supported at time t ,
 δA_c is a small area of concrete cross-section,
 T_c is the average temperature in element δA_c at time t ,
 $f_c (T_c)$ is the effective strength of concrete at temperature T_c and at time t ,
 A_s is the cross-sectional area of the steel,
 T_s is the average temperature of the steel at time t ,
 $f_s (T_s)$ is the effective steel strength at temperature T_s and time t .

Thomas and Webster assumed the ultimate strength of the reinforced concrete column at normal temperature condition was given by:

$$P_u = 0.65 f_{cu} A_c + f_y A_s \quad (2.3)$$

where: f_{cu} is the concrete cube strength,
 f_y is the yield strength of steel reinforcement,
 A_c is the cross-sectional area of the concrete.

The effects of fire on the strength of a column was allowed for by multiplying equation (2.3) with factors which were functions of the time of exposure. Thus:

$$P_u = \alpha_t (0.65 f_{cu} A_c) + \beta_t (f_y A_s) \quad (2.4)$$

where: α_t and β_t are parameters allowing for the time of exposure.

The expressions for α_t and β_t are obtained by equating equations (2.2) and (2.4):

$$\alpha_t = \frac{1}{0.65f_{cu}A_c} \sum f_c(T_c) \delta A_c \quad (2.5)$$

$$\beta_t = \frac{f_s(T_s)}{f_y} \quad (2.6)$$

A comprehensive series of full-scale tests were conducted on reinforced concrete columns by varying the percentages of reinforcement to establish empirical values of α_t and β_t directly from equation (2.4) as functions of :

- time of exposure to fire,
- dimension of the column,
- the properties of the concrete and steel.

Small scale tests were also conducted on the concrete and steel materials to determine the functions $f_c(T_c)$ and $f_s(T_s)$, and also to determine the temperature distributions across the column cross section .

Thomas and Webster could not determine the empirical values of both α_t and β_t directly from the observed endurance period due to the unsuitability of the method of analysis. The value of β_t had to be estimated from the measurement of steel temperatures in some of the columns and from data published by Lea in 1920 on the effect of temperature on the yield strength of steel. The empirical values of α_t at the time of collapse were then determined from equation (2.4) by inserting the values of β_t and equating P_u to the applied test load. Thomas and Webster

then gave an approximate indication of the relation between α_t , the column size and the time of exposure to the furnace test. These results are shown in Figure 2.3.

By adopting the values α_t and of β_t , a comparison was then made between the estimated load bearing capacity of the column and the actual applied test load, and between the estimated endurance period corresponding to the applied load, and the actual endurance period. However, agreement was poor due in part to the effects of spalling on the reinforcement cover at various positions on the surface of the column. Thomas and Webster suggested that it was desirable to modify equation (2.4) for the case of columns with side reinforcement, to allow for the different strengths of the side and corner bars at any time during the furnace test:

$$P_t = \alpha_t(0.65 f_{cu} A_c) + \beta_t f_y A_{s1} + \beta'_t f_y A_{s2} \quad (2.7)$$

where: A_{s1} is the cross sectional area of the corner bars,
 A_{s2} is the cross sectional area of the side bars,
 β_t is the reduction constant for the corner bars,
 β'_t is the reduction constant for the side bars.

Thomas and Webster's attempt to correlate the small scale material tests with the experimental results failed; the main reasons were given by Purkiss (1972) as threefold:

1. no account was taken of loading to a strain greater than that corresponding to the peak stress, i.e. descending branch behaviour of the concrete causing a redistribution of stress was not taken into consideration.

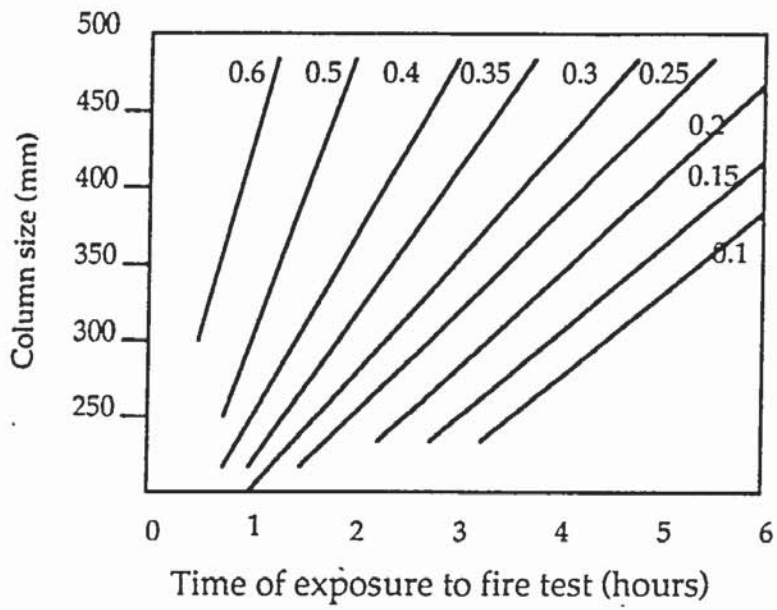


Figure 2.3: Tentative relationships between the values of α_t and the time of exposure to fire for various column sizes. (Thomas and Webster, 1953).

2. no account was taken of compatibility of strain due to temperature and loading.
3. the variation in peak stress was taken to be independent of any form of preloading.

Apart from the reasons mentioned above, Thomas and Webster had no knowledge of the complex stress-strain relationship at high temperatures for concrete.

However, the work undertaken by Thomas and Webster indicated that the magnitude of the applied test-load had a marked effect on the fire endurance period. A reduction in the test loads resulted in a considerable increase in the endurance period. The fire endurance also increased with higher concrete strength. The effect of age, from 7 months and beyond, was not found to be significant. Higher percentages of longitudinal reinforcement were also reported to produce a higher endurance period.

Clarke (1960) carried out a very similar analysis to Thomas and Webster (1953) which suffered from the same disadvantages, the difference being that Clarke suggested the ultimate load on reinforced concrete column when subjected to standard furnace test could be taken as:

$$P_u = a\Phi_c(T) \cdot f_{cu} A_c + \Phi_s(T)f_y A_s \quad (2.8)$$

where:

P_u is the ultimate load carried by a reinforced concrete column during a fire resistance test,

a is a constant determined by the size, age and relation of the test sample to concrete in the actual column,

$\Phi_c(T)$ is a function of the time during which the column has been exposed to the fire resistance test. This function relates to a column of specific size and concrete mix and is practically independent of the age of the column, provided that it exceeded 3 months,

t is the time of exposure (in hours),

f_{cu} is the concrete cube strength,

A_c is the net cross-sectional area of concrete,

$\Phi_s(T)$ is a function of the temperature of the reinforcement immediately prior to the collapse of the column,

f_y is the yield strength of the reinforcement

A_s is the cross-sectional area of the reinforcement.

Purkiss (1972) reported that the early work by Thomas and Webster in 1953, Clarke in 1960, Hull in 1918, 1919 and 1920, Ingberg *et al.* in 1921 and Seekamp *et al.* in 1964 provided the necessary information for the design codes to be laid down and also showed the value of plaster and other coverings in reducing the effect of fire. Later tests conducted by Haksever *et al.* (1982) and Haksever and Anderberg (1982) also contributed towards the development of the design codes.

Following the experimental investigations previously described, Lie and Allen (1972) proposed a method of calculation for the fire resistance of concrete columns as functions of significant parameters such as load intensity, slenderness of the column, concrete type, section size, eccentricity of load, equivalent buckling strength, percentage of steel and cover thickness to the steel. Two types of

concrete were selected for study; one containing a quartz aggregate representative of normal weight concrete and the other containing expanded shale representative of lightweight concrete.

The strength of the columns when exposed on all sides to a heating regime corresponding to the standard time-temperature curve was determined by the same methods as at room temperature, but by replacing the relevant ambient materials properties by their temperature dependent values. The cross sectional area was divided into a number of discrete elements and the strength calculated using values of the temperature dependent material properties combined with the temperature distribution in the column cross sections. The decrease in strength may then be determined as a function of time.

Creep was neglected in the analysis as it was assumed to have only secondary effects; however its omission is offset by the conservative approximations for the temperature-dependent strength and modulus of elasticity relations. Spalling also was not included since it was considered that it rarely occurred in cover less than 40 mm. In cover greater than 40 mm serious spalling was prevented by the inclusion of a wire mesh in the protection.

The temperature distribution was calculated using a numerical method described in Lie and Harmathy (1972). To verify the results, comparisons were then made between calculated fire resistances and those obtained from furnace tests under well-defined heating and loading conditions. The analysis was carried out for a pin ended short and slender columns subjected to a constant load eccentrically applied. The strength or the total load bearing capacity of the column is determined by dividing the cross section into small squares and integrating the

effects over the column cross section. For short columns the strength is determined from:

$$\text{Axial load: } P_t = \sum \Delta_j^2 f_{c,j} + \sum A_s f_y \quad (2.9)$$

$$\text{Bending Moment: } M = \sum u_j \Delta_j^2 f_{c,j} + \sum u_s A_s f_s \quad (2.10)$$

where:

$f_{c,j}$ is the temperature dependent concrete compressive strength of concrete element j ,

f_y is the temperature dependent yield strength,

Δ_j is the width of the square element,

u_j is the distance from the centroid of the cross section to the centre of element j ,

u_s is the distance from the centroid of cross section to the centre of steel bar,

A_s is the area of steel.

The strength of a slender column is governed primarily by the Euler buckling load P_c :

$$P_c = \pi^2 EI / (kL)^2 \quad (2.11)$$

where:

L is the column length,

kL is the equivalent length of a pin ended column where k depends on the end conditions,

EI is the stiffness of the cross section and the sum of the stiffness of the steel and concrete.

where: $EI = E_s I_s + C_c E_c I_c$ (2.12)

where: I_s is the second moment of area for steel,
 I_c is the second moment of area for concrete,
 E_s is the temperature dependent modulus of elasticity for steel,
 E_c is the temperature dependent modulus of elasticity for concrete,
 C_c is the factor which takes into account cracking of the section.

The value of C_c is adopted from Yokel *et al.* (1971):

$$C_c = 0.2 + P_u / P_a \leq 0.7$$
 (2.13)

where: P_u is the load at failure,
 P_a is the axial strength of the cross section.

As for short columns, the Euler strength of long columns during fire is determined from equation (2.11) by replacing the relevant material properties E_c and E_s by their temperature dependent values and integrating these effects over the column cross section:

$$E_c I_c = \Sigma E_{cj} (u_j^2 \Delta^2 + \Delta_j^4 / 12)$$
 (2.14)

$$E_s I_s = 4 E_s (u_s^2 A_s)$$
 (2.15)

The initial eccentricity at mid-height is increased by a magnification factor α given in Timoshenko and Gere (1961):

$$\alpha = 1 / (1 - P/P_c) \quad (2.16)$$

where: P is the applied load,
 P_c is the Euler load from equation (2.11).

Failure of the column is assumed to occur when the load and moment corrected by factor α reach the section capacity P_u and M_u . However, columns in buildings are subjected to different eccentricities at the top and bottom which is taken into account by multiplying α by a factor C_m :

$$C_m = 0.6 + 0.4M_1/M_2 \geq 0.4 \quad (2.17)$$

where: M_1 and M_2 are end moments with $M_1 > M_2$.

The strength of a slender column is thus determined in the same way as for short column but the eccentricity due to applied loads is increased by:

$$C_m / (1 - P_u/P_c).$$

Lie and Allen (1972) compared the results from the above analysis with the results of German tests by Becker and Stanke (1970) on axially loaded columns. The eccentricity was assumed to be 2.5 mm for the purpose of calculation. The analysis gave a consistent but somewhat conservative estimation of the fire resistance. The analysis by Lie and Allen indicated a substantial influence of the percentage of steel in cases of high eccentricity of load in that an increase of eccentricity reduces the fire resistance by about 20 to 30 percent for small percentages of steel. The calculations also indicated that the fire resistance increases for an oversized

column. For a small lightly reinforced column an increase in equivalent buckling length significantly decreased the fire resistance. The theory for eccentrically loaded columns was not checked due to the lack of suitable furnace test data.

Lie and Allen's method suffers from the drawback that stems from its failure to model additional moment as the column deflects. The other reasons that contributed to the disadvantages are given by Weeks (1985):

1. The basic equation for room temperature conditions that is used does not necessarily hold at elevated temperatures.
2. Failure to model structural interaction and material behaviour.
3. Limited models for slenderness have been used.

The fire tests previously described have all been on columns either axially loaded or with small eccentricity heated on all four sides in a standard furnace test. However, Haksever *et al.* (1982) carried out furnace tests on reinforced concrete columns, axially and eccentrically loaded, exposed on all four sides to a standard fire. The fire resistance period of eccentrically loaded columns was found to be significantly lower than those for axially loaded columns by values up to as much as 50%.

Haksever and Anderberg (1982) later carried out the qualitative verification of the structural behaviour of some pin ended reinforced concrete columns exposed to fire on three sides. The results indicated that moments applied in the same sense as the thermal gradient across the section decrease the fire resistance of the

column when compared to that corresponding to an axial load only. The tests also indicated that moments applied against the direction of the thermal gradient increase the fire resistance.

2.4 STRUCTURAL BEHAVIOUR OF A HEATED COLUMN

Dougill (1966) described the importance of restraint on the mode of failure of columns and gave an analysis that shows the effect of restraint on the type of failure incurred by a column that undergoes a furnace test with restraint. The analysis deals with a single heated column in the building frame shown in Figure 2.4 subjected to a local fire. The surrounding structure is assumed to be unaffected by heating and to behave linearly. The thermal expansion of the column is resisted by the axial restraint afforded by the surrounding structure inducing an additional load in the column to that carried before heating. The restraint to the column is mainly due to the stiffness of the beams and floors and hence increases with the number of floors N_{fl} above.

Dougill (1966) proposed that the condition for the displacements of the column and the surrounding structure to be compatible can be put in the form:

$$\frac{\varepsilon}{\varepsilon_0} + \frac{1}{R} \cdot \frac{P_v}{P_0} = \left(1 + \frac{1}{R}\right) + \frac{\alpha \bar{v}}{\varepsilon_0} \quad (2.18)$$

where: ε_0 is the initial shortening under load P_0 ,
 $\alpha \bar{v}$ is the thermal deformation,

ϵ is the displacement which is a function of the load P and temperature T ,

$R = N_{fl} K_s / K_c$ is a measure of the restraint afforded to the column from the surrounding structure and termed as the relative stiffness of the surrounding structure; K_s is the structural stiffness per floor and K_c is the column stiffness.

The equation of compatibility and the effect of restraint on mode of failure are solved by means of a graphical construction. The range of relative stiffness for flexible and hard structures is shown in Figure 2.5 and Figure 2.6 respectively. Dougill (1966) describes how in a flexible structure there is insufficient stiffness relative to the column stiffness to enable the column specimen to reach its ultimate strain when heated. It will eventually fail when the total load on the column is approximately equal to its maximum load capacity by the same mechanism of longitudinal instability as unrestrained columns in a standard furnace test. On the other hand, the load at failure on a column in a stiff structure will be small as the surrounding structure will relieve it of much of its load. Since limiting strain is the criterion for ultimate collapse, it is seen from Figure 2.6 that if the relative stiffness R is increased the thermal strain at failure must also increase. Since the thermal strain is a measure of temperature and time of exposure, a column in a stiff structure then will have a longer period of fire resistance than that for a similar column in a flexible structure.

In a later paper Dougill (1972a) set out a method of analysis for the stability of a plain concrete panel under the effect of axial and moment restraint. The analysis showed that structural instability leading to complete failure can occur in panels made of concrete, a strain softening material, during heating to high

temperatures. The mode of failure termed general, or destructive, spalling observed during early stages of fire tests has also been shown to correspond to compression failure that results from instability caused by strain softening, from the descending branch of the stress-strain curve of concrete in compression. The analysis also demonstrated that the occurrence of instability is considerably affected by the boundary conditions of loading and restraint applied to the panel and that it cannot occur when the panel is subjected to heavy flexural and axial restraint.

Dougill (1972b) carried out further numerical investigation on the occurrence of instabilities associated with general spalling of plain concrete panels shown in Figure 2.7 which illustrated the effects of restraint and loading upon the incidence of general spalling. The analysis also showed that the behaviour of a heated panel is very much influenced by the extent of cracking due to tensile stress and by the steepness of the descending branch of the stress-strain curve in compression described by the parameter β .

For a concrete panel with full flexural restraint in the absence of a longitudinal load, the heavy flexural restraint leads to the development of tensile stresses and early loss of stiffness due to cracking throughout the section. This results in progressive failure that is unlikely to be violent and the panel could still continue to act as a thermal barrier for some time though it has been effectively destroyed as a load bearing structure. With the presence of axial load the development of cracking is inhibited or delayed. For a high axial load the section is always in compression and instability occurs with a proportion of the section being loaded beyond the peak stress; the time to failure being greater than that for the case with no axial load.

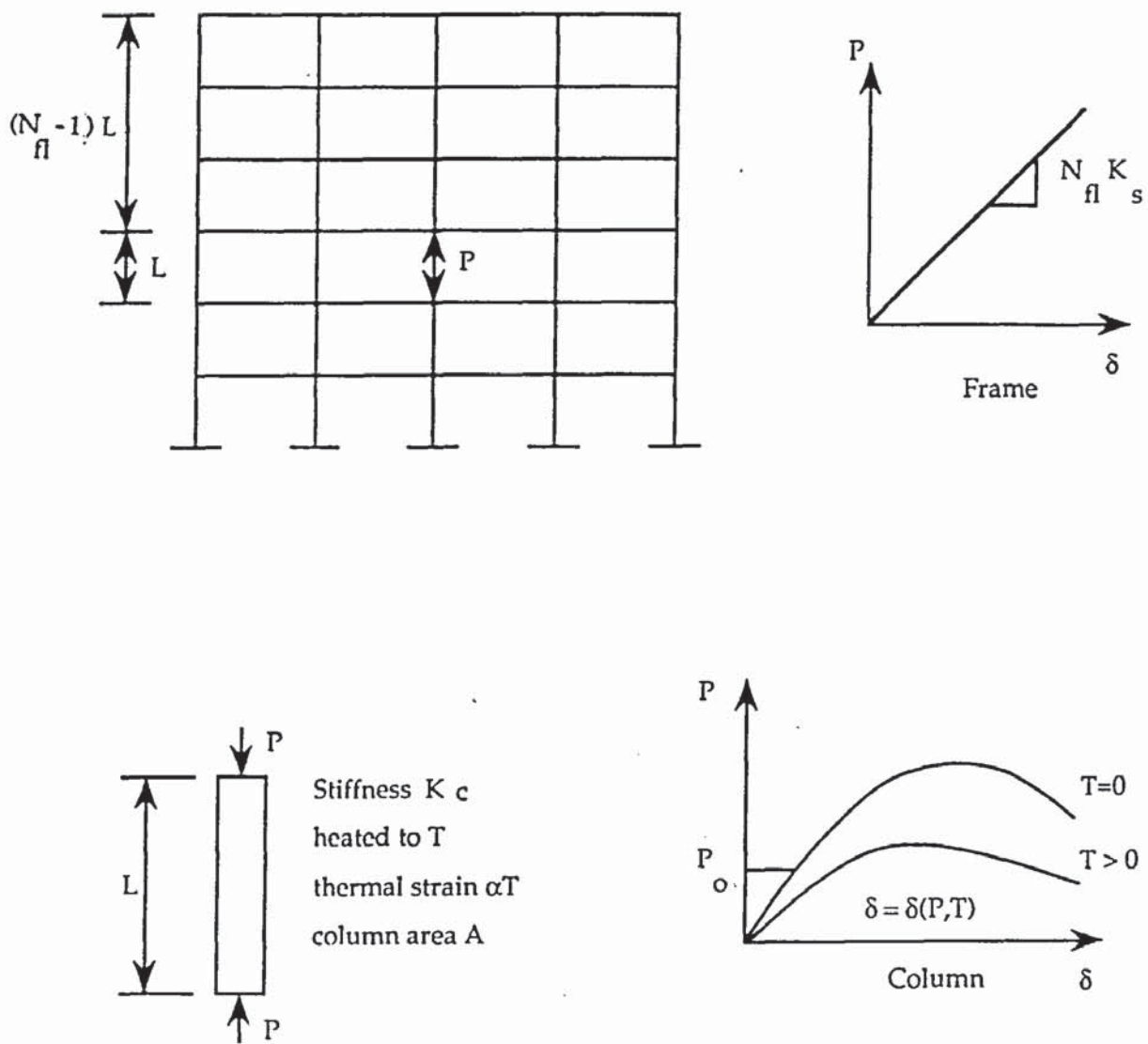


Figure 2.4: Structural arrangement of building frame and heated column. (Dougill, 1966).

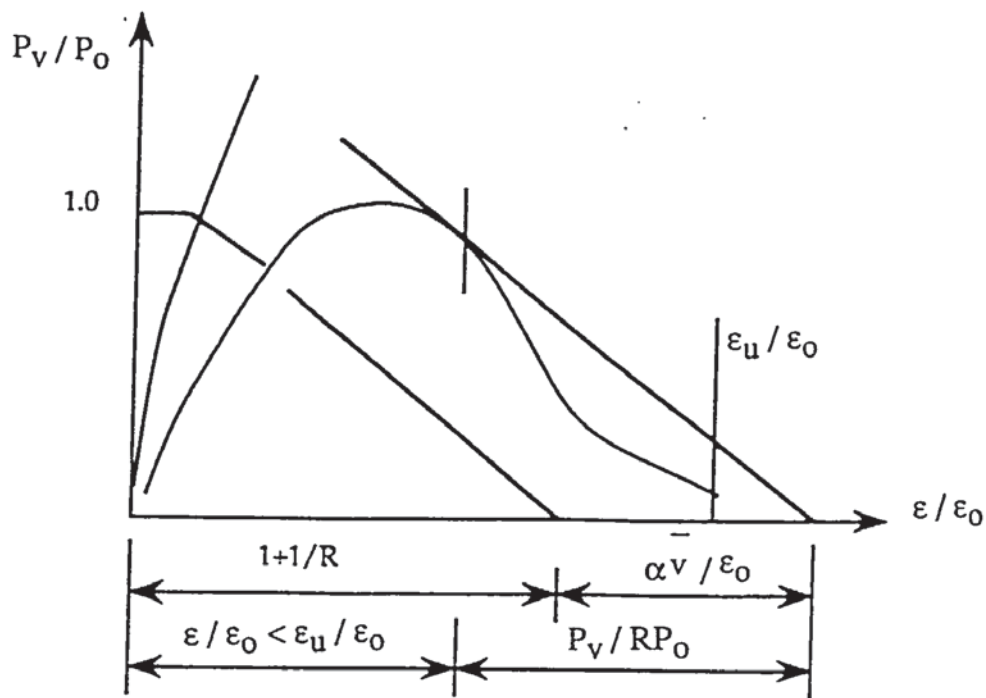


Figure 2.5: Loads and strains at failure of a column in a flexible structure. (Dougill, 1966).

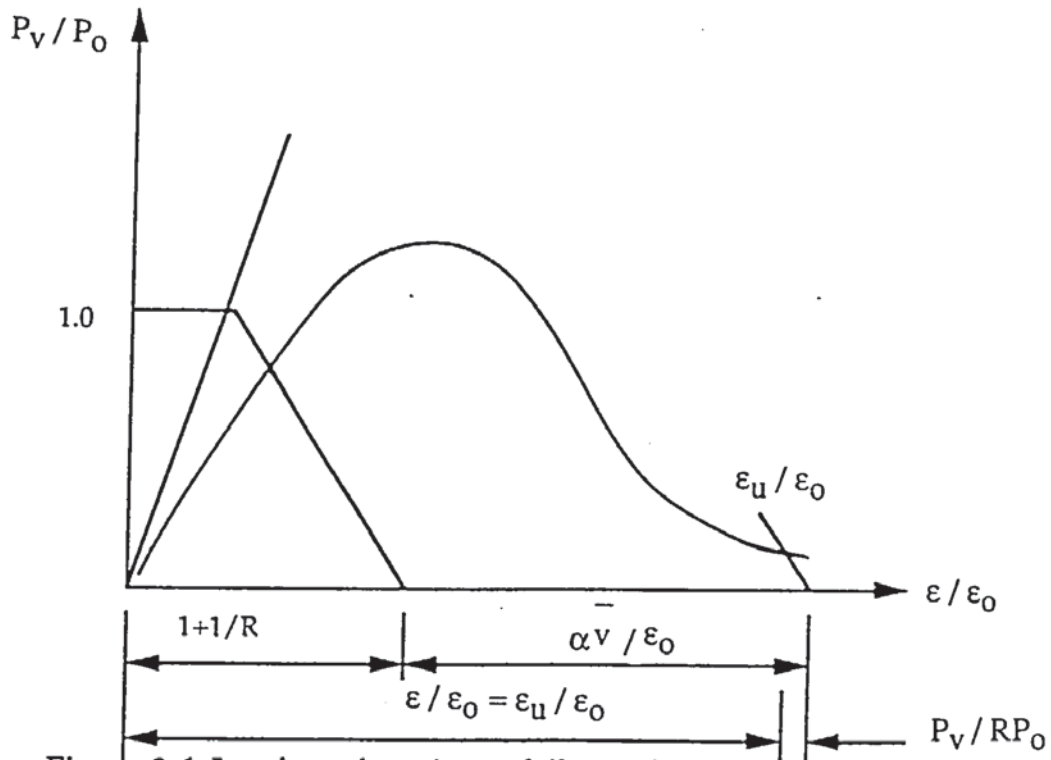


Figure 2.6: Loads and strains at failure of a column in a stiff structure. (Dougill, 1966).

The analysis also showed that, for a panel with full flexural restraint and intermediate axial loads, the time to failure can be increased further since tensile stresses are developed near the unheated face that lead to cracking. The onset of cracking has beneficial effect upon the behaviour of the panel in that it allows the section to unload and so avoid the conditions that contribute to instability. This is shown in Figure 2.8. It is clear that the panel carrying the intermediate axial loads survives because cracking provides some relief from the effects of restraint.

The effects of flexural restraint is shown in Figure 2.9. For small values of applied flexural restraint, the extent of cracking is reduced that reduces the period of exposure required for the occurrence of instability. On the other hand, an increase in flexural restraint leads to an increase in the time required to induce failure.

Dougill (1972b) also demonstrated that the form of the descending branch has a considerable effect upon the behaviour of the panel and that the occurrence of instability is no longer prevented by cracking for high values of β as shown in Figure 2.10.

The Portland Cement Association (Issen *et al.*, 1970) in the United States conducted some tests on restrained beams and slabs where the structural elements were allowed to expand by a given amount and were then completely restrained i.e. no movement was allowed. Although this clearly does not represent the type of behaviour that occurs in a structure, it does give a considerably better idea of structural response than a test with no restraint (Purkiss, 1972). The magnitude of restraint on a test specimen will have a considerable effect on the results of a

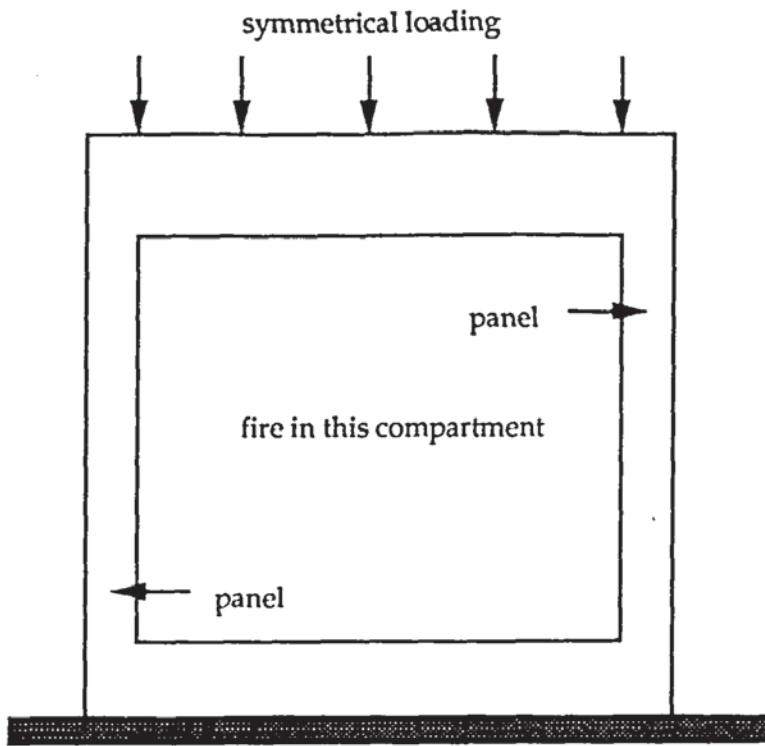


Figure 2.7: A possible structural arrangement that provides a combination of flexural restraint and axial load in a panel subject to heating. (Dougill, 1972b).

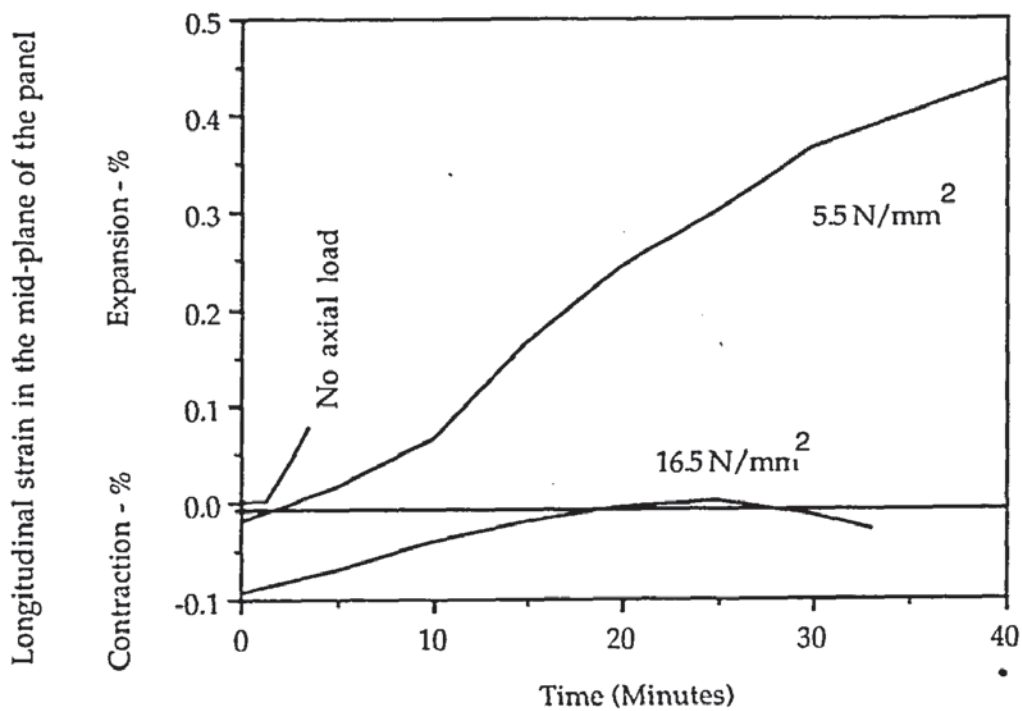


Figure 2.8: The effect of axial load on the behaviour of panels heated under full flexural restraint with $\beta=1$. (Dougill, 1972b).

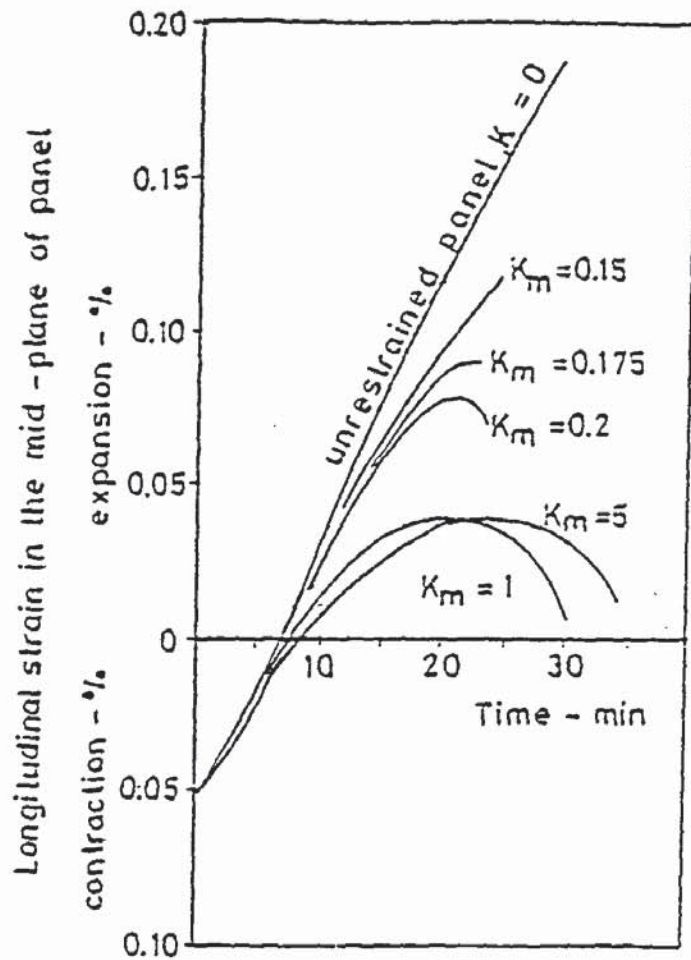


Figure 2.9: Expansion of panels heated under different degrees of flexural restraint and constant axial load of 11 N/mm² and with $\beta = 3$. (Dougill, 1972b).

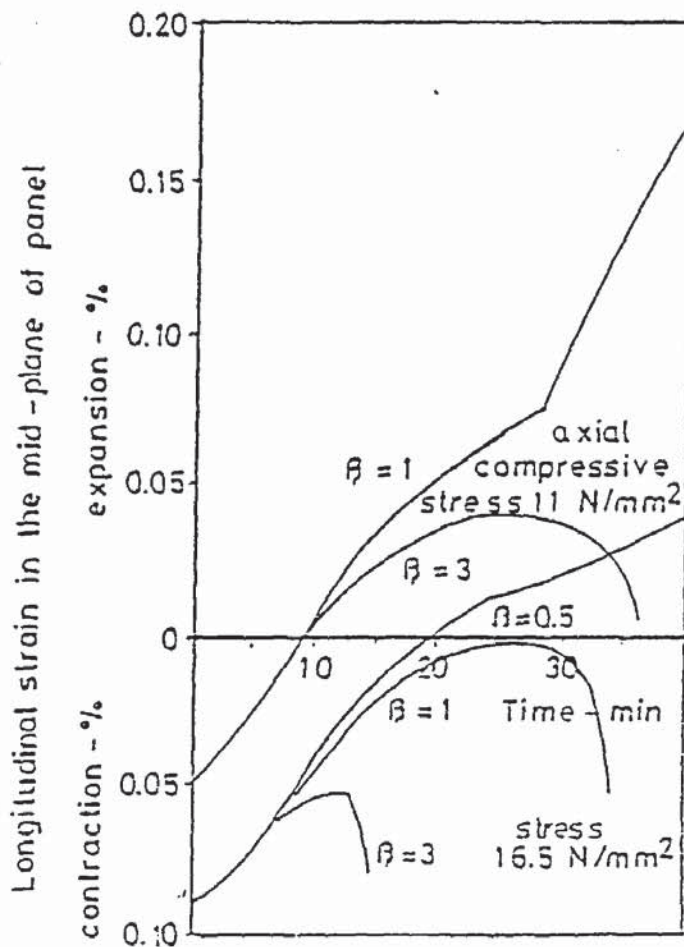


Figure 2.10: The effect of strain softening upon the performance of flexurally restrained panels. (Dougill, 1972b).

furnace test and Dougill (1972b) suggested that there exists an optimum restraint at which the specimen properties are enhanced to a maximum.

For beams and slabs, it is necessary to model continuity over the supports in order to obtain realistic structural conditions. This can be done either by replacing the continuity by deformation induced loads and moments or by testing real continuous structures. In some tests, beams have been cantilevered beyond the furnace and the cantilever is loaded together with the heated span. However, this only induces constant moment and therefore will not allow the redistribution of moments which will happen in an actual fire to occur .

Later, Allen and Lie (1974) carried out numerical investigation on the interaction of an interior column exposed to fire with the surrounding structure. As the column expands, the surrounding structure resists and the load on the column increases. The tendency to failure is relieved in two ways. First, the material becomes more deformable at higher stresses and temperatures, and this results in column contraction. Secondly, the column can bend or buckle sideways which results in a shortening of the column between its ends i.e. shortening of the column lengths. This tendency to bend sideways is enhanced by the reduced stiffness of the column.

Allen and Lie (1974) also demonstrated that the applied load increases and the fire resistance decreases as the vertical stiffness of the surrounding structure increases. However, when the vertical stiffness of the surrounding structure is further increased, a change in the fire resistance is observed. The increased applied load causes lateral bending, followed by chord shortening and relief of the applied load, so that failure does not take place. Eventually the column becomes shorter

than the initial length. Due to the transfer to adjacent support, the fire resistance is increased beyond that corresponding to no interaction. For very stiff vertical resistance, the column bends or buckle very early. The column continues to bend without failure well beyond the fire resistance calculated for the case of no interaction. If the structure is capable of transferring the total load to other supports, the column will never collapse.

Recently, Tassios and Chronopoulos (1991) proposed a step-by-step procedure for assessing the behaviour of reinforced concrete elements during fire by means of simple methods of statics and applied the method to three cases involving a fixed-end slab, two-span reinforced concrete beam and a simple reinforced concrete plane frame previously investigated experimentally. Owing to the non-linear temperature profiles through the depth of exposed elements, a non-linear distribution of strains exists that violates the principle of plane section remain plane. In order to fulfil planeness of cross sections under fire condition, self-generating self-equilibrating stresses are introduced that arise from the self-restraint of the cross section. The concept of thermoelements i.e. independent longitudinal fibres which are free to move axially is applied. Tassios and Chronopolous also proposed a diagram that may be used for the evaluation of the final effective imposed temperature of reinforced concrete elements under fire for a given maximum actual temperature reached on the exposed face. The diagram is shown in Figure 2.11.

Experimental and theoretical studies to predict the fire resistance of circular steel columns filled with bar-reinforced concrete was performed by Lie (1994) where a model to calculate the temperatures, deformations and fire resistance of the columns was presented. Comparisons between the calculated and measured results

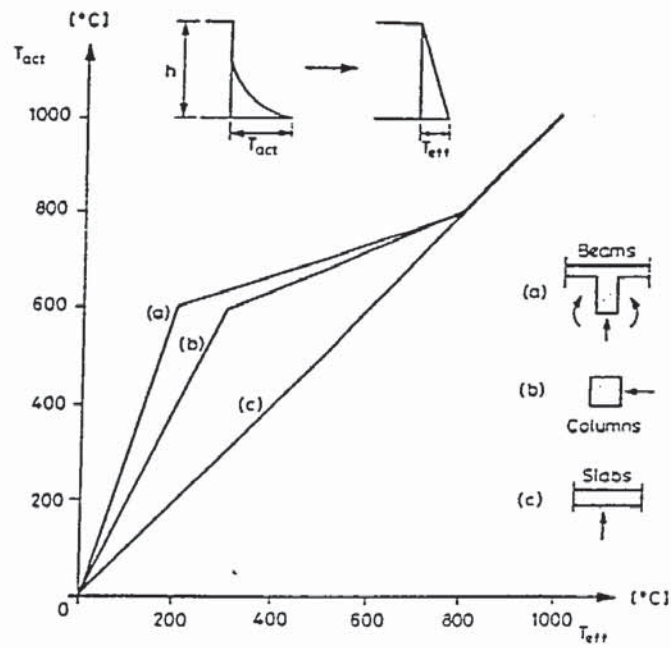


Figure 2.11: Practically effective temperatures for reinforced concrete elements (for a given actual temperature on the exposed face, e.g. according to the standard fire). (Tassios and Chronopoulos, 1991).

indicates that the model is capable of predicting the fire resistance of the column with an accuracy that is adequate for practical purposes. Using the model the fire resistance of circular concrete-filled steel columns can be evaluated for any value of significant parameters such as load, column-section dimensions, column length and percentage of reinforcing steel without the necessity of testing.

The fire tests and calculation methods described above have all neglected the effect of spalling on the behaviour of structural elements. The following section cover various aspects related to research work conducted on spalling and its effect on the performance of structural elements. The discussion is based largely on documentations on spalling by Malhotra (1984) and Connolly (1992).

2.5 SPALLING

Spalling is the breaking-off of layers or pieces of concrete from the surface of a structural element when it is exposed to high and rapidly rising temperatures experienced in a fire. The extent, nature and severity of occurrence of spalling vary. It may be insignificant in amount and consequence such as surface pitting, that is the removal of small pieces of concrete up to 20 mm in size from the surface of the concrete or as a result of corner break-off, that is the falling-off of the arises of beams or columns during fire exposure. Spalling can also seriously affect the stability of concrete construction in performing its design function. This situation arises due to extensive removal of concrete cover to the reinforcement as a result of explosive spalling.

Explosive spalling was suggested by Gary (1916) as the most important type of spalling due to its destructive effect on structural behaviour, though the actual

causes were unknown. The reduction of the concrete section leads to a more rapid rise of the temperature in the core which results in a reduction of the load bearing and separating functions of a structural element.

Malhotra (1984) reported that Endell in 1929, Bottke in 1931 and Hasenjager in 1935 carried out much of the research into spalling in the first half of this century. Investigations into the subject of spalling did not start in the United Kingdom until after the second world war. The Report of the Committee on the Fire Grading of Buildings (1946) suggested that spalling of concrete cover could greatly reduce the strength of columns when exposed to the standard furnace tests. After comprehensive series of tests on a range of elements constructed from different types of aggregates, Ashton and Davey (1953) noted that the 'process of disintegration' made it difficult to specify the thickness of concrete floors necessary to achieve the period of fire resistances.

In an investigation of the fire resistance of concrete columns, Thomas and Webster (1953) observed that larger columns suffered greater spalling of the arises. Spalling of the concrete cover to the main reinforcement caused a higher temperature rise of the bars and of the adjacent concrete within the core of the column. The investigation also showed that the use of light mesh reinforcement in the concrete cover could substantially reduce the incidence of spalling and hence significantly improve the performance of the columns. Clarke (1960) also indicated the importance of cover and the value of column renderings such as plaster in reducing the effects of fire. Clarke attributed spalling to the pressure built up by entrapped steam which could not readily force its way through dense concrete.

Ashton and Bate (1960), in a study of the behaviour of prestressed beams in fires, observed extensive spalling from the corners and noted the adverse effect on their fire resistance. In similar experiments conducted on reinforced and prestressed beams, Malhotra (1969) confirmed the occurrence of spalling with siliceous aggregate and the effectiveness of mesh reinforcement as a remedial measure.

In 1970, C.I.B Commission W14 undertook a survey of 13 national fire testing centres to determine the phenomenon of spalling in concrete. Malhotra (1972) reported that six factors were then suggested as having influence on the occurrence of spalling with the first three considered as the most important;

- nature of aggregate
- free moisture content
- restraint to thermal expansion
- density of concrete
- size of the aggregate, and
- age of concrete

At the conference on 'Fire Resistance of Prestressed Concrete' (1965), Kordina and Meyer-Ottens, Saito and Gustaffero all described their experiences of spalling. Saito (1965) proposed a theory of spalling based on the idea that concrete fails when the compressive stress at any point reaches a critical value. Explosive spalling was attributed to the non-linear temperature distribution across a concrete section leading to compression failure. On heating, the exposed face will try to expand due to the temperature gradient across the concrete section. This expansion will be restricted by the stiffness of the cooler central core. Consequently the exposed face will be in compression and the cooler central

region in tension. As the temperature gradient reduces with time, these stresses will diminish. Saito calculated the compressive stresses that may develop in the heated face using elastic analysis and considered spalling to be due to these thermally induced compressive stresses exceeding the compressive strength of the concrete. Saito also showed that tensile cracking within the concrete could relieve the compressive stresses and so inhibit spalling.

Harmathy (1965) ascribed explosive spalling to the steam pressure accumulated below the surface from 'moisture clogging'. On heating and as heat penetrates a slab exposed to fire, desorption of moisture starts in a thin layer adjoining the exposed surface. A major portion of the released vapours travel to colder zones and are reabsorbed which causes the dry zone to gradually get thicker. The moisture clog, which is a fully saturated layer, builds up a distance from the exposed face. A well defined front forms between the dry and the saturated layers and further absorption takes place from the interface. The rising exposed face temperature sets up severe thermal gradients across the dry layer. Heat flow increases through this layer as the temperature rises. The vapours leaving the interface are blocked from the colder depths by the saturated pores and thus they move across the dry layer. The further the interface is from the exposed face, the greater is the resistance to the movement of these vapours as the vapour flow is against the temperature gradient. As the temperature rises, the pressure at the interface builds up as the vapours are trapped between the zones of high pressure and temperature. The entire moisture begins to move into the cooler depths of the slab if the pore resistance in the saturated areas is not too high. However, for concrete with low permeability, the vapour simply cannot move and pore pressures at the interface builds up until they eventually exceed the tensile

strength of the concrete. When this occurs, the dry layer is dislodged from the concrete and hence the phenomenon of spalling.

An extensive experimental work to investigate the effect of concrete strength, thermal restraint, shape and compressive stress levels on the occurrence of spalling was conducted by Meyer-Ottens (1972). Three different concrete mixes with specified strength of 22.5, 45 and 60 N/mm² were used and subjected to three different heating regimes as shown in Figure 2.12. Higher compressive stresses in the concrete exposed to heating increased the probability of spalling of explosive type. Spalling was also encouraged by rapid heating. Meyer-Ottens also investigated the influence of moisture content by testing specimens with moisture contents ranging from 0.8 to 7.0% by weight. Results obtained suggested that explosive spalling was unlikely to occur for concrete section not less than 80 mm thick nor for concrete with moisture content below 2.5% by weight. For specimens 120 mm thick, spalling would only occur if the moisture content was at least 4.5% by weight.

Meyer-Ottens (1972) also plotted the results that considered the member thickness, ratio of compressive stress to concrete strength and moisture contents as boundary curves to distinguish between spalling and non-spalling conditions as shown in Figure 2.13. Sertmehemetoglu (1977) summarised the results from Meyer-Ottens, which is shown in Figure 2.14.

Christiaanse *et al.* (1972) studied the behaviour of 3 weeks old prestressed concrete beams with the moisture content estimated at 4.5% by weight. The fire tests exhibited severe spalling. A series of tests were then conducted on small and large scale lightweight concrete samples with different moisture contents and under

varying compressive stress levels. The investigation has shown that the occurrence of spalling depended on combinations of compressive stresses and moisture contents and that no spalling would occur for moisture content of concrete below 4% by weight. Christiaanse *et al.* plotted a spalling envelope diagram similar to that of Meyer-Ottens and is shown in Figure 2.15.

Akhtaruzzaman and Sullivan (1970) suggested that pore pressure was likely to be a major factor in spalling of concrete. The investigation showed that water-cured specimens were significantly more susceptible to explosive spalling than moist cured specimens. Akhtaruzzaman (1973) further concluded that spalling was possible for concrete younger than a certain critical age. This critical age depended on the curing conditions and the rate of heating.

Dougill (1972a) noted that the occurrence of spalling could seriously effect the performance of concrete members tested for fire resistance. Spalling occurred most often within the first-half hour of a furnace test in the form of local breakdown, and involved separation of external corners, splitting of aggregates or removal of shallow layers of surface materials. With prolonged heating, the regions affected by these forms of spalling may become extensive and eventually lead to the collapse of a member under test.

Dougill (1972a) further noted a more serious form of failure which was sudden and involved the complete or near complete destruction of a member under furnace test. This form of failure was also referred to as spalling within the context of work on fire resistance and most likely to occur in members with small cross sections and where the thermal expansion being restrained. Meyer-Ottens (1972) termed this form of failure as general or destructive spalling.

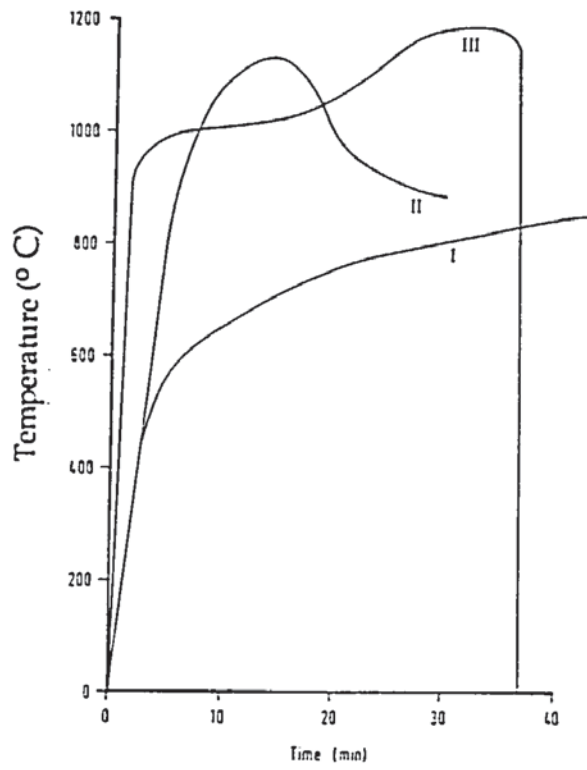


Figure 2.12: Different heating regimes. (Meyer-Ottens, 1972).

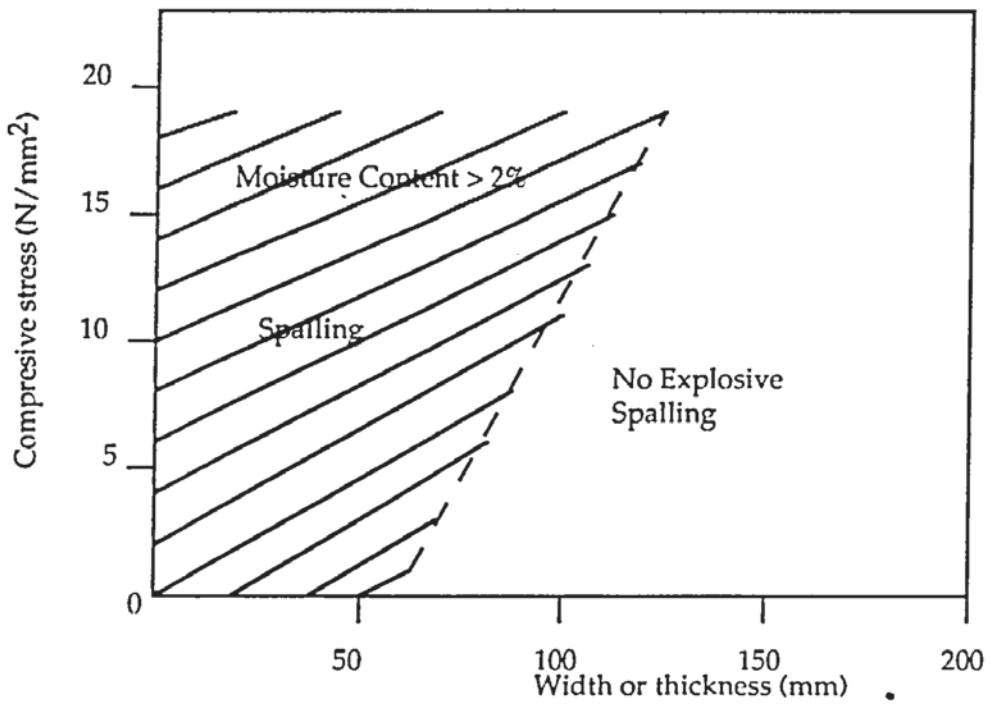


Figure 2.13: Approximate boundary between explosive and non-explosive spalling. (Meyer-Ottens, 1972).

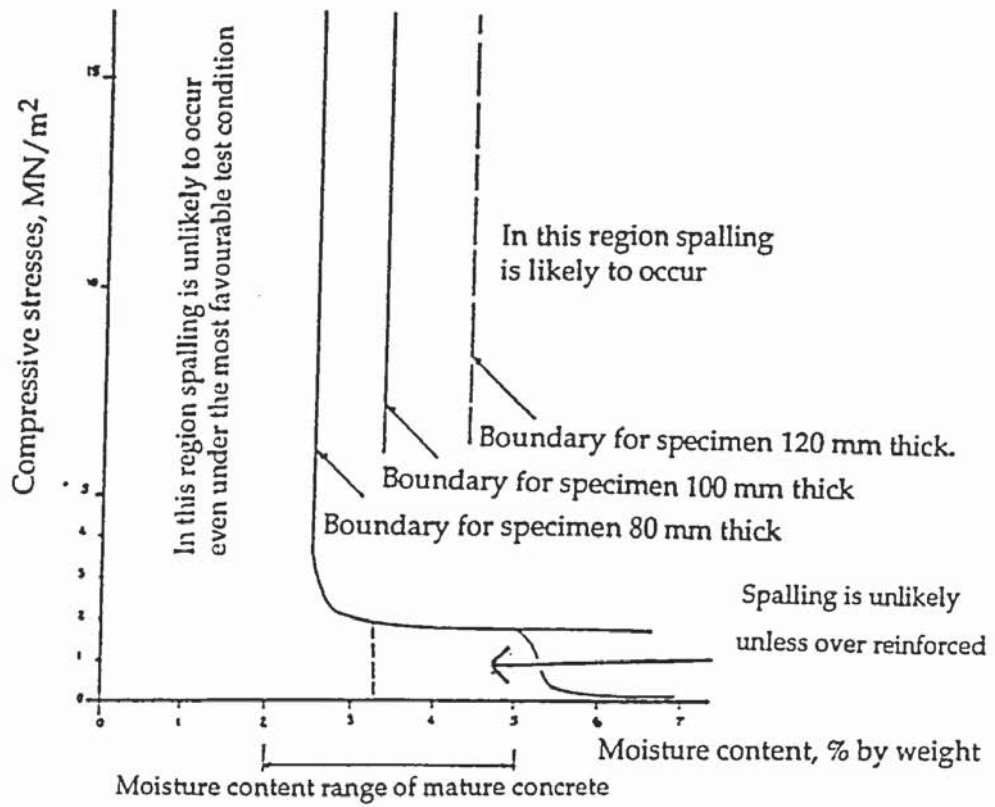


Figure 2.14: Summary of spalling test results of Meyer-Ottens. (Sertmehemetoglu, 1977).

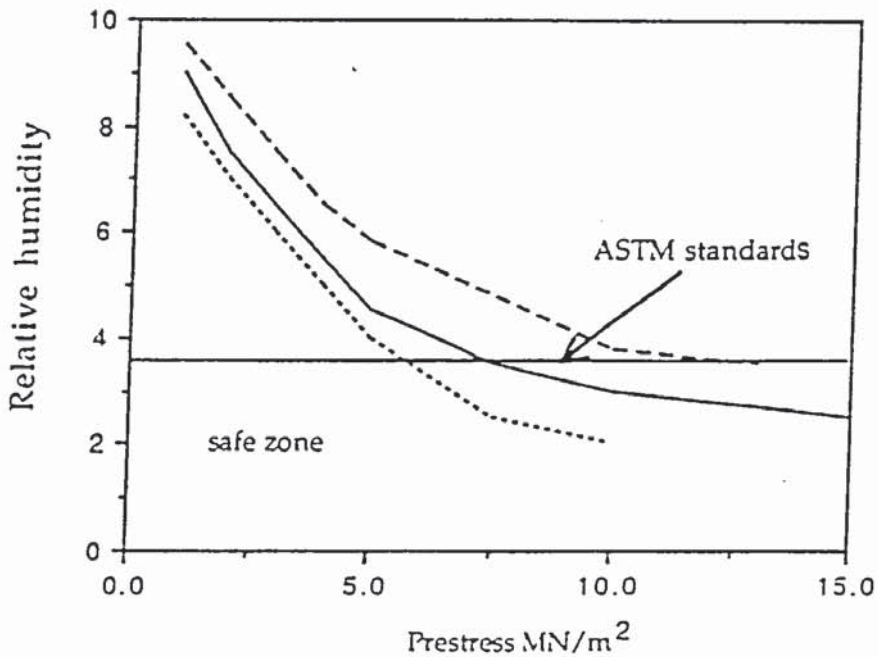


Figure 2.15: Safe spalling envelope (Christiaanse, 1972)

Copier (1979) conducted tests on prisms and slabs of lightweight concrete as an extension to the work of Meyer-Ottens. The specimens were heated from one and two sides following the standard temperature curve while varying the compressive stress, reinforcement and moisture content. Copier concluded that the principal cause of spalling was the moisture content of the concrete and noted that other contributory factors include the number of faces exposed, the presence of reinforcement, thickness of members and the presence of compressive stresses. However, the quantity of reinforcement, magnitude of compressive stress and the quality of concrete were thought to be of lesser importance.

During his extensive series of tests, Sertmehemetoglu (1977) developed special apparatus to measure pore pressures in 120 mm diameter concrete prisms heated from one end to create thermal gradient and to cause the movement and evaporation of free moisture. The investigation has shown that combinations of pore pressure, compression and internal cracking were needed to cause explosive spalling and that age of concrete up to 70 weeks had little effect on the occurrence of spalling.

The following section cover various aspects related to computer modelling of structural elements in a fire environment. A brief account of the historical development of research on computer modelling will also be given.

2.6 COMPUTER MODELLING

The long established approach to determine structural fire endurance has been through the use of standard laboratory tests conducted on a portion of

'representative' construction mounted in a furnace. The fire resistance of the element is determined from the time at which the specimen, through structural weakness or excessive heat transmission, ceases to be an effective bearer against the spread of fire. While this approach provides a reasonably simple solution to an otherwise complex problem, the standard furnace test does not provide the designer with a clear demonstration of how the actual structure will perform.

Selecting building elements that fulfil fire resistance requirements specified in the building codes is, however, no assurance that these building elements will function satisfactorily in a real-world building fire. Harmathy (1988) argued that specifying fire endurance requirements in terms of performance in test fires is justified only if:

- the severity of real-world fires can be described as a function of all significant parameters, and
- the relationship between the performance of building elements in a real-world fires and standard test fires is understood.

Computer simulation currently provides a more realistic situation corresponding to a column in a continuous structure using calculations based on heat transfer and the structural properties of materials at high temperature. The development of computational techniques has enabled the determination of heat transfer from the heated surface to the inside of the heated element and elaborate calculations can also be made regarding simulation of transient heating conditions and multi-dimensional heat flow.

Undoubtedly, further development is to be expected in the field of fire engineering that would have the objective of simulating a realistic fire environment and realistic structural behaviour as suggested by Malhotra (1986), Harmathy (1991) and Lie (1994).

Becker, Bizri and Bresler (1974) developed FIRES-T, a computer program for the Fire Response of Structures - Thermal that evaluates the temperature distribution history of structural cross sections in fire environments. The evaluation is formulated in two dimensions through the assumption that no heat is flowing along the longitudinal axis of a structural member. The heat flow problem solved by FIRES-T is non-linear due to the temperature dependence of the thermal properties of structural materials and the heat transfer mechanisms associated with fire environments. These non-linearities are handled by a local linearisation about a current temperature distribution that requires the use of an iterative approach within the given time steps.

In FIRES-T, the heat balance equation is solved in matrix form using a finite element method coupled with time step integration. This approach is based on the work of Wilson and Zienkiewicz but extended to the fire situation by Bizri (1973). The finite element mesh employed in FIRES-T can be made up of quadrilateral or triangular elements. Convective and radiative mechanisms are used to model the heat transfer from fire environment to which the structural member is exposed. A revised version of FIRES-T, FIRES-T3 has been developed by Iding *et al.* (1977a) that allows a three dimensional solution to the heat flow problem.

Wickström (1979) developed TASEF-2, a computer program for the Temperature Analysis of Structures Exposed to Fire that is similar to FIRES-T. It is based on

finite element method where the heat balance equation is solved in matrix form for a two dimensional field. The finite element meshes that may be employed are either quadrilateral or triangular elements. The fire exposure can be simulated using an arbitrary external temperature time curve defined by the user. TASEF-2 is sensitive to the choice of time increments which gives problems of overconvergence as a result of Wickström employing a smaller computer memory core than that required by FIRES-T (Weeks, 1985).

Allen and Lie (1974) used computer calculation to study the problem of a square reinforced concrete column in a fire. Their analysis takes into account the problems of restraint, interaction of the column with surrounding structure and considered fire curves for various fire loads. The temperature distribution in the column cross section was determined using the numerical method employed in Lie and Allen (1972). An approximate solution based on load deflection analysis was adopted. The correct solution requires an iterative determination of the moments, curvature and displacements along the column for each time interval. The column is said to have failed when convergence is very slow.

Allen and Lie (1974) calculated the lateral deflection based on the assumption that the column is fixed at both ends and that the curvature diagram varies linearly from mid-height to both supports. The curvature at mid-height and at the supports are assumed to be equal and opposite. This assumption is approximately correct as the column approaches failure with inelastic strains in the critical sections, but it is considerably in error for elastic conditions during the early stages of the fire. Allen and Lie's approximate numerical study of column-structure interaction indicated an increase in fire resistance with increased stiffness of the surrounding structure.

Lie (1983) employed a similar analysis to that used by Allen and Lie (1974) but with the boundary conditions substantially altered. The columns were idealised as pinned ended instead of fixed at both ends. A small eccentricity of 2.5 mm was assumed due to imperfections of the column and the loading device.

Becker and Bresler (1974) developed FIRES-RC (Fire Response of Structure - Reinforced Concrete Frames), a computer program for analysing the structural response of reinforced concrete frames in a fire using finite element techniques. Iding *et al.* (1977b) revised FIRES-RC by substituting the secant stiffness approach adopted by Becker and Bresler (1974) with a tangent stiffness approach and an allowance was made for the linear variation of the moment along the axis of the structural element. Further revision was made when Anderberg (1976) incorporated a material behaviour model developed at Lund Institute of Technology by Anderberg and Thelandersson (1976) into FIRES-RC. The model is based on the concept that the total strain can be separated into four components namely the thermal strain, instantaneous stress-related strain, creep strain and transient strain.

The analysis used in FIRES-RC is based on the finite element method with non-linear, direct stiffness formulation coupled with a time step integration. The deformed shape that results in equilibrium between the forces due to the external loads and internal stresses is determined through an iterative approach. However, FIRES-RC failed to take into account of geometrical non-linearities and second order effects. The additional moments that arise from the eccentricity of the axial force as the column deflects that would result in serious discrepancy between calculated and actual stress within the column cross section was not taken into

consideration. Hence, failure of a slender column due to buckling mode is likely to occur at an earlier time period than that predicted by FIRES-RC.

Haksever (1977) first considered geometrical non-linearities when analysing pin-ended slender L-frames exposed to fire. Forsén (1982) too considered geometrical non-linearities in CONFIRE; developed from the computer program CONFRAME originally written by Aldstedt (1975). CONFIRE uses the material model developed at Lund Institute of Technology by Anderberg and Thelandersson (1976) and takes into account the additional moment that arises from the eccentricity of axial force as the column deflects. However, an oversimplified model of restraint is used in CONFIRE where the ends are either considered as fully restrained or pinned.

The computer programs FIRES-RC and CONFIRE are designed to be used in conjunction with a program that predicts the thermal response of the reinforced concrete frames such as FIRES-T or TASEF-2 together providing an overall capability of predicting the structural response of reinforced concrete elements in fire environment.

Terro and Sullivan (1992) developed a model for the structural behaviour of reinforced concrete under transient temperature conditions. The analysis comprises two modules; TEMP that determines the incremental temperature gradients and STRUCT for the structural analysis calculations. The temperature file created in the thermal analysis is interfaced automatically with the structural analysis program.

TEMP is a non-linear finite element heat transfer analysis program for the prediction of the temperature distribution history in two dimensional continua. The general finite element formulation in TEMP is implemented in an incremental formulation to account for material non-linearities. It employs an implicit time differencing scheme that prevent divergence problems in the selection of time step. TEMP thus has the advantage that the mesh and time increment are not restricted in size to achieve convergence hence giving accurate predictions using less computer time.

STRUCT is a non-linear finite element program developed within the shell of a general purpose finite element program called LUSAS (London University Stress Analysis System) and has the capability to analyse three dimensional building structures. It takes account of material and geometrical non-linearities that occur due to the large displacements expected in structures exposed to fire. The constitutive model for concrete adopted in STRUCT is that the total strain is resolved into four strain components; free thermal strain, basic creep strain, transient creep strain and stress-related strain.

The models previously described were developed on the same concepts as those used to model concrete at ambient temperatures. The uniaxial model developed by Anderberg and Thelandersson (1976) make use of the non-linear theory of elasticity to model the non-linear behaviour in compression. Thelandersson (1982) then uses the theory of plasticity to describe the non-linear response assuming the existence of plastic and viscoplastic yield surfaces. The viscoplastic surface is used to describe the time-dependent effects, while the plastic surface is used to describe the instantaneous non-linear behaviour.

Khennane and Baker (1992) developed a model based on the theory of plastic to simulate the uniaxial thermomechanical response of concrete. The total strain is resolved into three individual components; mechanical strain, thermal strain and transient creep strain. Each component is formulated individually and the resulting constitutive equation is integrated over a time step. The mechanical strain is assumed to consist of an elastic strain and a plastic strain which itself is taken as temperature dependent. In describing the plastic strain rate, the non-linear part of the uniaxial stress-strain curves is assumed to be a quarter of an ellipse based on the proposal of Lin *et al.* (1987). The accuracy of the elliptical formulation describing the non-linear portion of the stress-strain curves at constant temperatures was then assessed using a combination of variable load and constant temperature and validated against the results obtained by Anderberg and Thelandersson (1976).

Although in general the computer models developed have been shown to be in good agreement with experimental data from a wide range of problems, there are still limitations and uncertainties in the use of computational techniques; the most important concerning the assumed behaviour of the concrete materials. Different models for determining the structural behaviour have been developed in that some use steady-state, transient state and some mixed data and have different degrees of sophistication. It is felt that further research needs to be done in this respect to verify the effect of modelling material models with and without incorporating the transient strain.

It should also be noted that no account is taken of spalling either in the thermal or structural analysis in all the computer models that have been developed to study the structural response of concrete structures when exposed to fire. The effect of

spalling is a loss of concrete and a resultant modification to the finite element meshes. Any incorporation of the effect of spalling would have the implication that the current mode of decoupling the thermal and structural analysis may no longer be appropriate.

For steel members, Tomecek and Milke (1993) conducted a study on the effect of partial loss of protection on the fire resistance. A series of computer simulations was used to make comparisons of the fire resistance to the percentage of protection lost. An array of three columns and three protection thickness was chosen for one series of simulations while three columns and two different material loss positions were used for a second set of simulations. The investigation has shown that the fire resistance of steel columns was found to decrease appreciably with any increase in protection loss. The effect were found to vary with the amount of protection loss, the size of the column and the position of protection loss.

Tomecek and Milke (1993) further noted that the severity of fire resistance loss varied with the initial rating of the column. A three-hour rated column would have a greater reduction in fire resistance than a one-hour rated column. In addition column size was also noted to have an effect on the loss of fire resistance in that the effect of protection loss on larger columns would be less than that on a small column.

There is also limitation as far as the consideration of moisture transport is concerned in the application of the computer simulation technique to study the response of concrete members in a fire environment. It is realised that lack of consideration of moisture transport will be critical where the concrete

compression face is exposed to the full effects of fire. Since the tension face, where moisture can easily escape due to the presence of cracks, is away from the exposed face, the moisture transport escape length will be large. Thus, full qualitative comparisons between tests and computer predictions cannot be expected. However, Haksever and Thelandersson (1982) and Weeks (1985) have indicated that moments applied in the same sense as the thermal gradient across a column section i.e. the case in which the concrete tension face is exposed to the full effects of fire, considerably reduce the fire resistance of the column. Thus the problem due to lack of consideration of moisture transport in computer modelling may not have a critical effect on the calculated results.

The following chapter, Chapter 3 deals with properties of materials at elevated temperature.

CHAPTER THREE

PROPERTIES OF MATERIALS AT ELEVATED TEMPERATURES

3.1 INTRODUCTION

All building materials, regardless of type, will experience a certain degree of degradation when exposed to fires. The material may burn, melt, spall, warp, expand, shrink or deflect. At some point, the elevated temperatures will adversely affect the material's strength and rigidity and therefore the structural performance. In order to understand and eventually predict the performance of structural members under fire conditions, it is thus necessary to have a knowledge of the relevant material properties that determine the behaviour of a member at elevated temperatures.

Material behaviour may be divided into two categories, thermal and mechanical. A knowledge of thermal properties is important since they influence the rate of heat transfer into the construction while that of mechanical properties is required to evaluate the ultimate limit state of structural integrity (Purkiss, 1986).

Many investigations on the effect of fire on concrete and steel have been reported. However, the test results are difficult to compare and interpret as a whole due to the variations in materials and experimental techniques employed by various researchers (Anderberg, 1983 and Schneider, 1985).

The mechanical properties of materials are highly influenced by the mode of testing. The classical method for the determination of material properties is to heat gradually a specimen to a desired temperature and apply an increasing load to failure. This procedure, known as steady state testing, is then repeated for different temperatures to obtain the relationship between the material parameter and temperature. However this procedure bears little relation to the conditions likely to be encountered in actual fire conditions as the temperature variation is progressive whilst the material is under load. The determination of material properties under transient heating conditions is a truer representation where the material is subjected to a degree of preload and transient type of heating.

The three main test parameters to determine the material properties are the heating process, application and control of load, and control of strain. These parameters can have constant values giving steady state conditions or varied giving transient conditions. Malhotra (1982) identified six different testing regimes in which material properties can be established. These are shown diagrammatically in Figure 3.1. A RILEM technical committee commissioned reports giving data on concrete and steel distinguishing between steady and transient tests and provided a basis for modelling such properties (Anderberg, 1983 and Schneider, 1985).

3.2 THERMAL PROPERTIES

In order to evaluate the thermal response of a concrete element, it is necessary to have data on the variation of thermal conductivity, specific heat, density and derived from those, thermal diffusivity. Knowledge of these data will enable the solution of the Fourier equation of heat diffusion to be used to determine the

temperature T within the structural element. The heat diffusion equation is given by:

$$\nabla^T(\gamma(\nabla T)) = \dot{T} \quad (3.1)$$

where: T is the space dependent temperature
 γ is the temperature dependent thermal diffusivity.

The value of diffusivity of a material is determined by the following relationship:

$$\gamma = \lambda / \rho C_p \quad (3.2)$$

where: γ is the thermal diffusivity (m^2/h),
 λ is the thermal conductivity ($W/m^{\circ}C$)
 ρ is the density (kg/m^3)
 C_p is the specific heat ($J/kg^{\circ}C$)

3.2.1 CONCRETE

The values of the thermal parameters for concrete are generally dependent on the type of aggregate, the mix proportions, the original moisture content and the age of the concrete (Purkiss, 1995). The data presented in this section are representative of typical concretes.



Figure 3.1: Different testing regimes for determining mechanical properties (Malhotra, 1982)

3.2.1.1 Thermal Conductivity

The temperature rise in a concrete member as a result of heat flow is a function of the thermal conductivity of the material. The thermal conductivity of concrete depends upon the nature of aggregate, porosity of the concrete and the moisture content for temperatures below 100°C. Harmathy (1970) investigated various concretes and obtained performance bands as shown in Figure 3.2 where the order of magnitude of the thermal conductivity of concrete is given as a function of temperature.

For normal weight concrete, thermal conductivity tends to decrease slightly with increasing temperature. The variation of thermal conductivity with temperature however, depends on the degree of crystallinity of the aggregate. The higher the crystallinity, the higher is the thermal conductivity and its decrease with temperature. A typical crystalline material in concrete is quartzite, which is often the main component in siliceous aggregate. The thermal conductivity of lightweight concrete tends to increase with temperature, but is nearly constant as shown in Figure 3.2, at around 0.5 W/m°C.

Eurocode 2 Part 10 (1992) gives the following equations for the values of thermal conductivity (W/m°C) for two normal weight concretes.

For siliceous aggregate:

$$\lambda = 2.0 - 0.24 (T_c / 120) + 0.012 (T_c / 120)^2 \quad (3.3)$$

For calcareous aggregate:

$$\lambda = 1.6 - 0.16 (T_c / 120) + 0.008 (T_c / 120)^2 \quad (3.4)$$

where: T_c is the temperature of the concrete.

3.2.1.2 Specific Heat

The specific heat of a material is the characteristic that describes the amount of heat input required to raise a unit mass of material a unit of temperature. Typical ranges for the volumetric specific heat, the product of specific heat and density, for normal weight and lightweight concretes are shown in Figure 3.3 (Harmathy, 1970). The peak at the 500°C temperature range is caused by the character of the specific heat of the cement paste which shows a sharp peak at around the temperature (Lie, 1992). Water in the concrete at temperatures below 150°C may also have a substantial effect on the value of the specific heat (Purkiss, 1986).

Schneider (1985) reported a study conducted by Collet and Tavernier in 1976 on the variation of specific heat as a function of temperature for concrete made with three different types of aggregate: gravel, limestone and lightweight aggregates. For dense aggregate concrete specific heat increases from 800 J/kg°C to 1200 and for lightweight aggregate and limestone concretes from 800 to 1000 J/kg°C. The results are shown in Figure 3.4. It can be seen that specific heat increases slowly with increasing temperature for all aggregates. The type of aggregate has only a small influence on the specific heat. Eurocode 2 Part 10 gives the following equation for the specific heat of normal weight concrete (J/kg°C):



Figure 3.2: Thermal conductivity of normal weight and lightweight concretes as a function of temperature. (Harmathy, 1970).



Figure 3.3: Ranges of volumetric specific heats of normal weight and lightweight concretes. (Harmathy, 1970).

$$C_p = 900 + 80 (T_c / 120) - 4 (T_c / 120)^2 \quad (3.5)$$

Lie (1992) suggested that 1170 J/kg°C is a reasonable approximation for the specific heat of concrete.

3.2.1.3 Thermal Diffusivity

The thermal diffusivity of a material is a measure of how effectively the heat is dissipated through the material. It is equal to the ratio of the thermal conductivity to the volumetric specific heat of the material. The larger the value of thermal diffusivity, the faster the heat is transported away from the surface being heated. Since the values of thermal conductivity and specific heat vary with elevated temperatures, the value of thermal diffusivity will so vary.

The relations between temperature and thermal diffusivity for normal and lightweight aggregate concretes are shown in Figure 3.5 (Malhotra, 1982). Thermal diffusivity decreases as temperature increases. For normal concrete at 700°C, thermal diffusivity is virtually half of the value at ambient temperature.

3.2.1.4 Density

Density of concrete depends primarily on the aggregate type and shows only minor temperature dependence as indicated in Figure 3.6 (Schneider, 1986). Density is mostly due to temperature rises during heating that drives away free moisture when the temperature exceeds 100°C. However, the effect of temperature on density is insignificant and it can be assumed constant for heating regimes up to 800°C when some aggregates start to decompose. Limestone

concrete shows a significant decrease in density at 800°C due to the decomposition of the calcareous aggregate. However, it is usually considered accurate enough to take the value of density of concrete as that at ambient temperature.

3.2.2 STEEL

The determination of thermal values of steel are less complex than that for concrete since the values are generally independent on either the use of the steel, either structural or reinforcing, or on the strength or grade of the steel (Purkiss, 1995).

3.2.2.1 Thermal Conductivity

As in concrete, the temperature rise in a steel member as a result of heat flow is a function of its thermal conductivity. The value of this property varies somewhat with chemical composition at room temperature; however, at elevated temperatures it may be considered identical for most structural steels. Figure 3.7 illustrates the typical variation in thermal conductivity of steel with temperature. As can be seen, thermal conductivity decreases with increasing temperature; at 800°C it is reduced by about 50% (Malhotra, 1982).

Eurocode 3 Part 10 (1992) gives the following equation for the thermal conductivity of steel:

$$\text{For } T_s < 800, \quad \lambda = 54 - 3.33 \times 10^{-2} T_s \quad (3.6)$$



Figure 3.4: Specific heat for different types of concrete. (Schneider, 1985).



Figure 3.5: Effect of temperature on thermal diffusivity of concrete. (Malhotra, 1982).



Figure 3.6: Density of structural concretes at high temperatures. (Schneider, 1986)



Figure 3.7: Thermal conductivity of steel at elevated temperatures.
(Malhotra, 1982).

$$\text{For } T_S > 800, \quad \lambda = 27.3 \text{ W/m}^\circ\text{C} \quad (3.7)$$

where: T_S is the temperature of the steel.

The thermal conductivity of steel at room temperature is about 50 W/m^{°C}, much higher than that for concrete. In the determination of its fire performance, steel is widely assumed as a perfect conductor due to its relatively high thermal conductivity. This would imply a uniform temperature distribution of the steel section. In reality, temperature gradients do exist in steel section which may give resultant in stress gradients.

3.2.2.2 Specific Heat

The specific heat of steel appears to be independent of the nature of the steel. For most structural steels, its value increases gradually with temperature. At 540^{°C}, there is a steep increase in specific heat over a narrow temperature range and nearly doubling in value up to 700^{°C} before reaching a peak and then decreasing. This is illustrated in Figure 3.8 where the volumetric specific heat of the steel is plotted as a function of temperature. Eurocode 3 Part 10 (1992) expressed the specific heat by the following equation for temperature up to 600^{°C} :

$$C_p = (425 + 7.73 \times 10^{-1} T_S) - (1.69 \times 10^{-3} T_S^2) + (2.22 \times 10^{-6} T_S^3) \quad (3.8)$$

$$\text{For } 600^\circ < T_S < 735^\circ, \quad C_p = 666 + 13002/(738 - T_S) \quad (3.9)$$

$$\text{For } 735^\circ < T_S < 900^\circ, \quad C_p = 545 + 17820/(T_S - 731) \quad (3.10)$$

$$\text{For } 900^{\circ} < T_s < 1200^{\circ}, \quad C_p = 650 \text{ J/kg}^{\circ}\text{C} \quad (3.11)$$

However, Eurocode 3 Part 10 (1992) proposed that for approximate calculation, the specific heat may be considered to be independent of steel temperature with the value should be taken as 600 J/kg^oC. Lie (1992) also suggested that a constant value of 600 J/kg^oC for the specific heat of steel for the entire temperature range as a good approximation due to the wide scatter of reported data in this narrow range and also due to its minor overall influence on behaviour in fire.

3.2.2.3 Thermal Diffusivity

The effect of temperature on the thermal diffusivity of steel is shown in Figure 3.9 (Malhotra, 1982). The thermal diffusivity has an almost linear relationship with temperature with a value of 0.84 m²/h at 20^oC decreasing linearly to 0.28 at 700^oC and can be represented by the following equation:

$$\gamma = 0.87 - (0.84 \times 10^{-3} T_s) \quad (\text{m}^2/\text{h}) \quad (3.12)$$

3.2.2.4 Density

The density of steel is unaffected by high temperature and may be taken as its ambient value of 7850 kg/m³ over the normally experienced temperature range.

3.3 MECHANICAL PROPERTIES

The general aim behind a study of the mechanical properties of a material is to enable a constitutive law governing the behaviour of that material at elevated

temperatures to be formulated. A complete formulation is required when it is necessary to undertake a full analysis in order to calculate deformations and displacements of structural elements in a fire (Purkiss, 1995).

Whilst the determination of mechanical properties at ambient condition are carried out according to various standard methods that have been laid down, there are no such standard for testing at elevated temperatures although the RILEM Committee is currently undertaking this. It thus necessary that care is taken in comparing test data from differing sources. Purkiss (1995) also stressed the importance of recognising that the rate of loading or strain used at elevated temperature testing plays a far more significant role than at ambient conditions owing to creep being much higher at elevated temperature. The rate of heating also plays an important role on the result of testing on a heated specimen.

3.3.1 CONCRETE

The mechanical properties of concrete are dependent on very wide variations of factors such as mix proportions, type of aggregates and age of concrete. Only representative results are presented in this section.

3.3.1.1 Compressive Strength

The compressive strength of concrete at elevated temperatures varies according to the type of aggregate and the aggregate/cement ratio (Schneider, 1985); the type of aggregate is the main factor. The decrease in strength of carbonate and lightweight aggregate concretes occur at higher temperature compared to siliceous concretes as shown in Figure 3.10 (Abrams, 1971). Pettersson (1965) also

investigated the influence of various aggregates on the elevated temperature compressive strength of concrete. The results are shown in Figure 3.11. As can be seen, the actual strengths will increase for some aggregates while others begin to decline immediately. These values, however, all tend to merge as temperatures reach 700°C .

Aggregate/cement ratio also significantly influences the shape of the strength-temperature relationship of concrete; the reduction in strength being significantly smaller for lean mixes than for rich mixes. The effect of aggregate/cement ratio and different load conditions are illustrated in Figure 3.12 (Malhotra, 1956). The presence of a compressive stress during heating is shown to have a favourable effect on the temperature dependent compressive strength. Weeks (1985) reported that Fisher in 1970 has also shown that, with preloaded specimens, there is a smaller strength loss at elevated temperatures.

3.3.1.2 Modulus of Elasticity

The variations with temperature of the modulus of elasticity of concrete, made from three types of aggregates, are shown in Figure 3.13. All three concretes experienced a rapid loss in elastic modulus as temperature increased. At 200°C, the modulus is around 70 - 80% of the modulus at room temperature and at 400°C, 40 - 50% of the original value. The variations in modulus of elasticity with different concrete strengths are shown in Figure 3.14 (Maréchal, 1970). It appears that aggregate type and concrete strength significantly effect the moduli at high temperatures. Lightweight aggregate concrete indicates the lowest decrease in the modulus of elasticity and siliceous aggregate concrete the highest.



Figure 3.8: Volumetric specific heat for steel at elevated temperatures. (Stirland, 1980).



Figure 3.9: Thermal diffusivity of steel. (Malhotra, 1982).



Figure 3.10: Compressive strength of concrete. (Abrams, 1971).



Figure 3.11: Influence of the aggregate on the compressive strength of concrete at elevated temperatures. (Petterson, 1965).



Figure 3.12: Influence of cement-aggregate ratio and load conditions on the concrete strength. (Malhotra, 1956).



Figure 3.13: Modulus of elasticity of concrete. (Schneider, 1985).



Aston University

Illustration removed for copyright restrictions

Figure 3.14: Variations in modulus of elasticity with different concrete strength. (Maréchal, 1970).

3.3.1.3 Stress-Strain Characteristics

The early work on stress-strain relationship for concrete suffered from the disadvantage that early researchers tended to be interested in only measuring specific properties such as compressive strength or elastic modulus rather than obtaining the complete stress-strain characteristics as suggested by Purkiss (1995). Early experimental work tended to be performed on specimens that were heated without applied load until it was realised that prehistory of stress had beneficial effects in that substantially smaller strength reductions were observed. Some typical stress-strain curves of Anderberg and Thelandersson (1976) are shown in Figure 3.15. Furumura (1966) appears to have been the first to obtain the complete stress-strain curve for concrete whose results indicated a reduction of the slope of the descending branch similar to that obtained for the compressive stress and elastic modulus. Later, the complete stress-strain curve has also been obtained by Purkiss (1972) and Bali (1984), amongst others.

Baldwin and North (1973) demonstrated that Furumura's data on the effects of temperature upon stress-strain characteristic can be normalised with respect to the maximum compressive stress and the strain value at peak stress, the curve obtained could be fitted with the equation:

$$\frac{\sigma}{\sigma_{\max}} = \frac{\epsilon}{\epsilon_{\max}} \exp\left(1 - \frac{\epsilon}{\epsilon_{\max}}\right) \quad (3.13)$$

where: σ_{\max} is the value of the maximum stress for the temperature
 ϵ_{\max} is the value of strain at the point of maximum stress.

Purkiss (1995) reported that a more general equation that can be fitted to any concrete stress-strain curve was suggested by Popovics in 1973 as below:

$$\frac{\sigma}{\sigma_{\max}} = \frac{\epsilon}{\epsilon_{\max}} \left(\frac{n}{n-1 + \left(\frac{\epsilon}{\epsilon_{\max}} \right)^n} \right) \quad (3.14)$$

Equation 3.14 needs only one parameter, n , to fit the data and n is found from equation:

$$\frac{n}{n-1} = \frac{\epsilon_{\max} E_0}{\sigma_{\max}} \quad (3.15)$$

where: E_0 is the initial modulus of elasticity.

Popovics suggested that n was only dependent on the concrete strength. However, Purkiss (1995) argued that, from the analysis of experimental stress-strain curves, n was more likely to be dependent on the aggregate-cement ratio.

3.3.1.4 Creep

Creep of concrete is determined by various factors; the most important of which are the temperature of the concrete and the stress (Lie, 1992). Data on creep at high temperatures of a carbonated aggregate concrete, for a 5-hour test period are shown graphically in Figure 3.16 (Cruz 1968). After heating to test temperature, a load equal to 45% of room-temperature strength of the concrete was maintained

during the test period. For this concrete, creep increased with temperature only moderately to 320°C. Above this point, the increase in creep was much greater.

Figure 3.17 shows creep information for two stress levels, i.e. 22.5% and 45% of the concrete strength, and several concrete temperatures for a 3-hour period (Anderberg and Thelandersson, 1976). From these data it appears that creep plays a limited role on the behaviour of concrete except when the temperature is above 400°C.

Anderberg and Thelandersson (1976) proposed a creep model from regression analysis for concrete under sustained load and constant temperature, where the creep is proportional to the ratio between the actual stress and the concrete strength for the test temperature. The mathematical formulation for the creep model is given by:

$$\epsilon_{cr} = \left[\frac{\sigma}{\sigma_{\max(T)}} \right] \left(\frac{t}{t_r} \right)^p \beta_0 e^{k_1(T-20)} \quad (3.16)$$

where: σ is the applied stress

$\sigma_{\max(T)}$ is the maximum compressive stress for temperature T

t is the time

t_r is the reference time = 3 hours

p is a dimensionless constant = 0.5

T is the concrete temperature

$\beta_0 = +0.53 \times 10^{-3}$

$k_1 = 3.04 \times 10^{-3} \text{ } ^\circ\text{C}^{-1}$



Figure 3.15: Stress-strain relationships for dense concrete (no preload).
(Anderberg and Thelandersson, 1976).



Figure 3.16: Creep of a carbonated aggregate concrete
at various temperatures. (Cruz, 1968).

Bažant and Panula (1978) investigated the effect of temperature on creep through a numerical analysis involving activation energy and demonstrated that the activation energy approach holds at every high temperatures. Bažant and Panula (1978) accept that activation energy remains constant for any particular concrete type. Maréchal (1970) demonstrated that the variation of creep with temperature above 500°C follows the equation:

$$\varepsilon_{cr} = C \sigma^{\alpha/kT} \cdot e^{-U_a/kT} \quad (3.17)$$

where: U_a is the activation energy,
 T is the absolute temperature,
 k is the Boltzman constant,
 α and C are constant varying with T .

This model does not seem to hold for temperatures below 150°C due to the presence of moisture. However, for concrete with no free moisture, the model appears to be satisfactory .

Gillen (1981) investigated the effects of temperature on creep and has shown the rate of creep strain to decrease continually with time, the magnitude of creep strains increased with temperature and that there is no consistent relation between age of concrete and creep.

Schneider (1976) conducted tests on creep and deformation characteristics of concretes up to 450°C and compared creep data that were measured at constant elevated temperatures with transient creep data, i.e. data derived from transient

temperature conditions. Schneider also highlighted the importance of transitional thermal creep in the temperature range 80°C to 300°C due to the physical disintegration and chemical decomposition. Schneider's results appear to be in good agreement with the results of other workers such as Maréchal (1970).

3.3.1.5 Thermal Expansion

The thermal expansion of concrete is influenced by cement, water content, aggregate type and age (Lie, 1992). However, the main factor affecting the thermal expansion of concrete is the type of aggregate (Schneider, 1985). The thermal expansion data for concrete made with different aggregates are shown in Figure 3.18 (Pettersson, 1965). Most concretes expand with increasing temperature; the expansion is not a linear function of temperature but increases with increasing temperature. Sanded expanded-shale concrete has the lowest expansion-temperature relationship over the temperature range of 20 - 875°C. Malhotra (1982) reported that Cruz in 1968, in some of his early experiments measuring the thermal expansion of concrete at elevated temperature, divided concrete into three groups depending on the aggregate used as shown in Figure 3.19.

Generally lightweight aggregates exhibit relatively little influence on expansion whilst hard aggregates have a more pronounced effect through the change in the molecular structure. The best example is quartz, which goes through a transformation at approximately 570°C and again at 870°C as shown in Figure 3.20 (Lie, 1992).



Figure 3.17: Effect of temperature and stress level on creep.
(Anderberg and Thelandersson, 1976).



Figure 3.18: Expansion with temperature of concretes made
with various aggregates. (Pettersen, 1965).

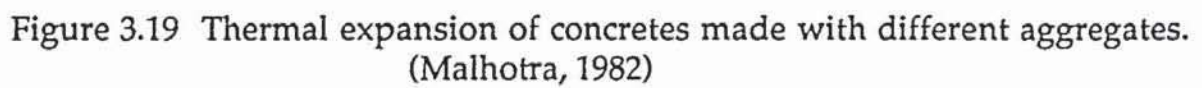


Figure 3.19 Thermal expansion of concretes made with different aggregates.
(Malhotra, 1982)

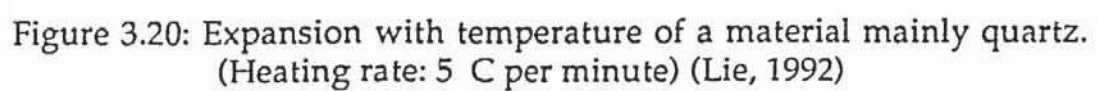


Figure 3.20: Expansion with temperature of a material mainly quartz.
(Heating rate: 5 C per minute) (Lie, 1992)

Anderberg and Thelandersson (1976) carried out an investigation of the effect of different load levels on thermal expansion of a siliceous-aggregate concrete heated at a rate of 5°C/min. The result is shown in Figure 3.21 where normal thermal expansion is represented by the zero curve. It can be seen that the effect of load reduces the expansion significantly.

Eurocode 2 Part 10 gives the following equations for the free thermal strain of two normal weight concretes:

For siliceous aggregate:

$$\text{For } 20 < T_c < 700 \quad \epsilon_{th} = -1.8 \times 10^{-4} + 9 \times 10^{-6} T_c + 2.3 \times 10^{-11} T_c^3 \quad (3.18)$$

$$\text{For } T_c > 700, \quad \epsilon_{th} = 14 \times 10^{-3} \quad (3.19)$$

For calcareous aggregate:

$$\text{For } 20 < T_c < 800, \quad \epsilon_{th} = -1.2 \times 10^{-4} + 6 \times 10^{-6} T_c + 1.4 \times 10^{-11} T_c^3 \quad (3.20)$$

$$\text{For } T_c > 800, \quad \epsilon_{th} = 12 \times 10^{-3} \quad (3.21)$$

The coefficients of thermal expansion of siliceous and calcareous aggregate concretes may be taken as $18 \times 10^{-6} \text{ deg}^{-1}\text{C}$ and $12 \times 10^{-6} \text{ deg}^{-1}\text{C}$ respectively over the whole temperature range for approximate calculations.

3.3.1.6 Transient Strain

Anderberg and Thelandersson (1976) conducted transient state tests on concrete specimens whereby the specimens were loaded to a certain stress level and then heated to failure. It is observed that the strains are functions of the applied stress as shown in Figure 3.21 with the strains being initially tensile. As the temperature is increased the strains turn compressive with the strain rate becoming very high at failure. At very high stress levels the strains may be entirely compressive.

Anderberg and Thelandersson (1976) suggested that if an attempt is made to calculate the total strains from the free thermal strains, the instantaneous stress related strains and the strains derived from the classical creep tests, then it is found that an additional term needs to be incorporated in the calculation to give the required strain balance as shown in Figure 3.22. This additional term is known as transient strain that is essentially due to stress modified thermally induced incompatibilities between the aggregate and the cement mortar matrix (Purkiss, 1995). Khoury *et al.* (1986) and Khoury (1992) also reported a substantial amount of data on transient strain.

Transient strains occur under stress as the temperature increases, essentially irrecoverable and only occur under first heating of the concrete. Its effect can be expressed as an increase in the compression deformability of concrete. Transient strain is temperature dependent and independent of time.

Anderberg and Thelandersson (1976) proposed that:

$$\varepsilon_{tr} = \sigma g(T) / \sigma_{max,0} \quad (3.22)$$



Figure 3.21: Effect-of load levels on concrete deformation.
(Anderberg and Thelandersson, 1976).



Figure 3.22: Different components of thermal strain.
(Anderberg and Thelandersson, 1976).

where: ϵ_{tr} is the transient strain
 $g(T)$ is a function of temperature and proportional to ϵ_{th}
 σ is the applied stress
 $\sigma_{max,0}$ is the compressive strength at ambient conditions.

3.3.1.7 Bond Strength

The bond strength between concrete and steel decreases with increasing temperature. It is generally agreed that the decrease in bond strength with temperature depends on the type of concrete and the surface of the reinforcing bars (Purkiss, 1995). Schneider (1985) suggested that concretes with lower thermal strain characteristics have higher bond strength at elevated temperatures than concretes with high thermal strain characteristics. Deformed bars or plain bars with heavily rusted rough surfaces show higher bond strengths than smooth bars. Figure 3.23 shows typical results obtained by Malhotra (1982) for the relative bond strengths of various reinforcing bars as a function of temperature.

Testing procedures also has an influence on the bond strength. The residual bond strength is always lower than bond strengths obtained from hot tests (Schneider, 1985).

3.3.2 STEEL

The main thrust on determining the effect of temperature on the properties of steel is on its strength behaviour. Generally the behaviour of steel at high temperatures depends primarily on the type of steel and the method of

manufacture. Considerable information on this is now available especially Anderberg (1983).

3.3.2.1 Strength Characteristics

The strength of hot-rolled structural steels is typically characterised by two values; its yield and tensile strengths. Figure 3.24 shows typical stress-strain curves for mild steel at various temperatures (Harmathy and Stanzak 1970). The strength loss at elevated temperatures is substantial even though there is a slight strength gain at relatively low temperatures. At ambient temperature, yield strength is characterised by a distinct point on the stress-strain curve at which a pronounced increase in strain is observed without a corresponding increase in applied stress. At elevated temperatures, this characteristic diminishes until the curve becomes rounded similar to a high yield steel. Under these conditions, the value of yield strength is defined by the 'offset' method. Figure 3.25 shows the variation of this characteristic yield strength with temperature where the yield strength is reduced by 50% at 600°C. Also, owing to the large strains exhibited at elevated temperatures, it is more usual to quote 1.0% or 2.0% proof stress i.e. the stress that produces a respective amount of residual strain, rather than the conventional 0.2% proof stress (Purkiss, 1995).

The tensile or ultimate strength of hot-rolled steel, as illustrated in Figure 3.25, is the maximum strength achieved before failure. The effect of temperature is similar to that of yield strength with the exception of a temporary 25% increase in strength in the 150 - 370° range. From this point, tensile strength decreases to values approaching yield strength at 760°C.



Figure 3.23: Reduction of bond strength for different steels. (Malhotra, 1982).



Figure 3.24: Stress-strain curves for a mild steel (ASTM A36) at various temperatures. (Harmathy and Stanzak, 1970).

Anderberg (1983) concluded that the relative decrease in strength of all hot-rolled and prestressing steels is almost the same. This means that the original strength has little influence on the strength-temperature curve. The 0.2% proof stress and the ultimate strength of such steels have 50% of its original value left at 500-550°C and about 20% at 700°C. For prestressing steel the 50% and 20% limits are reached at 350 - 400°C and 500°C respectively.

The strength changes in cold-worked steel are different in character from the changes found in hot-rolled steel at elevated temperatures. As shown in Figure 3.25, cold-worked steel loses its strength at relatively lower temperatures.

3.3.2.2 Modulus of Elasticity

The variation of modulus of elasticity of steel with temperature can be obtained directly from stress-strain relationship as the initial inclination of the curve. The modulus of elasticity decreases with increasing temperature as shown in Figure 3.26 (Anderberg, 1978). At 500 - 550°C the value is reduced by about 50%. The original strength characteristics seems to have little influence on the modulus. The modulus of elasticity for cold-drawn steel is typically 20% lower than the values for hot-rolled steel over a temperature range of 20 to 700°C.

3.3.2.3 Creep

Creep may be defined as the time dependent deformation of a material and is characterised by three periods: primary, secondary and tertiary as shown in Figure 3.27. The primary creep begins with load application and is reflected by a continuous but decreasing strain after the elastic deformation. The secondary

creep is the deformation that continues at a constant strain rate during the heating period. Finally, tertiary creep begins when the strain rate starts to increase eventually leading to failure by rupture. Data related to the primary and secondary phase are of most interest in fire conditions since heating period rarely exceeds a few hours. The creep depends not only on the temperature but is also strongly dependent on the stress in the steel. Figure 3.28 shows the rate of creep for two steels as obtained by Harmathy (1970). Anderberg (1983) suggested that creep starts to become significant at 250°C for cold-worked steel and 400°C for hot-rolled steel.

It is general practice to analyse creep data based on the Dorn (1954) temperature compensated time approach. The model can be extended so that it is applicable to variable stress by the use of the strain hardening rule. The creep strain is assumed to be dependent on the magnitude of the stress and on the temperature compensated time given by the following expression:

$$\theta = \int_0^t \exp(-\Delta H/RT) dt \quad (\text{hours}) \quad (3.23)$$

where: ΔH is the activation energy of creep (J/mol)
 R is the gas constant,
 t is the time.

The relation between creep strain and temperature compensated time is shown in Figure 3.29. Using Harmathy's comprehensive creep model with Dorn's theta method, the following equation can be obtained:



Figure 3.25: Strength of some steels at high temperature. (Lie, 1992)



Figure 3.26: Modulus of elasticity of steel at elevated temperatures. (Anderberg, 1978)



Figure 3.27: Typical creep curve. (Lie, 1992)



Figure 3.28: Creep rate for prestressing (ASTM A421) and mild steel (ASTM A36) - stressed. (Malhotra, 1982).

$$\frac{\delta \epsilon_{cr}}{\delta \theta} = Z \coth^2 \left(\frac{\epsilon_{cr}}{\epsilon_{cro}} \right) \quad (3.24)$$

where: ϵ_{cr} is the creep strain
 Z is the Zener-Hollman constant
 θ is the temperature compensated time,
 ϵ_{cro} is the y axis intercept of secondary creep phase.

3.3.2.4 Thermal Expansion

Thermal expansion of steel can be related to its temperature by a coefficient of expansion, which can be defined as the expansion of a unit length of the steel when it is raised one degree in temperature. The coefficient of thermal expansion is reported to be basically the same for all typical structural steels (Anderberg, 1983). Its value increases with increasing temperature. The thermal expansion of steel is commonly determined by heating steel specimens to various temperatures and measuring the increase in length. Figure 3.30 shows experimental data which apply to most steels. The thermal expansion of steel can be expressed by the following equation:

$$\alpha = (0.4 \times 10^{-8} T_s^2) + (1.2 \times 10^{-5} T_s) - (3 \times 10^{-4}) \quad (3.25)$$

where: T_s is the temperature rise of the steel.

Eurocode 3 Part 10 gives a slightly different version for the thermal expansion:

$$\text{for } T_s < 750^\circ\text{C}, \quad \epsilon_{th} = -2.416 \times 10^{-4} + 1.2 \times 10^{-5} T_s + 0.4 \times 10^{-8} T_s^2 \quad (3.26)$$



Figure 3.29: Harmathy's formulation of creep model. (Becker and Bresler, 1974).



Figure 3.30: Thermal expansion of steel. (Malhotra, 1982).

$$750 < T_s < 860, \quad \varepsilon_{th} = 11 \times 10^{-3} \quad (3.27)$$

$$860 < T_s < 1200, \quad \varepsilon_{th} = -6.2 \times 10^{-3} + 2 \times 10^{-5}T_s \quad (3.28)$$

However, a constant value for the steel coefficient of thermal expansion equal to 1.5×10^{-5} is often used in calculation.

The subject of this research is concerned with the development of an analytical process that models the effect of a fire environment on a reinforced concrete column. The following chapter, Chapter 4, deals with the constitutive model for both concrete and steel.

CHAPTER FOUR

MATERIAL BEHAVIOUR MODELS

4.1 INTRODUCTION

The last two decades have seen a surge of interest in numerical simulation of the behaviour of structures under a combination of thermal and mechanical loading. The development in computer technology as well as the difficulties encountered when experimenting with such structures has encouraged this trend. However, the success of a numerical simulation depends primarily on two main factors namely the reliability of the material model used and its numerical implementation as suggested by Khennane and Baker (1993).

Development of a reliable material model is a difficult task. This is especially so when the material in question experiences cracking, creep and shrinkage, elasto-plastic deformations, thermal expansion, transient strain, and degradation of the material properties as the temperature increases. Concrete is such a material and the difficulties encountered when modelling its response at elevated temperatures have previously been acknowledged (Anderberg and Thelandersson, 1976 and Khennane and Baker, 1993).

There are few publications relating to material models for the behaviour of concrete at elevated temperatures. The models use steady state, transient state and mixed data and have different degrees of sophistication. Schneider (1988) concluded that transient state models correspond largely to fire situations and that

concrete models should consider transient creep or at least the appropriate strain effects. However, there are still debates as to whether concrete exhibits transient strain in addition to classical creep strain and whether the effects of transient strain ought to be included in any material models used to predict the structural response. This is clearly shown in the different constitutive models developed by Anderberg and Thelandersson (1976), Schneider (1986) and Lie and Chabot (1990); which are the object of discussion in this chapter.

This chapter discusses the constitutive models formulated by various researchers. The calculated response using each model for a reinforced concrete column will then be compared in later chapters. For convenience, concrete and steel will be covered separately.

4.2 CONSTITUTIVE MODEL FOR CONCRETE

Following the availability of the total deformation test, a number of workers have attempted limited descriptions for concrete in compression subject to high temperature exposure. The approach generally used is by an extension of procedures used at normal or slightly elevated temperatures when cracking is insignificant and behaviour may be assumed to be linear.

Anderberg and Thelandersson (1976) first presented a computer oriented constitutive model for concrete in compression applied at transient temperatures based on the concept that the total strain ϵ_{tot} can be decomposed into four strain components namely the free thermal movement, instantaneous strain due to stress, creep and a correction term included to take account of the additional strain that occurs during temperature change. The constitutive model is given by:

$$\epsilon_{\text{tot}} = \epsilon_{\text{th}}(T) + \epsilon_{\text{cr}}(\sigma, T, t) + \epsilon_{\sigma}(\sigma, \bar{\sigma}, T) + \epsilon_{\text{tr}}(\sigma, T) \quad (4.1)$$

where:

ϵ_{th} is the thermal strain, including shrinkage, measured in specimens under variable temperature,

ϵ_{cr} is the creep strain or time dependent strain measured under constant stress and constant stabilised temperature,

ϵ_{σ} is the instantaneous, stress related strain, based on stress-strain relations obtained under constant stabilised temperature,

ϵ_{tr} is the transient strain accounting for the effect of temperature increase under stress, derived from tests under constant stress and variable temperature,

σ is the stress,

$\bar{\sigma}$ is the stress history,

t is the time,

T is the temperature.

Schneider (1986) then developed a similar general constitutive model for concrete under transient temperature conditions with the total strain being described by three components, namely the thermal strain, the instantaneous stress-related strain and the transient creep strain. The total strain is being described by the transient creep test method with the individual strains determined with respect to the material behaviour under transient conditions. The equation for the constitutive model is given by:

$$\epsilon_{\text{tot}} = \epsilon_{\text{th}}(T) + \epsilon_{\sigma}(\sigma, T) + \epsilon_{\text{tr,cr}}(\sigma, T) \quad (4.2)$$

where: $\epsilon_{tr,cr}$ is the strain increments that occur under rapid heating and drying of loaded concrete, known as transient creep.

The constitutive models described above have all been based on transient temperature conditions. However, Lie and Chabot (1990) proposed a model that omitted the effect of the transient strain component in the material model used to predict structural response in that the stress-related strain i.e. the strain determining the stress is obtained by adding the different strain components as follows:

$$\epsilon_{\sigma} = \epsilon_{axial} + \epsilon_{bending} - \epsilon_{thermal} \quad (4.3)$$

The following section describes the models used in this project for the respective strain components for concrete.

4.2.1 INSTANTANEOUS STRESS-RELATED STRAIN

The formulation of the stress-strain section of the constitutive model has been a subject of debate with regards to the most reliable approach for it (Purkiss, 1995). Anderberg and Thelandersson (1976) carried out the original research in this field. However, their analysis has been questioned by Schneider (1986 and 1988). The following section discusses the individual formulation of the stress-strain model. A model proposed by Khennane and Baker (1993) that uses the theory of plasticity to describe the non-linear response of concrete structures is also discussed. However, due to its late publication, the effect on the fire performance of a reinforced concrete column as predicted by Khennane and Baker's models will not be compared with others in this thesis.

4.2.1.1 Anderberg and Thelandersson's Model

Anderberg and Thelandersson (1976) calculated the instantaneous stress-related strain based on the concept that at every state a stress-strain relation is valid for the material and the relation at a given time depends on the current temperature and the prehistory of stress. The general description of the stress-strain relation takes the form of an idealised curve that consists of a parabolic branch followed by a linear descending branch as shown in Figure 4.1. The temperature dependence is introduced by varying the various parameters with respect to temperature that determine the diagram.

The boundary conditions of the parabolic curve of Figure 4.1 are determined by the following three equations:

$$\sigma = 0 \text{ when } \epsilon_{\sigma} = 0 \quad (4.4)$$

$$\sigma = \sigma_{\max} \text{ when } \epsilon_{\sigma} = \epsilon_{\max} \quad (4.5)$$

$$\frac{\partial \sigma}{\partial \epsilon_{\sigma}} = 0 \text{ when } \epsilon_{\sigma} = \epsilon_{\max} \quad (4.6)$$

where: σ_{\max} is the ultimate stress at current temperature

ϵ_{\max} is the value of strain at ultimate stress for current temperature

The equation for the parabolic branch obtained from these boundary conditions is as follows:

$$\sigma = \sigma_{\max} \frac{\epsilon_{\sigma}}{\epsilon_{\max}} \left(2 - \frac{\epsilon_{\sigma}}{\epsilon_{\max}} \right) \quad \text{for } 0 \leq \epsilon_{\sigma} \leq \epsilon_1 \quad (4.7)$$

where: ϵ_1 is the strain at transition between the parabolic branch and the linear descending branch such that $\epsilon_1 \geq \epsilon_{\max}$.

The initial elastic modulus E_0 is obtained from equation (4.7):

$$E_0 = 2 \frac{\sigma_{\max}}{\epsilon_{\max}} \quad (4.8)$$

The linear descending portion of the stress-strain envelope in compression is given by:

$$\sigma = \epsilon_{\max} E^* + \sigma_{\max} \left(1 - \frac{E^*}{E_0} \right)^2 \quad (4.9)$$

where: E^* is the slope of the descending branch which is negative.

The transition point ϵ_1 between the parabolic branch and descending portion is obtained from:

$$\epsilon_1 = \epsilon_{\max} \left(1 - \frac{E^*}{E_0} \right) \quad (4.10)$$

Anderberg and Thelandersson (1976) assumed E^* as independent of temperature based on Anderberg (1976) with E^* given a constant value of -880 N/mm^2 . σ_{\max} is assumed to be a unique function of temperature and the influence of prehistories of stress may be neglected.

The ultimate strain is stress history and temperature dependent. Anderberg and Thelandersson (1976) proposed a theoretical quantification of the stress history dependence of ϵ_{\max} with increasing temperature which is used as follows:

$$\epsilon_{\max} = \max (\epsilon_{\max,0}, \bar{\epsilon}_{\max} - \epsilon_{\text{tr}}) \quad (4.11)$$

where: compressive strains are positive

$\epsilon_{\max,0}$ is the value of strain corresponding to maximum stress at ambient conditions

$\bar{\epsilon}_{\max}$ is the temperature dependent maximum strain measured on specimens unloaded during heating

ϵ_{tr} is the transient strain which represents the stress dependent component of strain.

Figure 4.2 shows a graphical interpretation of equation (4.11) for a typical variation of ϵ_{\max} . The figure illustrates that the maximum strain due to a prehistory of stress is always less than or equal to $\bar{\epsilon}_{\max}$ but not reduced to a value less than $\epsilon_{\max,0}$.



Figure 4.1: General description of the stress-strain relation used in the material model. (Anderberg and Thelandersson, 1976).



Figure 4.2: Theoretical model of stress history dependence of concrete maximum strain. (Anderberg and Thelandersson, 1976).

4.2.1.2 Schneider's Model

Schneider (1988) expressed the stress-related strain part of the constitutive model based on the stress-strain relationship as follows:

$$\varepsilon_{\sigma} = \varepsilon_e + \varepsilon_p \quad (4.12)$$

where: ε_e is the elastic strain
 ε_p is the plastic strain due to stresses beyond half the concrete strength limit

A compliance function from Bažant (1982) that accounts for both strain elements in equation (4.12) was adopted that takes the form:

$$J(T, \sigma) = \frac{(1 + \kappa)}{E_c} \quad (4.13)$$

where: $J(T, \sigma)$ is the unit stress compliance function
 κ is a parameter allowing for non-linear stress-strain behaviour for stresses above half the concrete strength
 E_c the temperature dependent modulus of elasticity

The theoretical stress-strain relationship from Popovic (1973) is used to derive the expression for E_c which is given as:

$$E_c = \frac{\sigma_{\max}}{\varepsilon_{\max}} \times \frac{n(n-1) \left[1 - \left(\frac{\varepsilon}{\varepsilon_{\max}} \right)^n \right]}{\left[(n-1) + \left(\frac{\varepsilon}{\varepsilon_{\max}} \right)^n \right]^2} g \quad (4.14)$$

where: ε is the strain at current temperature

σ_{\max} is the value of stress at the point of maximum stress at current temperature

ε_{\max} is the value of strain corresponding to maximum stress in a stress-strain diagram at current temperature

g is a function that allows the increase of elasticity due to the external loads given by:

$$g = 1 + \left(\frac{\sigma}{\sigma_{\max,0}} \right) \left(\frac{T_c - 20}{100} \right) \quad (4.15)$$

where:

$\frac{\sigma}{\sigma_{\max,0}}$ is the ratio of the concrete stress at current temperature T to

the ambient strength

T_c is the concrete temperature ($^{\circ}\text{C}$)

An empirical boundary limit for the value of g is imposed such that $\sigma/\sigma_{\max,0} = 0.3$ is considered when $\sigma/\sigma_{\max,0} > 0.3$.

Schneider expressed κ as follows:

$$\kappa = \frac{1}{n-1} \left(\frac{\varepsilon}{\varepsilon_{\max}} \right)^n \quad (4.16)$$

where: $n = 3.0$ for normal concrete.

The initial tangent modulus, E_0 of the stress-strain curve is obtained by putting $\varepsilon \rightarrow 0$:

$$E_0 = \left(\frac{\sigma_{\max}}{\varepsilon_{\max}} \right) \left(\frac{n}{n-1} \right) g \quad (4.17)$$

4.2.1.3 Khennane and Baker's Model

Khennane and Baker (1993) termed the stress-related strain part of the constitutive model as instantaneous mechanical strain consisting of elastic strain rate, $\dot{\varepsilon}_e$ and plastic strain rate, $\dot{\varepsilon}_p$ where the overdot denotes derivative with respect to time. The calculation of the instantaneous mechanical strain is based on the same concept as that used by Anderberg and Thelandersson (1976); that is at every state of stress, a stress-strain relationship is valid.

Anderberg and Thelandersson (1976) described the stress-strain relation by assuming the stress-strain curves obtained under different but constant temperatures consist of parabolas. However, Khennane and Baker formulated the stress-strain relation at various constant temperatures based on the uniaxial stress-strain relation proposed by Lin et. al (1987). According to the formulation, the non-linear part of the stress-strain curve is assumed to be a quarter of an ellipse, see Figure 4.3 whose equation is given by:

$$\frac{(\sigma - f_{yT})^2}{(\sigma_{\max,T} - f_{yT})^2} + \frac{(\Delta p - \epsilon_p)^2}{\Delta p^2} = 1 \quad \text{for } f_{yT} < \sigma \leq \sigma_{\max,T} \quad (4.18)$$

where: T is the current temperature
 σ is the current stress
 $\sigma_{\max,T}$ is the ultimate compressive strength at current temperature
 f_{yT} is the yield strength at current temperature identified as the point where the stress-strain curve deviates from linearity
 ϵ_p is the plastic strain
 Δp is the horizontal offset of the peak stress from the initial elastic tangent.

where:
$$\Delta p = \epsilon_{\max,T} - \frac{\sigma_{\max,T}}{E_T} \quad (4.19)$$

where: $\epsilon_{\max,T}$ is the ultimate strain at current temperature
 E_T is the current elastic modulus

From Hooke's Law, the elastic strain ϵ_e is written as:

$$\epsilon_e = \frac{\sigma}{E_T} \quad (4.20)$$

where: E_T is the elastic modulus at temperature T.



Figure 4.3: Elliptical idealisation of the non-linear parts of the uniaxial stress strain curves. (after Khennane and Baker, 1993).

:

The elastic strain rate is obtained by differentiating equation (4.20) with respect to time and where the overdot denotes derivative with respect to time:

$$\dot{\epsilon}_e = C_e \dot{\sigma} + \dot{C}_e \sigma \quad (4.21)$$

where: C_e is the elastic compliance parameter given by:

$$C_e = \frac{1}{E} \quad (4.22)$$

and $\dot{C}_e = -\frac{\dot{E}}{E^2}$ (4.23)

The plastic strain ϵ_p occurs only once the stress has exceeded the yield strength and is obtained from (4.18) as:

$$\epsilon_p = \Delta p \left\{ 1.0 - \left[1.0 - \frac{(\sigma - f_{yT})^2}{(\sigma_{\max, T} - f_{yT})^2} \right]^{0.5} \right\} \quad (4.24)$$

The plastic strain rate is obtained by differentiating equation (4.24) and is written as:

$$\dot{\epsilon}_p = C_p \dot{\sigma} + \dot{C}_p \sigma \quad (4.25)$$

where: C_p is the plastic compliance parameter given by:

$$C_p = \frac{1}{H} \quad (4.26)$$

and $\dot{\epsilon}_p = -\frac{\dot{H}}{H^2}$ (4.27)

where: H is the hardening parameter obtained from (4.18) as:

$$H = \frac{(\sigma_{\max, T} - f_{yT})^2}{\Delta p^2} \times \frac{\Delta p - \epsilon_p}{(\sigma - f_{yT})} \quad (4.28)$$

where both the expressions for ϵ_p and H depend on the current stress σ .

4.2.1.4 Baldwin and North on Furumura

This section is largely based on Weeks (1985) that described the instantaneous stress-strain relationship for concrete under compression at high temperatures developed by Baldwin and North (1973) on Furumura that takes the form:

$$\frac{\sigma}{\sigma_{\max}} = f\left(\frac{\epsilon}{\epsilon_{\max}}\right) \quad (4.29)$$

where: f is a function independent of temperature

σ_{\max} is the value of the maximum stress for the temperature

ϵ_{\max} is the value of strain at the point of maximum stress for the temperature

On plotting the normalised stress against normalised strain, Baldwin and North described the stress-strain relationship for any temperature by the following expression:

$$\frac{\sigma}{\sigma_{\max}} = \frac{\varepsilon}{\varepsilon_{\max}} \exp\left(1 - \frac{\varepsilon}{\varepsilon_{\max}}\right) \quad (4.30)$$

The expression shows that the stress-strain curve for concrete at high temperatures can thus be derived from the stress-strain relationship at room temperature together with the location of the maximum of the stress-strain curve at high temperatures.

The required tangent modulus of elasticity is then equal to the gradient of the stress-strain curve for any given value of strain and can be found from the differentiation of the relationship with respect to strain.

$$\frac{d\sigma}{d\varepsilon} = E_C = \frac{\sigma_{\max}}{\varepsilon_{\max}} \left[\exp\left(1 - \frac{\varepsilon}{\varepsilon_{\max}}\right) \left(1 - \frac{\varepsilon}{\varepsilon_{\max}}\right) \right] \quad (4.31)$$

For the stress-strain relation in tension, the slope of the relation is equal to the initial slope of the stress-strain relation for compression. The concrete element is assumed to fail in tension once the ultimate tensile stress has been exceeded. This idealised stress-strain relationship in tensile zone is shown in Figure 4.4 and is essentially similar to that established by Anderberg (1976). From equation (4.31) the initial tangent modulus of the stress-strain relation under compression E_0 or the slope of the stress-strain relation under tension is given by:

$$E_0 = \frac{\sigma_{\max}}{\epsilon_{\max}} \exp(1) \quad (4.32)$$

However, the importance of the tensile properties of concrete is relatively small in this research since tensile stress in concrete contributes relatively insignificantly to the total load bearing capacity of a reinforced concrete.

Unloading behaviour of the concrete in the stress-strain relation is idealised as a straight line with a slope equal to the instantaneous initial modulus as shown in Figure 4.4. The stress-strain follows the linear behaviour when load is reapplied until the original curve is reached. With further increase in load the relation follows the curve that would have been described if unloading had not taken place. Actual unloading-reloading behaviour of concrete is characterised by a hysteresis loop. However, tests have shown that with reloading the relation does return to the curve that would have been described had unloading and subsequent reloading not taken place.

If σ_i and ϵ_i are the current stress and strain respectively, and σ_{i-1} and ϵ_{i-1} are the stress and strain from the previous time step, where ϵ_i is less than ϵ_{i-1} , then the current state of stress σ_i is given by:

$$\sigma_i = \sigma_{i-1} - E_0 (\epsilon_{i-1} - \epsilon_i) \quad (4.33)$$

4.2.2 TRANSIENT STRAIN

The following section discusses the transient strain component formulated by Anderberg and Thelandersson (1976) and Schneider (1988). Anderberg and

Thelandersson (1976) proposed that this strain component accounts for the effect of strain increase under increasing temperature. Schneider (1988) proposed a slightly different notation, subsequently named as transient creep, that comprises not only the creep strains which are due to rapid drying of capillary water but also accounts for the total loss of gel water and chemically bounded water.

4.2.2.1 Anderberg and Thelandersson's Model

Anderberg and Thelandersson (1976) proposed that:

$$\epsilon_{tr} = \frac{\sigma g(T)}{\sigma_{max,0}} \quad (4.34)$$

where: $g(T)$ is a function of temperature
 σ is the applied stress
 $\sigma_{max,0}$ is the compressive strength at ambient conditions.

Anderberg and Thelandersson (1976) suggested that $g(T)$ is approximately proportional to ϵ_{th} i.e. the temperature dependence of transient strain is very similar to that of thermal strain as shown in Figure 4.5. Hence:

$$\epsilon_{tr} = -k_2 \frac{\sigma}{\sigma_{max,0}} \epsilon_{th} \quad \text{for } 20^{\circ}\text{C} \leq T < 500^{\circ}\text{C} \quad (4.35)$$

where: k_2 is a dimensionless constant varying with cement type.

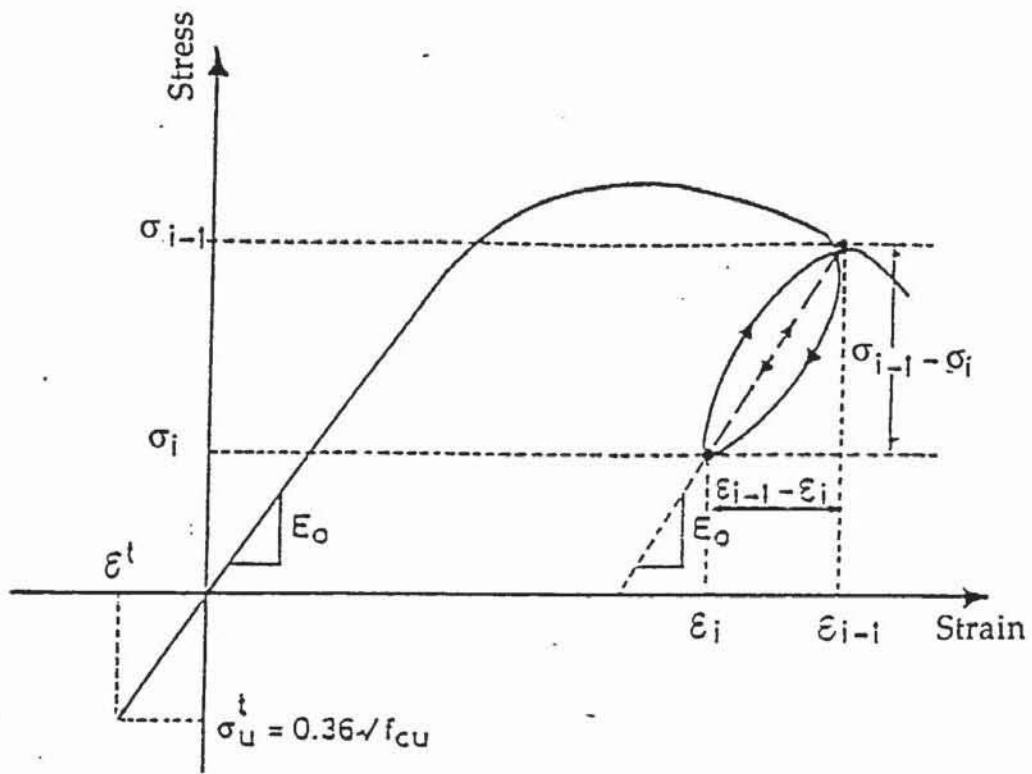


Figure 4.4: Idealised stress-strain relation showing tensile zone and unloading characteristics.



Figure 4.5: $\frac{\epsilon_v}{\left(\frac{\sigma}{\sigma_{\max,p}}\right)}$ plotted against thermal strain ϵ_{th} .

(Anderberg and Thelandersson, 1976).

Anderberg and Thelandersson (1976) found by means of linear regression that a value of k_2 equal to 2.35 best describes the quartzite concrete used in their tests. From investigation of the strain component ϵ_{tr} against test series by Weigler and Fisher (1967) and Schneider (1976), Anderberg and Thelandersson demonstrated that good agreement was obtained if k_2 was given values of 2.0 and 1.8 respectively. The variation in the factor k_2 is assumed to be due to the different mix proportions used in the test series. A value of k_2 equal to 2.35 is used in this research.

For temperature above 500°C there is an accelerated effect on transient strains. Anderberg (1976) proposed the following expression for the incremental change in ϵ_{tr} :

$$\Delta \epsilon_{tr} = 0.1 \times 10^{-3} \frac{\Delta T \sigma}{\sigma_{max,o}} \quad \text{for } 500^\circ\text{C} \leq T < 800^\circ\text{C} \quad (4.36)$$

where: σ is the stress from the previous time increment,
 $\sigma_{max,o}$ is the compressive strength at ambient conditions.

4.2.2.2 Schneider's Model

Schneider (1988) named the strain components that occurs under rapid heating and drying of loaded concrete as transient creep which accounts for the total loss of gel and chemically bounded water apart from the creep strain due to rapid drying of capillary water. Schneider used a model based on the classic analysis of creep data and adopted an important simplification in that, for creep in a fire, the duration of couple of hours exposure is short compared with the age of concrete.

Hence, the strain components would be time invariant within a period of a few hours being the duration of exposure.

Schneider (1988) proposed a compliance function that accounts for transient creep strain component as:

$$J(T, \sigma) = \frac{\Phi}{E_c} \quad (4.37)$$

where: Φ is the creep function given by:

$$\Phi = g\phi + \left(\frac{\sigma}{\sigma_{\max,0}} \right) \left(\frac{T_c - 20}{100} \right) \quad (4.38)$$

where: ϕ being given by:

$$\phi = C_1 \tanh \gamma_w (T_c - 20) + C_2 \tanh \gamma_o (T_c - T_g) + C_3 \quad (4.39)$$

where: γ_w accounts for the moisture content defined by:

$$\gamma_w = 0.001 \times (0.3w + 2.2) \quad (4.40)$$

where: w is the moisture content in % by weight.

E_c and g are given by equation (4.14) and (4.15) respectively.

Table 4.1 gives the values of C_1 , C_2 , C_3 , T_g and γ_0 as proposed by Schneider.

Parameter	Dimension	Quartzite Concrete	Limestone Concrete	Lightweight Concrete
C_1	1	2.60	2.60	2.60
C_2	1	1.40	2.40	3.00
C_3	1	1.40	2.40	3.00
γ_0	$^{\circ}\text{C}^{-1}$	7.5×10^{-3}	7.5×10^{-3}	7.5×10^{-3}
T_g	$^{\circ}\text{C}$	700	650	600

Table 4.1: Parameters for transient creep functions ϕ of structural concretes
(Schneider, 1988)

Schneider (1988) also argued that Anderberg and Thelandersson's (1976) presentation of transient creep strain into two separate components namely transient strain, that accounts for the effects of the strain increase under increasing temperatures and creep strain, that comprises drying creep and basic creep, does not yield any advantages as creep strain is small with respect to the fire situation.

4.2.3 THERMAL STRAIN

Thermal strain during heating is a simple function of temperature, directly given by the thermal expansion curve. The thermal expansion depends on the initial water content since drying shrinkage is included. However, the shrinkage will be modelled separately due to the irrecoverability of the shrinkage strain and due to

the possibility that the structural response program may be used to determine the residual strength of a reinforced concrete column.

The thermal expansion curve, including shrinkage, for quartzite aggregate derived by Anderberg (1976) is shown in Figure 4.6 which indicates that the thermal strain is considerably non-linear with respect to temperature. Forsén (1982) found that the experimental curve established by Anderberg may be represented by the following two fourth degree polynomials:

$$\epsilon_{th} = - (a\tau^4 + b\tau^3 + c\tau^2 + d\tau + e) \quad \text{for } \tau \leq 6 \quad (4.41)$$

$$\epsilon_{th} = - (a'\tau^4 + b'\tau^3 + c'\tau^2 + d'\tau + e') \quad \text{for } \tau > 6 \quad (4.42)$$

where: $\tau = T / 100$ (°C)

$$a = 0.02837 \quad a' = 0.02102$$

$$b = -0.2447 \quad b' = -0.4972$$

$$c = 0.7376 \quad c' = 3.791$$

$$d = 0.3229 \quad d' = -8.265$$

$$e = 0.09218 \quad e' = 5.561$$

Thermal strain is a negative strain component since tensile strains (expansion) are taken as negative in this research.

4.2.4 CREEP STRAIN

Anderberg and Thelandersson (1976) proposed the variation of creep strains with time as a power function through a mathematical formulation as follows:

$$\epsilon_{cr} = \left[\frac{\sigma}{\sigma_{\max(T)}} \right] \left(\frac{t}{t_r} \right)^p \beta_0 e^{k_1(T-20)} \quad (4.43)$$

where:

$$\beta_0 = +0.53 \times 10^{-3}$$

$$k_1 = 3.04 \times 10^{-3} \text{ } ^\circ\text{C}^{-1}$$

σ is the applied stress

$\sigma_{\max(T)}$ is the maximum compressive stress for temperature T

t is the time

t_r is the reference time = 3 hours

p is a dimensionless constant taken to be 0.5.

Equation (4.43) expresses the creep versus time for any given combination of temperature and stress. For variable stress and temperature, the strain hardening principle is used to describe the creep development. Throughout a time history the creep is calculated incrementally with both stress and temperature assumed to be constant during a time increment, see Figure 4.7.

The principle of strain hardening is formulated according to the following procedure. Initially, it is assumed that the stress σ_i , the temperature T_i and the accumulated creep strain $\epsilon_{cr,i}$ are known at the time t_i . At a subsequent time $t_{i+1} = t_i + \Delta t_i$, the accumulated creep strain $\epsilon_{cr,i+1}$ has to be determined. If, at time t_{i+1} , the temperature T_{i+1} and the stress σ_{i+1} are known, the material time $t_{m,i}$ can be calculated that would give a creep strain equal to the accumulated value $\epsilon_{cr,i}$ corresponding to stress σ_{i+1} and temperature T_{i+1} . Using equation (4.43) to solve for $t_{m,i}$ explicitly and rearranging yields the following expression:



Figure 4.6: Thermal expansion of quartz aggregate concrete. (Anderberg, 1976).

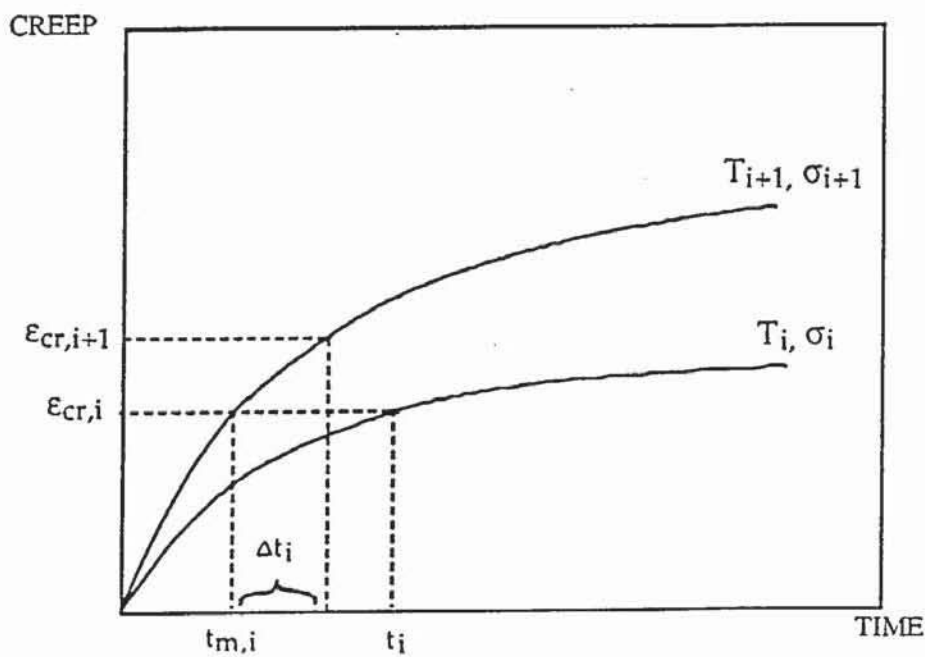


Figure 4.7: Strain hardening principle for temperature dependent concrete creep strain.

$$t_{m,i} = t_r \left[\frac{\epsilon_{cr,i}}{\beta_0 \left[\frac{\sigma_{i+1}}{\sigma_{\max}(T_{i+1})} \right] e^{k_1(T_{i+1}-20)}} \right]^{\frac{1}{p}} \quad (4.44)$$

The expression for the creep strain is obtained by adding the actual time increment Δt_i to the material time $t_{m,i}$ as follows:

$$\epsilon_{cr,i+1} = \beta_0 \left[\frac{\sigma_{i+1}}{\sigma_{\max}(T_{i+1})} \right] \left[\frac{(t_{m,i} + \Delta t_i)}{t_r} \right]^p e^{k_1(T_{i+1}-20)} \quad (4.45)$$

However, if the stress σ_{i+1} is unknown when the creep strain $\epsilon_{cr,i+1}$ is evaluated, a simplification is made with sufficient accuracy using the stress σ_i from the previous time step t_i . It should be noted that the true time is not explicitly used in the model, apart from the very first time when accumulated creep strain is zero due to the use of material time at each time step. Significant analytical errors caused by this simplification may be avoided provided the time increments are set sufficiently small when a rapid change in stress is expected. No creep recovery is accounted for in the above mentioned formulation.

4.2.5 SHRINKAGE STRAIN

Shrinkage strain in concrete is due to the loss of moisture and this loss increases when the temperature increases up to 100°C where the free water evaporates. The shrinkage model described here is taken from Becker and Bresler (1974). The

maximum shrinkage potential is set to 0.001 mm/mm at 100°C. All shrinkage is assumed to have occurred at temperatures above 100°C.

The basic shrinkage model is:

$$\frac{d\epsilon_{shr}}{dt} = a(T) (\epsilon_{\infty}(T) - \epsilon_{shr}) \quad (4.46)$$

Where: ϵ_{shr} is the current cumulative shrinkage strain

$\epsilon_{\infty}(T)$ is the total potential shrinkage

$a(T)$ is the shrinkage rate constant

$$a(T_i) = (0.001 + ((T_i - 20) \times 0.0125)^2) \quad (4.47)$$

$$\epsilon_{\infty}(T_i) = 0.0005 \times (1 + (T_i - 20) \times 0.0125) \quad (4.48)$$

$$\partial\epsilon_i^{shr} = a(T_i)(\epsilon_{\infty}(T_i) - \epsilon_{shr}) \Delta t_i \quad (4.49)$$

where: $\partial\epsilon_i^{shr}$ is the incremental shrinkage strain

Δt is the time step.

The shrinkage strain within a given time step is calculated from the given equation. The total amount of shrinkage occurring within any time step cannot cause the cumulative shrinkage strain to exceed the total potential shrinkage for the temperature at that time step. The equation holds for the range of temperature 20 to 100°C.

4.3 CONSTITUTIVE MODEL FOR STEEL

It is generally agreed that the deformation process of steel at elevated temperatures can be described by three strain components namely thermal strain, instantaneous stress-related strain and creep strain. Thus the constitutive equation for steel is given by:

$$\varepsilon = \varepsilon_{th} (T) + \varepsilon_{\sigma} (T, \sigma) + \varepsilon_{cr} (t, T, \sigma) \quad (4.50)$$

where: ε_{th} is the thermal strain
 ε_{σ} is the instantaneous stress-related strain based on stress-strain relationship obtained under constant, stabilised temperature
 ε_{cr} is the creep strain or time dependent strain.

The following section described the models used in this project for the respective strain components for steel based largely on Forsén (1982). Unlike concrete, steel does not undergo transient strain.

4.3.1 STRESS-STRAIN MODEL

An analytical description of the stress-strain curve as a function of temperature can be made in different ways as illustrated in Figure 4.8 and Figure 4.9. In Figure 4.8 the curve is approximated by two straight lines as used in FIRES-RC and CONFIRE or can be refined as shown in Figure 4.9 where an elliptic branch is placed between the straight lines.

Forsén (1982) described the temperature dependent instantaneous stress-strain law for the reinforcing steel, adopted in this research, based on a bi-linear stress-strain envelope following Becker and Bresler (1974). The envelope, shown in Figure 4.10, can be determined using three parameters namely the elastic modulus $E_s(T)$, the yield stress $f_y(T)$ and the strain hardening modulus $E^*(T)$ which are all temperature dependent. Numerical values for these parameters are presented in Anderberg (1976). The model adopted also includes the unloading path, determined by the current inelastic strain ϵ_0 and the temperature dependent initial elastic modulus E_s .

An envelope for the stress-strain relationship is obtained by means of two parallel lines with a slope of E^* for the upper and lower bounds as follows:

- upper bound: $\sigma_u = f_y + E^*(\epsilon - \epsilon_y)$ (4.51)

- lower bound: $\sigma_l = -f_y + E^*(\epsilon + \epsilon_y)$ (4.52)

where: ϵ_y is the temperature dependent yield strain = f_y / E_s

A third line intercepts the axis at ϵ_0 with a slope of E_s :

- $\sigma_E = E_s(\epsilon - \epsilon_0)$ (4.53)

where:

ϵ_0 is the calculated using the stress-strain from previous time step:

$$\epsilon_0 \text{ for } i = \epsilon_{i-1} - \sigma_{1-i} / E_s \quad (4.54)$$

It can be seen from Figure 4.10 that the stress corresponding to the current strain

$\epsilon_{\sigma} = \epsilon_i$ and the inelastic strain ϵ_o , increases with further loading in accordance with the modulus E_s until the upper bound is reached. Along the upper bound, the tangent modulus is reduced to E^* the strain hardening modulus which is taken equal to $E_s/20$ for increasing ϵ_{σ} . Failure of the steel is assumed to occur when the steel ruptures at a value of stress related strain equal to $10\epsilon_y$. It is assumed that the stress-strain relation in compression is identical to that in tension.

The state of stress is then determined from the statement:

if $\sigma_E > \sigma_u$ then $\sigma = \sigma_u$
 or if $\sigma_E < \sigma_1$ then $\sigma = \sigma_1$
 else $\sigma = \sigma_E$.

4.3.2 THERMAL STRAIN MODEL

The thermal strain is a function of the temperature dependent coefficient of thermal expansion, α_s and the temperature of the element. Forsén (1982) suggested that within a normal temperature range i.e. at temperatures not much higher than ambient, a constant value of $\alpha_s = 15.0 \times 10^{-6} \text{ } ^\circ\text{C}^{-1}$ is often used in calculation. However, at elevated temperatures, α_s has higher values. Anderberg (1976) presented the following values for the steel type $K_S40 \phi 10$:

$$\alpha_s (20^\circ\text{C}) = 12.0 \times 10^{-6} \text{ } ^\circ\text{C}^{-1} \quad (4.55)$$

$$\alpha_s (800^\circ\text{C}) = 20.0 \times 10^{-6} \text{ } ^\circ\text{C}^{-1} \quad (4.56)$$



Figure 4.8: Simplified model of the stress-strain curve for steel (used in CONFIRE). (Anderberg, 1983).



Figure 4.9: Refined model of stress-strain curve for steel. (Anderberg, 1983).

A linear interpolation may be used to determine the value of α_s in the temperature range of 20°C to 800°C.

Determination of the thermal strain of steel is achieved through the application of the expression:

$$\epsilon_{th} = - \int_{20^{\circ}\text{C}}^T \alpha_s(T) dT \quad (4.57)$$

where: α_s is the temperature dependent coefficient of expansion

T is the temperature

ϵ_{th} is a negative strain component (expansion)

or
$$\epsilon_{th} = aT^2 + bT + c \quad (4.58)$$

where: $a = 5.128 \times 10^{-9} \text{ }^{\circ}\text{C}^{-2}$

$b = 1.179 \times 10^{-5} \text{ }^{\circ}\text{C}^{-1}$

$c = 2.379 \times 10^{-4}$

4.3.3 CREEP MODEL

The model for creep in reinforcing steel in most cases is based on the concept put forward by Dorn (1954) that considered the effect of varying temperatures, extended to variable stress by the use of a strain hardening rule. The model for creep adopted in this investigation is similar to that used in FIRES-RC based on Harmathy's Comprehensive Creep Model (1970) with Dorn's Theta Method (1954) for temperature variation. Creep in steel is considered to be a function of the



Aston University

Illustration removed for copyright restrictions

Figure 4.10: Steel stress-strain envelope. (Becker and Bresler, 1974).

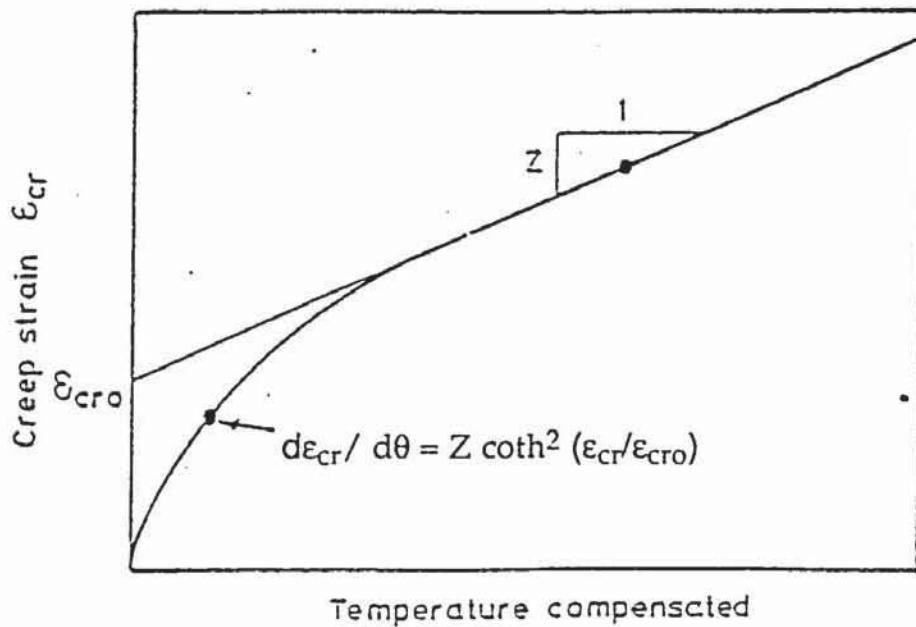


Figure 4.11: Hamathy's formulation of creep model.

current state of strain and is primarily a function of the shear strain and is therefore assumed to be identical in both tension and compression. Only the primary and secondary phases of creep are considered.

Using Harmathy's formulation of creep as shown in Figure 4.11 the creep rate is a constant in the domain of temperature compensated time, hence:

$$\frac{d\varepsilon_{cr}}{d\theta} = Z \quad (4.59)$$

where: ε_{cr} is the creep strain
 θ is the temperature compensated time
 Z is the Zener-Holloman constant.

Harmathy (1970) suggested that this relationship can be extended for use in both primary and secondary phases of creep with the following modification:

$$\frac{d\varepsilon_{cr}}{d\theta} = Z \coth^2 \left(\frac{\varepsilon_{cr}}{\varepsilon_{cro}} \right) \quad (4.60)$$

where: ε_{cro} is the y-axis intercept of the secondary creep phase.

The temperature compensated time, θ , which combines temperature and time into one single parameter, can be calculated from the following expression:

$$\theta = \int_0^T [\exp(-\Delta H/R(T + 273))] dt \quad (4.61)$$

where: ΔH is the activation energy of creep
 R is the gas constant
 T is the temperature in °C.

Harmathy (1974) computational algorithm follows, combining Dorn's Theta Method and a strain hardening rule that allows the computation of the incremental creep strain for varying stress and temperature:

$$\Delta \epsilon_{cr} = Z(\sigma) \Delta \theta (T, \Delta t) \coth^2 \left(\frac{\bar{\epsilon}_{cr}}{\epsilon_{cro}} \right) \quad (4.62)$$

where: $\Delta \theta (T, \Delta t) = \Delta T \times e^{-\frac{\Delta H}{R(T+273)}}$
 $\bar{\epsilon}_{cr}$ is the accumulated creep strain
 $Z(\sigma)$, $\Delta H/R$, ϵ_{cro} are constants varying with steel type.

The steel hardening rule combined in the Harmathy (1974) algorithm for the determination of creep strain in the steel for varying stress and temperature is applied in a way analogous to that for concrete, see Figure 4.7. It is assumed that the stress σ_i , the accumulated creep strain $\epsilon_{cr,i}(\theta_i, \sigma_i)$ are known at the temperature compensated time θ_i . To evaluate the creep increment from θ_i to θ_{i+1} when the stress is σ_{i+1} a fictitious temperature compensated material time $\theta_{i,m}$ is introduced that would give the same creep $\epsilon_{cr,i}$ at the stress σ_{i+1} as at σ_i . The incremental creep strain $\Delta \epsilon_{cr,i}$ is then calculated for the temperature compensated time $\theta_{i+1} =$

$\theta_{i,m} + \Delta\theta_i$ and the total strain is therefore given by $\epsilon_{cr,i+1} = \epsilon_{cr,i} + \Delta\epsilon_{cr,i}$.

The current state of creep strain is given by the sum of the accumulated creep strain and the incremental creep strain for the current time step or the accumulated creep strain for the next time step.

In the first time step where $\bar{\epsilon}_{cr} = 0$, the hyperbolic cotangent term tends towards infinity, thus the creep strain for the first time step is calculated from the following equation as suggested by Harmathy (1967):

$$\Delta\epsilon_{cr} = \left(3Z\theta\epsilon_{cro}^2\right)^{\frac{1}{3}} + Z\theta \quad (4.63)$$

which is a good approximation for strain values of ϵ_{cr} up to $0.5\epsilon_{cro}$. It should be noted that no model of creep recovery is accounted for in the above mentioned model of creep.

Following the discussion of the constitutive models for both concrete and steel, the succeeding chapter, Chapter 5, describes the computer programs used in this project. In order to present the computer programs, the analysis is broken down into two stages, the thermal analysis and structural analysis.

CHAPTER FIVE

DESCRIPTION OF COMPUTER PROGRAMS

5.1 INTRODUCTION

Computer modelling on reinforced concrete columns exposed to fire used in this research separates the thermal and structural responses into two distinct programs. The thermal response for the structural cross sections of the column system is calculated using a modified version of FIRES-T, a computer program for the Fire Response of Structures - Thermal, developed by Becker, Bizri and Bresler (1974). FIRES-T is used to evaluate the temperature distribution histories of general cross sections subjected to fire environments. It is assumed that the longitudinal thermal response is uniform throughout the structural member. Therefore each segment of the column under analysis is subject to the same temperature distributions. The error caused by this assumption is likely to be small and is consistent throughout the research.

The structural response is calculated using a modified version of SAFE-RCC, Structural Analysis of Fire Exposed Reinforced Concrete Columns developed by Weeks (1985). SAFE-RCC is an analytical tool developed to study the fire response of reinforced concrete column subjected to restraint and continuity likely to be experienced in a total structure.

Details of the finite element mesh for each structural cross section are passed directly from FIRES-T to SAFE-RCC to ensure consistent cross sections in both the

thermal and structural analysis. The temperature distribution histories generated by FIRES-T are then used in conjunction with SAFE-RCC together providing an overall capability of predicting the structural response of reinforced concrete column subjected to fires. Figure 5.1 shows the main composition of the computer analysis.

5.2 THERMAL RESPONSE PROGRAM: FIRES-T

FIRES-T evaluates the temperature distribution history of structural cross sections in fire environments by solving the heat balance equation in matrix form using a finite element method coupled with a time step integration. FIRES-T is used in a form essentially as that developed by Becker, Bizri and Bresler (1974) but modified by Weeks (1985) with a substantially different output subroutine to suit the requirements of SAFE-RCC where all the finite element details and results of the thermal analysis are written into a specified file which can be used as input data for the structural analysis program.

The heat flow problem solved by FIRES-T is non-linear due to the temperature dependence of the thermal properties of structural materials and the heat transfer mechanisms associated with fire environments. The non-linearities encountered in the analysis are handled by a local linearisation about a current temperature distribution which then requires the use of an iterative approach within the given time steps.

The fire environment is simulated through the use of a standard International Organisation of Standardisation (ISO) fire which is expressed as a time dependent curve. Convective and radiative mechanisms are used to model the fire boundary

conditions. The finite element mesh employed in FIRES-T can be made of quadrilateral or triangular elements.

The following section on the thermal model and solution procedure is based largely on the documentation of FIRES-T from Becker, Bizri and Bresler (1974) except that a new output subroutine has been compiled to suit the requirements of the structural analysis program.

5.2.1 THERMAL MODEL AND SOLUTION PROCEDURE

The two dimensional heat flow problems are modelled mathematically by the following partial differential equation:

$$\rho C_p \frac{\partial T}{\partial t} = \frac{\partial}{\partial x} \left(\lambda \frac{\partial T}{\partial x} \right) + \frac{\partial}{\partial y} \left(\lambda \frac{\partial T}{\partial y} \right) \quad (5.1)$$

where: x, y are Cartesian co-ordinates,
 ρ is the space dependent density,
 C_p is the temperature and space dependent specific heat,
 λ is the temperature and space dependent isotropic conductivity,
 T is the temperature,
 t is the time.

A finite element, time step integration technique is used in the solution of the above equation which can be simplified by the following statement of heat balance equation:

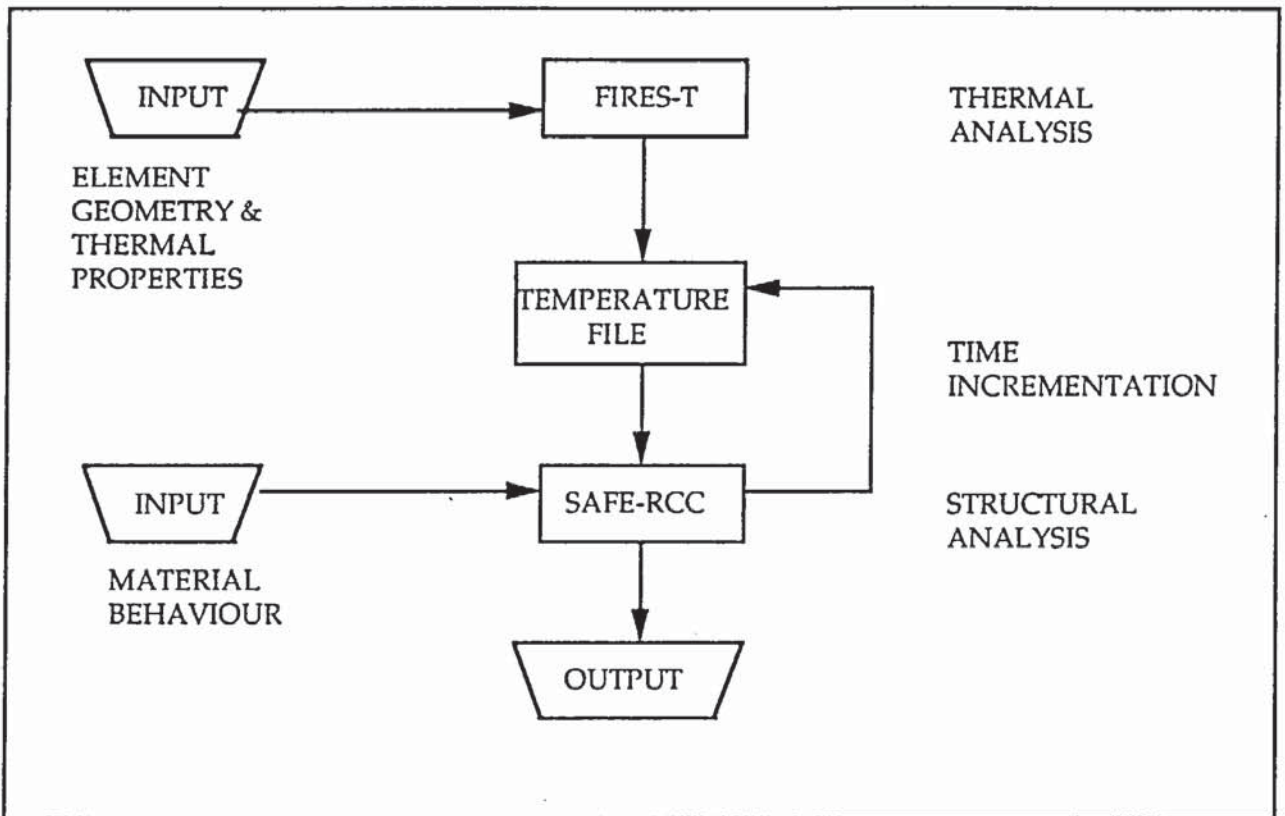


Figure 5.1: Main Composition of the computer analysis

$$\left| \begin{array}{l} \text{Rate at which heat} \\ \text{is stored in elements} \\ \text{adjacent to a node} \end{array} \right| + \left| \begin{array}{l} \text{Rate at which heat} \\ \text{flows from elements} \\ \text{adjacent to a node} \end{array} \right| = \left| \begin{array}{l} \text{Rate at which} \\ \text{external heat} \\ \text{enters a node} \end{array} \right| \quad (5.2)$$

This heat balance equation is given in matrix form by the following equation:

$$\underline{C}(\rho(T), C_p(T)) \dot{\underline{T}} + \underline{K}(\lambda(T)) \underline{T} = \underline{Q}(\underline{T}, F(t)) \quad (5.3)$$

where: \underline{C} is the capacity matrix,
 \underline{K} is the conductivity matrix,
 \underline{Q} is the external heat flow vector,
 \underline{T} is the temperature vector,
 $\dot{\underline{T}}$ is the temperature rate of change vector,
 $\rho(T)$ is the density as a function of temperature,
 $C_p(T)$ is the specific heat as a function of temperature,
 $\lambda(T)$ is the conductivity as a function of temperature,
 $F(t)$ is the external heat source (e.g. standard fire).

5.2.2 CONDUCTIVITY MATRIX K

The terms of the conductivity matrix are associated with the rate of heat flow from the elements adjacent to each node. The conductivity matrix for the system being analysed is assembled from element conductivity matrices, initially condensed from a system of triangular elements with linear temperature distributions. A process of static condensation is used to reduce the system of linear triangles to an element conductivity matrix.

The conductivity matrix of a triangular element with a linear temperature distribution is:

$$k^m = \frac{\lambda(T)}{2l} \begin{vmatrix} e^2 + d^2 & y_k e - x_k d & -y_j e + x_j d \\ y_k^2 + x_k^2 & -y_j y_k - x_j x_k & \\ & & y_j^2 + x_j^2 \end{vmatrix} \quad (5.4)$$

where: x_k, x_j, y_k, y_j, e, d and l are defined in Figure 5.2(a).

A quadrilateral element is constructed from four linear triangles through the addition of a fifth node (see Figure 5.2b). The co-ordinates of this node are specified as the average of the original four nodes which places this node at the centroid of the quadrilateral element. These triangles are assembled into a 5×5 element matrix which is reduced to a 4×4 matrix due to the assumption that there is no external heat flow at node 5. A typical term for the quadrilateral conductivity matrix is given by:

$$K_{i,j} = K_{i,j} - \frac{K_{i,5} K_{j,5}}{K_{5,5}} \quad (5.5)$$

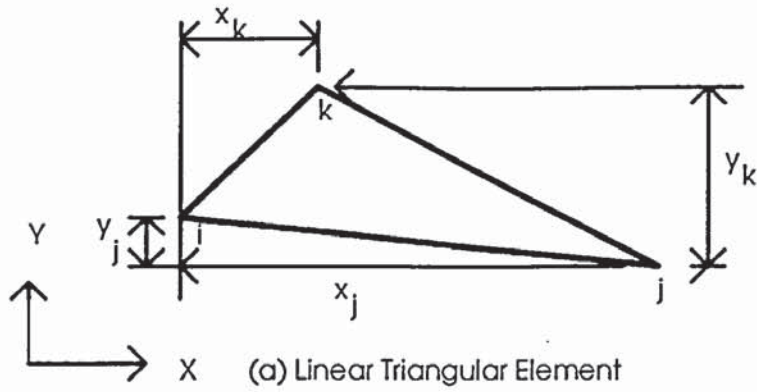
These element conductivity matrices are then assembled into the conductivity matrix for the system, where:

$$\underline{K} = \sum_i K^i \quad (5.6)$$

$$l = x_j y_k - x_k y_j$$

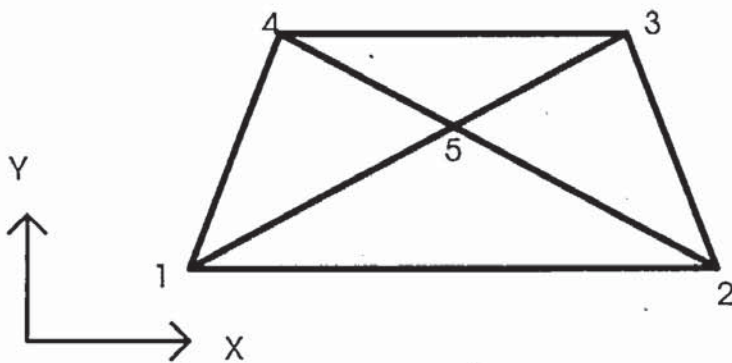
$$d = x_k - x_j$$

$$e = y_j - y_k$$



$$x_5 = \frac{x_1 + x_2 + x_3 + x_4}{4}$$

$$y_5 = \frac{y_1 + y_2 + y_3 + y_4}{4}$$



(b) Quadrilateral Assembly of Four Linear Triangles

Figure 5.2: Quadrilateral finite element

5.2.3 CAPACITY MATRIX C

The heat capacity associated with a node is the rate at which heat is absorbed for a unit rate of change of the temperature of that node. The capacity matrix contains terms that are dependent on the heat capacity $C_p(T)$ and density $\rho(T)$ of the elements immediately adjacent to each node.

The capacity matrix is idealised through a system analogous to the lumping of mass for a dynamic analysis. This lumping is achieved by delineating the volume adjacent to a node by a parameter drawn through the midpoints of element boundaries and the internal nodes previously associated with the conductivity matrix as shown in Figure 5.3.

The heat capacity for an element is given by:

$$C_m = V_m \rho(T) C_p(T) \quad (5.7)$$

where: V_m is the volume of each element which is equal to unit thickness times the area of the element.

Since the areas are a function of the linear triangles associated with an element, the contribution of an element, m , to a particular node i , is given by:

$$C_{m,i} = \rho(T) C_p(T) \frac{(A_j + A_k)}{2} \quad (5.8)$$

where: A_j, A_k are areas of triangles in elements adjacent to node i .

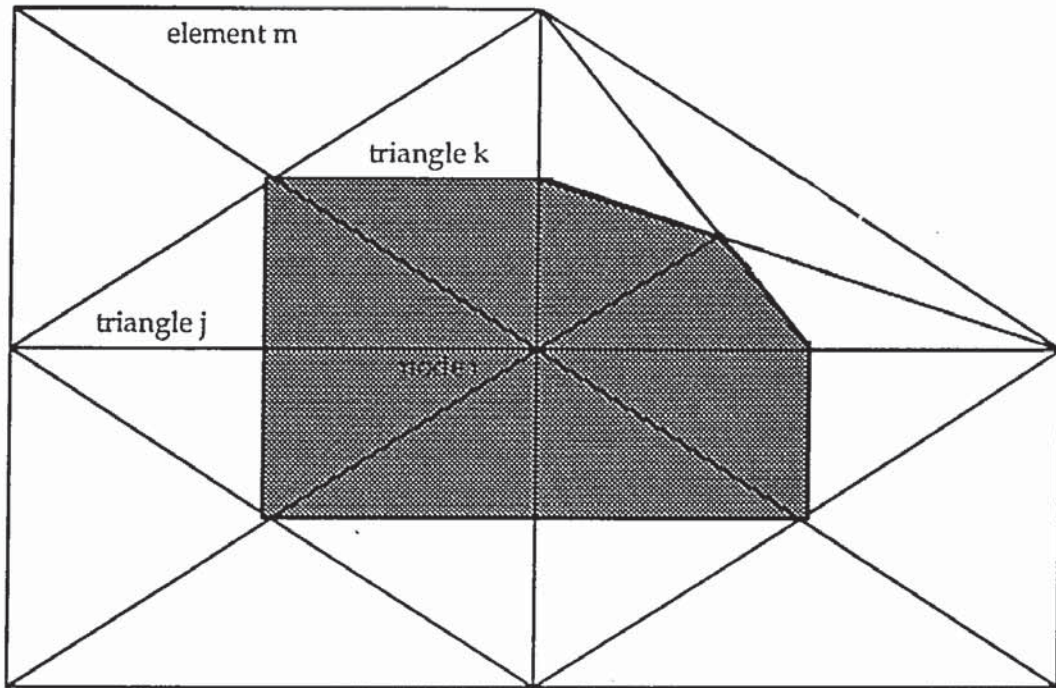


Figure 5.3: Heat Capacity Idealisation

Therefore the heat capacity of a node i is:

$$C_i = \sum^{m'} C_{m,i} \quad (5.9)$$

where: m' is the number of elements adjacent to node i.

The capacity matrix is then given by:

$$\underline{C} = \sum_{i=1}^n C_i \quad (5.10)$$

where: n is the number of nodes.

5.2.4 EXTERNAL HEAT FLOW VECTOR Q

In solving the heat flow problem, either one of two conditions must be known for each node i.e. either the temperature of the node or the external heat flow into the node. The external heat flow is expressed in the following summation:

$$Q = Q_K + Q_E + Q_F \quad (5.11)$$

where: Q_K is a prescribed heat flow,
 Q_E is the resultant of an exothermic reaction within the system,
 Q_F is the heat flow caused by the exposure of the system to an external source.

The basic concern of this program lies with the contribution from Q_F , therefore it is assumed that $Q_E = 0$. Q_K is directly input as data. Q_F is considered to be a function of both convective and radiative mechanisms. The time-temperature relationship for the fire is represented by the function $F(t)$.

The boundary of the system exposed to the fire is assumed to be made up of surfaces of unit thickness connecting adjacent nodes. Therefore the external heat flow over a surface can be represented by:

$$Q_F = l * q(T_s, T_f) \quad (5.12)$$

where: l is the length between adjacent nodes i and j ,
 q is the rate of heat flow per unit area,
 T_s is the average surface temperature = $(T_i + T_j)/2$
 T_f is the temperature of the standard fire $F(t)$.

The heat flow per unit area of the exposed surface can be modelled in two ways either as linear or non-linear heat transfer.

5.2.4.1 Linear Heat Transfer

$$q = h(T') (T_f - T_s) \quad (5.13)$$

where: $h(T')$ is the heat transfer coefficient,
 $T' = (T_f + T_s) / 2$

5.2.4.2 Non-Linear Heat Transfer

$$q = A(T') (T_f - T_s)^{N(T')} + \sum_{i=1}^{rs} V\sigma [a(T_s)\epsilon_f(T_r)\theta_r^4 - \epsilon_s(T_s)\theta_s^4] \quad (5.14)$$

where: $A(T')$ is the convection coefficient,
 $N(T')$ is the convection power factor,
 V is the radiation view factor,
 σ is the Stefan-Boltzman constant,
 $a(T_s)$ is the absorption of the surface,
 $\epsilon_f(T_r)$ is the emissivity radiation source,
 $\epsilon_s(T_s)$ is the surface emissivity,
 θ_r is the absolute temperature of radiation source,
 θ_s is the absolute temperature of surface,
 rs is the number of sources of radiation.

A simplified version of the above formula is achieved through the elimination of the temperature dependence of the controlling parameters and the assumption that the standard fire is the only radiation source. Thus formula (5.14) is reduced to:

$$q = A(T_f - T_s)^N + V\sigma (a\epsilon_f\theta_f^4 - \epsilon_s\theta_s^4) \quad (5.15)$$

where:

ϵ_f is the emissivity of the flame associated with the standard fire,
 θ_f is the absolute temperature of the standard fire.

5.2.5 NUMERICAL SCHEME

The heat flow equation and associated boundary conditions are solved using a finite element method. The technique reduces the differential equation to a system of algebraic equations. Equation (5.3) can now be simplified into:

$$\underline{C}\dot{\underline{T}}_i + \underline{K}\underline{T}_i = \underline{Q} \quad (5.16)$$

where: i represents the i^{th} time step.

Substituting a linear approximation for the temperature rate of change vector:

$$\dot{\underline{T}}_i = \frac{(\underline{T}_i - \underline{T}_{i-1})}{\Delta t} \quad (5.17)$$

where: Δt is the time step interval,

into equation (5.16) gives:

$$\underline{C} \frac{(\underline{T}_i - \underline{T}_{i-1})}{\Delta t} + \underline{K}\underline{T}_i = \underline{Q} \quad (5.18)$$

Defining two new matrices as the modified conductivity matrix and the modified external heat flow vector respectively as:

$$\underline{K}^* = \underline{K} + \frac{\underline{C}}{\Delta t} \quad (5.19)$$

and:

$$\underline{Q}^* = \underline{Q} + \frac{\underline{C}\underline{T}_{i-1}}{\Delta t} \quad (5.20)$$

the solution to equation (5.16) is from the solution of the following set of linear equations:

$$\underline{K}^*\underline{T}_i = \underline{Q}^* \quad (5.21)$$

It should be noted that \underline{K}^* , \underline{Q}^* , \underline{K} , \underline{C} and \underline{Q} are all functions of \underline{T}_i . This equation can be resolved through two basic approaches by either using the temperature distributions from the previous time step, \underline{T}_{i-1} to calculate the necessary values and thus solve equation (5.21) directly, or by using an iterative solution technique that allows the necessary variables to be continually revised on the basis of converging solution. The latter option is adopted in FIRES-T through the triangularisation of \underline{K}^* on the basis of previous temperature distribution followed by back substitution for \underline{Q}^* to obtain \underline{T}_i .

In order to accelerate convergence, an overconvergence factor β is used in the iterative process to estimate the temperature distribution for the next iteration, $j+1$ such that:

$$\underline{T}_i^{j+1} = \underline{T}_i^j + \beta(\underline{T}_i^j - \underline{T}_i^{j-1}) \quad (5.22)$$

Values of β up to -0.60 have been necessary to achieve convergence in the application of FIRES-T undertaken in this thesis. Convergence is achieved when the temperature distributions of two successive iterations coincide within a prescribed level of error expressed as:

$$\frac{2|T_i^j - T_i^{j-1}|}{|T_i^j + T_i^{j-1}|} < \text{permissible error} \quad (5.23)$$

Flow charts of FIRES-T is presented in Figure 5.4.

5.2.6 COMMENTARY ON THE USE OF FIRES-T

The computer program FIRES-T models the fire environment through the use of a standard fire curve, expressed as time dependent, and the use of the radiative and convective mechanisms of the fire boundary.

When using FIRES-T, the origin of the co-ordinate axis is arbitrary. However, in order for it to be used in conjunction with the structural response program SAFE-RCC, the origin must correspond with the longitudinal axis of the column. This is because the finite element mesh used in FIRES-T is passed directly over to SAFE-RCC in the form of elemental areas and centroidal distances of the element to the xx-axis. This condition is necessary in order to produce the correct balance of positive and negative distances about the principal axis of bending for the calculation of stresses and strains in the structural response program SAFE-RCC (see Figure 5.5).

In order to use FIRES-T, the column cross section must be discretised into a series of finite element meshes that may be constructed either from triangular or quadrilateral elements. Since concrete is not a highly conductive material, it is advisable to use finer element meshes near the surface of the column section and coarser meshes at the interior to overcome the effect of high thermal gradient that

occurs near the surface of the column. Once the mesh has been chosen, the number and co-ordinates of the nodal points are entered as data.

The number of elements and details of their corresponding nodal points, in addition to the material type designation for each element, are then entered. The corresponding nodal points must be prescribed in a counter-clockwise order. The materials data are then entered for each thermal property allowing for their temperature variation. Specification of the boundary conditions for different surface elements with the parameters of the heat flow equation for each material exposed to fire are the data next required. Details of the convergence criteria are then entered. This is followed by the fire history data in the form of a series of fire temperatures against time, and the elements of the column cross sections that are exposed to the fire. The required time increments are also entered. The elemental temperatures of the column cross section are then calculated for each time increment in accordance with the theory covered in the previous sections. FIRES-T allows the use of up to four temperature-time fire curves and as many surface boundary conditions as are necessary to represent the fire exposure. For full user instructions, the user manual of FIRES-T (Becker, Bizri and Bresler (1974)) should be consulted.

The phenomena associated with heat flow in a turbulent environment of a fire is difficult to model exactly. Heat flow through the column surface is highly dependent on the values chosen for the parameters of the heat flow equation. The critical parameters appear to be the emissivities of both the flame and the surface of the column. With regard to these values and other thermal boundary conditions, the data given in Table 5.1 are taken to be reasonable for this project.



Figure 5.4: Flow chart for program FIRES-T
(Becker, Bizri and Bresler (1974))

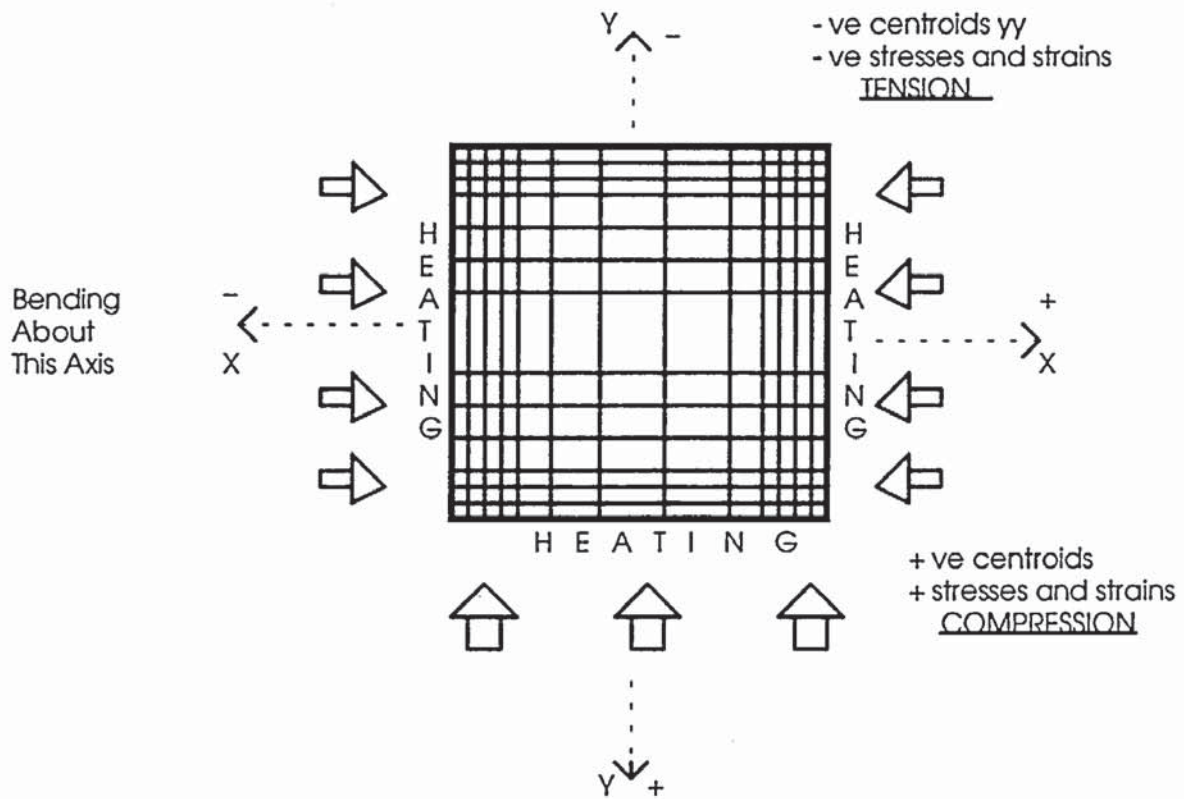


Figure 5.5: Origin of co-ordinate axis with respect to finite element mesh for tension and compression sign convention incorporated in SAFE-RCC for column cross sections

For further discussion of background to this, Odeen (1972), Weeks (1985) or Mooney (1991) should be consulted.

In order to ensure consistent cross sections in both the thermal and structural analysis, FIRES-T passes details of the finite element mesh for each structural cross section over to the structural response program SAFE-RCC.

	Parameter	Value
Fire Exposed Face	Convection Factor (A)	$3600 \text{ J/hm}^2\text{K}^{1.33}$
	Convection Power (N)	1.33
	Absorption (a)	0.9
	Fire Emissivity (ϵ_f)	0.7
Cool Face	Convection Factor (A)	$7920 \text{ J/hm}^2\text{K}^{1.25}$
	Convection Power (N)	1.25
	Absorption (a)	1.0
	Fire Emissivity (ϵ_f)	0.9
	View Factor (V)	0.5
	Surface Emissivity (ϵ_s)	0.9
	Stefan-Boltzman Constant	$2.04 \times 10^{-4} \text{ J/hm}^2\text{K}^4$

Table 5.1: Values of concrete parameters for non-linear heat flow equation

5.3 STRUCTURAL RESPONSE PROGRAM: SAFE-RCC

The computer program SAFE-RCC is a non-linear structural analysis program which was developed by Weeks (1985) as an analytical tool to study the fire response of reinforced concrete columns subjected to restraint and continuity as experienced in a total structure. SAFE-RCC provides a description of the column response in the form of the time history of lateral displacements, rate of deflection, axial deformation, end slopes, end moments, axial force, internal stresses and strains in the concrete and steel elements, and an indication of the state of the concrete with respect to cracking at a particular time step (see also Purkiss and Weeks, 1987).

The structural analysis used in SAFE-RCC is based on the method developed by Cranston (1967) for the computer analysis of restrained columns in a non-fire environment. The analysis is designed such that solutions for a given column bent about one of the principal axes of the cross section are obtained in stages using an iterative method as loading is applied from zero up to a maximum load in specified load increments or to a specified deflection. The model of the mechanical properties for both concrete and steel reinforcement incorporated in SAFE-RCC takes into account both the variation due to temperature and the stress dependence of transient strain, thermal strain, creep strain, and shrinkage strain.

The geometric discretisation of the column under analysis allows a maximum of 20 segments; the segment division points can be further subdivided into a maximum of 150 concrete and steel finite elements which are directly passed over from FIRES-T. Since only half of the section is modelled due to the symmetry of

the analysis, the subdivision corresponds to 300 elements for the whole segment cross section .

SAFE-RCC can employ a maximum of 65 time steps, the size of which is at the discretion of the user. However, numerical problems may arise if the time step increments are set too large resulting in slow convergence particularly at the beginning of the fire period where the fire curve is normally very steep. Weeks (1985) suggested that a time increment of 3 minutes during the steepest portion of the temperature-time curve i.e. for the first half hour for the International Organisation of Standardisation (ISO) 834 curve should be taken to give acceptable convergence. Thereafter the time increments can be increased as the rate of temperature rise decreases.

Figures 5.6 and 5.7 show the hierarchical structures of the computer program SAFE-RCC. Brief descriptions of the individual elements of the program structure and the corresponding program subroutines are described in the following sections which are based largely on the documentation of SAFE-RCC from Weeks (1985) and Purkiss and Weeks (1987).

5.3.1 SAFERCC - The Primary Solution Executor

The main body of the computer program SAFERCC is the primary solution executor that controls the execution of the analysis and comprises essentially a series of Fortran call statements to the various subroutines that contain the analytical methods and numerical procedures. It is also concerned with the initialisation of certain arrays and variables and inputs the data necessary for the determination of the array dimensions required for the program run.

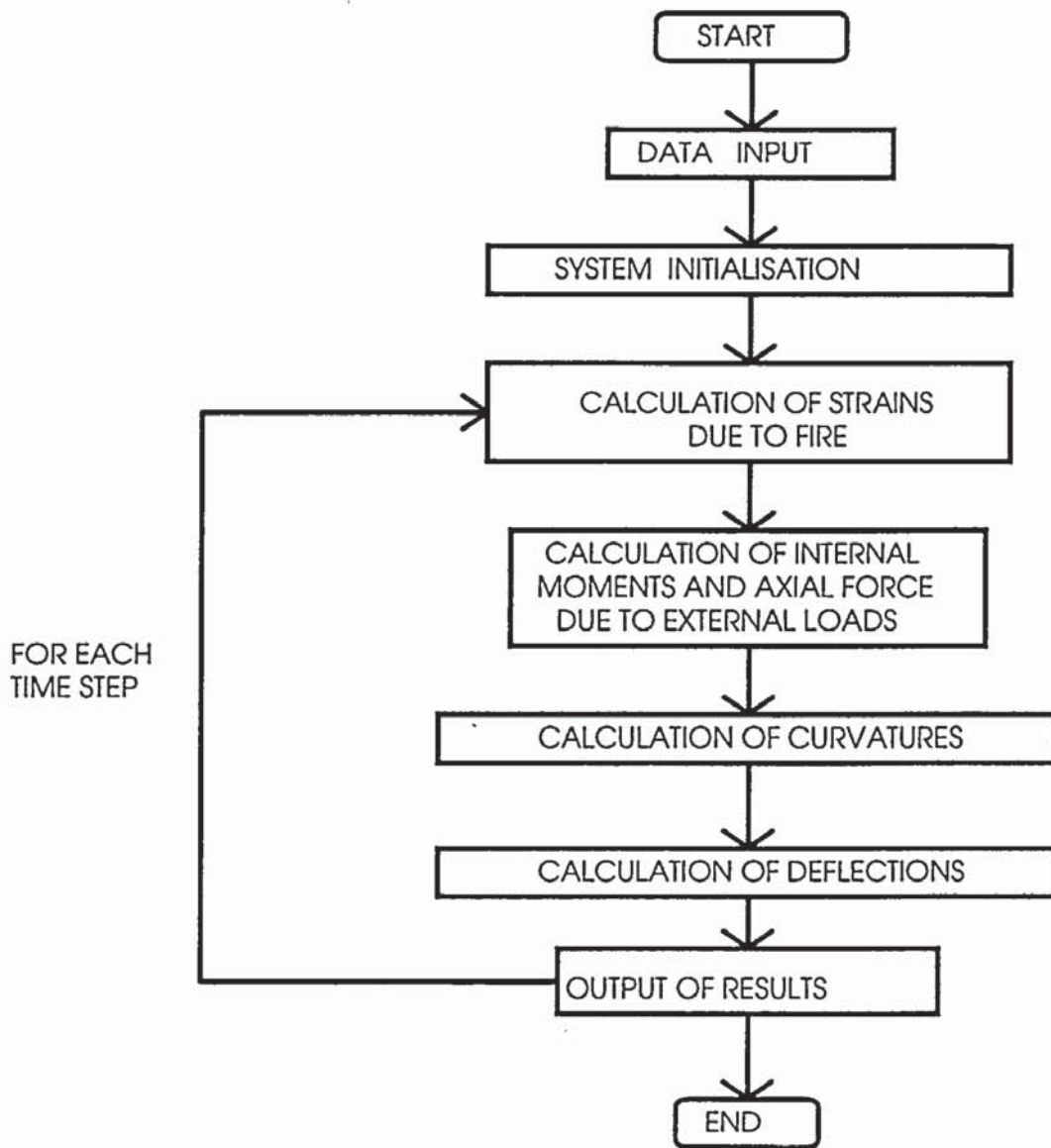


Figure 5.6 : Macro flow diagram showing the structure of the computer program SAFE-RCC

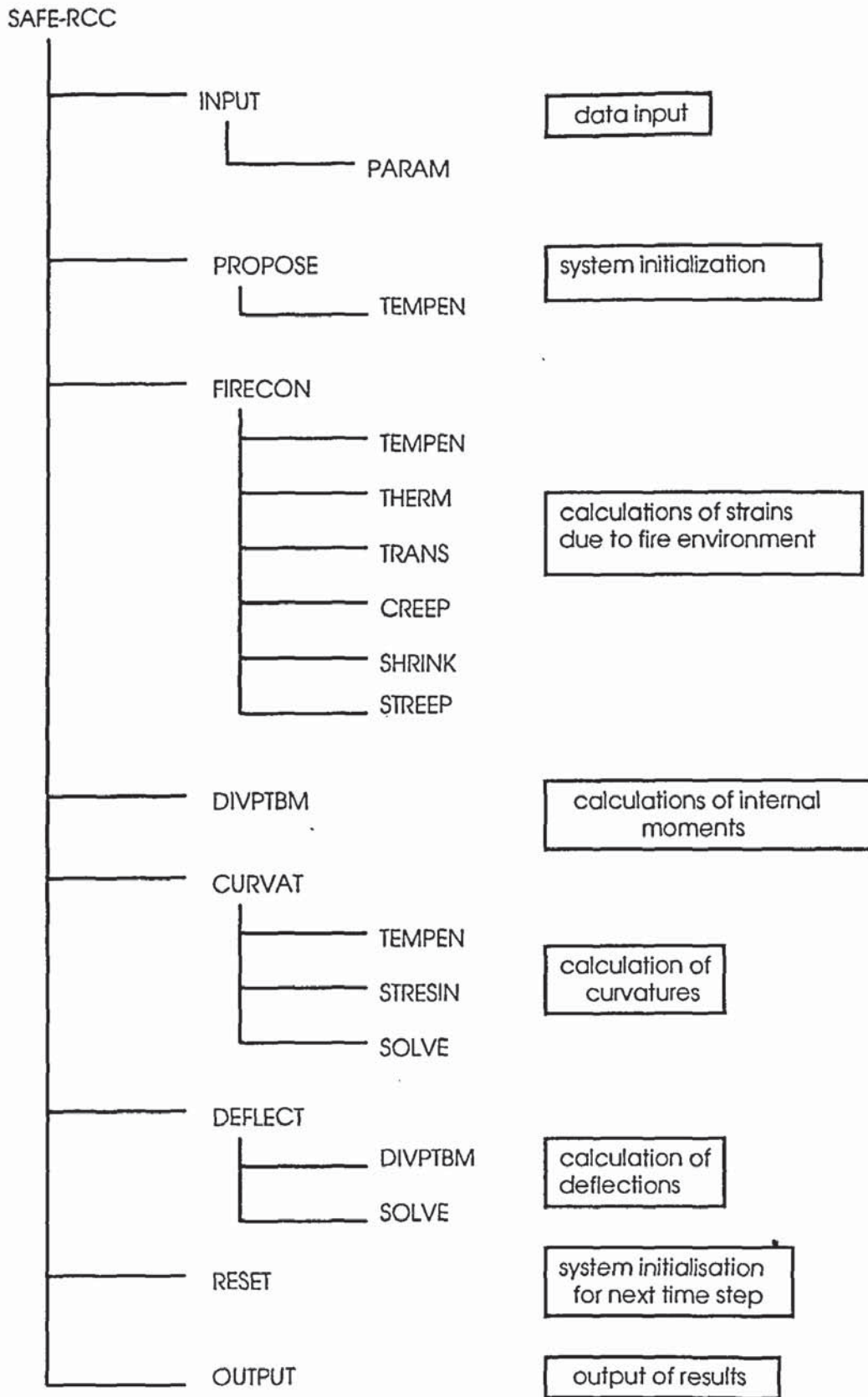


Figure 5.7: Hierarchical structure of SAFE-RCC

5.3.2 DATA INPUT

The majority of the data input is carried out by subroutine INPUT which reads from a file prepared by the user.

5.3.2.1 Subroutine PARAM

The temperature dependent material properties for both concrete and steel are modelled as linear segments. The description of these is accomplished through the entering a series of eight ordered pairs of temperature-property values by subroutine PARAM. The ordered pairs of values then describe the nodes of the segments.

5.3.3 SYSTEM INITIALISATION

Subroutine PROPOSE executes the system initialisation through the calculation of the proposed values necessary to commence the structural response analysis. Initial values must be calculated for the end moments, end slopes, axial force, division point deflections, curvatures and direct strain at the column axis. Subsequently, the system is initialised for the next time step through the execution of subroutine RESET; by setting the proposed values listed above for the next time step equal to the calculated values from the current time step.

The theory behind the numerical procedures contained in subroutine PROPOSE is described as follows.

5.3.3.1 Calculation of Proposed End Moments

The end moments for pinned end conditions of a column exposed to fire as shown in Figure 5.8 are calculated using the following formulae:

$$M_A = -Pe \quad (5.24)$$

and $M_B = Pe \quad (5.25)$

where: P is the axial force that is entered as item in data,
 e is the eccentricity of the application of axial force (entered as item of data and taken as positive to the right of line AB).

5.3.3.2 Calculation of Proposed End Slopes

For a column pinned at both ends, the proposed end slopes are calculated using the following formulae based on Macaulay's method:

$$(\theta_A)_p = \frac{\left(\frac{M_A L}{3} - \frac{M_B L}{6} \right)}{EI} \quad (5.26)$$

$$(\theta_B)_p = \frac{\left(\frac{M_B L}{3} - \frac{M_A L}{6} \right)}{EI} \quad (5.27)$$

where: L is the length of the column under analysis
 E is the initial elastic modulus of concrete at ambient temperature
 I is the second moment of area of the column cross section.

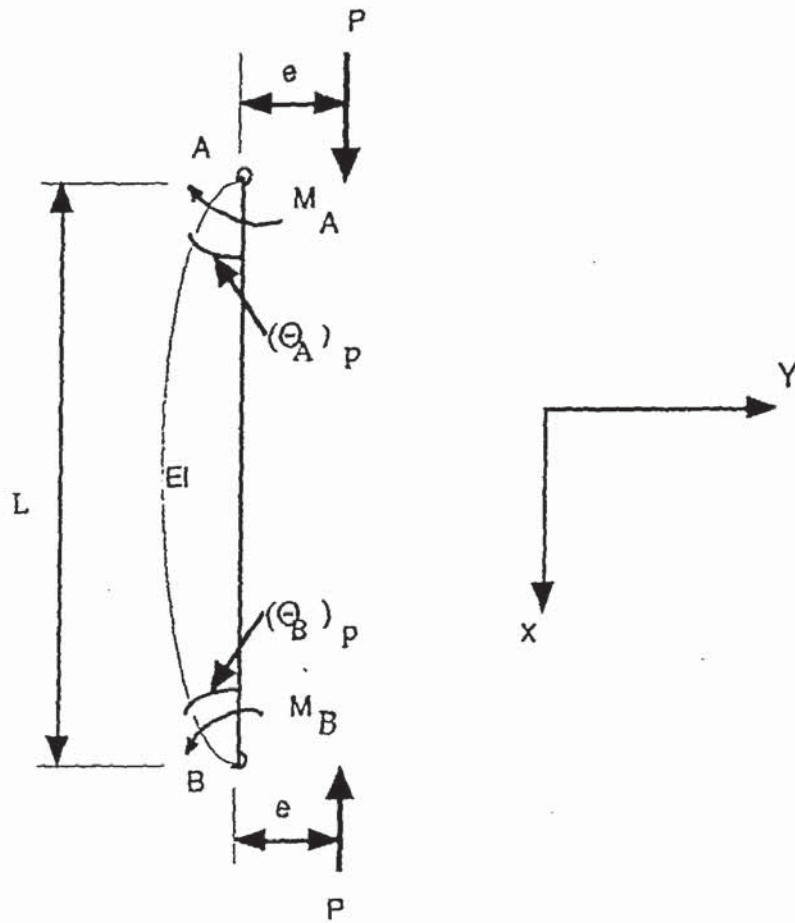


Figure 5.8: System analysed for pinned rotational restraint at both ends of the column exposed to fire.

5.3.3.3 Calculation of Proposed Division Point Deflections

The proposed division point deflections are calculated taking into consideration the column end moments and the axial force eccentricities at each division point.

The division point deflections are obtained from the following equation:

$$(y_x)_p = -\frac{1}{EI\alpha^2} \left(M_A \cot\alpha L + \frac{M_B}{\sin\alpha L} \right) \sin\alpha x + \frac{M_A}{EI\alpha^2} \cos\alpha x - \frac{M_A}{EI\alpha^2} \dots + \left(\frac{M_A + M_B}{EI\alpha^2} \right) \left(\frac{x}{L} \right) \quad (5.28)$$

where: $\alpha^2 = \frac{P}{EI}$,

x is the distance from the end A to the division point.

5.3.3.4 Calculation of Proposed Curvatures

The proposed curvature of the column ϕ is expressed by the following equation:

$$\frac{1}{R} = \frac{\left(\frac{(M_A + M_B)x}{L} - M_A \right)}{EI} \quad (5.29)$$

where: R is the radius of the circle the deflected column would describe.

5.3.3.5 Direct Strain at the Column Axis

The proposed value of the direct strain at the column axis for each division point is assumed to be zero. This assumption is justified since the axial strains at the

initial stages of the fire are low. Bending strains will be more significant than direct axial strains in a column. Furthermore the direct strain specified is only a proposed value in order to start the structural analysis and is adjusted as the analysis proceeds.

5.3.3.6 Calculation of Second Moment of Area

The second moment of area for the column is calculated on the basis of a transformed section. This is done to ensure that to a 'true' equilibrium condition of end slopes and induced moments at each end of the column is obtained.

The uncracked transformed I value for the column is given by the equation:

$$I_{\text{uncracked}} = \frac{bh^3}{12} + (\alpha_e - 1)A_{sc}d_2^2 \quad (5.30)$$

where:

b is the breadth of the column

h is the overall depth of the column

$$\alpha_e = E_s/E_c$$

E_s is the initial tangent modulus of the steel stress-strain relation for the average current temperature

E_c is the initial tangent modulus of the concrete stress-strain relation for the average current temperature

A_{sc} is the area of steel

d_2 is the distance between the centroid of the section and the centroid of the steel

When the structural system is under load the member sections will crack resulting in a reduced I value. Cracking of the column under analysis will be increasingly significant as time proceeds due to the effects of the fire. Automatic consideration is taken of this within the structural analysis.

5.3.4 CALCULATIONS OF STRAINS DUE TO FIRE

The induced strains as a result of the fire environment are determined using the material behaviour models which are presented in Chapter 4. The appropriate subroutine containing the material behaviour models according to the material type are controlled and selected by subroutine FIRECON. Subroutine FIRECON is used essentially as developed by Weeks (1985) except that it has been modified to incorporate the constitutive models of Anderberg and Thelandersson (1976), Schneider (1986) or Lie and Chabot (1990).

5.3.4.1 Subroutine THERM

Subroutine THERM calculates the induced strains due to the thermal expansion. Concrete thermal strains are calculated using the polynomial fit established by Forsén presented in Section 4.2.3. The thermal strain model predicts a zero value of induced thermal strain at 20°C. This is done to satisfy compatibility since SAFE-RCC has been developed for a structural response analysis starting with an initial temperature of 20°C. For this reason, the value of thermal strain predicted by Forsén polynomial fit at 20°C (1.8345×10^{-4} m/m) is subtracted from the current calculated value.

The steel thermal strain is calculated on the basis of the induced thermal strain which is a function of the temperature dependent coefficient of thermal expansion and the elemental temperature, as presented in Section 4.3.2. Referring to Figure 5.9 the coefficient of thermal expansion is given by:

$$\alpha_s(T) = T_3 + \frac{(T_4 - T_3)(T - T_3)}{(\alpha_4 - \alpha_3)} \quad (5.31)$$

or, for $T_n < T < T_{n+1}$

$$\alpha_s(T) = T_n + \frac{(T_{n+1} - T_n)(T - T_n)}{(\alpha_{n+1} - \alpha_n)} \quad (5.32)$$

and the thermal strain is given by:

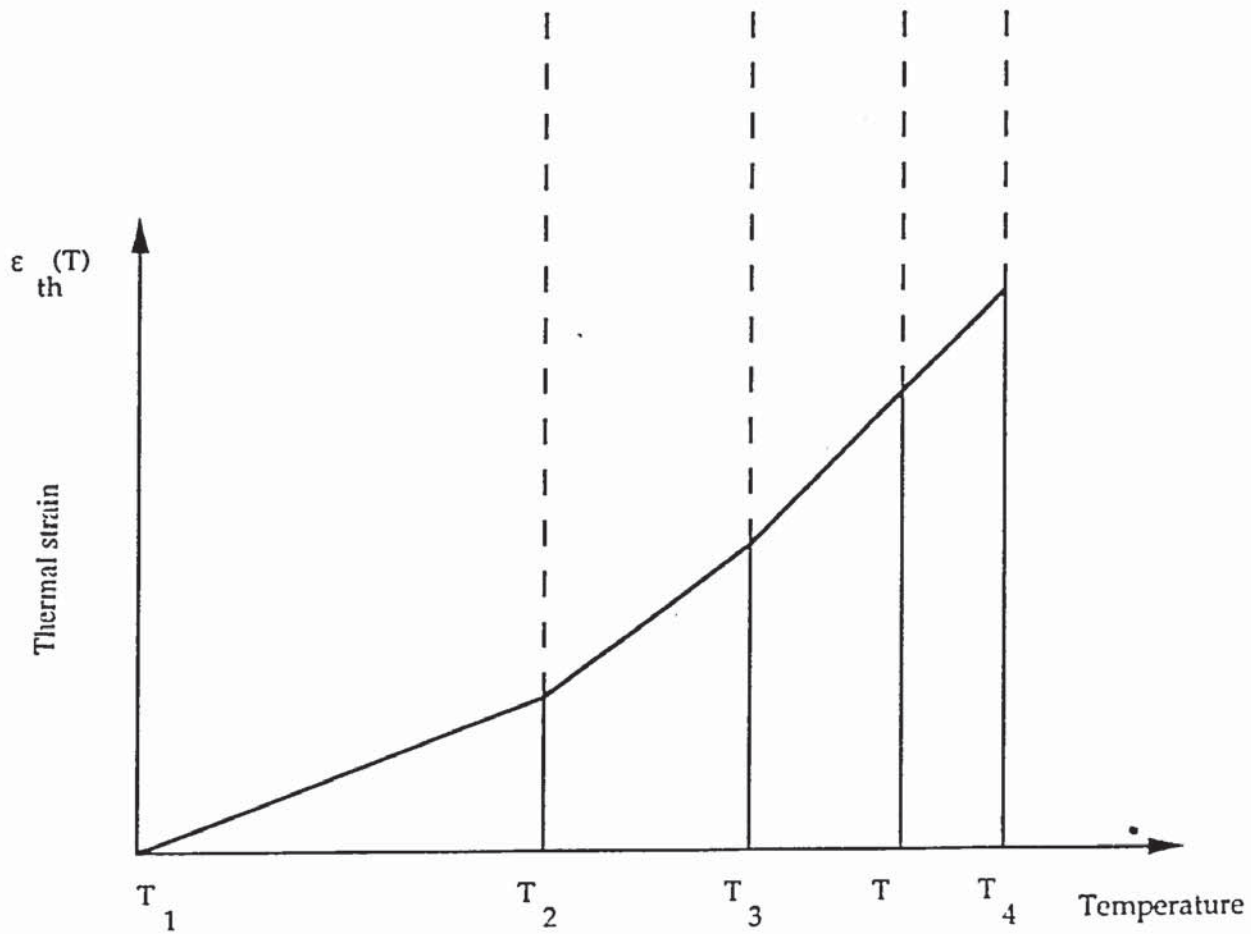
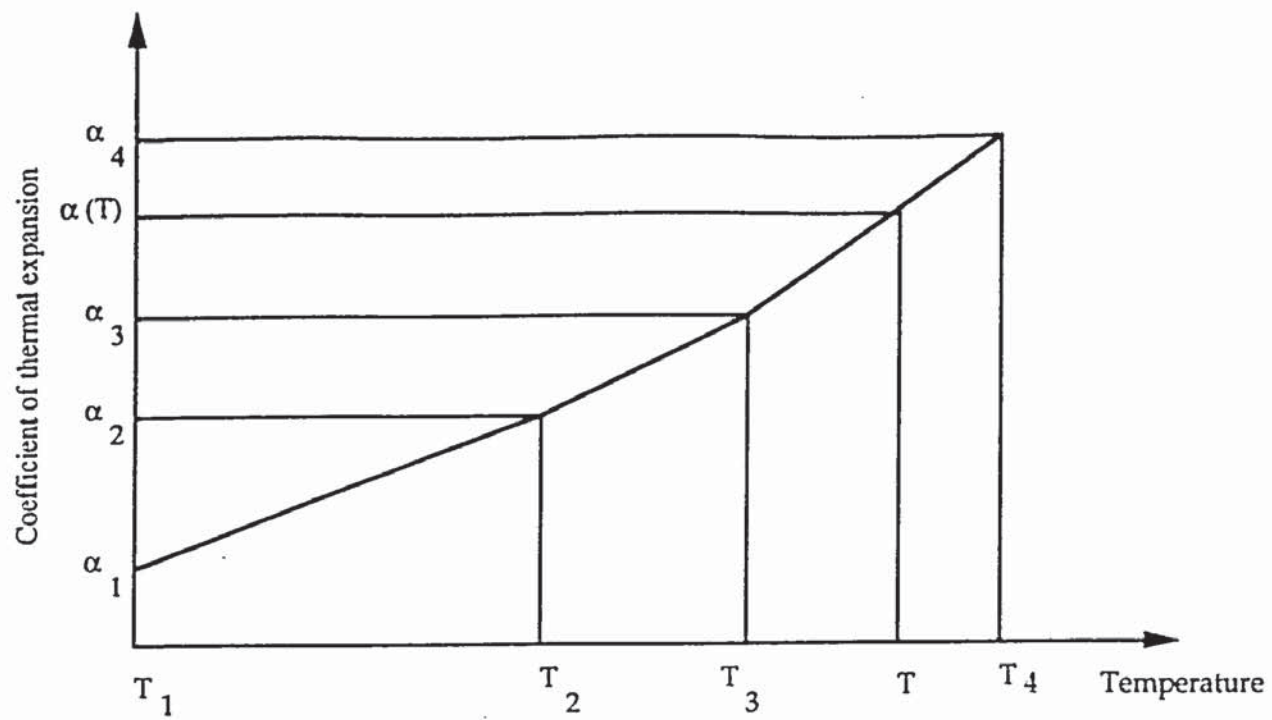
$$\epsilon_{th}(T) = \alpha_1(T_1 - 20) + \alpha_2(T_2 - T_1) + \alpha_3(T_3 - T_2) + \alpha(T)(T - T_3) \quad (5.33)$$

or, for $T_n < T < T_{n+1}$

$$\epsilon_{th}(T) = \alpha_1(T_1 - 20) + \alpha_1(T_2 - T_1) + \dots + \alpha_n(T_n - T_{n-1}) + \alpha(T)(T - T_n) \quad (5.34)$$

5.3.4.2 Subroutine TRANS

Subroutine TRANS calculates the induced transient strain in concrete elements from the Anderberg and Thelandersson (1976) model presented in Section 4.2.2.1 and from Schneider's transient creep model in Section 4.2.2.2. The concrete transient strain is a function of the current state of stress; since this has yet to be



$$\alpha(T) = \alpha_3 + (\alpha_4 - \alpha_3) \frac{(T - T_3)}{(T_4 - T_3)}$$

$$\epsilon_{th} = \alpha_1(T_1 - 20) + \alpha_2(T_2 - T_1) + \alpha_3(T_3 - T_2) + \alpha(T)(T - T_3)$$

Figure 5.9: Calculation of steel thermal strain (Subroutine THERM).

determined, the transient strain is calculated using the elemental stress from the previous time step. The errors caused by this assumption are negligible, again provided that the time step increments are kept relatively small. The transient strain model is set to give a zero value for Lie and Chabot's constitutive model for concrete.

5.3.4.3 Subroutine CREEP

Subroutine CREEP calculates the induced creep strain in concrete elements using the Anderberg and Thelandersson (1976) model for primary and secondary creep presented in Section 4.2.4. Using Fortran data statements, the constants β_0 , k_1 , t_r and p are set equal to 0.53×10^{-3} , 3.04×10^3 , 3.0 and 0.5 respectively. The concrete creep strain is a function of the current state of stress. However, the elemental stress from the previous time step is used to determine the creep strain since the current stress state has yet to be determined. To account for the variable stress and temperature, a strain hardening principle is employed. It is assumed that no creep strains occur for concrete in tension.

The creep model is set to give a zero value for the creep component of Schneider's constitutive model for concrete. Since Lie and Chabot's model allows for creep by values used in the stress-strain curve, the classical creep term is also set to give zero value.

5.3.4.4 Subroutine SHRINK

Subroutine SHRINK calculates the incremental shrinkage strain of concrete during a time step using the shrinkage model from Becker and Bresler (1974)

presented in Section 4.2.5. The shrinkage strain is calculated incrementally for the temperature range of 20°C to 100°C. The maximum total shrinkage at 100°C is 0.001 m/m. All remaining shrinkage is assumed to occur upon reaching 100°C. However, at any time step, the shrinkage occurring may not exceed the potential shrinkage.

5.3.4.5 Subroutine STREEP

Subroutine STREEP calculates the induced incremental strain due to creep in a steel element using the Harmathy (1970) comprehensive creep model with the Dorn (1954) Theta Method for temperature variation. A strain hardening principle is used to account for variation of stress. The model is presented in Section 4.3.3.

The parameters Z and ϵ_{cro} are functions of the current state of stresses, since these have yet to be determined the elemental stresses from the previous time step are employed. Creep recovery is not accounted for in the model and is therefore assumed not to occur. The steel model is assumed to be identical in both tension and compression.

5.3.5 CALCULATION OF INTERNAL MOMENTS AND AXIAL FORCE

Subroutine DIVPTBM calculates the division point moments about the axis of the column due to the external loads taking into account the second order effects due to axial load eccentricity at the division points as a result of the deflected column profile. The division point bending moments calculated about the axis of the column are given by:

$$M_r = -M_A + \frac{(M_A + M_B) + \left(g_A + \sum_{r=0}^r \sqrt{\left(l_r^2 - \left((y_r)_p - (y_{r-1})_p \right)^2 \right)} \right)}{L} - P(y_r)_p \quad (5.35)$$

where: g_A is the gusset length at end A,
 y_r is the division point deflections.

Internal variation of the axial force throughout the deflected column segments lengths is accounted for by vertical resolution at the division points. This procedure is contained within subroutine CURVAT.

5.3.6 CALCULATION OF CURVATURES

Subroutine CURVAT calculates the column curvature at each division point corresponding to the cross section loading. The procedure is iterative, with initial proposals being made for ϵ_r , the direct strain at the column axis and ϕ_r , the curvature. These proposals define the strain profile across the section from which the calculated values of axial load and bending moment are obtained. If these calculated values are reasonably close to the specified values, the proposal values of ϵ_r and ϕ_r are taken as correct. The magnitude appropriate for the permissible differences are defined by the allowable incompatibilities. Otherwise the proposals for ϵ_r and ϕ_r are modified and the procedure repeated until it converges to a solution. Full details of the numerical procedure is given in Cranston (1967). Failure is assumed to occur when equilibrium between the cross sectional column strength and applied loads cannot be obtained .

Contained within subroutine CURVAT is the total strain model by Anderberg and Thelandersson (1976), Schneider (1986) or Lie and Chabot (1990) as presented in Section 4.2. The corresponding stress and tangent modulus is determined through the application of subroutine STRESIN for each cross sectional element. The compatibility equations are solved using subroutine SOLVE where a series of simultaneous equations written in matrix form is solved using the numerical procedure of Gaussian elimination.

5.3.6.1 Subroutine STRESIN

Subroutine STRESIN represents the stress-strain relationship for the column subslice for concrete and steel. The stress-strain relationships for concrete are presented in Section 4.2.1 whilst that for steel in Section 4.3.1. However, some additional features are discussed in this section.

For the Baldwin and North (1973) stress-strain model, the following statement is used in order to determine whether the linear unload relation corresponding to 'true unloading' should be followed (Figure 5.10). For a given state of strain, if the stress predicted by the linear unload line (equation 4.33) yields a stress greater than that predicted by expression (equation 4.30), the true state of stress is given by the latter's expression. Otherwise, the true state of stress is that predicted by the linear unload relation.

Figure 5.10 shows some typical stress-strain paths. When the concrete has unloaded and cracked any state of strain will predict zero stress if it is less than the value of strain at which the linear unload relation crosses the strain axis of the

stress-strain relation. Subsequent reloading is assumed to continue from the point at which the linear unload line crosses the strain axis.

The maximum stress attained is σ_{\max} . Any increase in strain beyond σ_{\max} will therefore give a smaller value of stress ($< \sigma_{\max}$) due to the descending branch behaviour, or unloading behaviour, of the concrete stress-strain relation. It is then not possible, by virtue of the stress-strain relation, for any concrete element to crush when there is a solution to the analysis.

However, if an element is strained beyond ϵ_{\max} , the consequences for the computer analysis are that the element must unload and the surrounding elements must take up the stress deficiency. This implies a shift in the neutral axis position. When many elements are strained into the descending branch portion of the stress-strain relation the neutral axis may shift right out of the section resulting in failure of the column.

Subroutine STRESIN also employs a concrete tension flag to indicate whether any concrete element is cracked. This situation arises when an element attains a tensile strain greater than the permissible value. Tensile strain will no longer be sustained when a concrete element is cracked; a corresponding zero stress is therefore predicted. However, the element may still be 'reloaded' into compression.

For steel, a bi-linear stress-strain relation is employed where the stresses are computed on the basis of the permanent inelastic strain. The steel strain hardening modulus has been set equal to one twentieth of the modulus of elasticity. The steel

is assumed to rupture when strains greater than ten times the yield strain are attained. The relation is assumed to be identical in tension and compression.

5.3.7 TEMPERATURE DEPENDENCE OF MATERIAL PARAMETERS

Subroutine TEMPEN calculates the temperature dependent material properties, such as the stress and strain corresponding to the maximum concrete stress, the yield strength and elastic modulus of steel and the coefficient of thermal expansion of steel. The temperature dependent material properties is represented in subroutine TEMPEN as linear segments by a series of points and connecting lines where the y-axis corresponds with the material parameter and the x-axis the temperature. The value of material property f for a given temperature T_i is given by:

$$f(T_i) = f(T_n) + (T_i - T_n) S_n \quad (5.36)$$

where: $T_n \leq T_i \leq T_{n+1}$

S_n is the slope between points n and $n+1$.

5.3.8 CALCULATION OF DEFLECTIONS

Subroutine DEFLECT calculates the division point deflections by double integration of the curvature making allowance for any initial deflections. The calculations are made using the assumption that the curvature varies linearly between division points. However, under zero load it is assumed that the segments are straight. The numerical procedure adopted is iterative, with initial proposals being made for $(\theta_A)_p$ and $(\theta_B)_p$, the end slopes. These proposals define

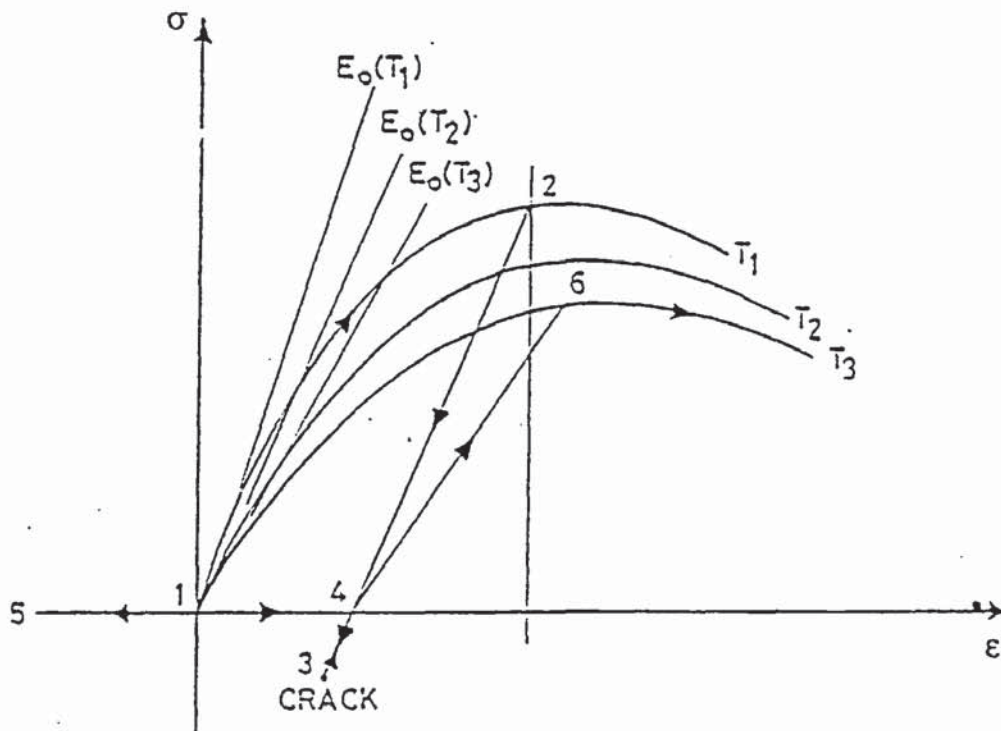
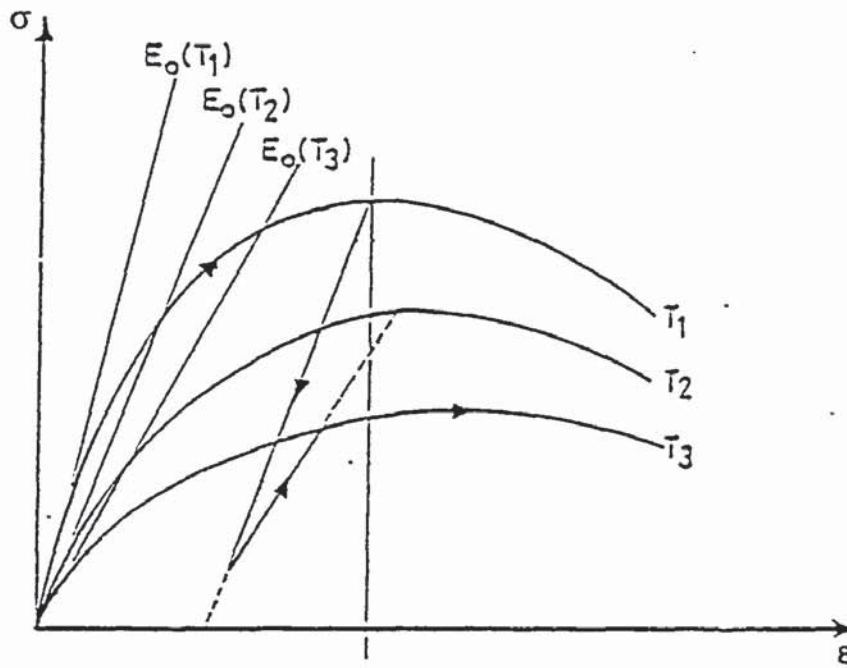
the provisional slopes and deflections of each division points from which the calculated values of end slopes and deflections are obtained. For a valid solution, the difference between the calculated values and the proposed values must be within their allowable incompatibilities. Otherwise the proposals are modified and the procedure repeated until a valid solution is obtained. The procedure is described in detail in Cranston (1967). The partial differential equation is solved using subroutine SOLVE. When division point deflections do not converge to a solution the column is assumed to have failed.

Calculation of the column axial deformation is also contained within subroutine DEFLECT. The axial deformation is calculated from the consideration of the average segment total strain.

The rate of deflection is also calculated, to ensure convergence, within subroutine DEFLECT according to the equation:

$$\frac{d(y_r)_c}{dt} = \frac{\Delta(y_r)_c}{\Delta t} \leq \frac{L^2}{15b} \quad (5.37)$$

where: $d(y_r)_c/dt$ is the rate of deflection,
 $\Delta(y_r)_c$ is the change in deflection for the current time step,
 Δt is the time interval for the current time step,
 L is the column length,
 b is the breadth of the column.



strain path: 1-2, 2-3, 3-4, 4-5, 5-4, 4-6, 6-5 - previously uncracked
 1-2, 2-4, 4-5, 5-4, 4-6, 6-5 - previously cracked

Figure 5.10: Examples of stress-strain path.

5.3.9 OUTPUT OF RESULTS

The results of the structural analysis is given in printed form by subroutine OUTPUT. The printed output includes the time history of lateral displacements, rate of deflection, axial deformation, end slopes, end moments, axial force and internal stresses and strains in the concrete and steel elements.

Indication is given if any concrete is cracked and a warning message is given if the rate of deflection exceeds the permissible rate. A statement of the type of column failure is also given with the corresponding failure time.

The next chapter, Chapter 6 describes the procedures adopted for modelling the concrete material models and for the modelling of reinforced concrete columns exposed to fire which incorporates the effect of spalling.

CHAPTER SIX

DESCRIPTION OF MODELLING PROCEDURE

6.1 INTRODUCTION

In a fire environment thermal gradients and thermal expansion of structural elements are sources of internal stresses. As a consequence of internal stresses, cracking, crushing or spalling can occur and reduction in strength and stiffness of the structural members results. Reduction in strength is also due to the degradation of material properties as the temperature rises. This combination of phenomena controls the fire response of structural elements.

Computer simulation is generally thought to provide a realistic correlation corresponding to the response of structural elements in an actual fire. However, there are limitations and uncertainties in the use of computer simulation, the most important of which concerns the assumed behaviour of one of the constituent materials, namely concrete. These uncertainties refer to the different constitutive models proposed by Anderberg and Thelandersson (1976), Schneider (1986) and Lie and Chabot (1990). Anderberg and Thelandersson (1976) and Schneider (1986) both incorporate the effects of transient strain or the appropriate strain effect in their constitutive models whilst Lie and Chabot (1990) propose a model that omits the effect of the transient strain component.

This chapter describes the method that incorporates the three concrete material models described above in the computer simulation. The assessment of the

relative effect of the three concrete material models on the structural response of reinforced concrete columns in a fire environment is described in Chapter 7.

This chapter is also concerned with the description of a method to model concrete columns exposed to fire which incorporates the effect of spalling. It seems that there is general recognition of the potential problems of spalling but no real investigation into what effect spalling has on the fire resistance of reinforced concrete members. The question arises as to how much the fire resistance may decrease with the partial loss of concrete cover, and the magnitude of the protection loss on the likely detrimental effect on the structural behaviour. The relationship of fire resistance with the extent of spalling and the time of exposure at which the concrete spalls are thus the principal concerns.

In an attempt to address this situation, a series of computer simulations was used to model concrete columns exposed to fire which incorporated the effect of spalling by varying the amounts of concrete lost during a specified period of exposure to fire. An array of six percentages of spalling was chosen for one range of simulations while a two stage progressive spalling regime was used for a second range. The assessment of the relative effect of spalling on the fire resistance and the deformation of reinforced concrete columns is described in Chapter 8.

In order to model the fire response of a reinforced concrete column, it has been assumed that the heat flow is separable from the structural analysis. The computer analysis is therefore carried out in two stages. The thermal response of the member is evaluated using FIRES-T. The structural response of the reinforced concrete column is predicted using SAFE-RCC.

6.2 PROCEDURE FOR MODELLING MATERIAL BEHAVIOUR MODELS

This section describes the procedure for modelling the concrete material models presented by Anderberg and Thelandersson (1976), Schneider (1986) or Lie and Chabot (1990) in the structural analysis program SAFE-RCC. The program requires the calculation of strains as a result of the fire environment.

The induced strains as a result of the fire environment are determined using the material behaviour models which are presented in Chapter 4. The models of the mechanical properties of concrete incorporated in SAFE-RCC take into account the variation due to temperature and stress dependence of transient strain, creep strain and thermal strain. These strains are contained within subroutines TRANS, CREEP and THERM respectively. The appropriate subroutines are controlled and selected by subroutine FIRECON.

Subroutine TRANS calculates the induced transient strain in concrete from the Anderberg and Thelandersson (1976) model presented in Section 4.2.2.1 and from Schneider's transient creep model in Section 4.2.2.2. The transient strain model is set to give a zero value for Lie and Chabot's (1990) constitutive model for concrete.

Subroutine CREEP calculates the induced creep strain in concrete elements using the Anderberg and Thelandersson (1976) model for primary and secondary creep presented in Section 4.2.4. The creep model is set to give a zero value for the creep component for Schneider's constitutive models for concrete. Since Lie and Chabot's model allows for creep by using values used in the stress-strain curve, the classical creep term is also set to give zero value.

Subroutine THERM calculates the induced strains due to the thermal expansion for all three constitutive models. Concrete thermal strains are calculated using the polynomial fit established by Forsén presented in Section 4.2.3.

The constitutive model by Anderberg and Thelandersson (1976), Schneider (1986) or Lie and Chabot (1990) are contained within the subroutine CURVAT. Subroutine CURVAT calculates the column curvature and longitudinal strain at each divisional point corresponding to the cross section loading. The flexural strain and longitudinal strain define the total strain profile across the section. The instantaneous stress-related strain is then given by the total strain less the strain components due to the effects of exposure to the fire.

The corresponding stress and tangent modulus are determined through the application of subroutine STRESIN for each cross sectional element. The stress-strain model of Anderberg and Thelandersson (1976) is slightly modified and incorporates the Baldwin and North characterisation for the stress-strain relationship presented in Section 4.2.1.4 whilst Schneider's stress-strain model is presented in Section 4.2.1.2..

The resultant axial load and moment on the column cross section are computed when the stresses in all the elements have been found. At any section the calculated forces should be within the magnitudes appropriate for the permissible differences with the applied forces. In general the curvature and longitudinal strain must be iterated to achieve this equality.

6.3 PROCEDURE FOR MODELLING SPALLING OF CONCRETE

This section describes the method adopted for the computer modelling of reinforced concrete columns exposed to fire which incorporate the effect of spalling by varying the amounts of concrete lost during a specified period of exposure to fire. Two ranges of spalling regime were considered as described below.

6.3.1 FIRST RANGE OF SPALLING

Six different percentages of spalling namely 0%, 3.0%, 7.2%, 14.5%, 29.5% and 39% were considered for this range of simulations. Sections of concrete material were deleted to simulate spalling of concrete after two periods of exposure of either 15 or 30 minutes to the furnace environment.

For this range, with the column size already known the first step was to decide the finite element mesh for the unspalled column. Figure 6.1 shows the reinforced concrete column as well as a typical mesh design with 132-elements where the elements were divided between steel and concrete. Once a mesh was developed data files were created for input into FIRES-T. The data files include number and coordinates of nodal points, number of elements and details of corresponding nodal points, material property information, boundary surface definitions, the time increments and characteristics of the fire environment.

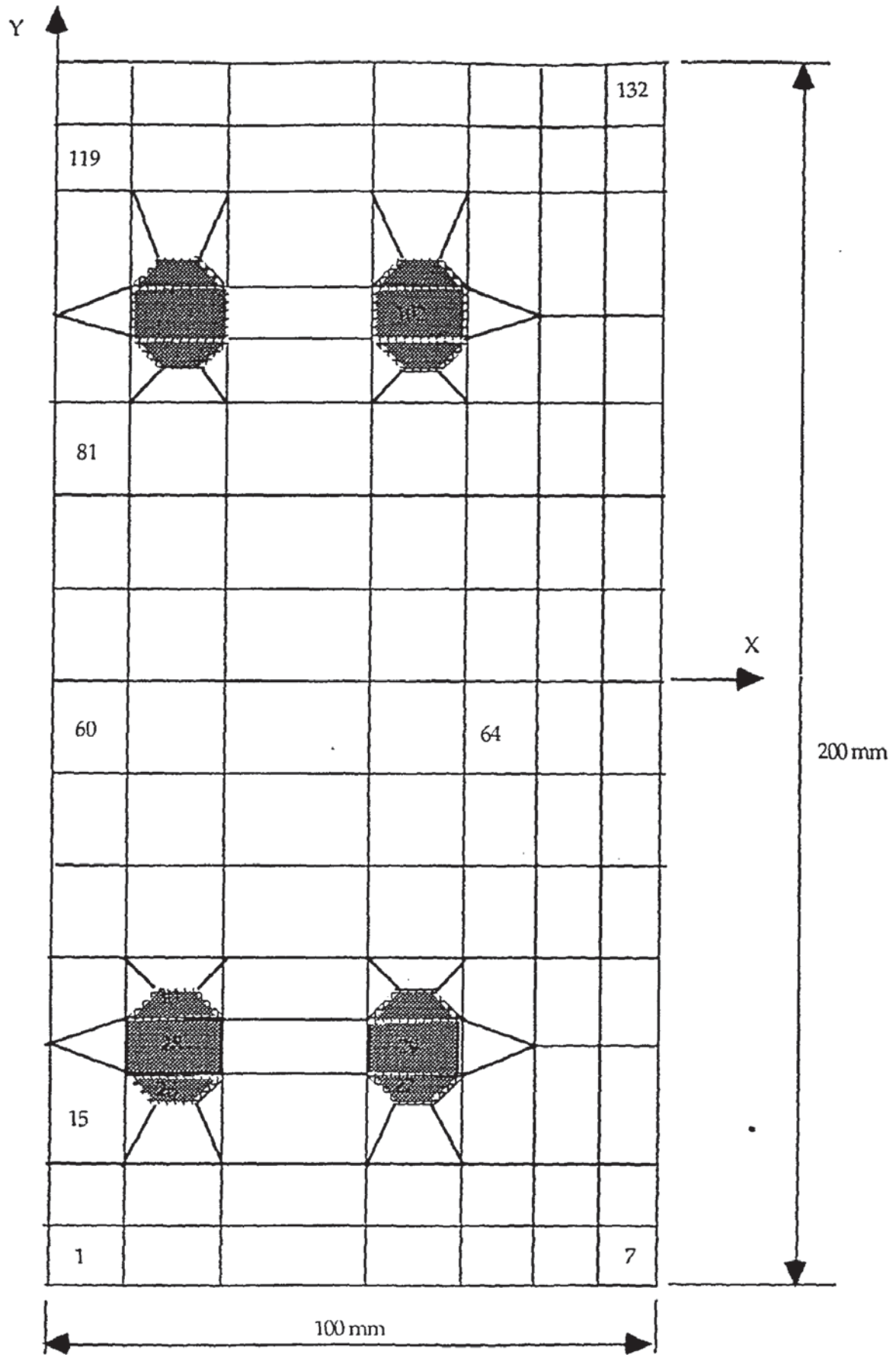


Figure 6.1: Example of finite element mesh for column cross section with 132 elements (8x32 mm diameter bars)

6.3.1.1 Simulation of Spalling After 15 Minutes

Firstly, FIRES-T was employed to calculate the temperature distribution histories in the column cross sections when exposed to the ISO furnace environment for 15 minutes with no spalling. Once execution of the simulation was completed, the nodal temperatures at 15 minutes were extracted to be used as part of the input data for the next FIRES-T run where the simulation of spalling of concrete cover was to be performed. An area of concrete was removed to simulate spalling; the first spalling condition represented was 3% of the total area (see Figure 6.2). A new finite element mesh was developed to represent the spalled cross section. Data files were then created for input into the next FIRES-T run taking into consideration the new boundary conditions, surface elements and elemental geometry. For this second FIRES-T run the initial time was specified at 15 minutes and the simulation was run for a further two hours.

Once execution of the simulation was completed, the elemental temperatures obtained from the first run were combined with those from the second run. These elemental temperatures were to be used as input data for the structural analysis program SAFE-RCC. However, the elemental temperatures from the second run were first edited by increasing the number of elements from 126 to 132 with the elements considered to have spalled were all assigned a temperature of 960°C. This would effectively render the strength of the spalled elements as negligible for the structural analysis run. SAFE-RCC was then employed to determine the structural response of the column until failure occurred. The same type of analysis as described above was performed with the other percentages of spalling. Typical cross sections with various percentages of spalling are shown in Figures 6.3 and 6.4.

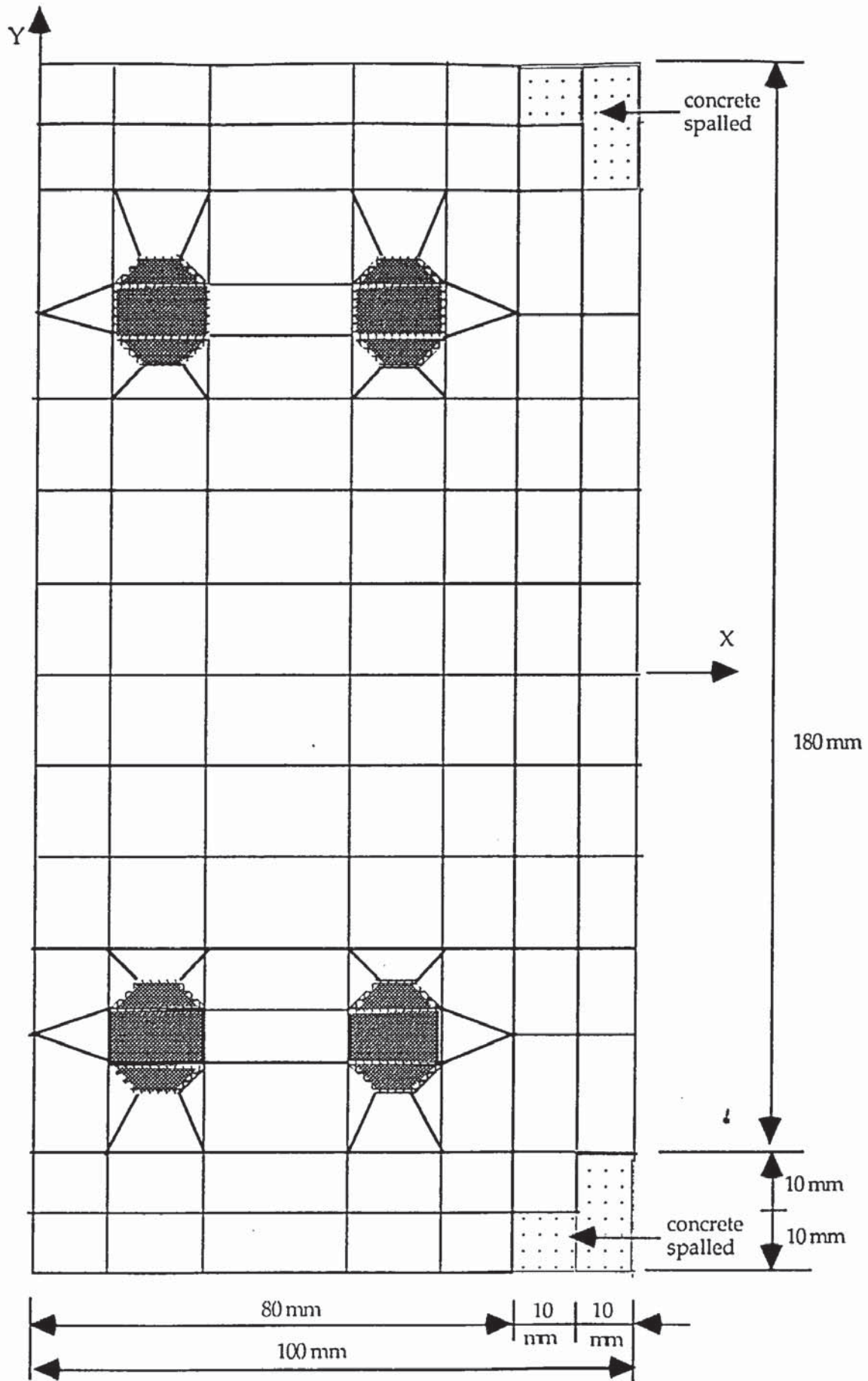


Figure 6.2: Example of finite element mesh for spalling condition representing 3% of the total area

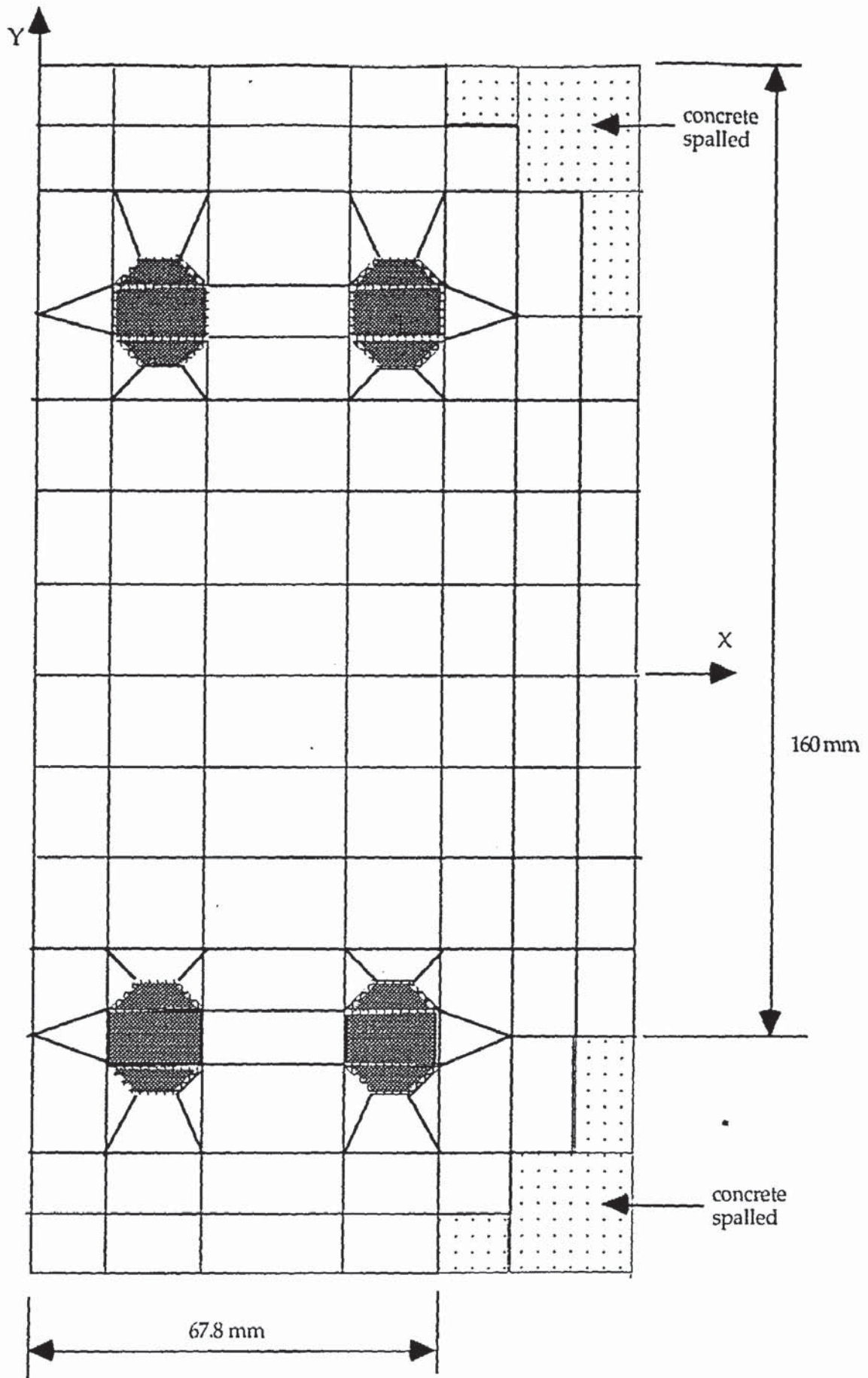


Figure 6.3: Example of finite element mesh for spalling condition representing 7.2% of the total area

6.3.1.2 Simulation of Spalling After 30 Minutes

As in the previous case, the same procedure was performed for each percentage of spalling except that for this set of simulations FIRES-T was first employed to calculate the temperature distribution histories in the column cross sections for 30 minutes. A further two-hour simulation was then performed for the second FIRES-T run with the initial time specified at 30 minutes. Following the edition to the elemental temperatures obtained from the second FIRES-T run, SAFE-RCC was then employed to determine the structural response until failure.

6.3.2 SECOND RANGE OF SPALLING

A two stage progressive spalling regime was used for a second range of simulations to model a gradual loss of concrete after periods of exposure of 15 minutes and 30 minutes to the furnace environment. In this regime, sections of concrete material were progressively deleted on the sides of the column cross sections and as well on the corners.

For the case of gradual loss of concrete cover on the corners, FIRES-T program was first employed for 15 minutes with no spalling. Once execution of the simulation was completed, the nodal temperatures at 15 minutes were extracted to be used as part of input data for the next FIRES-T run where the simulation of spalling of concrete cover was to be performed. An area of concrete representing 7.2% of the total area was removed to simulate spalling on the sides of the cross section (see Figure 6.3). A new mesh design was developed to represent the spalled cross section and data files created for input into the next FIRES-T run taking into consideration the new boundary conditions, surface elements and

elemental geometry. FIRES-T program was then run for the next stage for a further 15 minutes.

Once execution of the second FIRES-T run was completed the nodal temperatures at 30 minutes were extracted to be used as part of input data for the next FIRES-T run where the simulation of a further 22.3% spalling of concrete cover was to be performed representing a total of 29.5% of the total area (see Figure 6.4). Similarly, a new finite element mesh design was developed to represent the new cross section and data files were created for input into the final stage of FIRES-T run.

Upon the completion of the final simulation the elemental temperatures obtained from the first, second and third runs were all combined to be used as input data for structural analysis program SAFE-RCC. However, the elemental temperatures from the second run were first edited by increasing the number of elements from 120 to 132 and those from the third run were increased from 90 to 132 elements. Similarly the elements which were considered to have spalled were all assigned a temperature of 960°C in the SAFE-RCC run.

The same type of analysis as described above was performed with the progressive spalling that occurs on the sides of the column cross sections as illustrated in Figures 6.5 and 6.6. In this case, spalling condition representing 14.5% of the total area was considered to have spalled after 15 minutes and a further 13.5% after 30 minutes representing a total of 28% of the total area.

The next chapter, Chapter 7 deals with the effect of variation in modelling parameters on the behaviour of reinforced concrete columns in a fire environment.

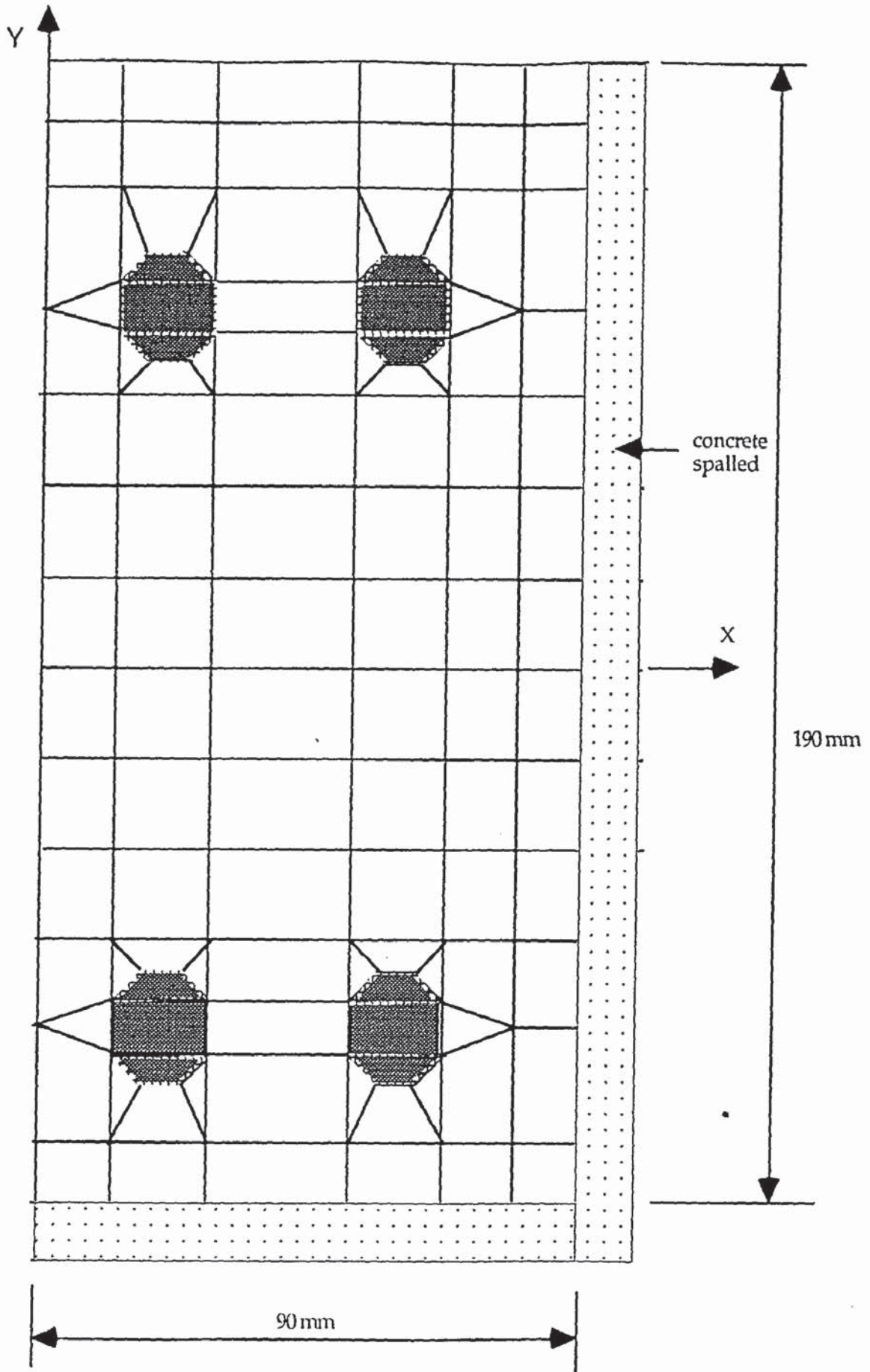


Figure 6.5: Example of finite element mesh for spalling condition representing 14.5% of the total area

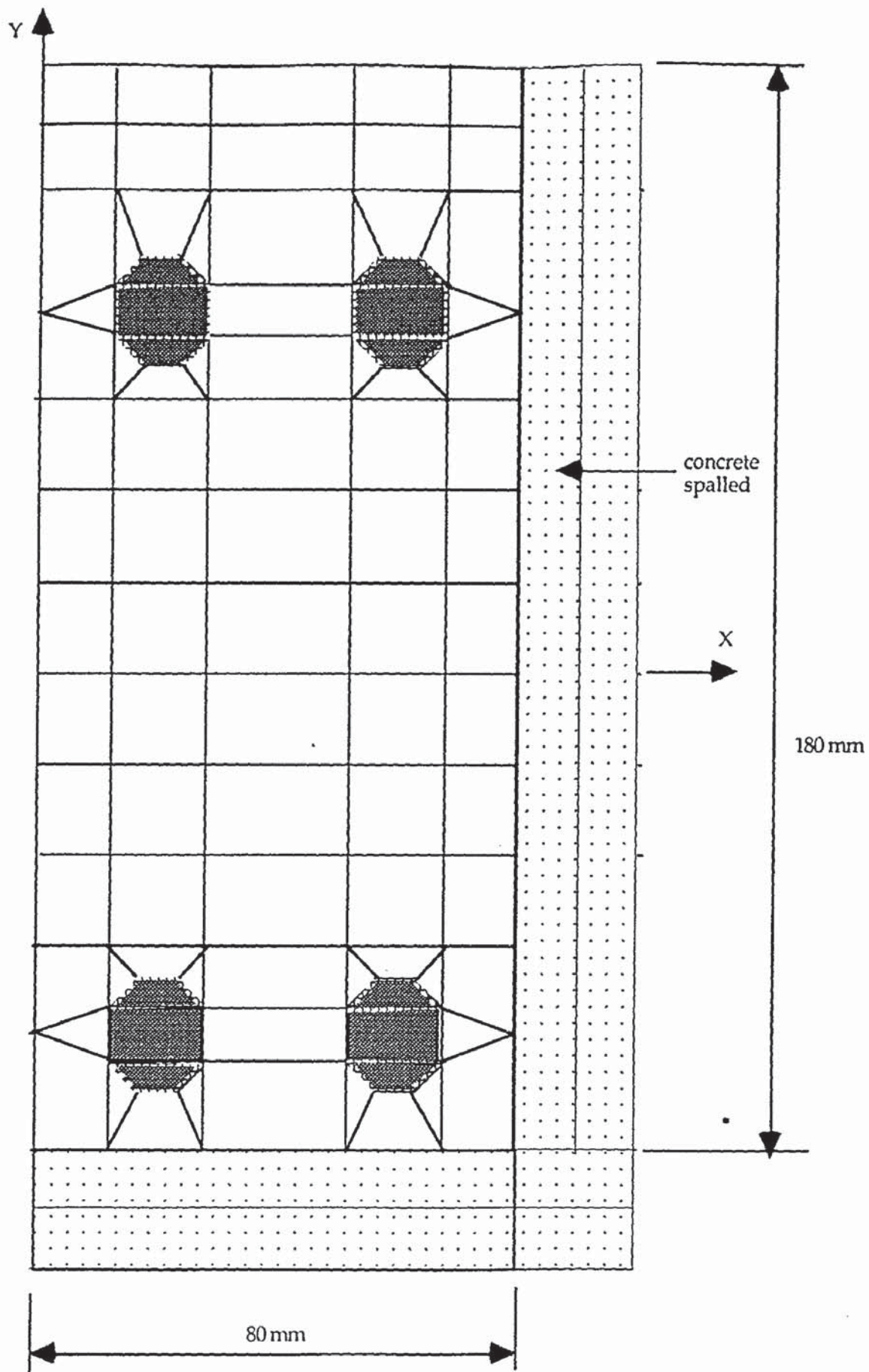


Figure 6.6: Example of finite element mesh for spalling condition representing 28% of the total area

CHAPTER SEVEN

EFFECT OF VARIATION IN MODELLING PARAMETERS ON COLUMN BEHAVIOUR

7.1 INTRODUCTION

The advent of computer modelling has opened new ways to assess the fire risks of intricate structural systems. Through an approach of a parametric study computer models can be employed to study the effect of different mesh designs on the temperature distribution histories across cross sections of structural elements. Alternative methods can be used to simulate a boundary condition that defines the interaction between a structural element with the surrounding fire environment. Several formulations have also been proposed by various researchers for determining the effect of different concrete material models on the fire resistance of concrete elements exposed to fire. These formulations pertain to those proposed by Anderberg and Thelandersson (1976), Schneider (1986) and Lie and Chabot (1990) and have been discussed in preceding chapters.

In this chapter comparisons are made between the effect of various mesh designs on the temperature distribution histories across a column cross section as well as the possible alternative methods to simulate a cool face boundary condition. Comparisons are also made between the calculated response using each model for a reinforced concrete column subjected to various loading conditions exposed to a standard fire. The constitutive model of Anderberg and Thelandersson (1976) adopted in this research is slightly modified and incorporates the Baldwin and

North formulation for the stress-strain relationship. For simplicity, the constitutive model of Anderberg and Thelandersson (1976) is henceforth referred to as Anderberg whilst that due to Lie and Chabot (1990) as Lie.

The validation of the computer models is achieved through a quantitative verification against actual tests performed by Haksever and Anderberg (1982) to determine the performance of reinforced concrete columns after exposure to fire. The reinforced concrete columns loaded either concentrically or eccentrically through an hydraulic system were exposed to heating from three sides to the usual regime of ISO 834. The columns were 200 mm square, 2 m long reinforced with 8 No. 16 mm bars. The test arrangement is illustrated in Figure 7.1. Comparisons were then made between the measured and calculated temperatures, deformations and fire resistances of each model.

In order to predict the thermal response of the column cross section FIRES-T was employed. For continuity, the thermal properties and values of parameters used in the calculation are similar to those used by Weeks (1985) and are shown in Tables 7.1 to 7.4. The values of concrete and steel densities used are 2400 and 7850 kg/m³ respectively. A schematic diagram indicating the boundary conditions and the material types used in FIRES-T are shown in Figures 7.2 and 7.3. In the FIRES-T run, the time step increments were set to 3 minutes for the first 48 minutes. Thereafter, the increments were increased to 6 minutes.



Figure 7.1: Illustration of testing arrangement (Haksever and Anderberg, 1982)

Temperature (°C)	Value (J/hm°C)
20	6480
100	4680
225	4320
380	4320
600	3420
900	3240
1000	2950

Table 7.1: Values of thermal conductivity for quartzite concrete used in calculation. (Anderberg, 1976).

Temperature (°C)	Value (J/kg°C)
20	850
200	1100
400	1250
1000	1300

Table 7.2 : Values of specific heat for quartzite concrete used in calculation. (Harmathy, 1970).

Temperature (°C)	Value (J/hm°C)
20	180,000
200	171,000
800	135,000
1000	135,000

Table 7.3: Values of thermal conductivity for steel used in calculation. (Malhotra,1982).

Temperature (°C)	Value (J/kg°C)
20	475
700	775
900	650
1000	650

Table 7.4 : Values of specific heat for steel used in calculation. (Malhotra, 1982).

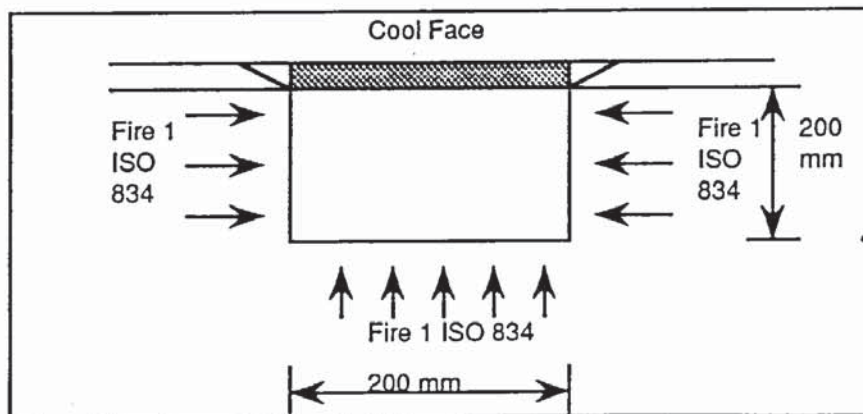


Figure 7.2: Schematic diagram indicating the boundary conditions used in FIRES-T run for the test column.

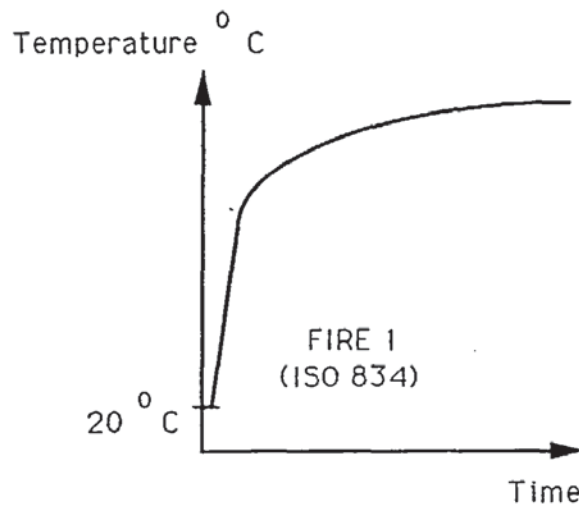
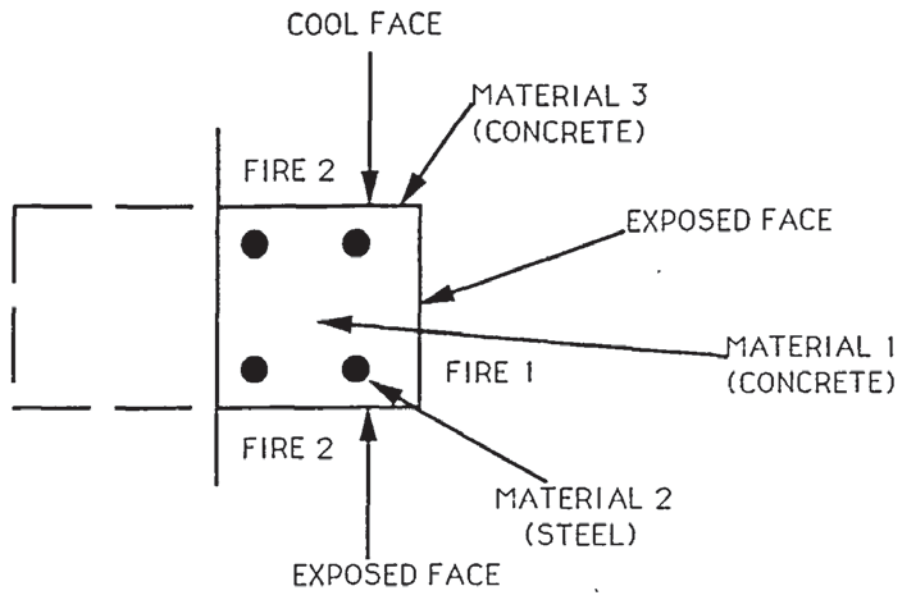


Figure 7.3: Schematic diagram indicating the material types used in the FIRES-T run for the test column.

7.2 EFFECT OF MESH DESIGNS ON THE TEMPERATURE DISTRIBUTION HISTORIES

The effect of mesh designs on the temperature distribution histories across the column cross section was investigated first. Three different mesh designs were employed for the column, each containing 112, 132 and 152 elements over half of the cross section. The difference in the mesh designs was due to the size of the finite element meshes employed to discretise the cross section. The choice of mesh was based on the need to employ a fine element in the vicinity of the fire boundary since a steep temperature gradient is to be expected. A coarser mesh was employed at the centre of the column where the gradient is expected to be lower. A typical mesh design with 132 elements is shown in Figure 6.1. The plane of symmetry in each case is modelled as an insulated surface with $Q_k = 0$.

The calculated concrete temperatures obtained were compared to those measured at various depths in the column under test as illustrated in Figures 7.4 to 7.6. The comparisons illustrate that good agreement is achieved between the modelled concrete temperatures and the temperatures measured during the test. Temperatures at 200 mm depth measured from the cool face which corresponds to the fire exposed face exhibit the largest disagreement where the measured temperatures are higher than those calculated. Weeks (1985) suggested that this could be due to the thermocouple at this point measuring the furnace temperatures rather than the surface of the column whilst the calculated temperatures correspond to the surface.

The next section deals with the effect of modelling the cool face behaviour on the temperature distribution histories across the column cross section.

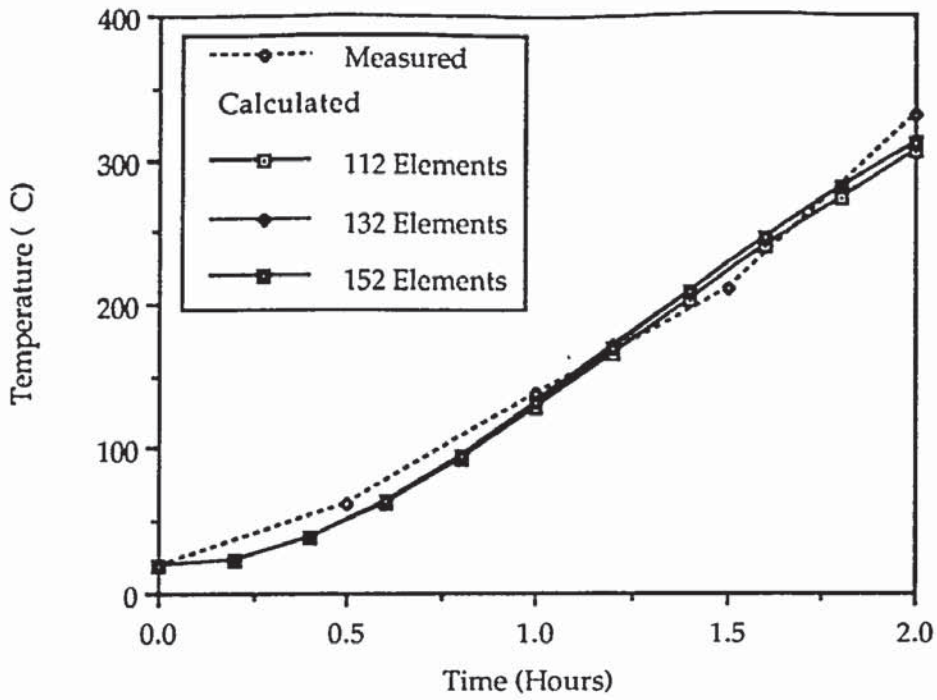


Figure 7.4: Temperature at 100 mm depth in a reinforced concrete column as a function of time (fire exposure time: 2 hours)

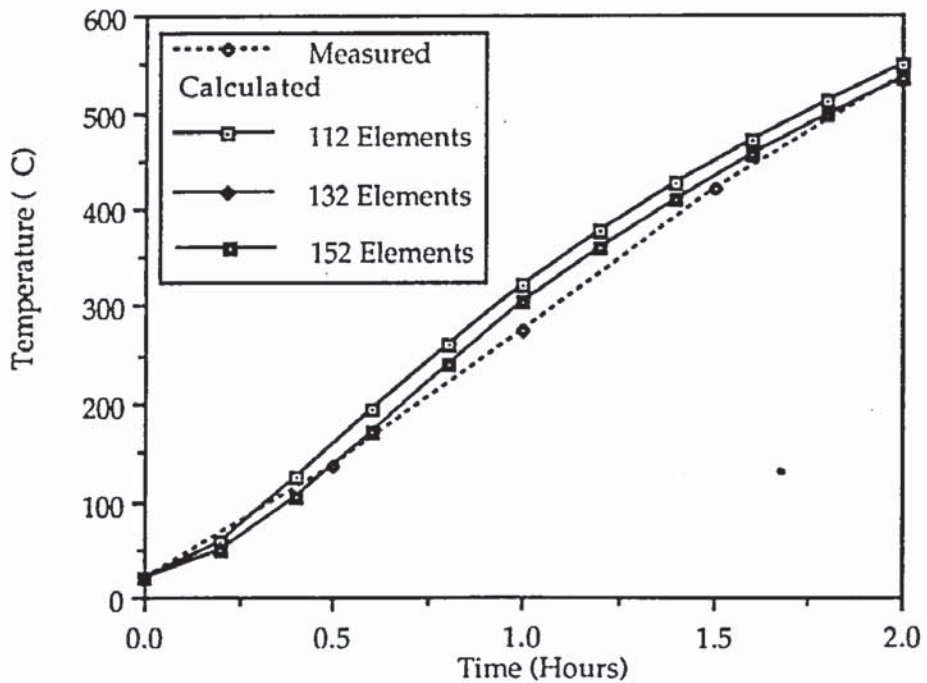


Figure 7.5: Temperature at 160 mm depth in a reinforced concrete column as a function of time (fire exposure time: 2 hours)

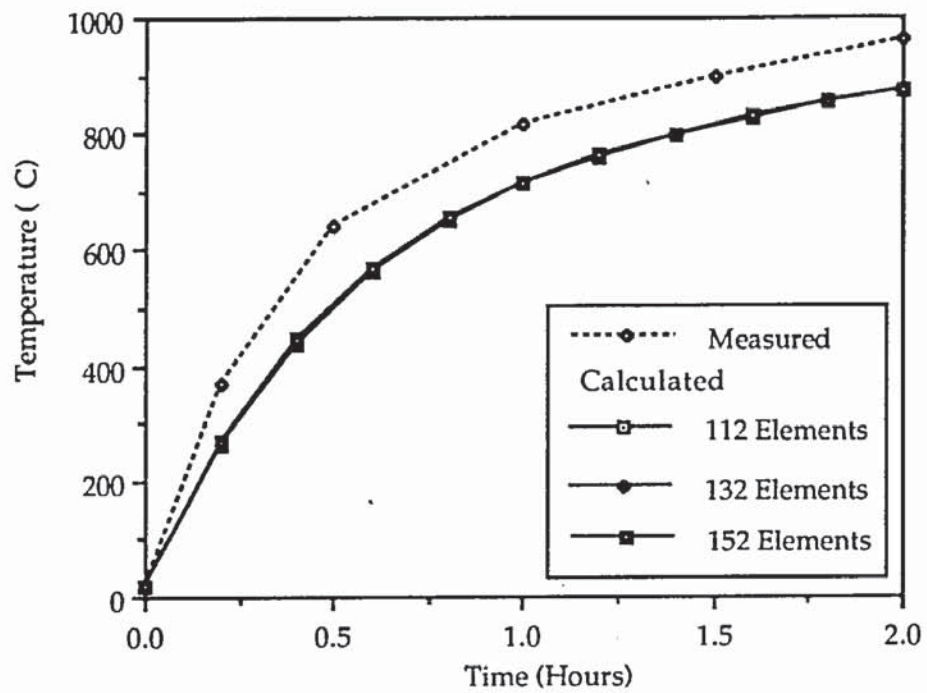


Figure 7.6: Temperature at 200 mm depth in a reinforced concrete column as a function of time (fire exposure time: 2 hours)

7.3 EFFECT OF BOUNDARY CONDITIONS ON THE TEMPERATURE DISTRIBUTION HISTORIES

An investigation was also made of possible alternative methods to simulate the cool face behaviour (see Figure 7.2). Three different boundary conditions were considered. Firstly, the nodal temperatures at the cool face were specified as known temperature condition of 20°C whilst the 21 surface elements on the fire-exposed face (see Figure 6.1) were subjected to the regime of ISO 834. Secondly, the surface elements on the cool face were specified as second material type having values of cool face parameters (see Table 5.1) whilst the fire-exposed face subjected to ISO 834. Thirdly, the surface elements were considered as being exposed to two fire types with the cool face exposed to a linear fire curve of constant temperature 20°C whilst the fire-exposed face subjected to the non-linear ISO 834. In all three cases the fire-exposed face was assigned the values of fire-exposed parameters specified in Table 5.1. Table 7.5 summarises the different boundary conditions. Comparisons were then made of the calculated temperatures from each boundary condition with the measured temperature distributions across the column cross section from Haksever and Anderberg (1982). The results are shown in Figures 7.7 to 7.9 for various depths in the column. Comparisons between the different boundary conditions indicate that there is no significant difference in the temperature distribution histories generated for this range of temperatures.

The temperature distribution histories obtained from the 132-finite element meshes with the cool face modelled as specified temperature boundary conditions

Types	Description of Boundary Conditions
BC1	Specified Boundary Condition: Cool face specified at 20°C
BC2	Flow Boundary Condition: Cool face specified as second material type
BC3	Fire Boundary Condition: Cool face specified as exposed to fire with temperature constant at 20°C

Table 7.5: Boundary conditions for simulating cool face.

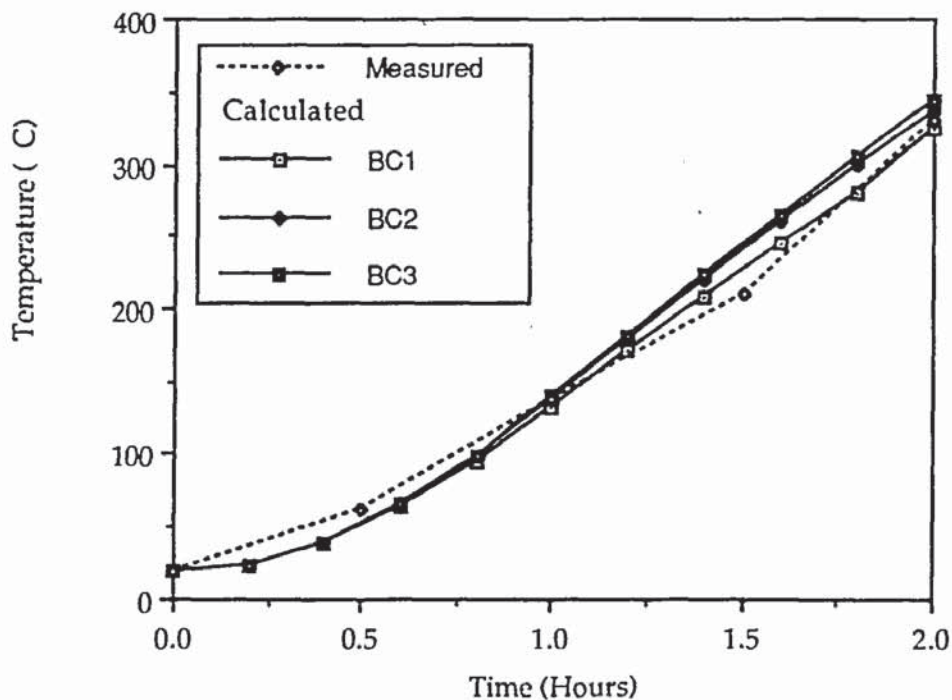


Figure 7.7: Temperature at 100 mm depth in a reinforced concrete column as a function of time (fire exposure time: 2 hours)

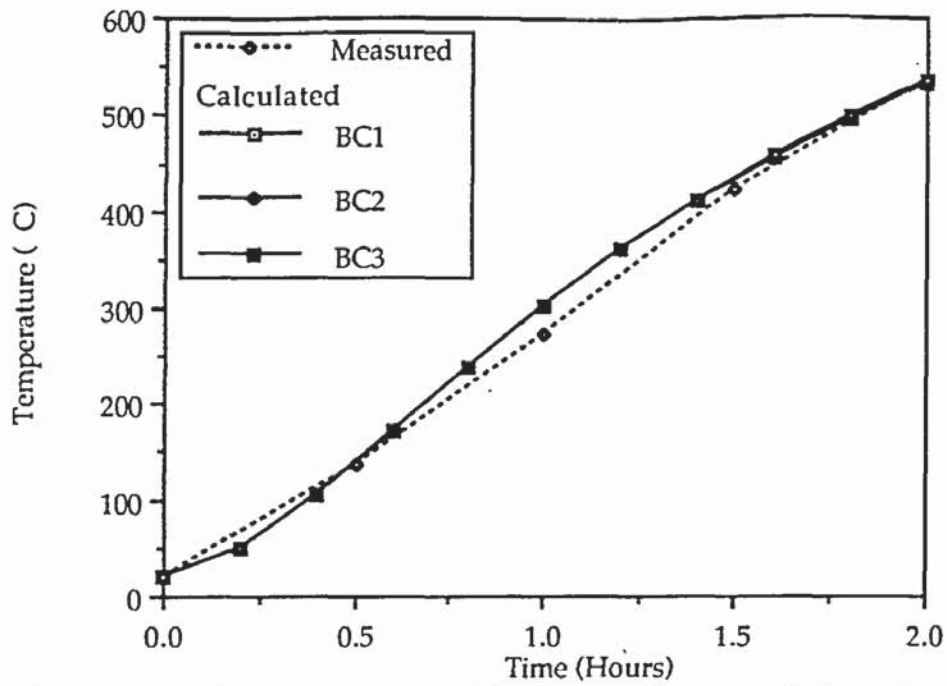


Figure 7.8: Temperature at 160 mm depth in a reinforced concrete column as a function of time (fire exposure time: 2 hours)

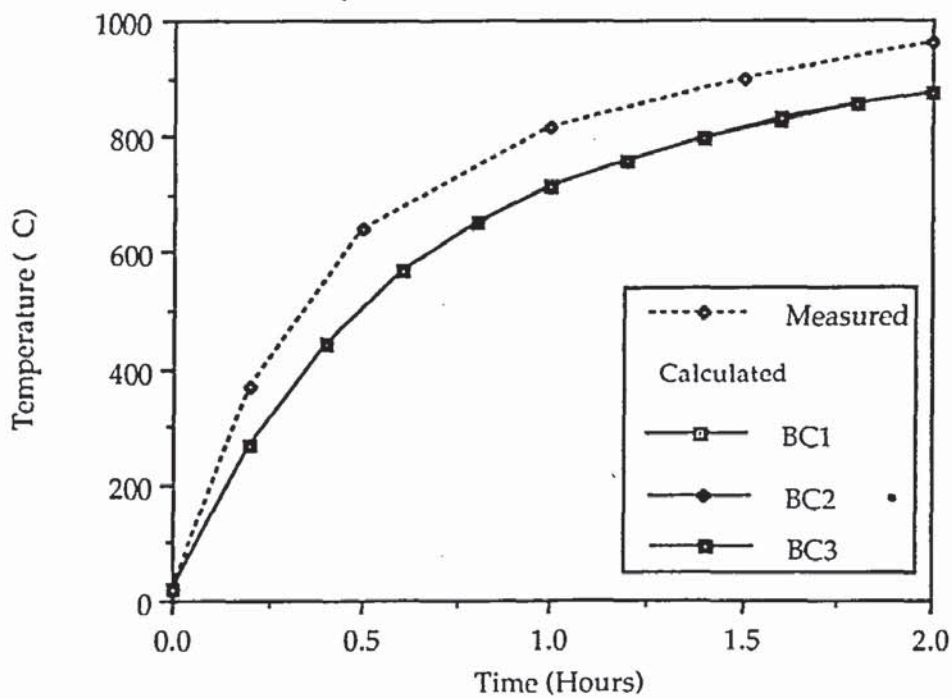


Figure 7.9: Temperature at 200 mm depth in a reinforced concrete column as a function of time (fire exposure time: 2 hours)

(case BC1) were then used as data for the structural response program SAFE-RCC in all the subsequent sections.

7.4 COMPARISONS BETWEEN THE EFFECT OF DIFFERENT CONCRETE MATERIAL MODELS ON THE STRUCTURAL RESPONSE

Comparisons between the effects of the different concrete material models on the column behaviour in fires are made under various loading conditions. Three columns were tested; one loaded concentrically and two eccentrically. Column C1 was concentrically loaded to 900 kN, column C2 to 600 kN with eccentricity of 60 mm directed away from the furnace whilst column C3 was loaded to 300 kN with an eccentricity of 60 mm towards the furnace. The loading arrangement is summarised in Table 7.6.

In order to predict the structural response using SAFE-RCC the two metre long column was divided into 10 equal segments. The 11 segment division points were further subdivided into 132 elements for the half column section or 264 elements for the whole section due to symmetry. The basic materials data for the concrete and reinforcing steel used in the calculation of the structural response are presented in Tables 7.7 to 7.10. A constant value of 15×10^{-6} per °C was used for the value of the steel coefficient of thermal expansion. The materials data adopted are similar to those used by Weeks (1985) and are taken to be reasonable for this project since this investigation concerns with the comparisons between the effects of the different concrete material models on the column behaviour in fires.

The mid-height deflection and axial deformation that occurred during the actual tests on the columns are shown in Figures 7.10 to 7.12 by the dashed line curves

whilst the calculated values for the concrete models are shown by the full lines. Deflection away from furnace and axial elongation are taken as positive for all columns. The calculated and measured fire resistances of the columns are tabulated in Table 7.11. M1 and M2 refer to the constitutive models of Anderberg and Schneider respectively that incorporate the transient strain effects whilst M3 refers to the constitutive model of Lie that omits the transient strain effects.

Haksever and Anderberg (1982) commented that column C1 exploded after 52 minutes in the test due to high moisture content of about 6% and due to high load level. The estimated failure time was about 60 to 65 minutes. As can be seen from Figure 7.10(a) and Figure 7.10(b) the measured curves and calculated curves from M1 are relatively close together followed by those from M2. The curves from M3 appear to lag behind and give a significantly longer fire resistance time than M1 and M2. As illustrated in Figure 7.10(a), the measured mid-height deflection was initially towards the furnace but changed sign at 30 minutes. A similar trend is also observed with M1 and M2. However, M3 predicts that the column would continue to deflect towards the furnace until failure occurred.

Figure 7.10(b) also shows that the axial deformation during the first 30 minutes of the test was almost zero. Increased column shortening then occurs with increased deflection. Calculated axial deformations from M1 and M2 both show axial elongations during the initial stages of the fire. In a similar trend to the test, increased deflection then causes increased shortening. However, M3 predicts that the column would continue to expand until failure occurred. As can be seen from the figure, M1 and M2 give a significantly better prediction for the deformation behaviour of the column.

For column C2, Haksever and Anderberg (1982) indicated that the test measurements were terminated after 30 minutes due to a support failure. The estimated failure time was 48 minutes. However, a comparison between measured and calculated deformations is still of interest.

Figure 7.11 (a) and (b) respectively show the measured and calculated mid-height deflection and axial deformation for column C2. As can be seen from the figures the calculated curves are almost parallel to those measured and agreement between the deformation and calculated failure times is generally quite good for M1 and M2. However, M3 gives a large mid-height deflection and axial deformation at a much longer time of failure. Similarly to C1, M1 and M2 give a significantly better prediction for the deformation behaviour of column C2 than M3.

Comparison between the measured and calculated mid-height deflections for column C3 is shown in Figure 7.12 (a). The calculated mid-height deflections from M1 and M2 were directed towards the furnace for the first 75 minutes but then changed sign and followed the measured curve until failure occurs. However, M2 gives a much smaller deflection at failure than M1 with both being lower than that measured. The mid-height deflection from M3 does not follow a similar trend in that the column continued to bend towards the furnace until failure.

Figure 7.12 (b) shows that for measured axial deformation and for that calculated by M1 and M2, the column expanded axially during the first 80 minutes but then changed into compression although the calculated axial deformations are less than 50% of that measured at failure. On the contrary, M3 predicts axial expansion of the column throughout the period of fire exposure.

Types of Column	Load (kN)	Eccentricity (mm)	Comments
C1	900	0.0	Exposed to heating on 3 sides
C2	600	+60.0*	Exposed to heating on 3 sides
C3	300	-60.0**	Exposed to heating on 3 sides

* eccentricity away from furnace

** eccentricity towards furnace

Table 7.6: Types of column and loading conditions.

Temperature (°C)	Proportionate loss of strength (Anderberg (1976))	σ_{\max} (N/mm ²)
20	1.0	36.80
135	1.02	37.54
265	0.95	34.96
400	0.95	34.96
450	0.75	27.60
500	0.55	20.24
650	0.35	12.88
960	0.05	1.84

Table 7.7: Variation of maximum concrete stress with temperature.

Temperature (°C)	ϵ_{\max}
20	0.0024
100	0.0030
200	0.00325
300	0.0036
400	0.0044
500	0.0055
600	0.0070
960	0.0142

Table 7.8: Variation on the concrete strain at maximum stress with temperature. (Anderberg and Thelandersson, 1976).

Temperature (°C)	Proportionate loss of strength (Crook (1980))	Proof strength f_v (N/mm ²)
20	1.00	453.0
100	0.96	434.9
200	0.83	376.0
300	0.82	371.5
400	0.75	339.8
500	0.59	267.3
600	0.37	167.6
700	0.21	95.2

Table 7.9: Variation of steel proof strength with temperature.

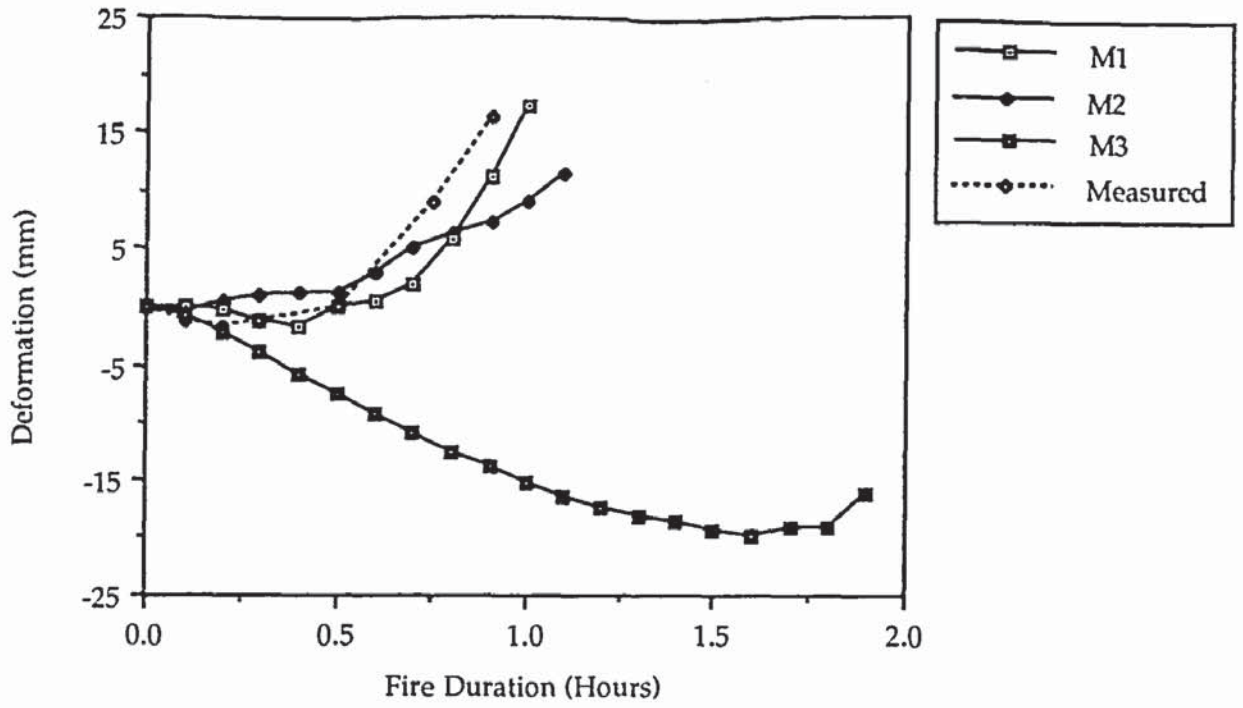
Temperature (°C)	Proportionate loss of strength (Anderberg (1976))	Elastic Modulus E_s (KN/mm ²)
20	1.00	210.0
100	1.00	210.0
200	0.98	205.8
300	0.89	186.9
400	0.77	161.7
500	0.62	130.2
600	0.40	84.0
700	0.15	31.5

Table 7.10: Variation of steel initial tangent modulus with temperature.

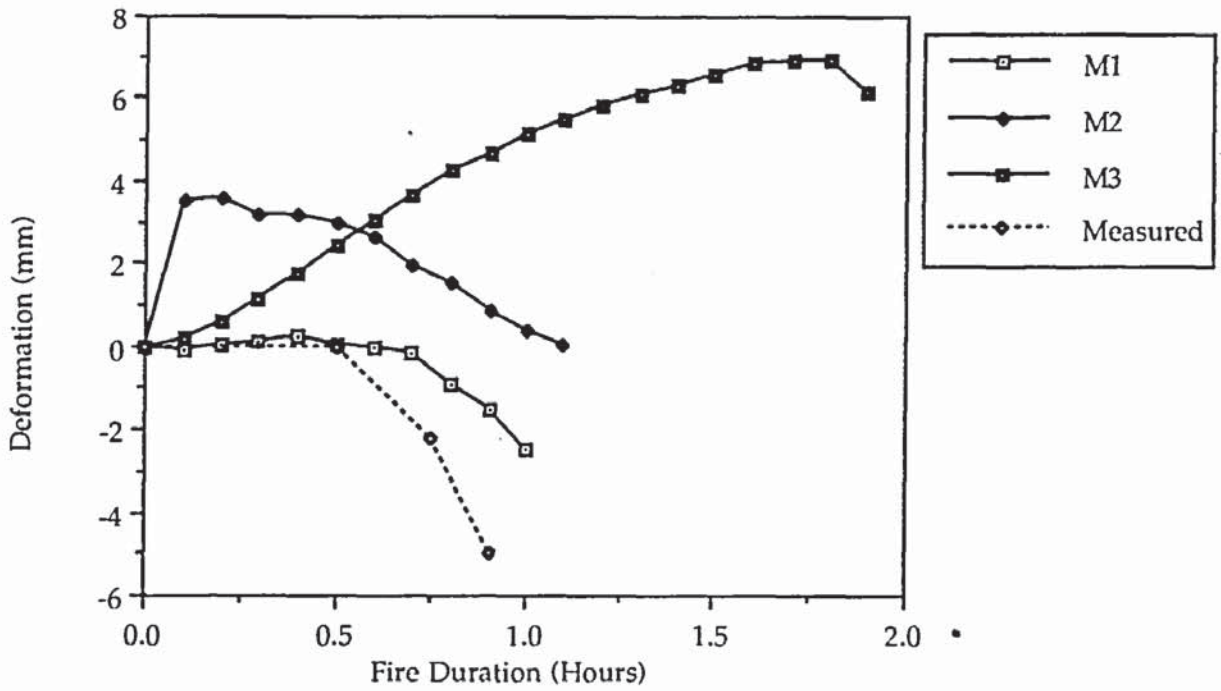
Model	Time to Failure (Minutes)		
	C1	C2	C3
M1	60	39	96
M2	66	36	90
M3	114	84	132
Test	52	30*	108

*test terminated due to a support failure

Table 7.11: Calculated and measured fire resistances of the columns.

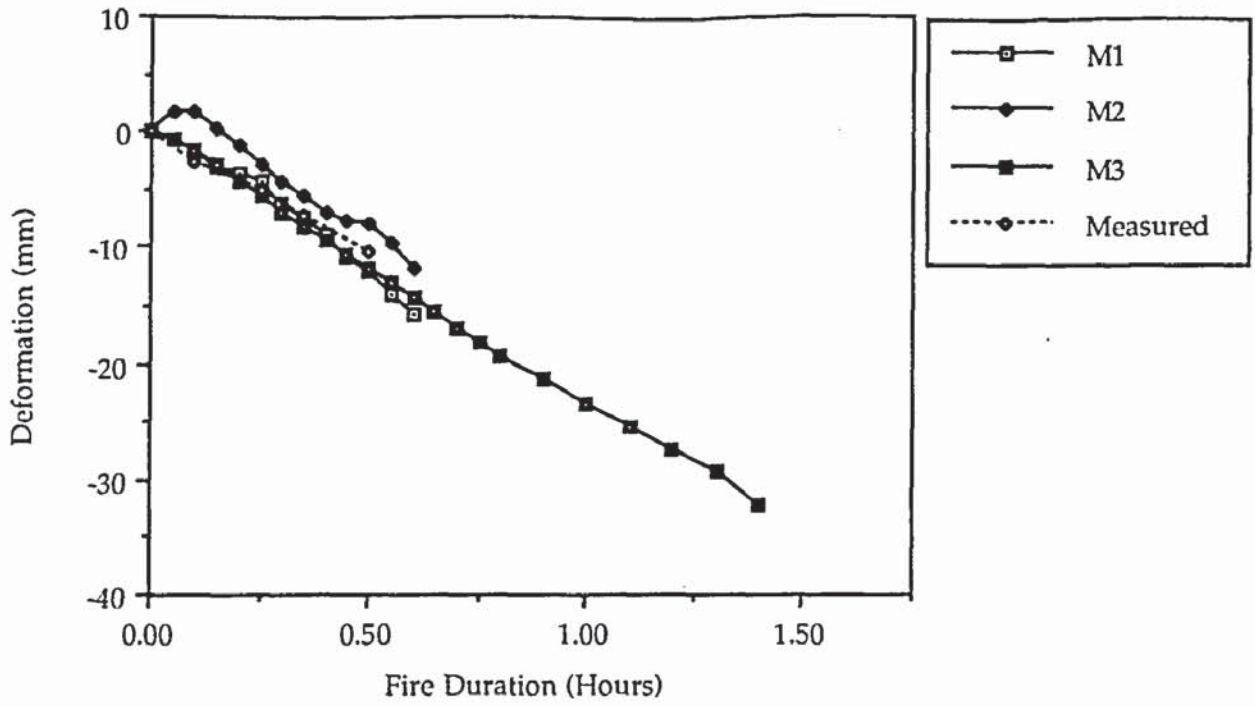


a) mid-height deflection

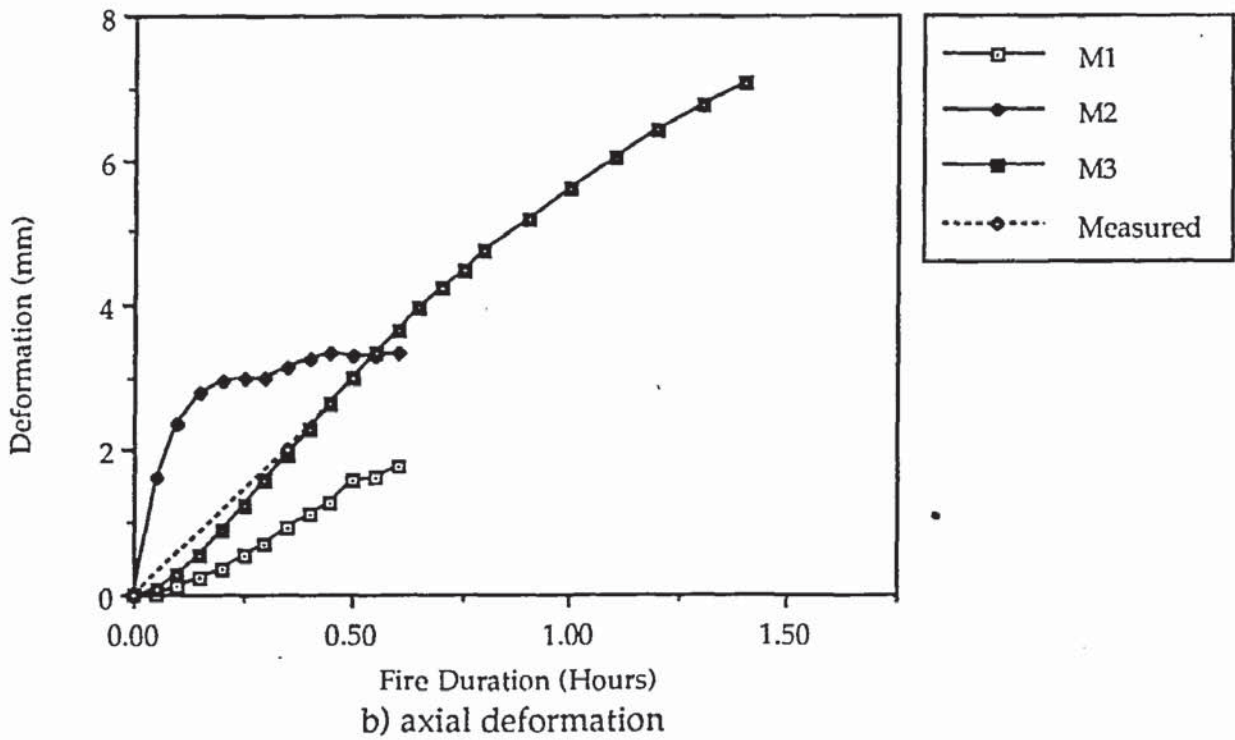


b) axial deformation

Figure 7.10: Measured and calculated behaviour of column C1

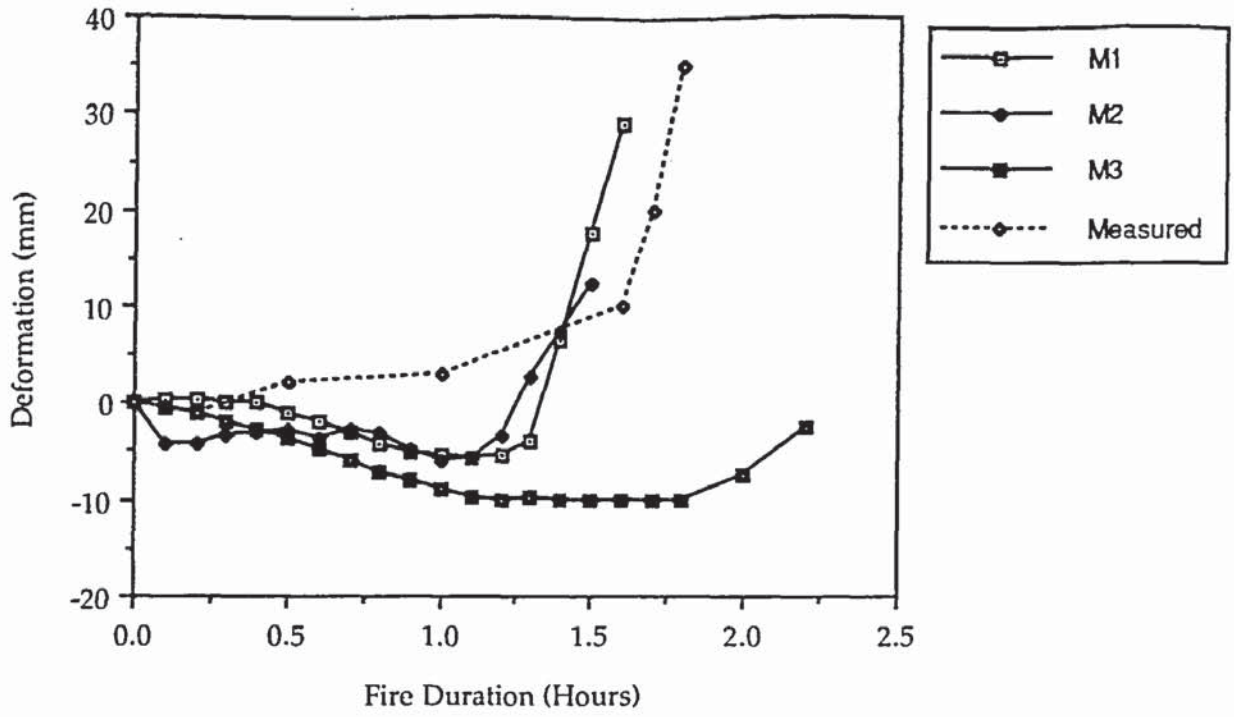


a) mid-height deflection

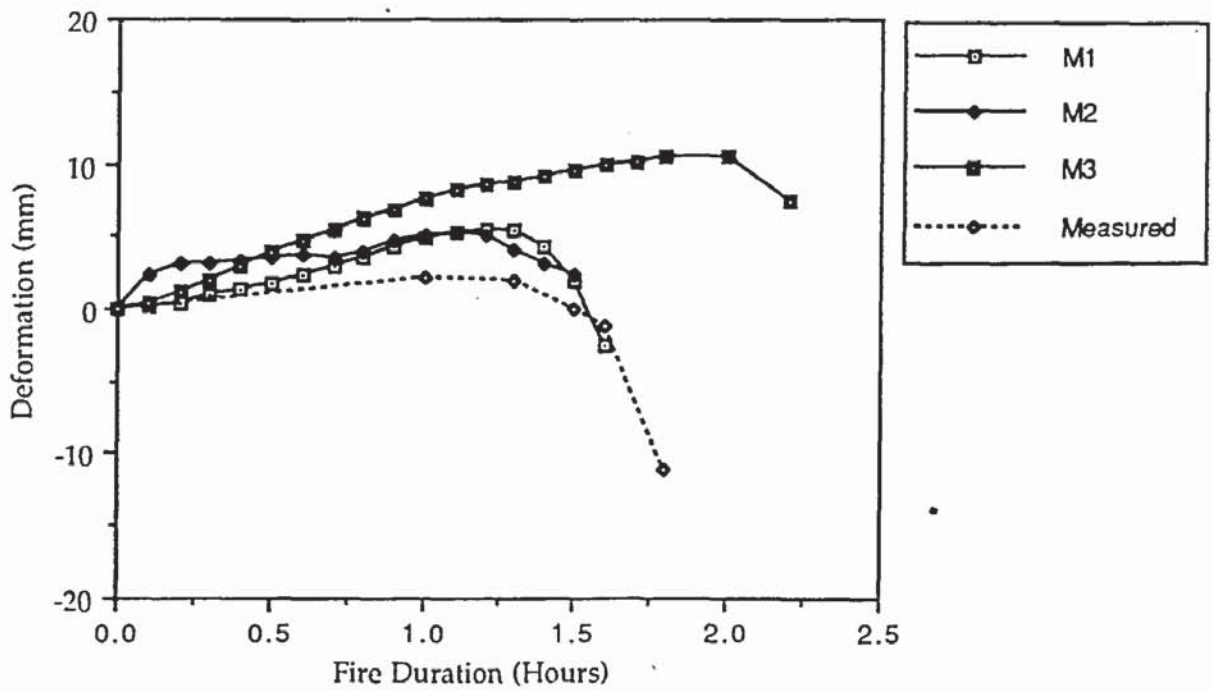


b) axial deformation

Figure 7.11: Measured and calculated behaviour of column C2



a) mid-height deflection



b) axial deformation

Figure 7.12: Measured and calculated behaviour of column C3

For column C3 the measured and calculated deformations are only qualitatively in agreement with M3 which predicts the longest fire resistance time. However, it can be seen from the figure that M1 gives a better prediction for the behaviour of the column where the mid-height deflection and axial deformation are closer to those measured.

7.5 CONCLUSION

It has been shown in this chapter that computer simulation lends itself ideally to an extensive parametric study which could be carried out to determine the structural response of a concrete element in fire environment. The effect of mesh design on the temperature distribution history in a column cross section, the possible alternative methods to simulate a boundary condition and its effect on the temperature distribution history and the effect of any material model adopted on the calculated response of a reinforced concrete column are some of the examples.

It has been shown that for this range of temperatures the different boundary conditions and mesh designs have a limited effect on the temperature distribution history in the column cross section.

It is generally known that in order to obtain a good correlation between test and calculated measurements, reliable material models will have to be developed that allow for the effect of degradation of the material properties as temperature increases. Unlike steel, the development of concrete material models is subjected to much debate as to whether the effects of transient strain ought to be included in any models used to predict the structural response. This chapter has illustrated

that good correlation between measured and calculated measurements can only be obtained with models M1 and M2 representing that of Anderberg and Schneider respectively. On the other hand, model M3 representing Lie does not give a reliable correlation between the measured and calculated measurements.

It should be noted that for column C3 the concrete compression face is exposed to the full effects of the fire and thus any problem due to variations in the concrete material models adopted has a significant effect on the calculated response of the column. On the other hand, the concrete compression face of column C2 corresponds to the cool face and the consequence of different concrete models will be far less marked. This explains the fact that the constitutive model of Lie exhibits the largest disagreement with the measured curves for column C3. For column C2 a similar trend is predicted to that observed although Lie predicts a much larger mid-height deflection and axial deformation at the time of failure. An intermediate state exists for column C1 as seen by the results.

For column C3, since the tension face where moisture can easily escape due to the presence of cracks is away from the exposed face, the moisture transport escape length will be large. Thus full quantitative comparison between test and computer calculation may not be achieved. On the contrary for column C2, the moisture content will be reduced very quickly since the tension face where cracks provide an easy moisture escape route is directly exposed to the fire.

It should be remembered that the computer calculation involves a number of simplifying assumptions which are unlikely to hold for the test column. Temperature variation along the column axis has not been considered and all the cross sections are assumed to be identical throughout the column. It has also been

assumed that moisture transport has no effect on either material or thermal properties. Complete agreement therefore cannot be expected between the observed test and calculated deformations. However, it can be expected that the overall trends should exhibit agreement.

The data plotted in Figures 7.10 through 7.12 clearly illustrate that a better response of a reinforced concrete column exposed to fire in all cases is given by a constitutive model with transient creep or appropriate strain effect of Anderberg or Schneider with Anderberg which gives a slightly better response. A model that does not include the transient strain such as that due to Lie gives less good results although in certain circumstances the difference may not be significant. A constitutive model for concrete that considers the effects of transient creep or appropriate strain effect therefore gives a significantly better prediction for the deformation behaviour of a reinforced concrete column compared to a model that omits the effect of transient strain component. Transient state models thus correspond largely to fire situations and bear closer relation to the conditions likely to be encountered in an actual fire conditions as the temperature variation is progressive whilst the material is under load.

CHAPTER EIGHT

THE EFFECT OF SPALLING ON COLUMN BEHAVIOUR

8.1 INTRODUCTION

The previous chapter established that the calculated response of a reinforced concrete column in a fire environment is significantly affected by the constitutive model adopted to simulate the behaviour of concrete at elevated temperatures. Investigation is now directed towards determining the extent to which the column behaviour is affected by the occurrence of spalling of concrete cover. Spalling of concrete in structural members as a result of exposure to fire is generally recognised as a problem though presently little information is available to quantify its effect.

It is accepted that computer simulation provides an alternative method of assessing the fire performance of a column. However, to date modelling capability is limited in that no account is taken of the phenomenon of spalling either in the thermal or structural analysis. The effect of spalling is a loss of concrete which can be represented by modifications to the finite element meshes used for the subdivision of the cross sectional area of the column.

The method adopted for the modelling of concrete columns exposed to fire which incorporate the effect of spalling by varying the amounts of concrete lost during a specified period of exposure to fire was described in Chapter 6. FIRES-T was used to simulate the thermal response of concrete columns with

the occurrence of spalling when exposed to ISO 834 furnace environment. Based on the predicted thermal response, the fire resistance of each column with varying amounts of spalling was determined using the structural response program SAFE-RCC. The material properties for the concrete and steel used to predict the thermal response of the cross sections and the data used to predict the structural response were as in Chapter 7.

8.2 DISCUSSION OF RESULTS

An array of three columns C1, C2 and C3 (see Table 7.6) and six different percentages of spalling namely 0%, 3.0%, 7.2%, 14.5%, 29.5% and 39% were considered for one range of simulations while a two stage progressive spalling regime conducted on similar columns was used for a second range of simulations. In both cases, sections of concrete material were deleted to simulate spalling of concrete after two periods of exposure of 15 and 30 minutes to the furnace environment. A similar procedure was also performed on a reference column C4 which was subjected to an axial load of 900 kN and exposed to the heating regime of ISO 834 on all four sides. The test arrangement and the dimension of column C4 are similar to columns C1, C2 and C3 as illustrated in Figure 7.1. As in Chapter 7, M1, M2 and M3 refer to the constitutive models of Anderberg, Schneider and Lie respectively.

The validation of column C4 is achieved through a quantitative verification against actual tests performed by Haksever, Haß and Kordina (1982). The original tests were conducted on axially loaded columns exposed to heating on all four sides with the ends fixed. Haksever, Haß and Kordina (1982) indicated that the fire resistances fell within the range 123 to 168 minutes. In this

investigation, a reduction in fire resistance is therefore expected due to changes in the buckling length as column C4 is idealised as pinned. A reduction to around 75 minutes for models M1 and M2 would seem reasonable.

After the computer simulations were completed four series of comparisons were made. The first involved comparisons of the effect of spalling on the temperature distribution history for concrete and steel elements in columns C1, C2, C3 and C4. The second, third and fourth comparisons were made between M1, M2 and M3. The second comparison was a determination of the effect of progressive spalling on the structural response of columns C1, C2, C3 and C4. The third involved comparisons of the mid-height deflection of columns C1, C2, C3 and C4 at failure with the percentage of spalling. The fourth involved comparisons of the fire resistance of the columns with the percentage of spalling to determine the severity of the loss of concrete on fire resistance. In both third and fourth comparisons, the mid-height deflections and the fire resistances obtained at the time of failure were compared using the amount of spalling evaluated as a percentage of total protection for an unspalled column.

For the first and second series of comparisons, designations SP1 to SP4 are employed as reference to the regime of progressive spalling that occurs on the sides of the column cross sections whilst designations SP5 to SP8 refer to that for progressive spalling on the corners. SP1 denotes the case with 14.5% of cross sectional area spalled after 15 minutes and a further 13.5% spalled after 30 minutes, SP2 denotes 14.5% of spalling occurring after 15 minutes, SP3 denotes 14.5% of spalling after 30 minutes whilst SP4 refers to that without spalling. SP5 denotes the case with 7.2% of cross sectional area spalled after 15 minutes and a further 22.3% spalled after 30 minutes, SP6 denotes 7.2% of

spalling occurring after 15 minutes, SP7 denotes 7.2% of spalling after 30 minutes whilst SP8 refers to that without spalling. Table 8.1 summarises the two regimes of progressive spalling as described above whilst Table 8.2 summarises the number of computer runs performed.

Comparisons between the effect of spalling on the temperature distribution history for various elements either steel or concrete (see Figure 6.1) in the columns are shown in Figures 8.1 to 8.11. Figures 8.1 to 8.6 illustrate the temperature history for elements in columns C1, C2 and C3 for the series of progressive spalling that occurs on the sides of the column cross sections. Figures 8.7 to 8.11 illustrate the temperature history for column C4 as a result of progressive spalling on the corners.

Figures 8.1 and 8.2 for columns C1, C2 and C3 and Figures 8.7 and 8.8 for column C4 appear to indicate that the effect of spalling causes more rapid temperature rises in the steel reinforcement. The SP5 case of column C4 exhibits the highest temperature rise as can be seen from Figure 8.7. In this case the steel reinforcement is directly exposed to the fire due to the loss of concrete cover. In addition, the figures reveal that comparison between the temperature distribution histories of SP2 and SP3 and between SP6 and SP7 shows a slight difference in that SP2 and SP6 respectively attain a slightly greater temperature than SP3 and SP7 especially for the first 60 minutes.

Comparisons between the temperature history for concrete elements are plotted in Figures 8.3 to 8.6 for columns C1, C2 and C3 and in Figures 8.9 to 8.11 for column C4. The figures appear to indicate a similar trend of behaviour of temperature distribution history as previously described for steel elements.

Series	Designation	Description on Amount and Time of Spalling
Regime 1	SP1	14.5% spalled after 15 minutes and a further 13.5% spalled after 30 minutes
	SP2	14.5% spalled after 15 minutes
	SP3	14.5% spalled after 30 minutes
	SP4	Reference column - no spalling
Regime 2	SP5	7.2% spalled after 15 minutes and a further 22.3% spalled after 30 minutes
	SP6	7.2% spalled after 15 minutes
	SP7	7.2% spalled after 30 minutes
	SP8	Reference column - no spalling

Table 8.1: Description of the amount and time of spalling for the two stage progressive spalling regimes.

Types of Column	Thermal Analysis		Structural Analysis	
	First Range of Spalling	Second Range of Spalling	First Range of Spalling	Second Range of Spalling
C1	22	6	36	6
C2			36	6
C3			36	6
C4	22	6	36	6

Table 8.2: Description of the number of computer runs performed

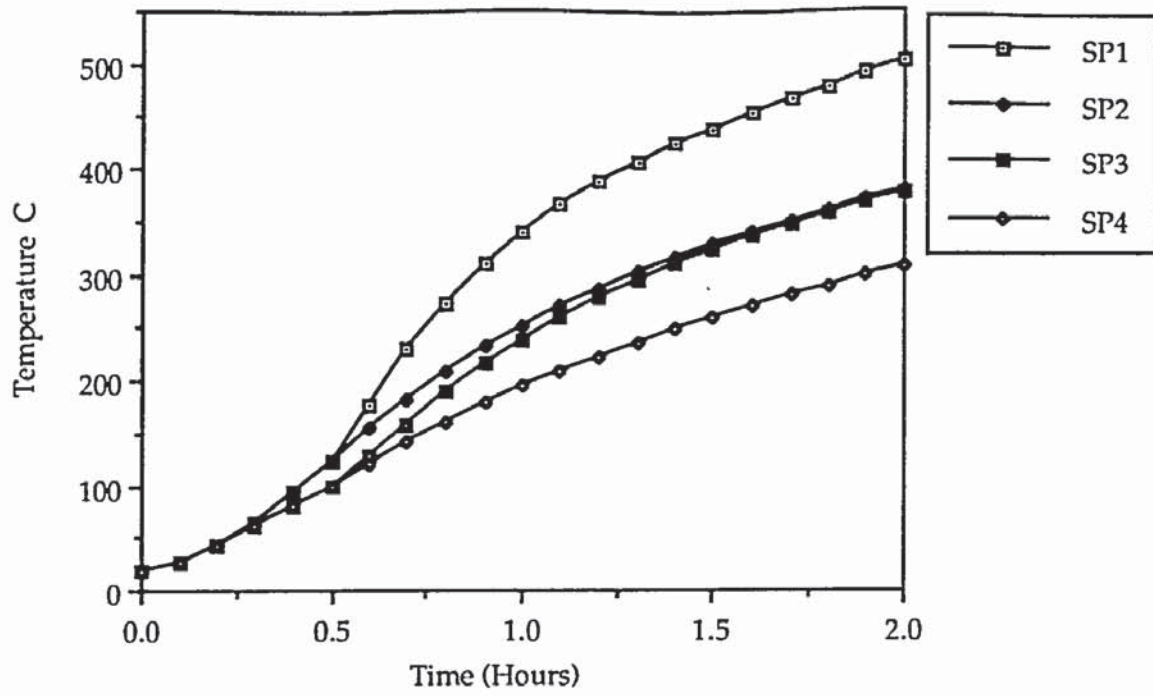


Figure 8.1: Temperature history for element 102 (steel) in columns C1, C2 and C3

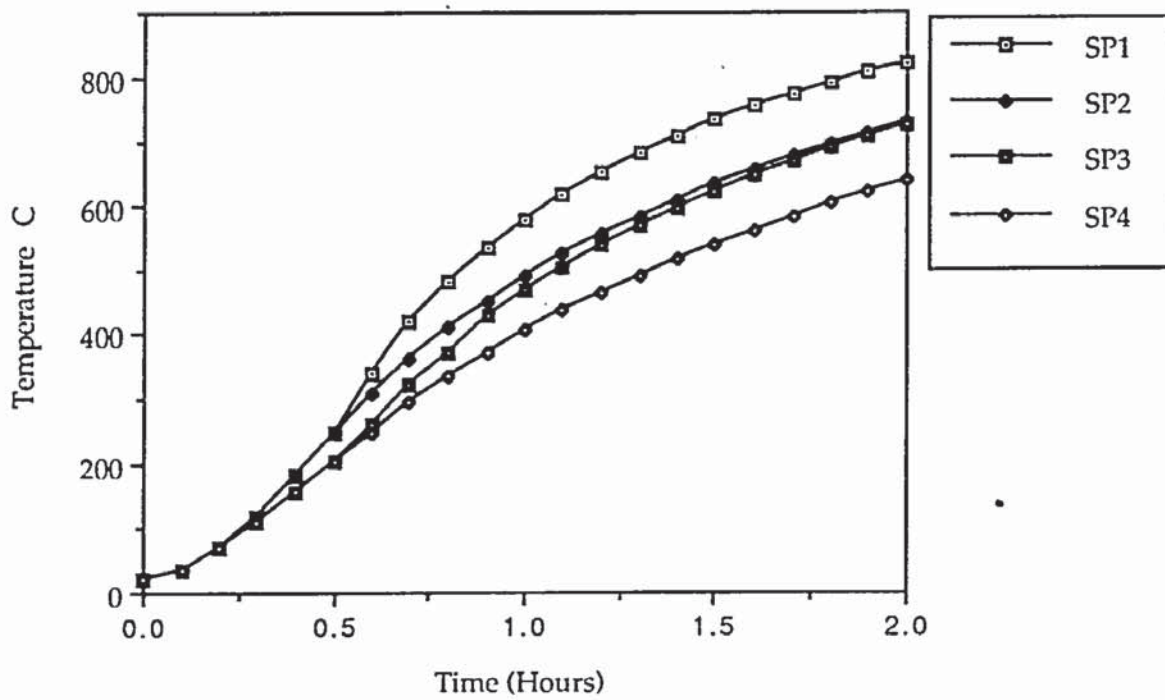


Figure 8.2: Temperature history for element 29 (steel) in columns C1, C2 and C3

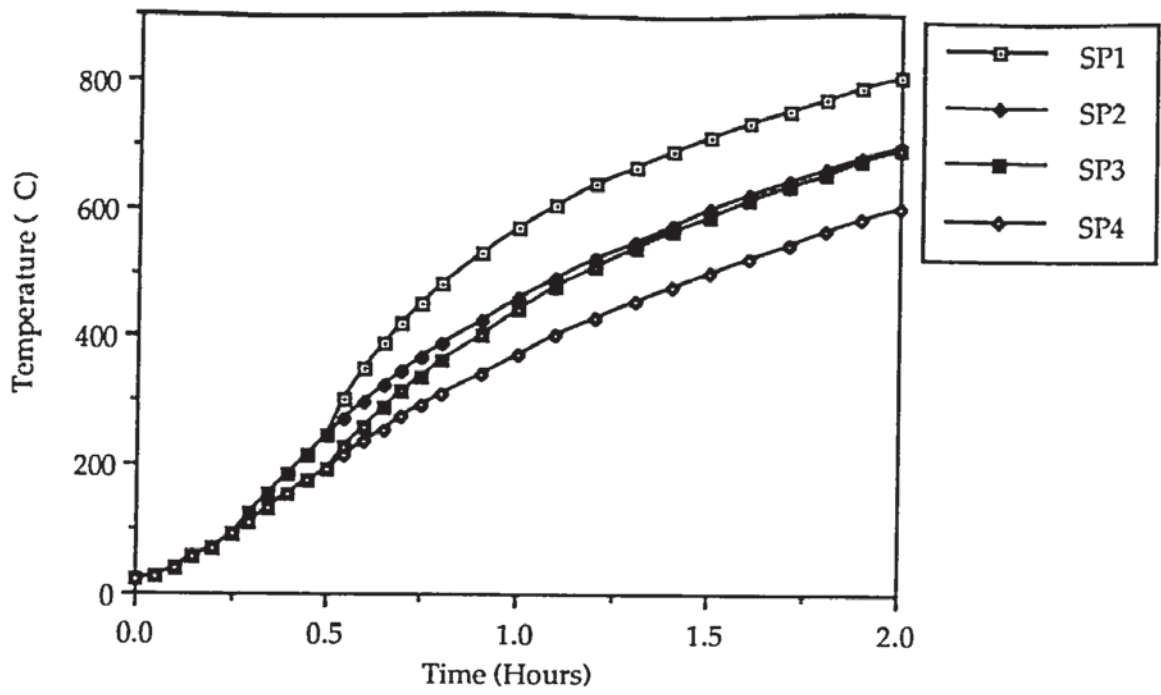


Figure 8.3: Temperature history for element 15 (concrete) in columns C1, C2 and C3

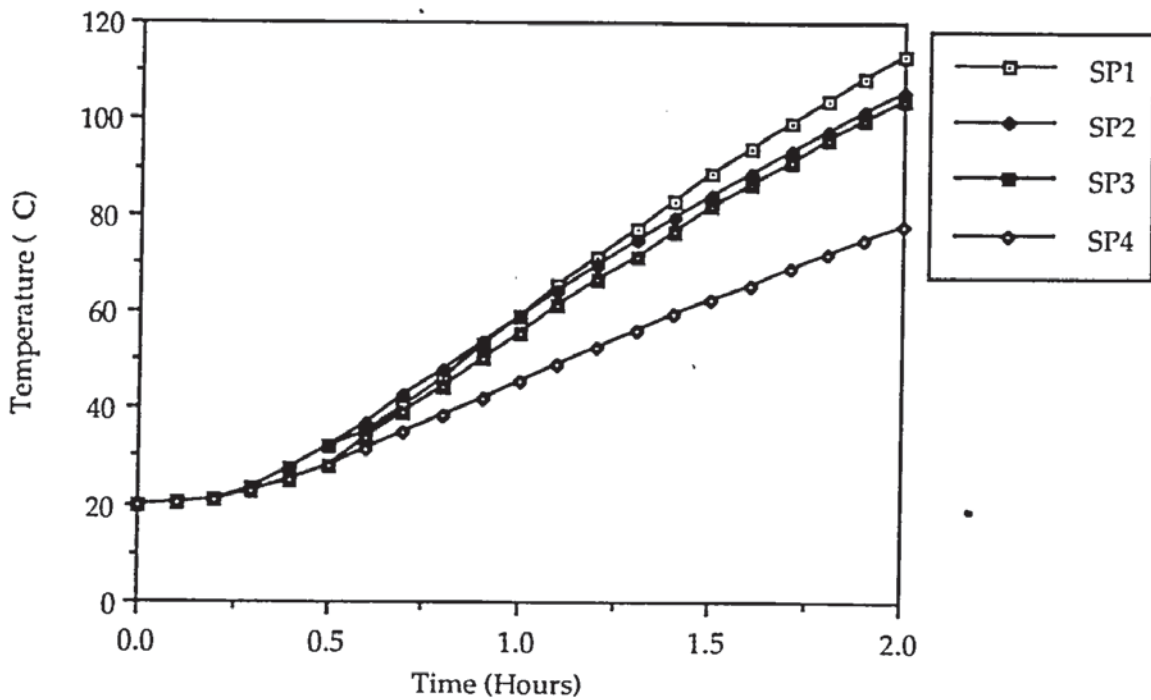


Figure 8.4: Temperature history for element 119 (concrete) in columns C1, C2 and C3

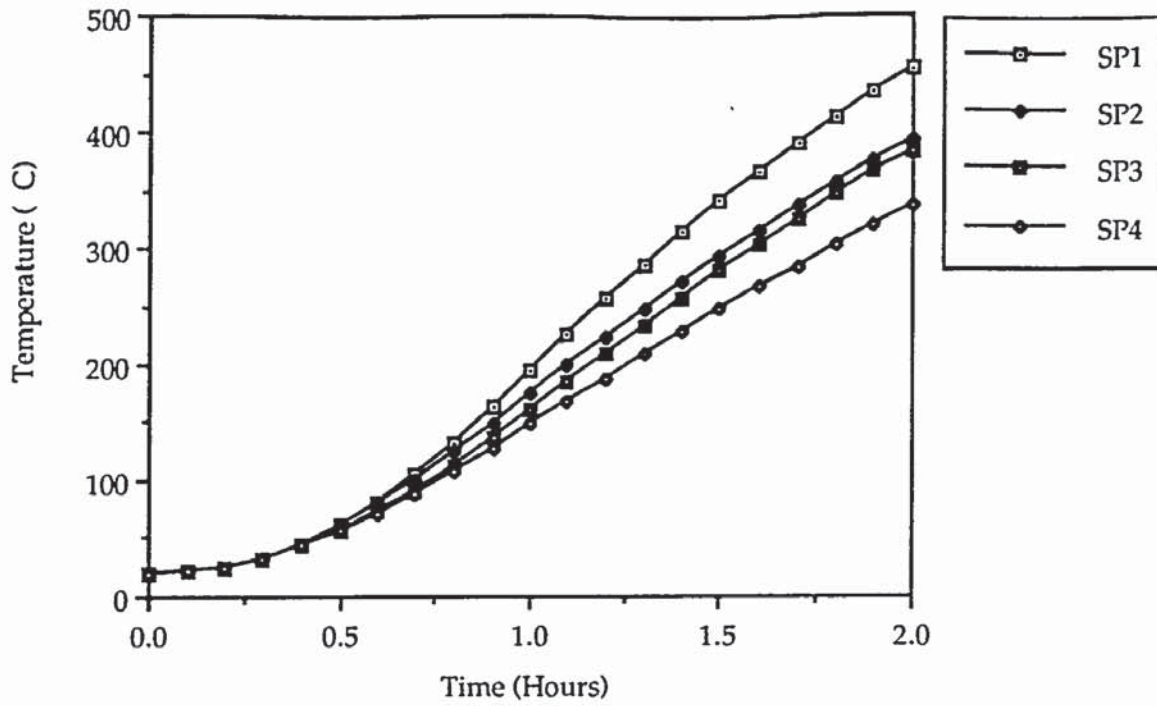


Figure 8.5: Temperature history for element 60 (concrete) in columns C1, C2 and C3

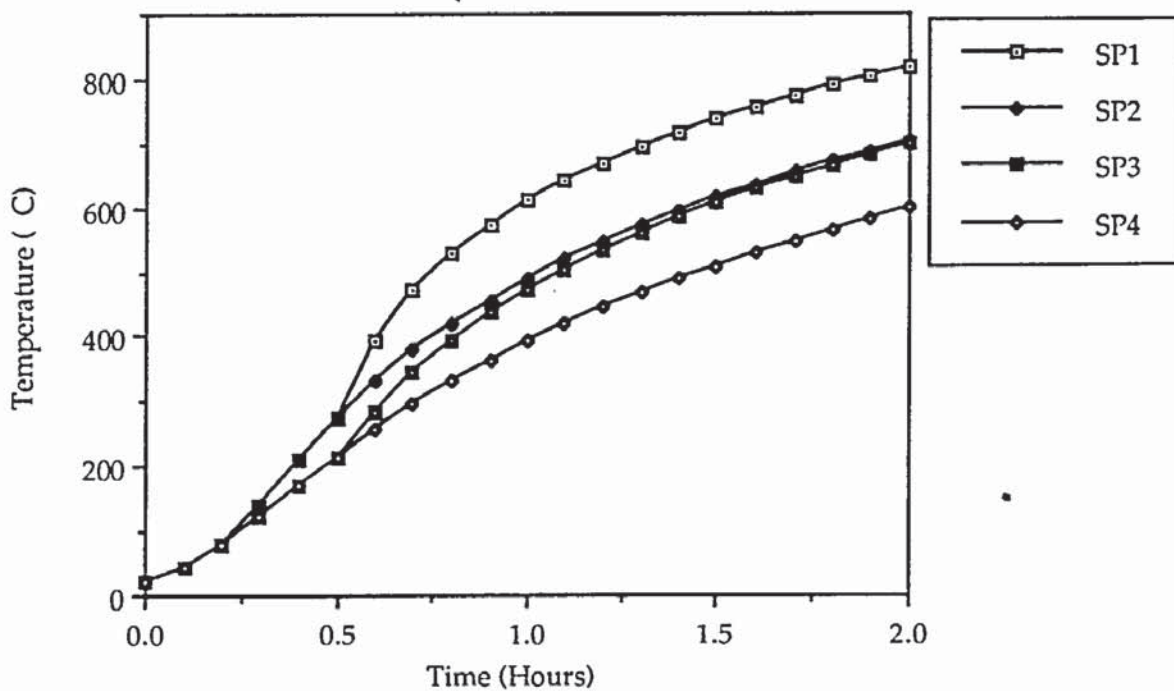


Figure 8.6: Temperature history for element 64 (concrete) in columns C1, C2 and C3

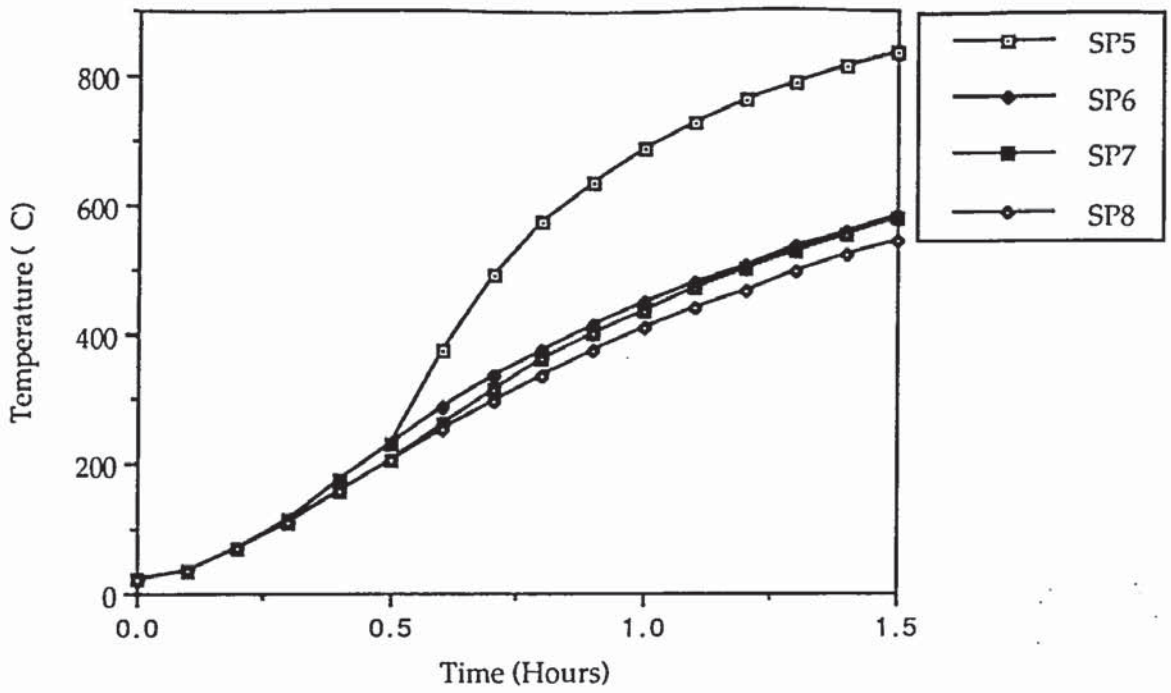


Figure 8.7: Temperature history in element 102 (steel) in column C4

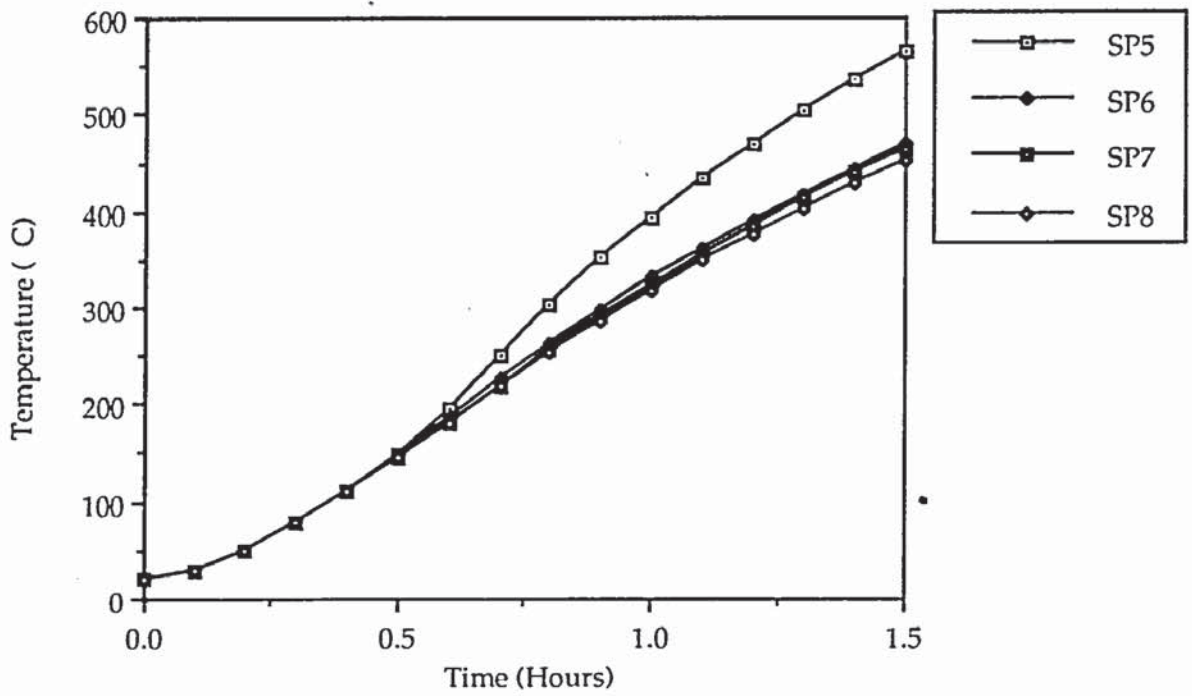


Figure 8.8: Temperature history in element 28 (steel) in column C4

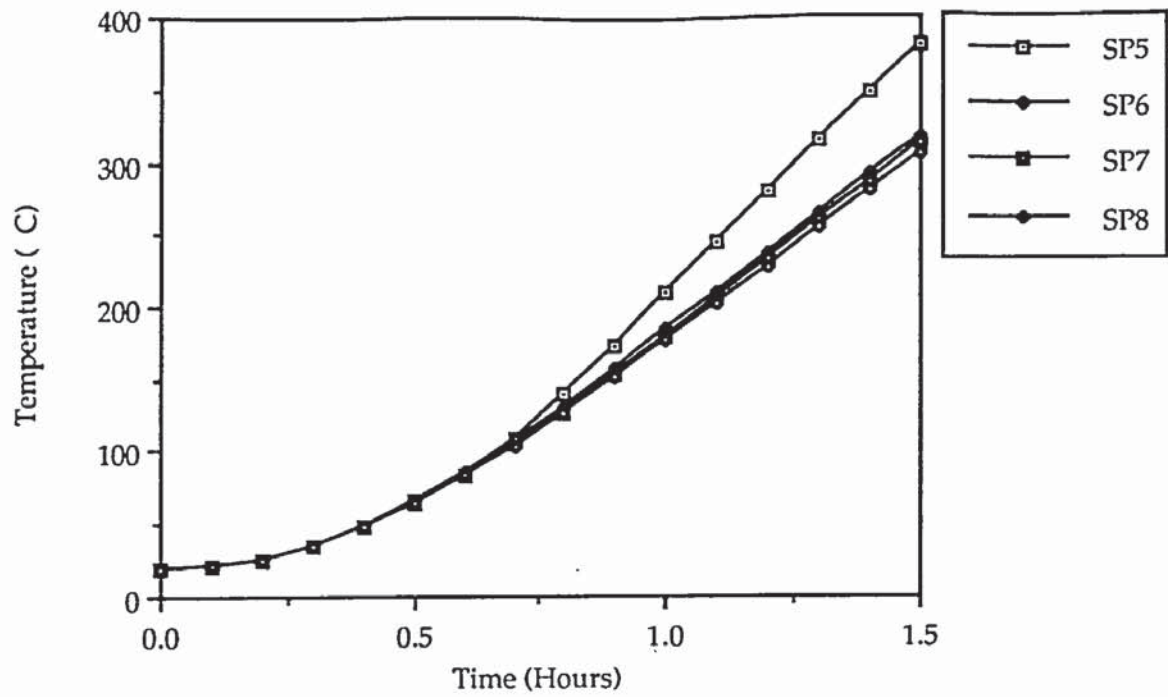


Figure 8.9: Temperature history in element 60 (concrete) in column C4

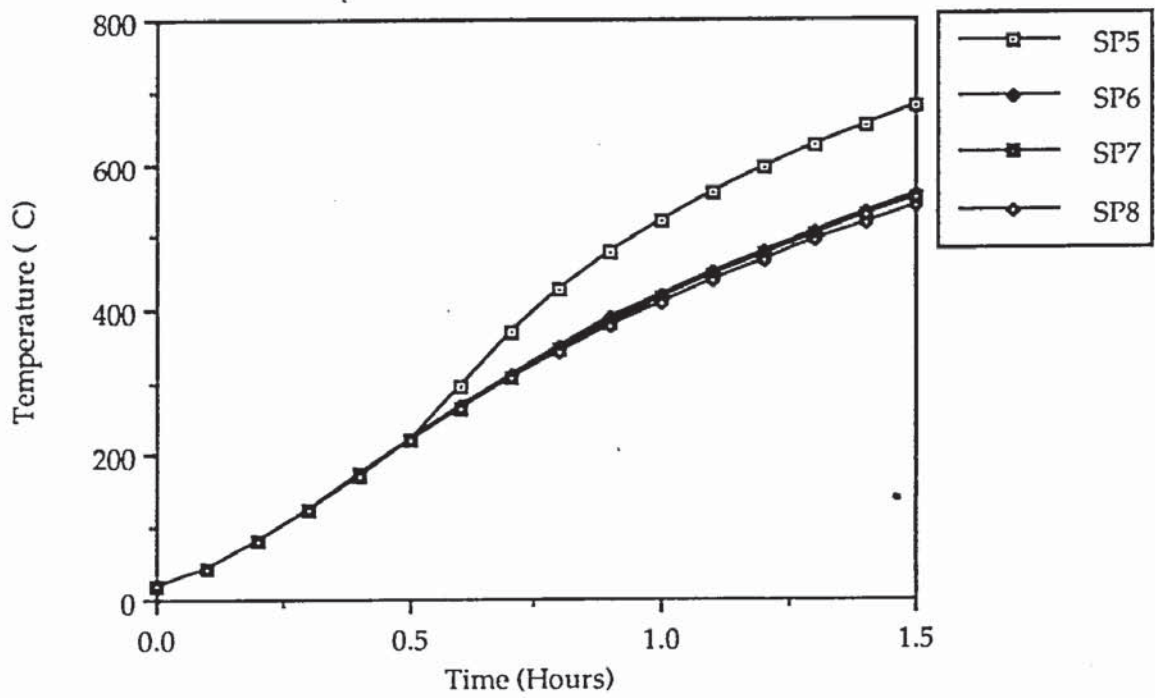


Figure 8.10: Temperature history in element 64 (concrete) in column C4

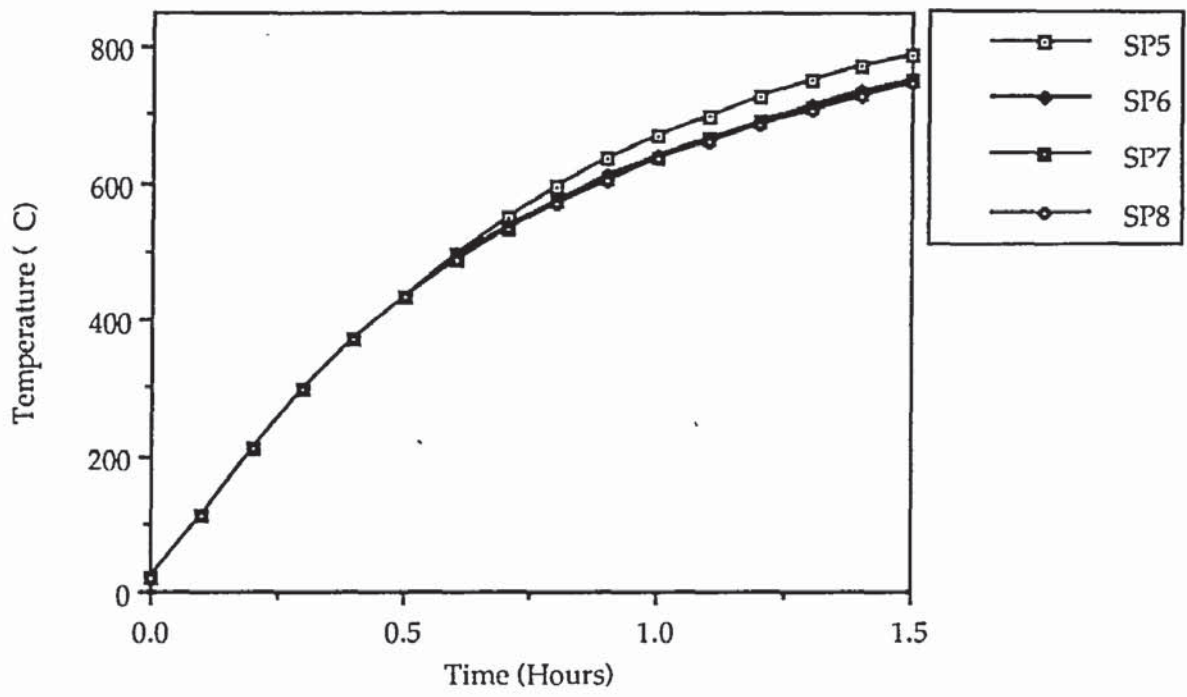


Figure 8.11: Temperature history for element 1 (concrete) in column C4

The effect of spalling would cause greater temperature rises especially in elements in the vicinity of the fire boundary as is the case with element 15 and element 64. The high temperatures would cause the concrete to lose strength and this would have an effect of reducing the fire resistance. Figures 8.5 and Figures 8.9 illustrate that the temperature rise in element at the centre of the columns is not as rapid as that for elements near the surface. An intermediate state will exist for other elements which are shielded from the furnace radiation by the concrete material.

Comparisons between the effect of progressive spalling on the structural response for M1, M2 and M3 are illustrated in Figures 8.12 to 8.23 for typical columns. Figures 8.12 to 8.14 and Figures 8.15 to 8.17 illustrate the mid-height deflections and axial deformations of column C1 and C3 respectively for the series of progressive spalling that occurs on the sides of the column cross sections. Figures 8.18 to 8.20 illustrate the mid-height deflection and axial deformation for C2 as a result of progressive spalling on the corners whilst Figures 8.21 to 8.23 illustrate the axial deformations for C4 for a similar case of progressive spalling as that for C2.

Comparisons between the columns whose results are plotted in Figures 8.12 to 8.23 indicate that the performance of a column is affected by the extent of spalling and the time of exposure at which the concrete spalls. The effect of spalling on the exposed faces is to reduce the fire resistance.

Comparison between Figures 8.12 to 8.14 for column C1 reveals that there is no significant difference in the mid-height deflections or axial deformations for any of the columns in this series even though the effect of spalling is to reduce

the fire resistance period. The exception is only for the SP1 case of model M2 whose deflection is very much smaller compared to the other cases of spalling as illustrated in Figure 8.13. The SP1 case of M3 exhibits a reversal in the deflection at failure where it bends away from the furnace in contrast to those for SP2, SP3 and SP4 as can be seen in Figure 8.14.

Figures 8.15 to 8.17 appear to indicate a similar trend behaviour of mid-height deflections and axial deformations for column C3 as previously described for C1 although the fire resistances in this series are much longer than that for C1. However, M1 exhibits an exception for this series where the deflections for SP1 and SP3 cases are much smaller than those for SP2 and SP4 as illustrated in Figure 8.15. Similarly to column C1, the deflection at failure of model M2 is drastically reduced for the SP1 case as illustrated in Figure 8.16. Figure 8.17 illustrates a deflection away from the furnace for SP1 in contrast to those for SP2, SP3 and SP4 in a similar trend behaviour to column C1.

Comparison between Figures 8.18 to 8.20 for column C2 also reveals that there is no significant difference in the mid-height deflections or axial deformations for any of the columns in this series. However, it can be seen from the figures that the effect of spalling is to reduce the fire resistance period. The figures also illustrate that M1 and M2 predict a similar range of mid-height deflections at failure whilst M3 predicts a larger deformations at a much longer time of failure.

Figures 8.21 and 8.22 illustrate that the calculated axial deformations of column C4 obtained from M1 and M2 seem to follow the same basic shape in that the deformations both show small elongations during the initial stages of the fire

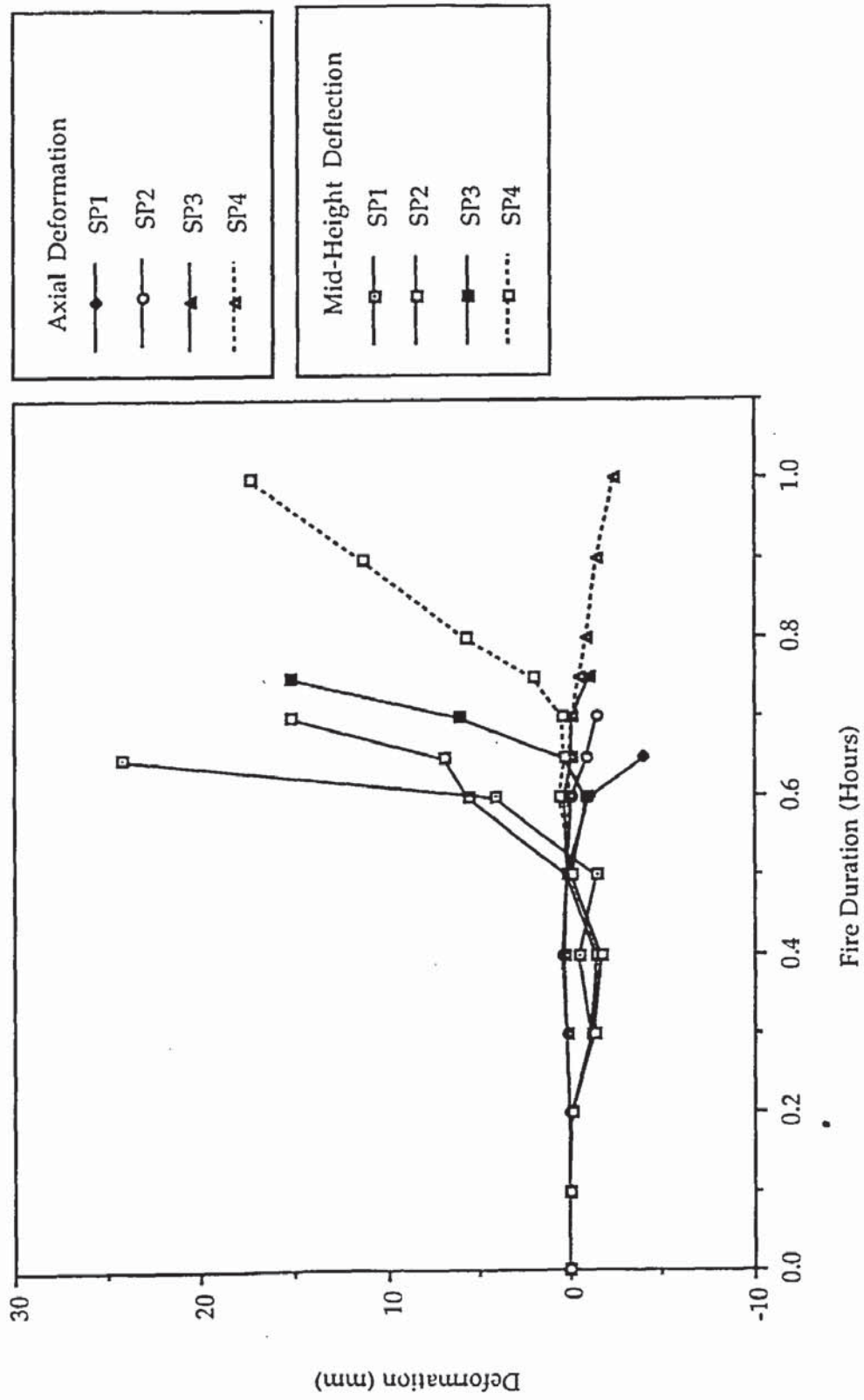


Figure 8.12: Calculated behaviour of column C1 for model M1

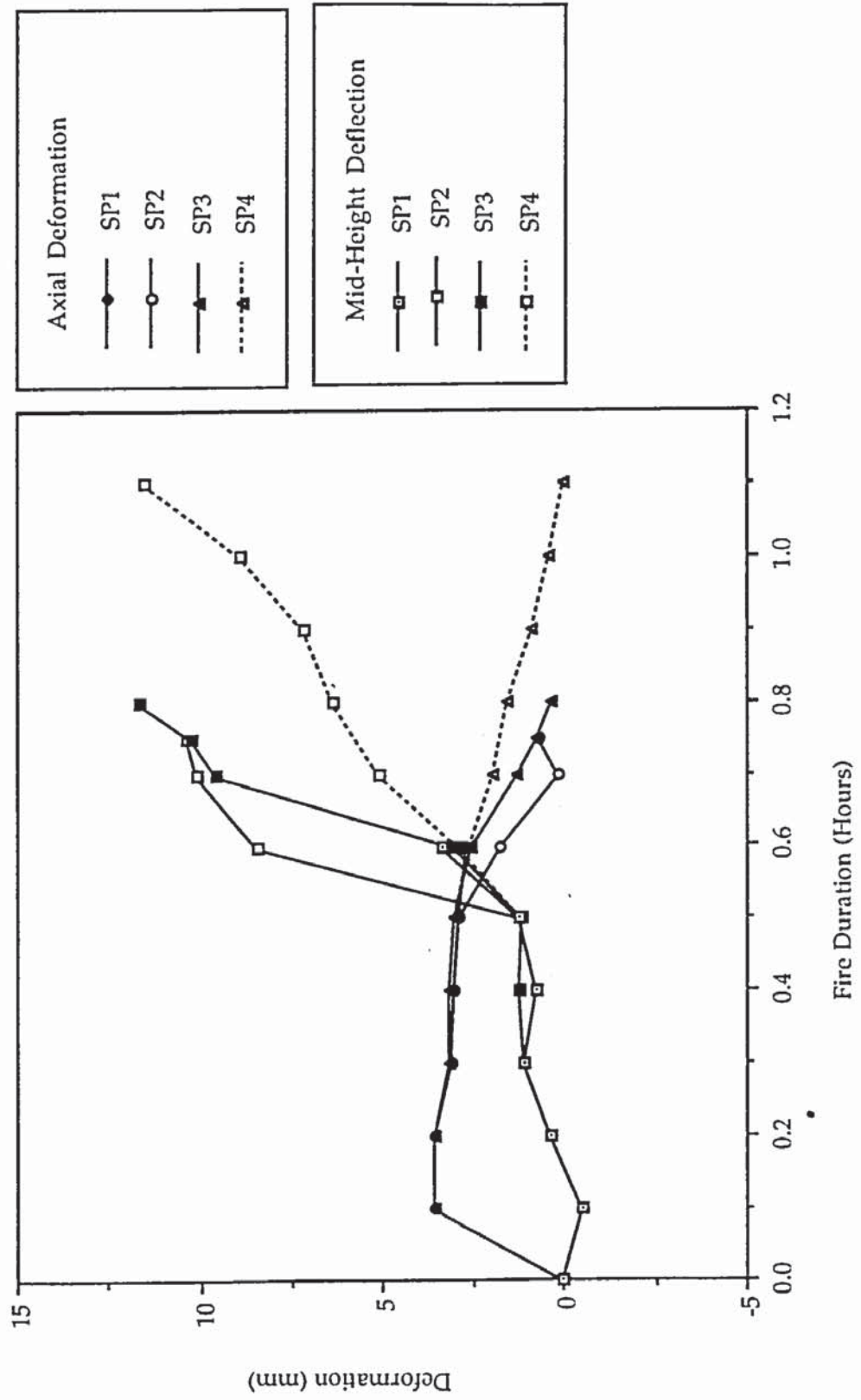


Figure 8.13: Calculated behaviour of column C1 for model M2

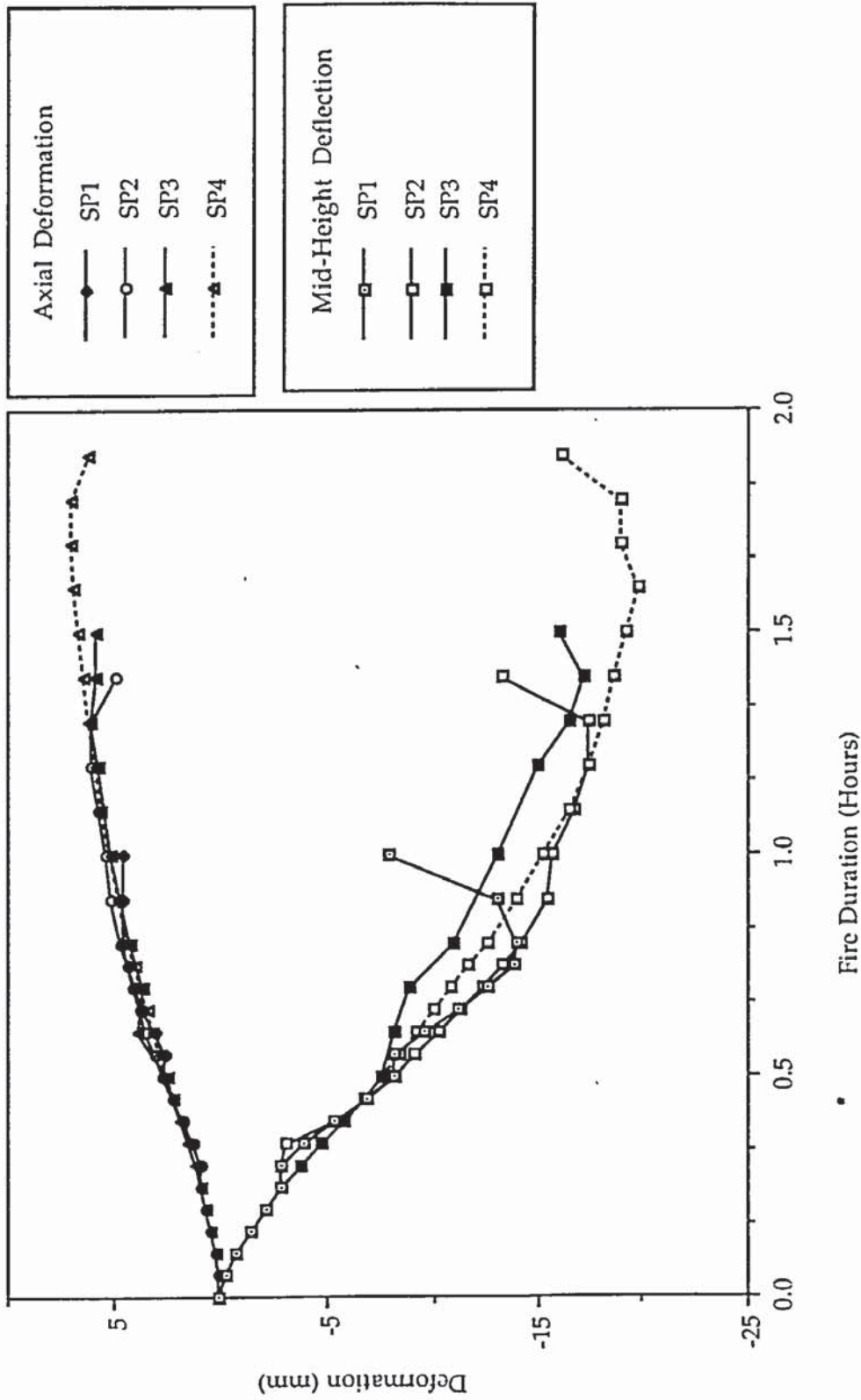


Figure 8.14: Calculated behaviour of column C1 for model M3

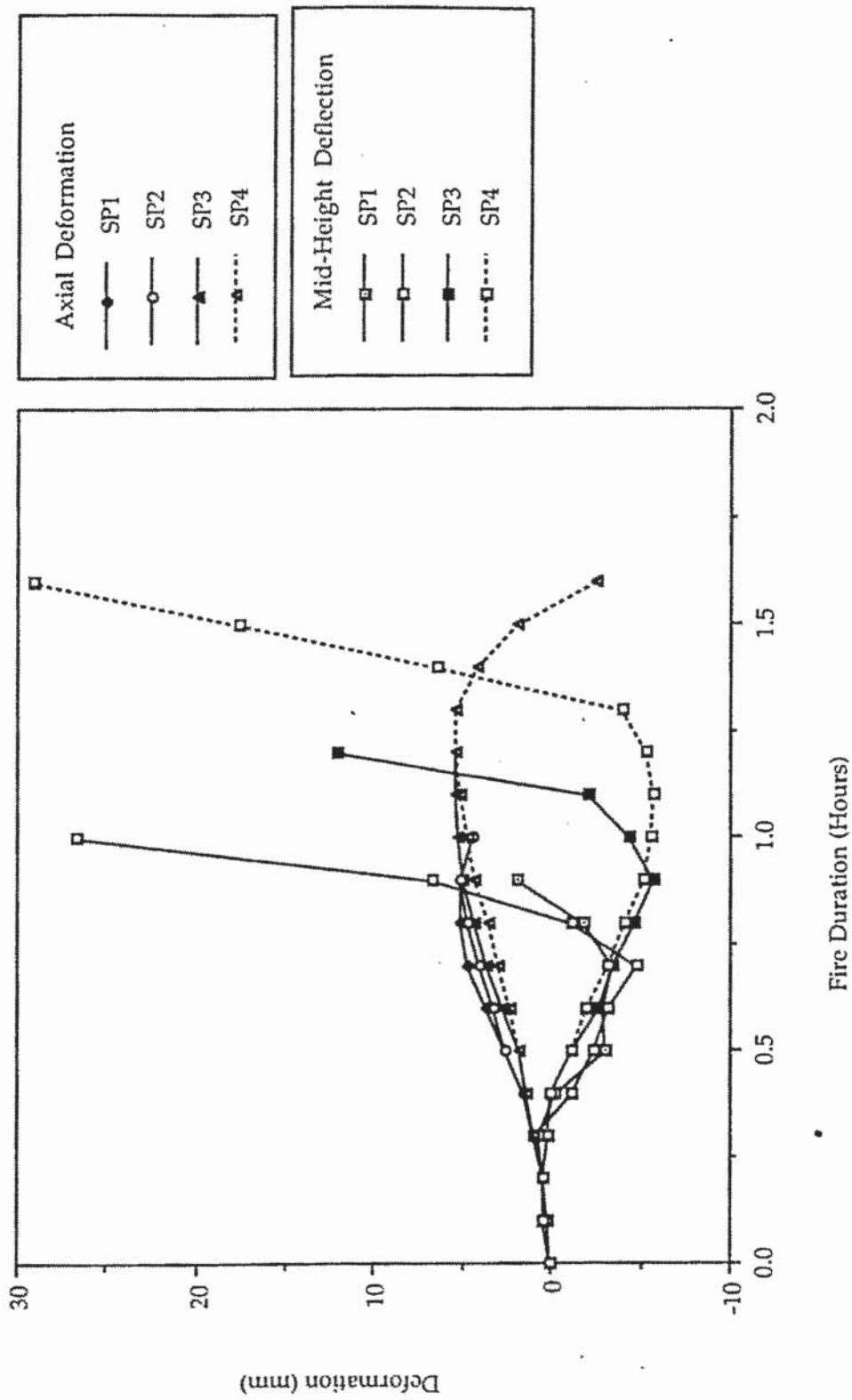


Figure 8.15: Calculated behaviour of column C3 for model M1

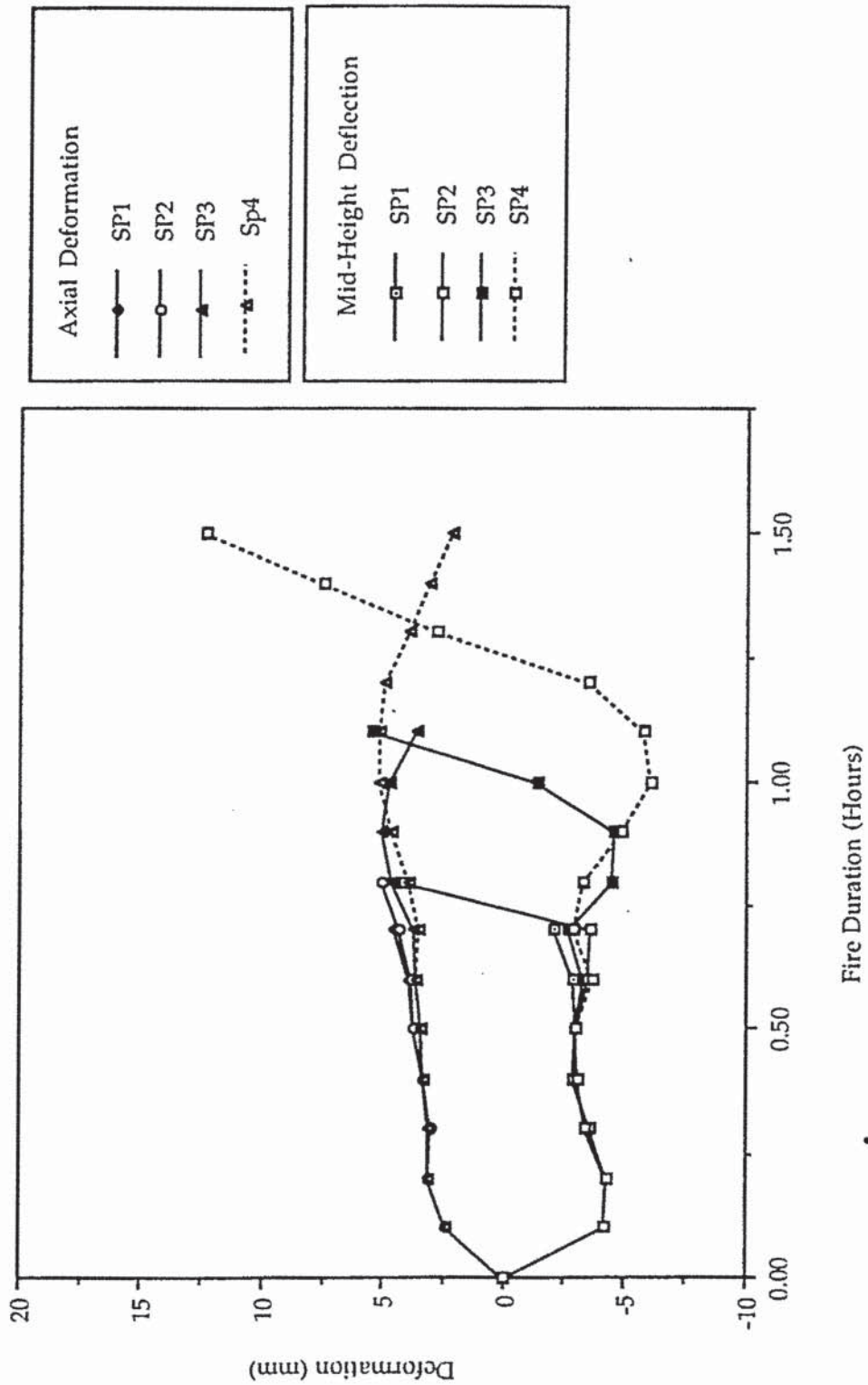


Figure 8.16: Calculated behaviour of column C3 for model M2

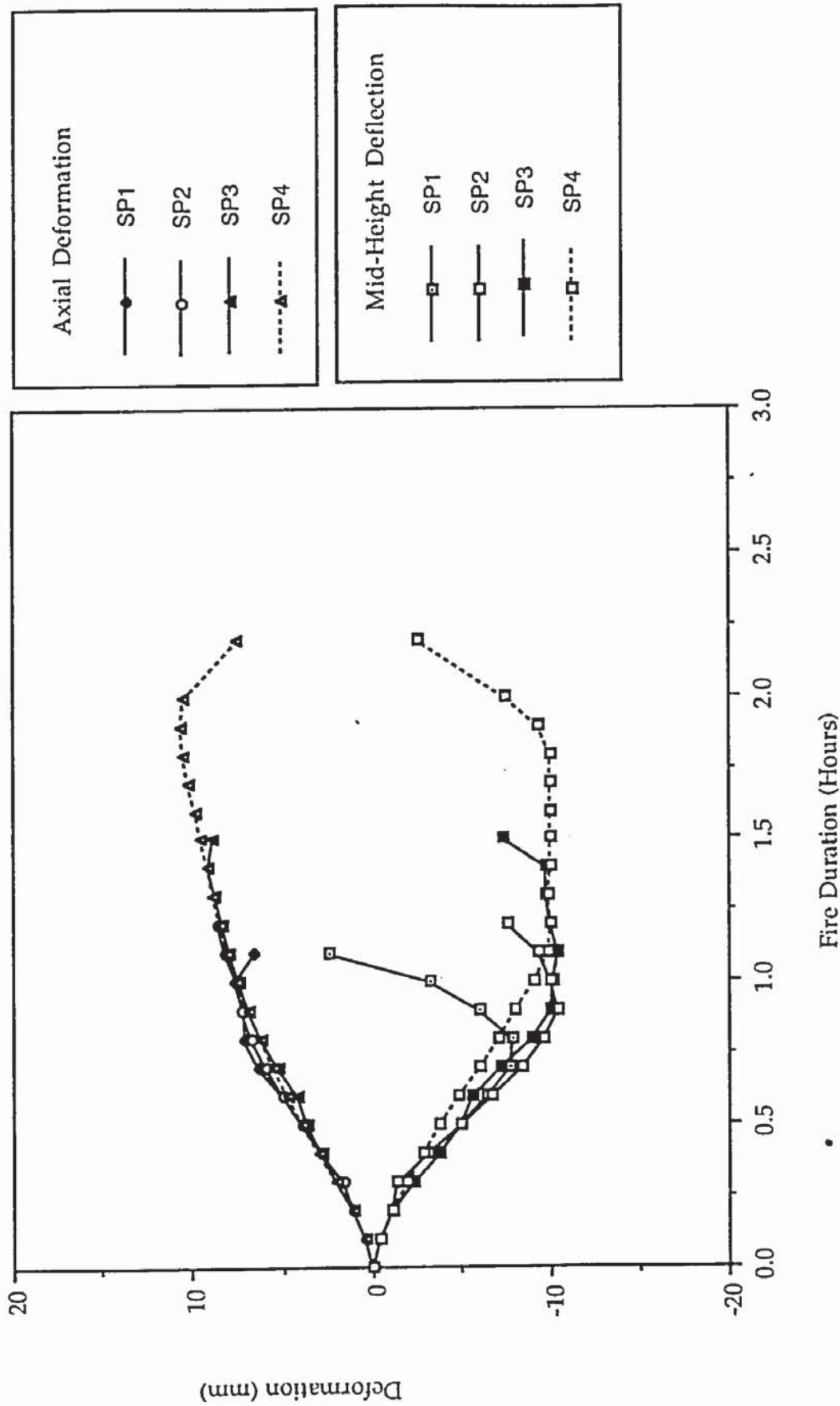


Figure 8.17: Calculated behaviour of column C3 for model M3

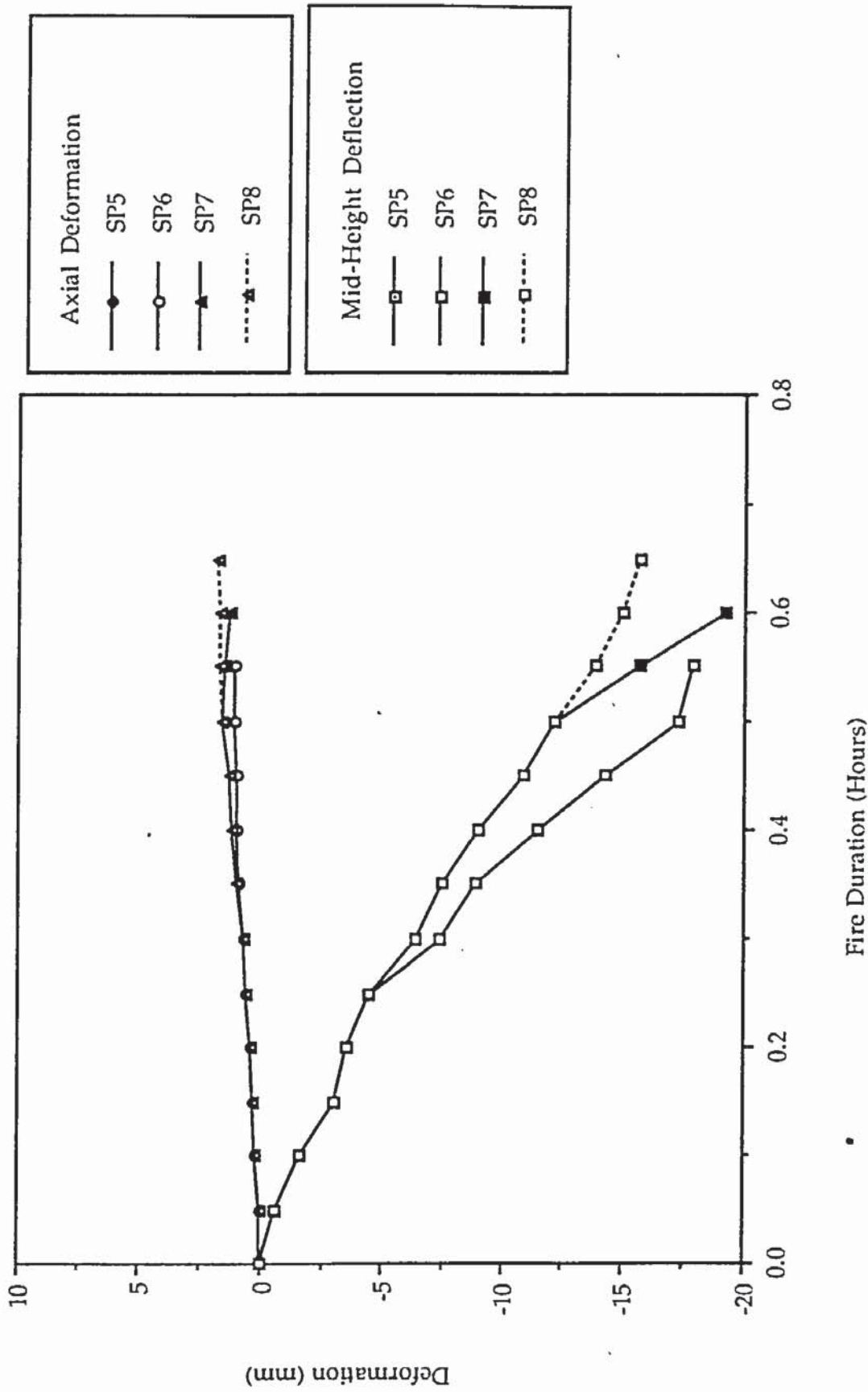


Figure 8.18: Calculated behaviour of column C2 for model M1

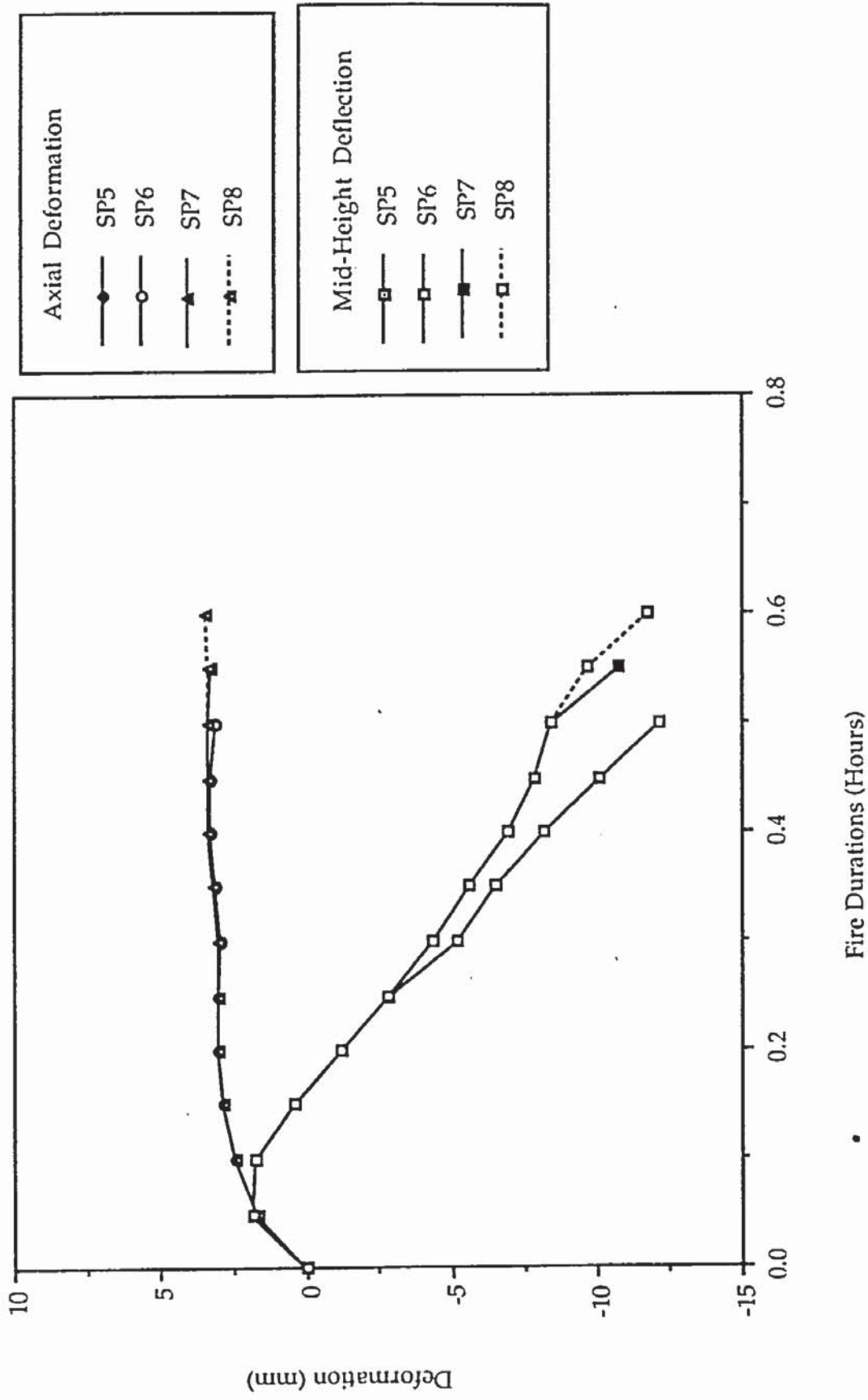


Figure 8.19: Calculated behaviour of column C2 for model M2

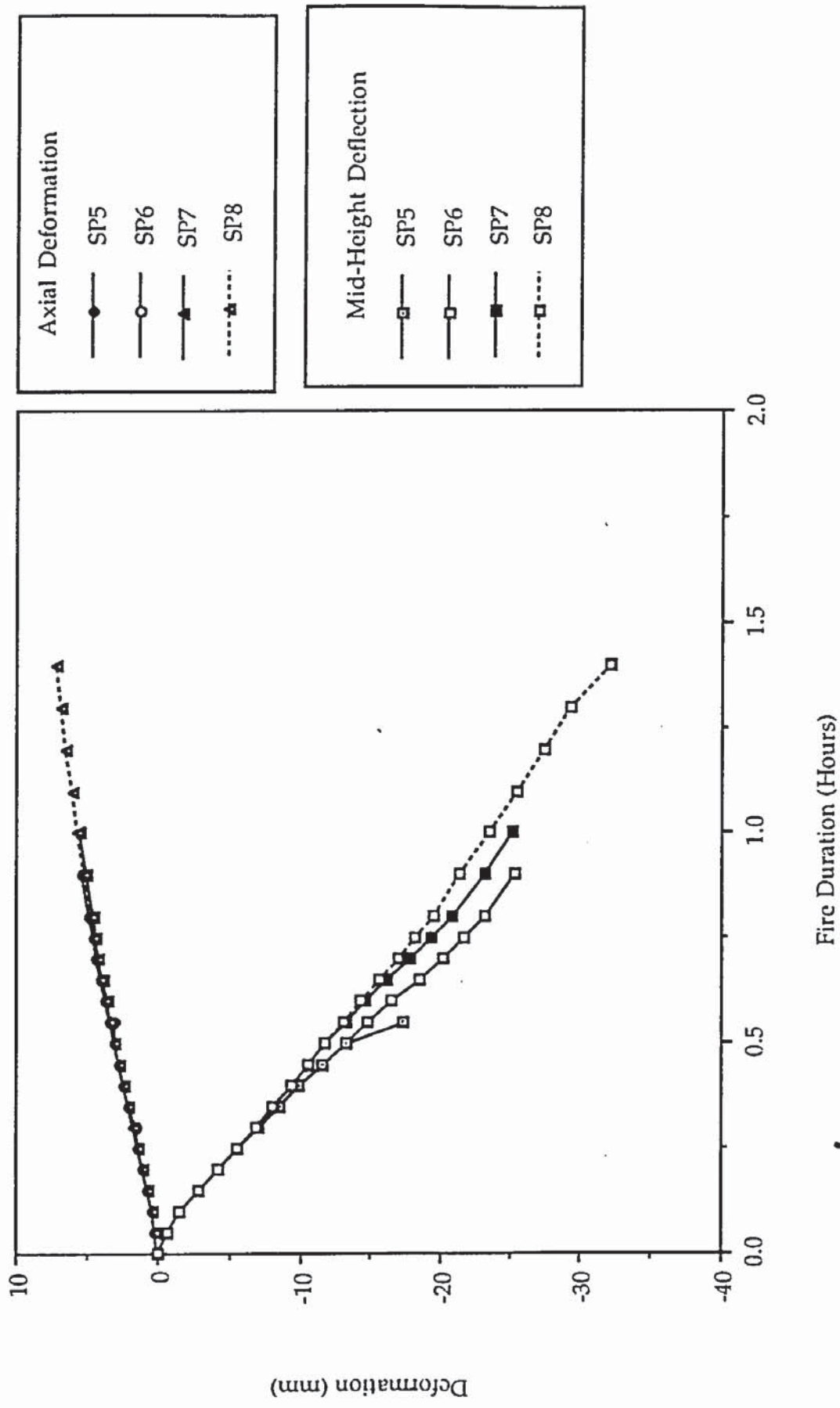


Figure 8.20: Calculated behaviour of column C2 for model M3

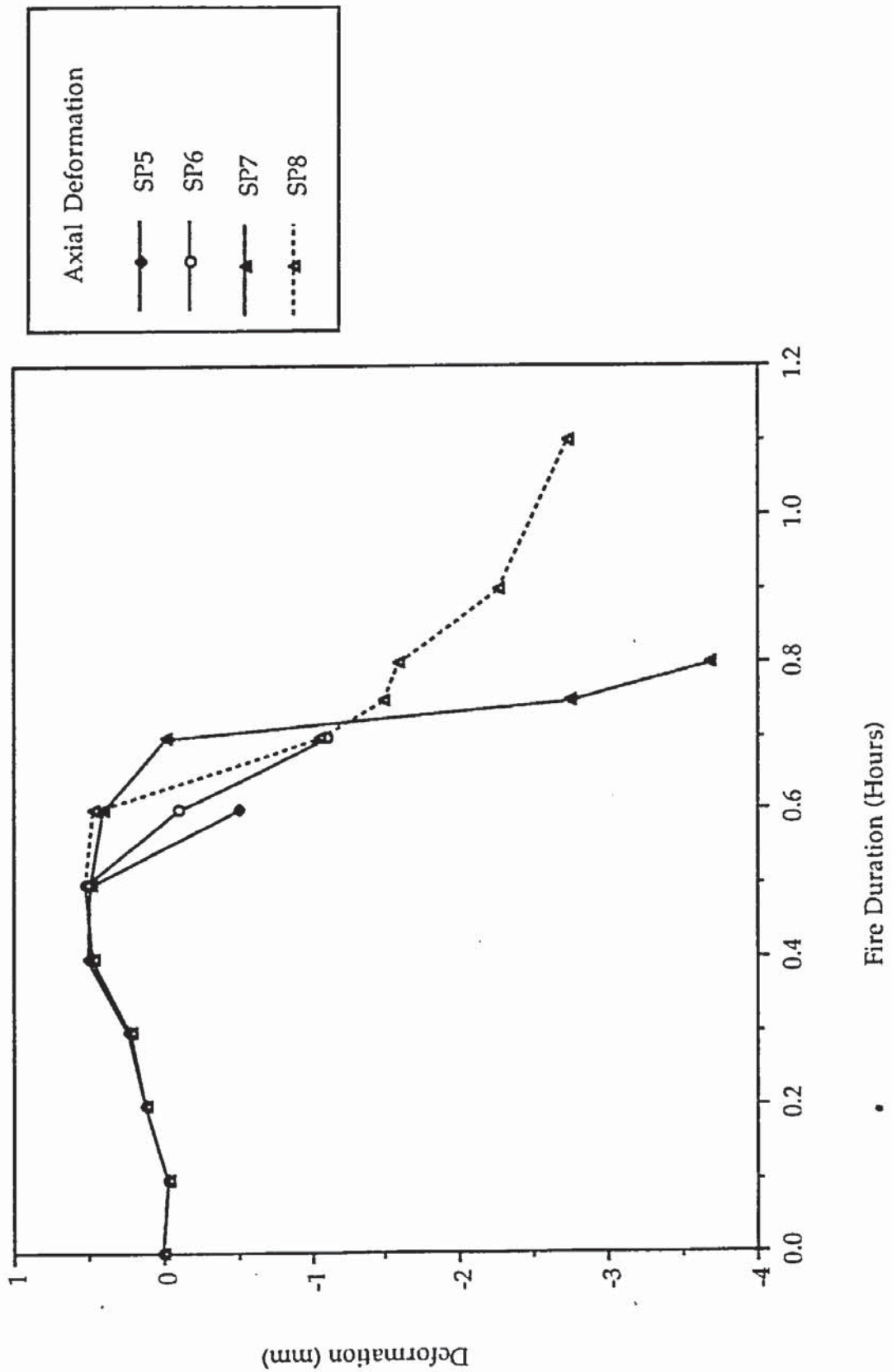


Figure 8.21: Calculated behaviour of column C4 for model M1

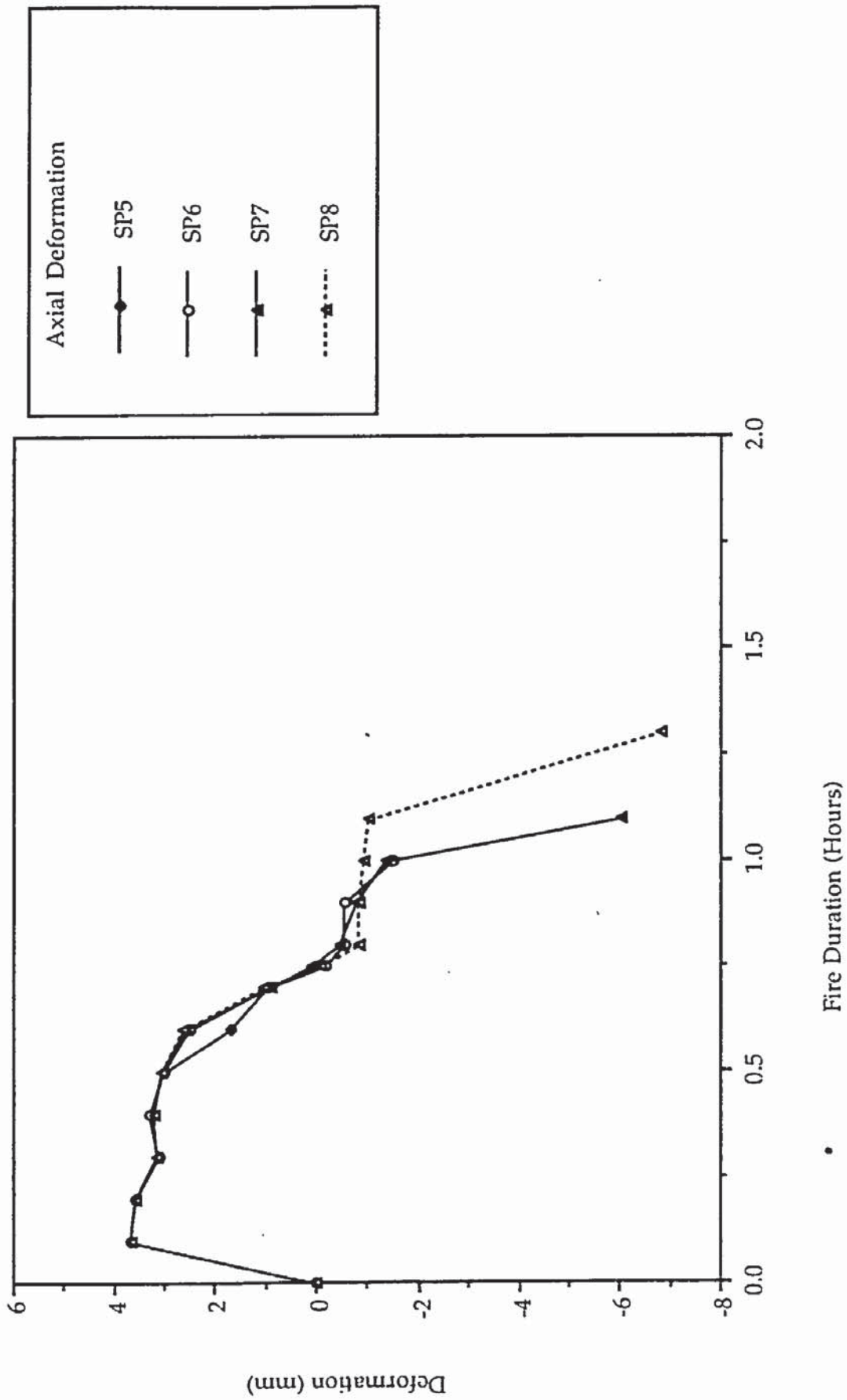


Figure 8.22: Calculated behaviour of column C4 for model M2

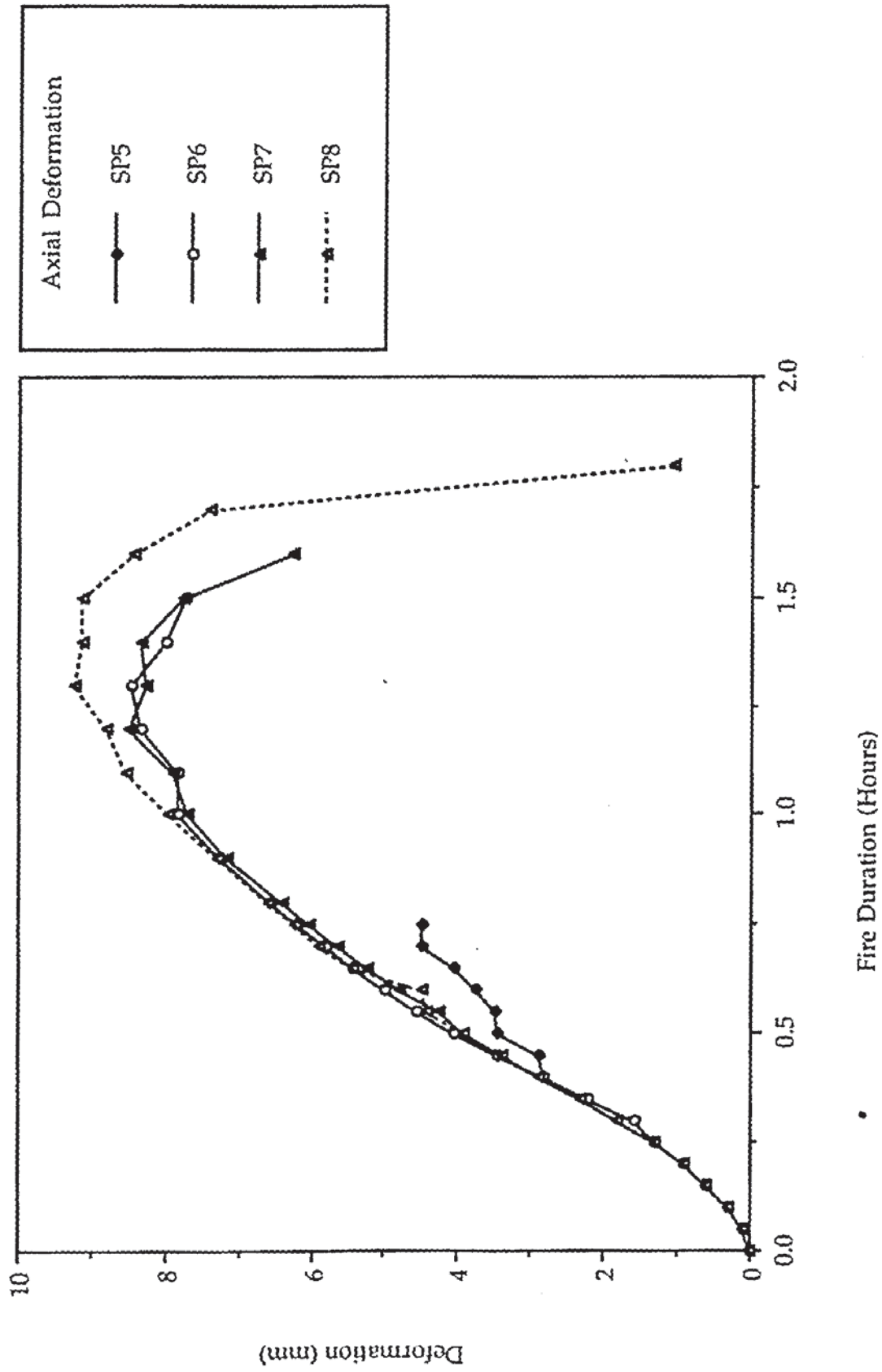


Figure 8.23: Calculated behaviour of column C4 for model M3

but then changes into compression until failure occurs for all cases of spalling. In contrast, M3 predicts axial expansion throughout the period of fire exposure as shown in Figure 8.23.

Figures 8.24 to 8.26 compare the mid-height deflections at failure of columns C1, C2 and C3 respectively for the three models. Mid-height deflections for column C4 were not plotted as the deflections at failure were not significant. This is due to the symmetrical exposure of column C4 to the heating regime and the loading is axial.

As illustrated in Figure 8.24 the comparison between the mid-height deflection responses of M1, M2 and M3 for column C1 at failure exhibits a slight difference in that the concrete models adopted appear to influence the deflection response. M1 and M2 exhibit a similar response where the deflections are always directed away from the furnace; except that M2 gives smaller deflections than M1. However, M3 does not exhibit a similar response in that the deflections are always directed towards the furnace for all spalling cases. It can also be seen from Figure 8.24 that each model predicts a consistent magnitude of mid-height deflections at failure for all percentages of spalling.

For column C2 plotted in Figure 8.25 shows that all the curves seem to follow the same trend in that the deflections are all directed towards the furnace with M3 which predicts the largest deflection whilst M1 and M2 are again relatively close to each other. The similarity in the trend can be explained by the fact that column C2 was eccentrically loaded with an eccentricity of 60 mm directed away from the furnace. The column is thus expected to bend towards the furnace with the cool side in compression.

Figure 8.26 reveals a similar trend behaviour of mid-height deflections for column C3 as that described for column C1 although the deflection of M3 towards the furnace is less pronounced than those for the previous case and that M1 exhibits a greater deflection away from the furnace for low percentages of spalling. For this case it is expected that the column C3 would bend away from the furnace with the cool side in tension since the column was eccentrically loaded with an eccentricity of 60 mm towards the furnace.

The calculated fire resistances of columns C1, C2, C3 and C4 from the exposure simulations for the three models are plotted against the percentage of spalling in Figures 8.27 to 8.30. The fire resistances for 39% spalling case were not plotted as there was no significant difference with the fire resistances at 29.5% spalling for all columns. The plots reveal that the concrete model adopted has a large influence on the reduction of the fire resistance. As illustrated in the figures, M3 is shown to predict a consistently higher fire resistance for all four columns. The calculated curves from M1 and M2 seem to follow the same basic shape and are relatively close together except for column C4 where M2 appears to give slightly longer fire resistances times when compared to M1.

In addition, it can be observed that the decrease in fire resistance for M3 is significantly greater when compared to the decrease for M1 and M2 for all four columns. The fire resistance for M3 is approximately decreased by a third of its initial rating with 15% spalling and by a half with 30% spalling. The effect is not as drastic for M1 and M2 but in each case a significant reduction in fire resistance occurs.

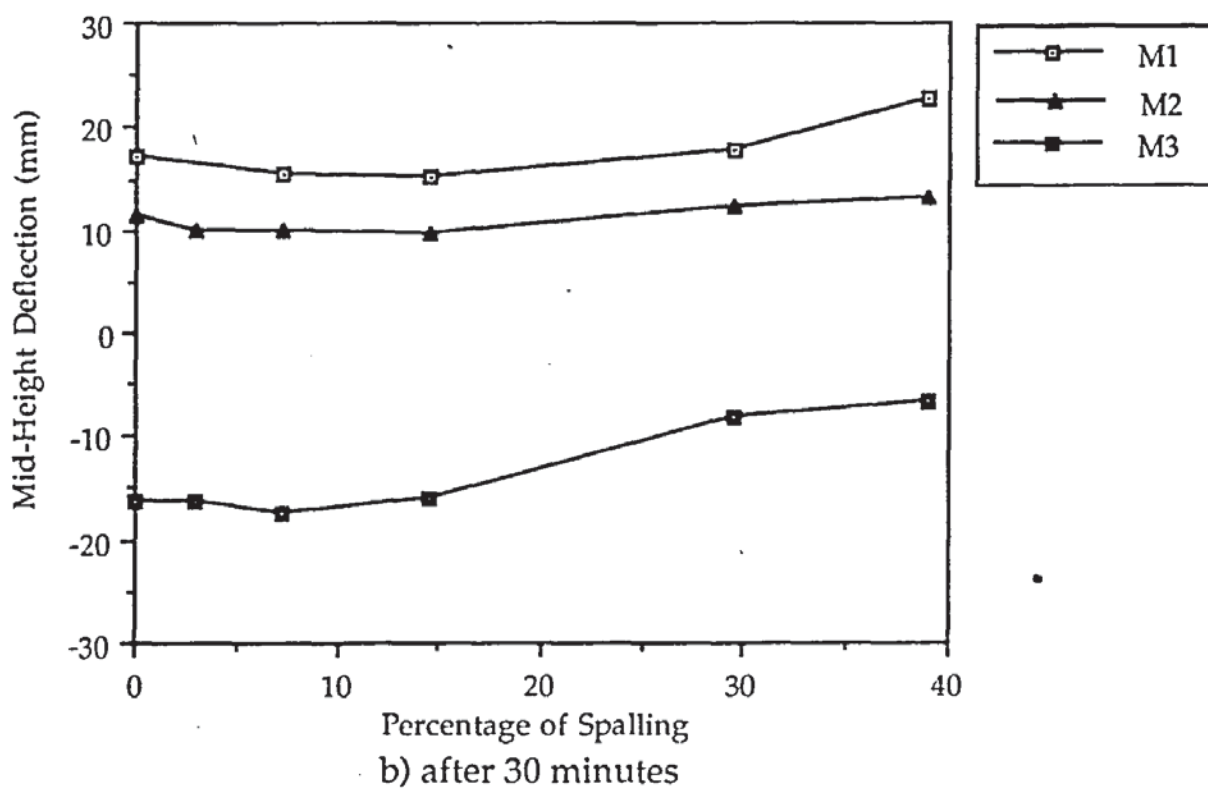
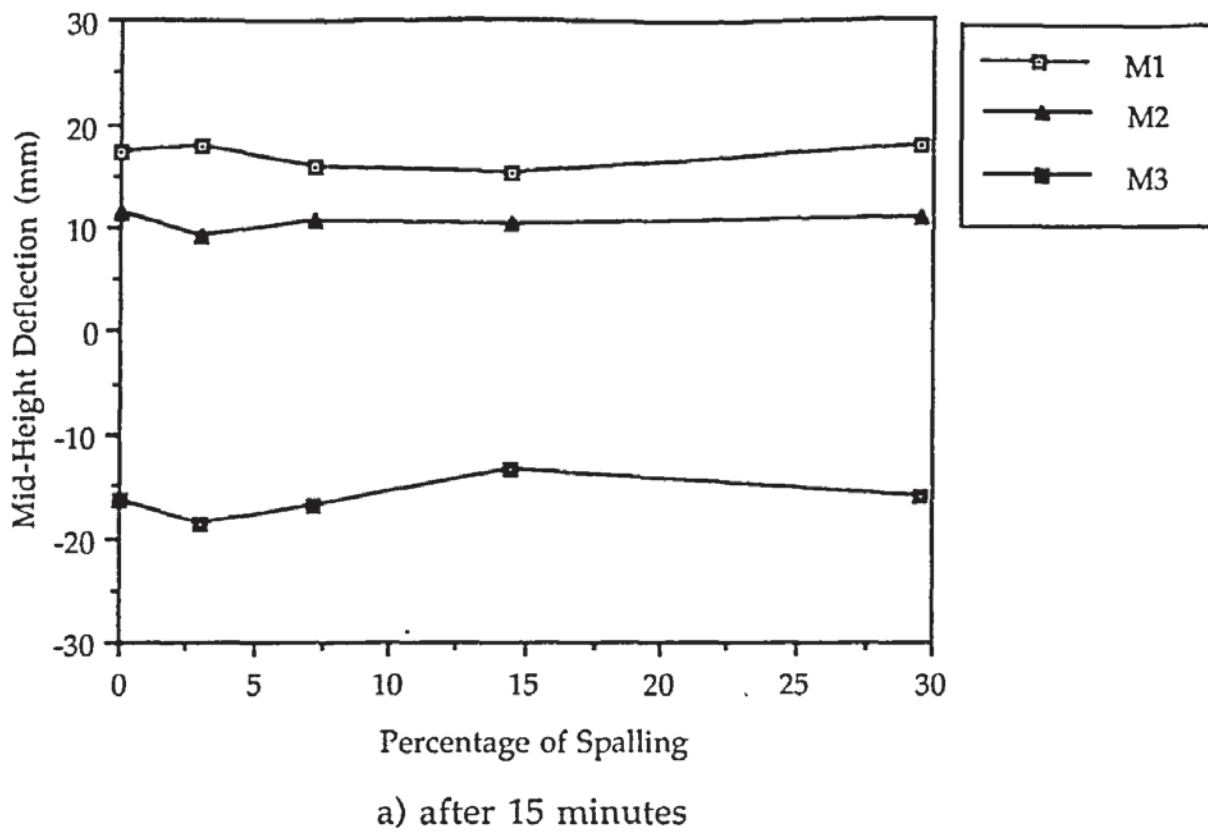
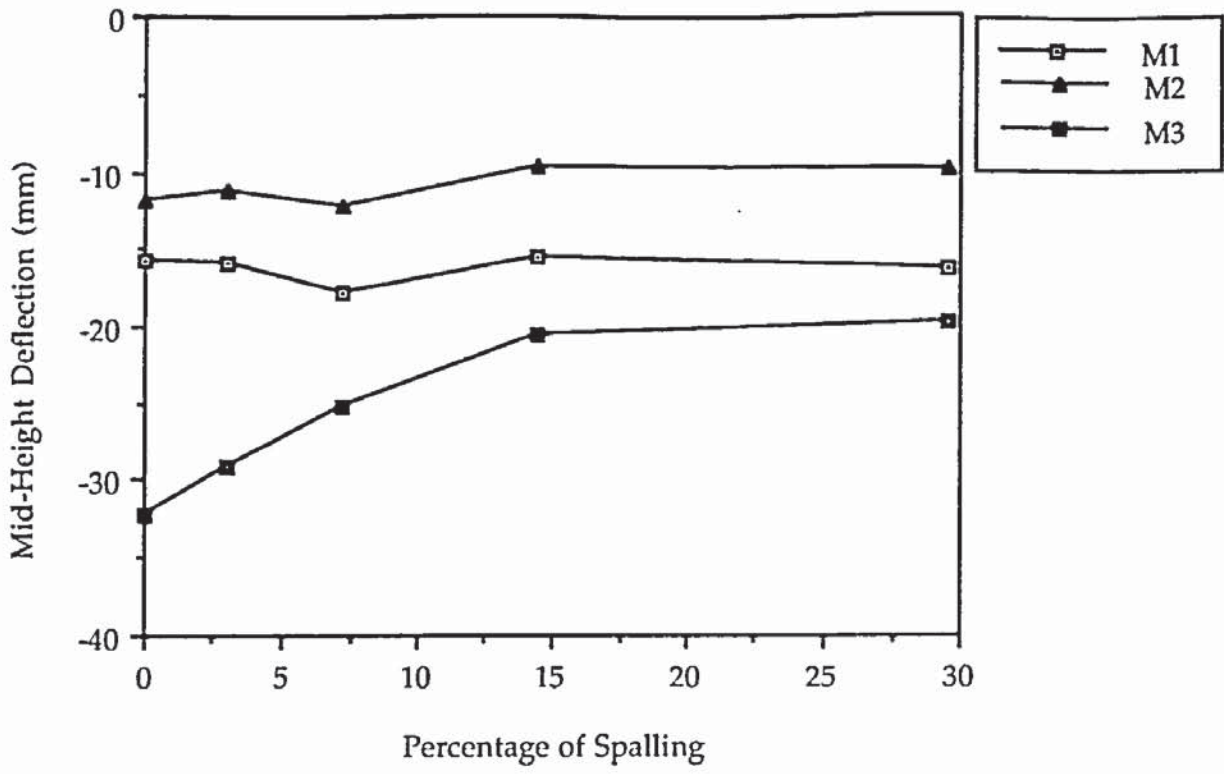
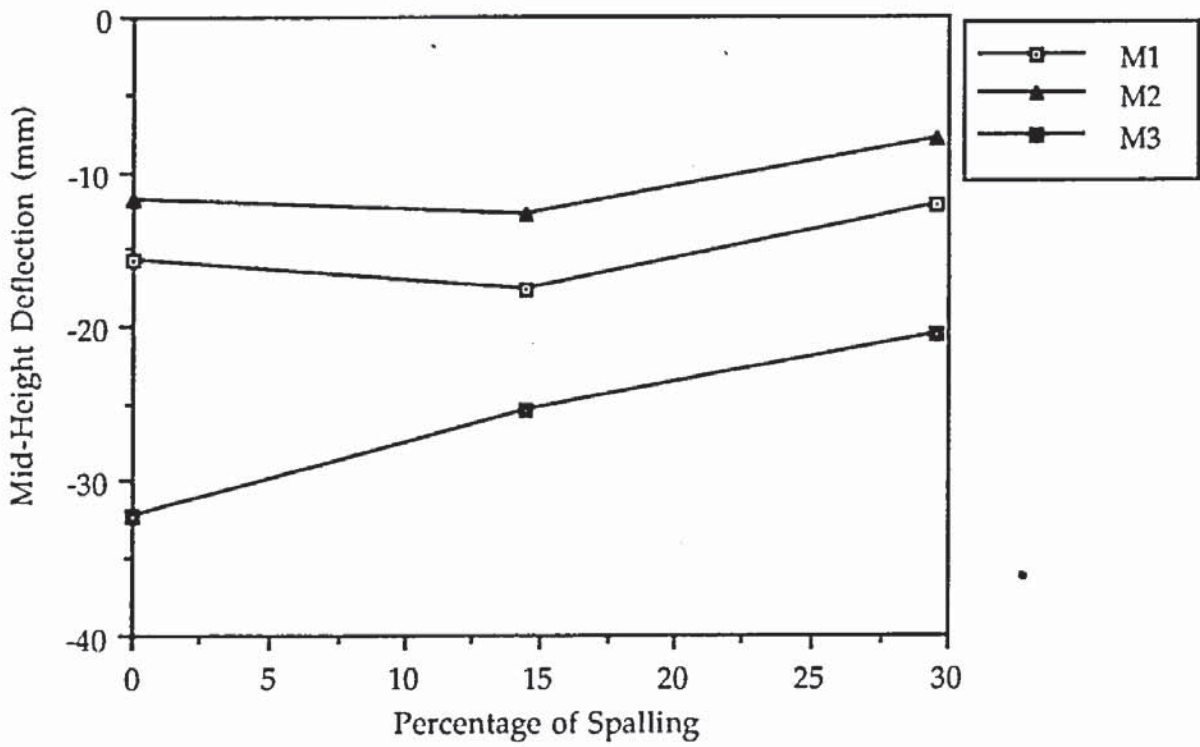


Figure 8.24: Mid-height deflection versus percentage spalling for column C1



a) after 15 minutes



b) after 30 minutes

Figure 8.25: Mid-height deflection versus percentage spalling for column C2

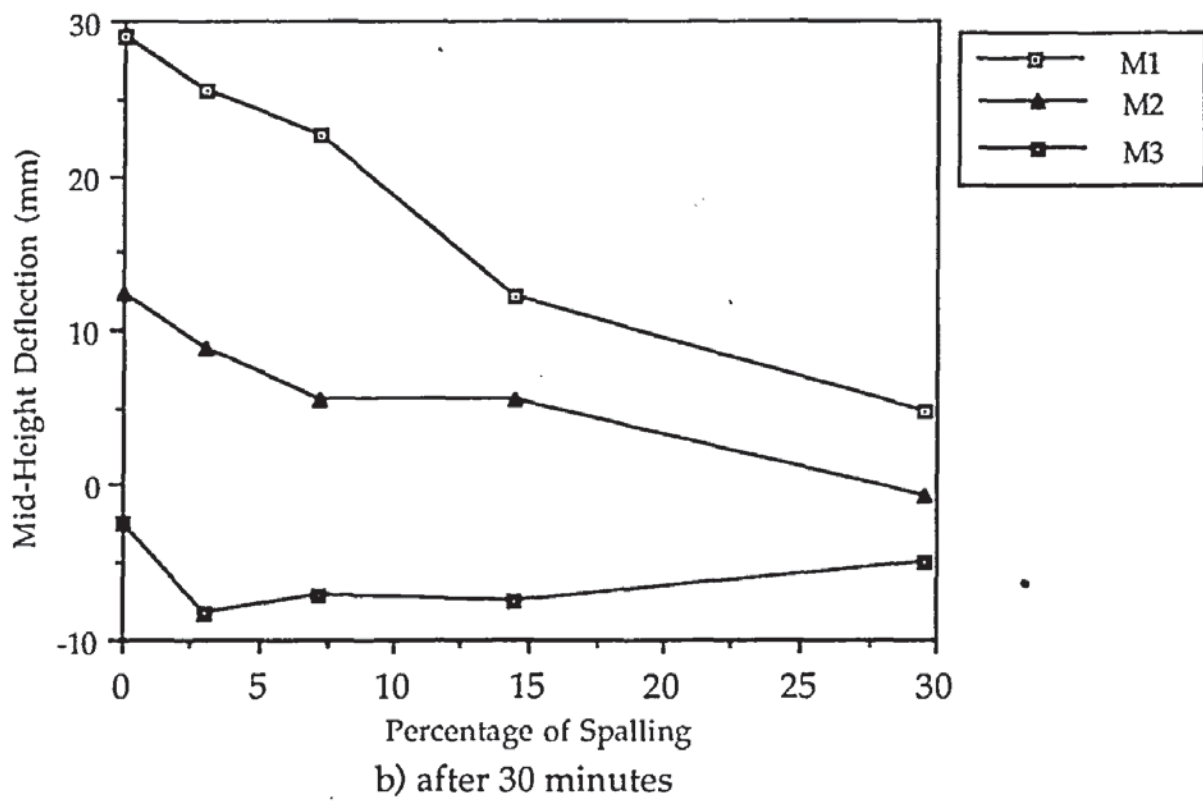
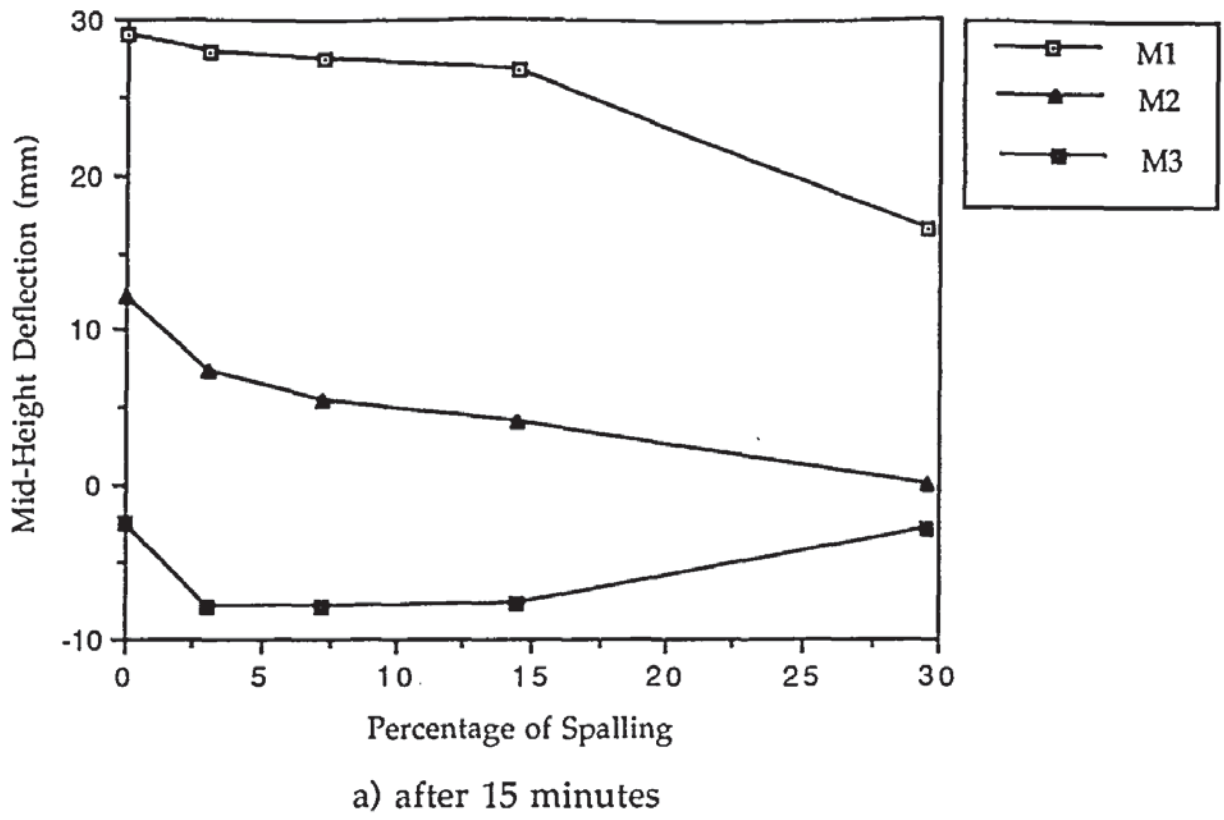
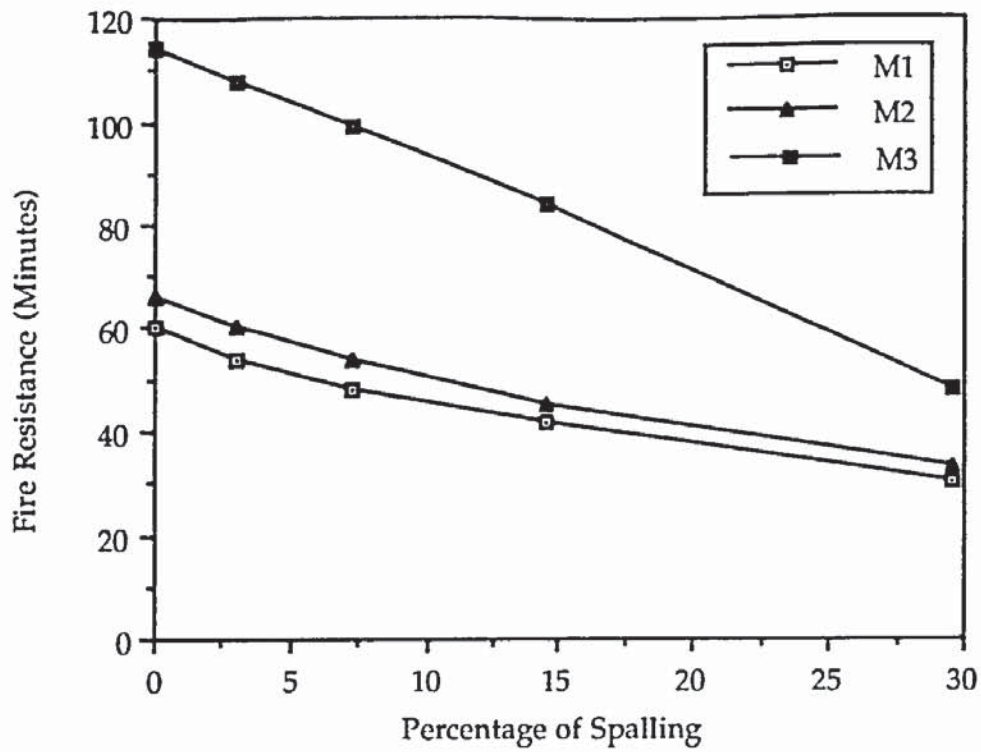
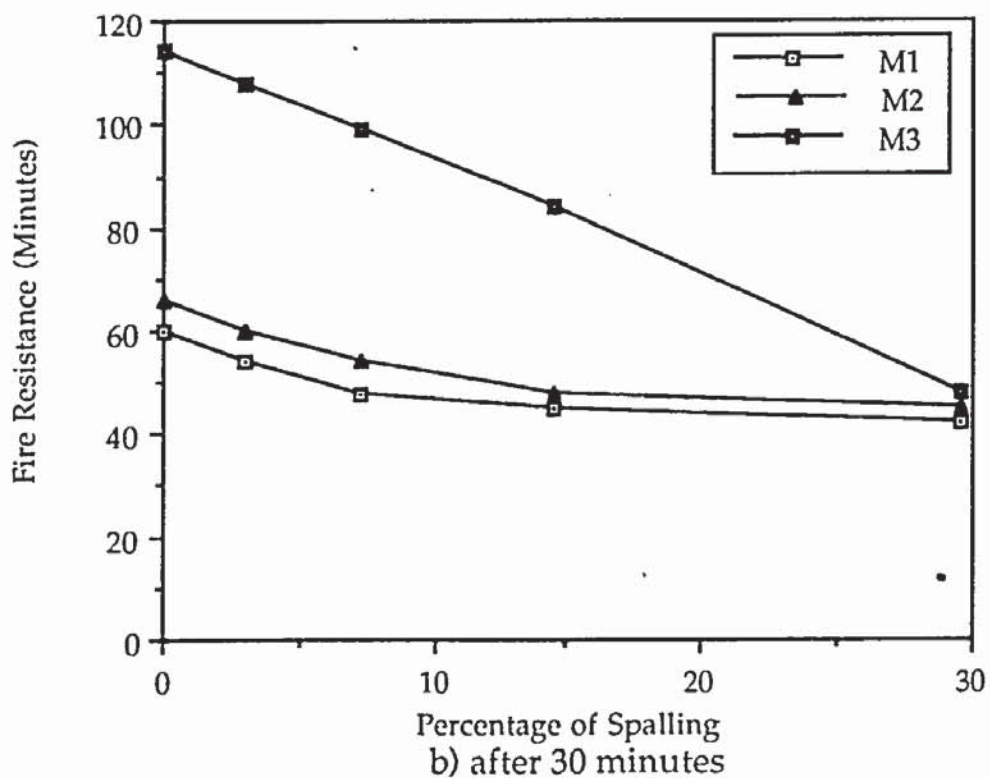


Figure 8.26: Mid-height deflection versus percentage spalling for column C3

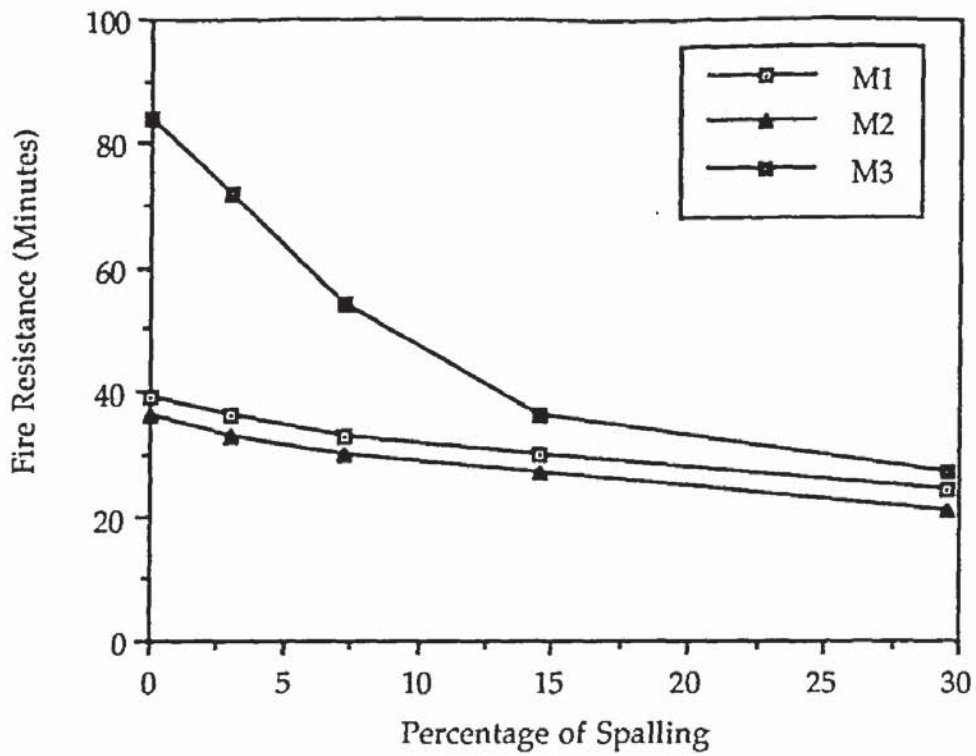


a) after 15 minutes

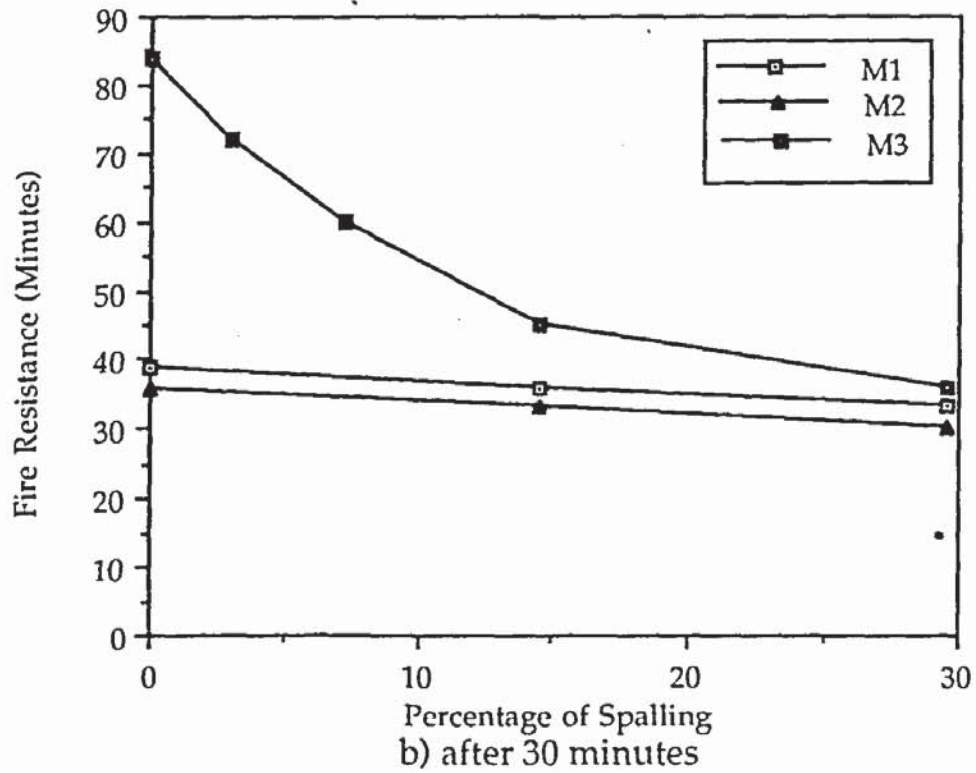


b) after 30 minutes

Figure 8.27: Fire resistance versus percentage spalling for column C1



a) after 15 minutes



b) after 30 minutes

Figure 8.28: Fire resistance versus percentage spalling for column C2

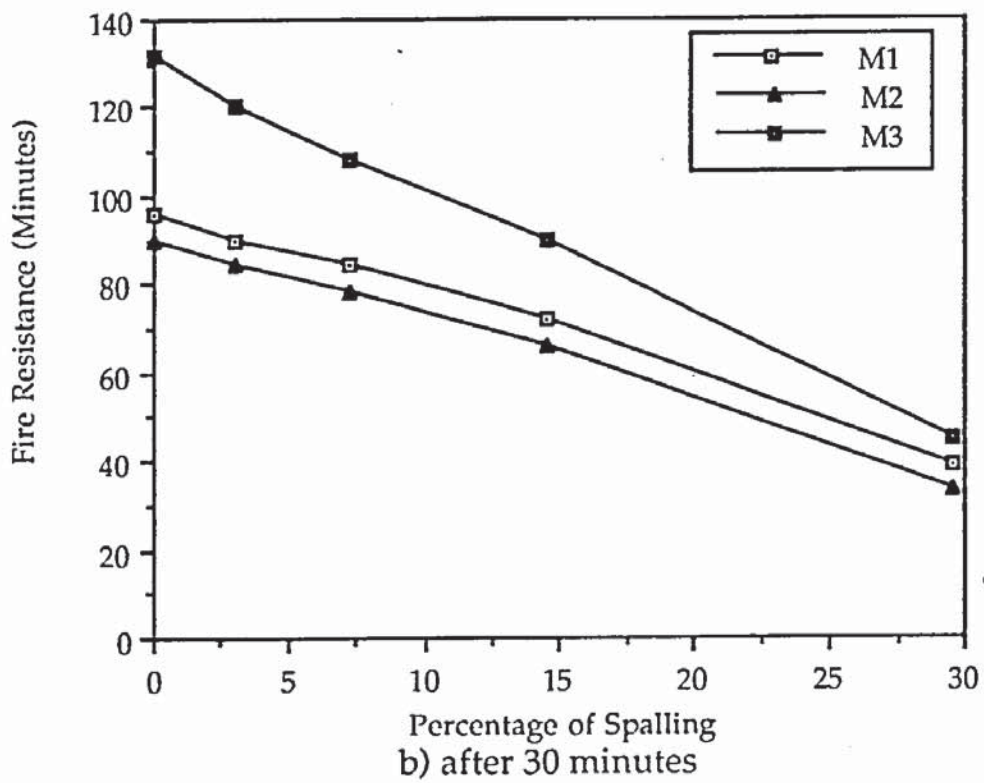
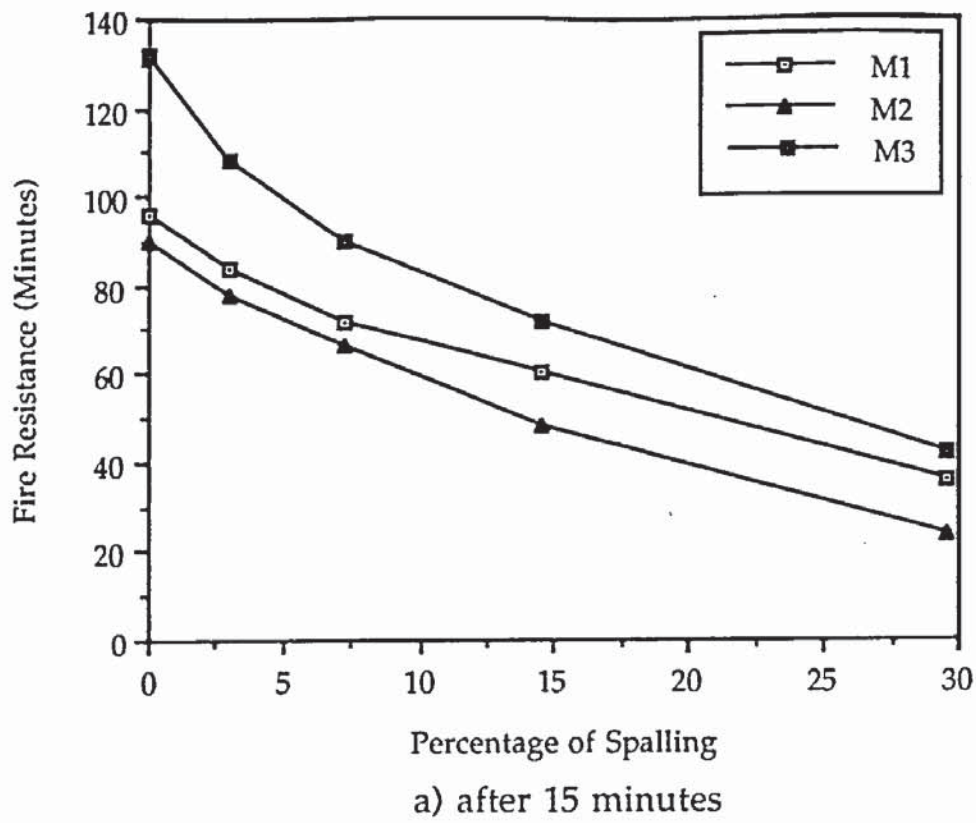
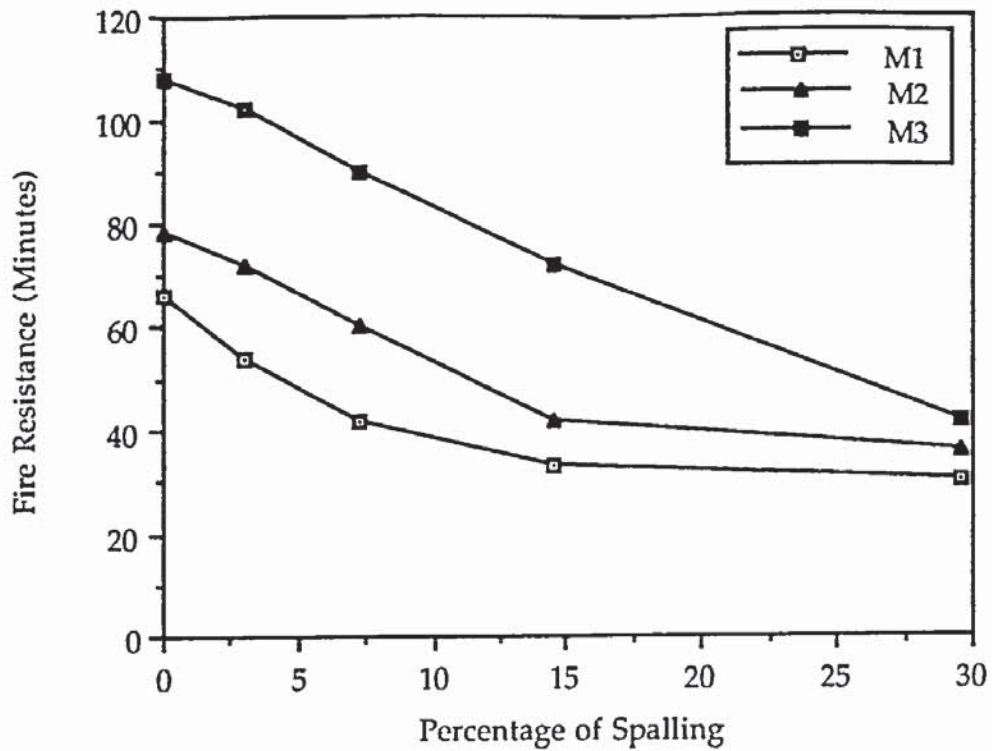
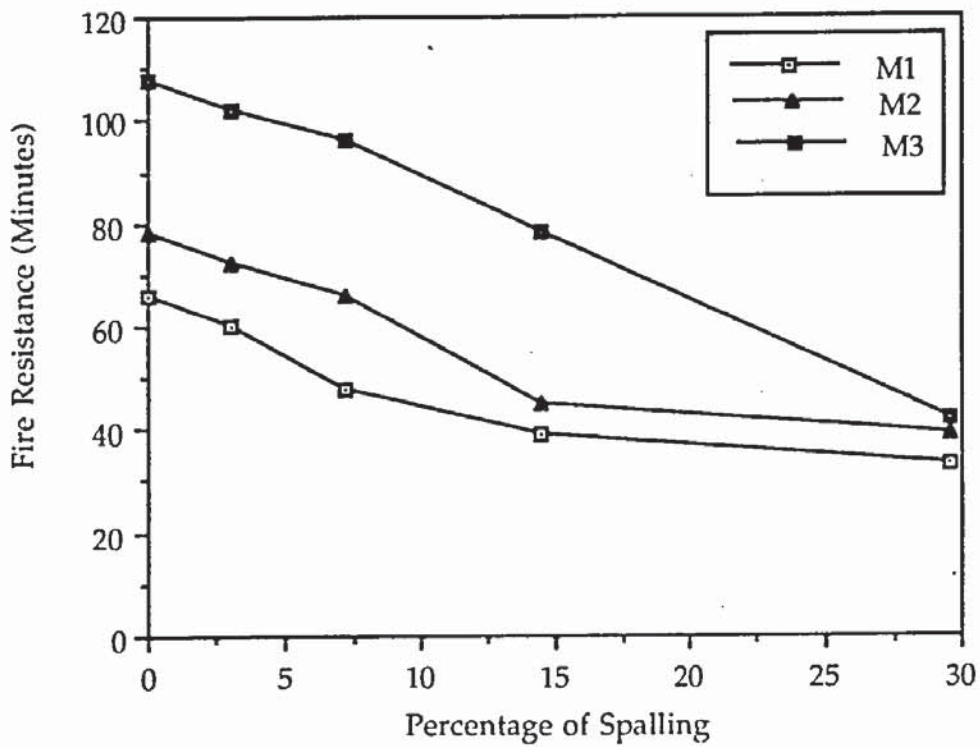


Figure 8.29: Fire resistance versus percentage spalling for column C3



a) after 15 minutes



b) after 30 minutes

Figure 8.30: Fire resistance versus percentage spalling for column C4

Figures 8.27 to 8.30 also reveal that in comparing the endpoints of the curves representing M1, M2 and M3 for the columns, the fire resistance is found to be approximately equal. Since the percentage of spalling is the same for all columns it would appear that the fire resistance of all three models are comparable at that percentage of spalling.

On the basis of the plots drawn in Figures 8.27 to 8.30, the extent of spalling and the time of exposure at which the concrete spalls for each column can be related. The average of M1 and M2 was used for fitting either linear or bi-linear equations since there was no significant difference between the results obtained from the two models as illustrated in the figures. Since the times to failure are only known to an accuracy of 3 minutes (upto 48 minutes) and 6 minutes beyond 48 minutes, a linear or bi-linear fit was considered accurate enough.

The following formulations are proposed for the range of spalling between 0.0% to 29.5% unless otherwise stated :

For column C1 with spalling occurring after 15 minutes:

$$t = t_0 (1.0 - 0.026x) \quad \text{for } 0.0\% < x < 7.2\% \quad (8.1a)$$

where:

x is the percentage of spalling

t is the fire resistance in minutes with x% spalling

t₀ is the fire resistance in minutes with no spalling (62.6 minutes)

$$R^2 = 0.991$$

and

$$t = 0.91t_0 (1.0 - 0.015x) \quad \text{for } 7.2\% < x < 29.5\% \quad (8.1b)$$

with: $R^2 = 0.996$

For column C1 with spalling occurring after 30 minutes:

$$t = t_0 (1.0 - 0.026x) \quad \text{for } 0.0\% < x < 7.2\% \quad (8.2a)$$

with: $R^2 = 0.991$

$$t_0 = 62.6$$

and

$$t = 0.84t_0 (1.0 - 0.006x) \quad \text{for } 7.2\% < x < 29.5\% \quad (8.2b)$$

with: $R^2 = 0.906$

For column C2 with spalling occurring after 15 minutes:

$$t = t_0 (1.0 - 0.022x) \quad \text{for } 0.0\% < x < 7.2\% \quad (8.3a)$$

with: $R^2 = 0.991$

$$t_0 = 37.3$$

and

$$t = 0.92t_0 (1.0 - 0.012x) \quad \text{for } 7.2\% < x < 29.5\% \quad (8.3b)$$

with: $R^2 = 1.00$

For column C2 with spalling occurring after 30 minutes:

$$t = t_0 (1.0 - 0.013x) \quad (8.4)$$

with: $R^2 = 0.970$

$$t_0 = 36.1$$

For column C3 with spalling occurring after 15 minutes:

$$t = t_0 (1.0 - 0.029x) \quad \text{for } 0.0\% < x < 14.5\% \quad (8.5a)$$

with: $R^2 = 0.978$

$$t_0 = 90.5$$

and

$$t = 0.85t_0 (1.0 - 0.021x) \quad \text{for } 14.5\% < x < 29.5\% \quad (8.5b)$$

with: $R^2 = 1.00$

For column C3 with spalling occurring after 30 minutes:

$$t = t_0 (1.0 - 0.021x) \quad (8.6)$$

with: $R^2 = 0.994$

$$t_0 = 93.9$$

For column C4 with spalling occurring after 15 minutes:

$$t = t_0 (1.0 - 0.034x) \quad \text{for } 0.0\% < x < 14.5\% \quad (8.7a)$$

with: $R^2 = 0.985$

$$t_0 = 70.5$$

and

$$t = 0.59t_0 (1.0 - 0.007x) \quad \text{for } 14.5\% < x < 29.5\% \quad (8.7b)$$

with: $R^2 = 1.00$

For column C4 with spalling occurring after 30 minutes:

$$t = t_0 (1.0 - 0.029x) \quad \text{for } 0.0\% < x < 14.5\% \quad (8.8a)$$

with: $R^2 = 1.00$

$$t_0 = 72.1$$

and

$$t = 0.66t_0 (1.0 - 0.008x) \quad \text{for } 14.5\% < x < 29.5\% \quad (8.8b)$$

with: $R^2 = 1.00$

It should be noted that the formulation is concerned with evaluating trends rather than proposing definitive formulae. The equations serve to provide an indication of the effect of spalling in that if a column failed after a period of exposure to fire with a known percentage of spalling an estimate could then be made of the fire resistance had there been no spalling.

Equations 8.1(a) to 8.8(b) reveal that the coefficients of the amount of spalling range between 0.026 to 0.034 for the case of spalling occurring after 15 minutes and between 0.021 to 0.029 for spalling after 30 minutes. The exception is only with column C2 for spalling occurring after 30 minutes which gives a slight anomaly. In this case the fire resistance without spalling is just above 30 minutes; the effect of spalling would not therefore be significant. Comparisons between the equations illustrate that the change in fire resistance with respect to spalling tends to suggest that the amount of spalling is the more significant factor whilst heating and loading patterns may be of lesser importance. There is some evidence that the earlier spalling occurs the higher the possible decrease in fire resistance.

8.3 CONCLUSION

The investigation reported in this chapter has demonstrated the application of the computer simulation and the verification of the effect on the response of a structural element after exposure to fire.

It has been shown in this chapter that the occurrence of spalling has a significant effect on the fire resistance of a reinforced concrete column in that the fire resistance decreases appreciably with any increase in spalling. However, the eventual effects were found to vary with the extent of spalling and the time of exposure at which the concrete spalls. The effect of spalling is that there is a loss of concrete which would cause more rapid temperature rises in the steel reinforcement and the remaining concrete. This would have an effect of reducing the fire resistance.

Tomecek and Milke (1993) observed similar results when investigating the effect of partial loss of protection on the fire resistance of steel columns. The fire resistances were found to decrease significantly with any increase in protection loss. The effects were found to vary with the amount of protection loss, the size of the column and the position of the protection loss.

This chapter has also illustrated that the calculated severity of fire resistance loss varies with the concrete model incorporated in the computer calculation. The models of Anderberg and Schneider have been shown to exhibit a similar response in most cases whilst the model of Lie gives an anomalous results. A similar conclusion can also be made for the calculated deformation at failure.

The constitutive models of Anderberg and Schneider both consider the effects of transient creep or appropriate strain effect whilst a similar strain component is omitted in the model of Lie. A better response in the spalling cases is therefore given by a model with transient strain component. A model that does not include the transient strain effect gives less good correlation as seen by the results.

The data plotted in Figures 8.1 to 8.30 present very good information on the effect of spalling. An attempt has been made to quantify the reduction in fire resistance against the extent of spalling for reinforced concrete columns where equations that serve to provide an indication of the effect of spalling have been proposed. Comparisons between the equations reveal that changes in fire resistance with respect to spalling tend to suggest that the heating pattern, loading pattern and time of spalling may be of lesser importance compared to the effect of the amount of spalling. Although of these the time of spalling may be the most significant. However, further investigation may be necessary to verify and augment this observation in that a wider variety of columns should be tested to possibly obtain design curves or equations. In addition, the effect of three-dimensional heat transfer should also be investigated.

CHAPTER NINE

CONCLUSIONS AND RECOMMENDATIONS FOR FUTURE WORK

9.1 INTRODUCTION

This chapter reviews the work presented in this thesis and presents the conclusions that can be drawn from it. Possible areas that warrant further research effort will be suggested.

In general this research is concerned with the application of the computer simulation technique as an alternative method to study the performance of structural elements in a fire environment. In the preceding chapters, the following aspects of the parametric study of the behaviour of reinforced concrete columns in fire have been examined through computer simulation:

1. The investigation of the effects of mesh designs and boundary conditions that defines the interaction between the column face and the surrounding fire environment on the temperature distribution histories across the column cross section.
2. The assessment of the relative effect of the concrete material models proposed by Anderberg and Thelandersson (1976), Schneider (1985) and Lie and Chabot (1990) on the structural response of reinforced concrete columns exposed to fire.

3. The development of a method to model reinforced concrete columns exposed to fire which incorporates the effect of spalling by varying the amounts of concrete lost during a specified period of exposure to fire. The effect of the severity of fire resistance loss is then compared between the three concrete material models incorporated in the computer calculation.
4. The quantification of the reduction in fire resistance against the amount of spalling, heating and loading patterns, and the time at which the concrete spalls.

9.2 THE APPLICATION OF THE COMPUTER SIMULATION TECHNIQUE

The investigation reported in this thesis has demonstrated the application of the computer simulation in the study of structural response to fire. It has been shown that computer simulation lends itself ideally to an extensive parametric study which could be carried out to determine the structural response of concrete elements in fire environment.

The approach of a parametric study can be used which take into account the effect of spalling, mesh designs, boundary conditions and the effect of different concrete material models. However, comparisons between the different mesh designs and boundary conditions indicate that there is no significant difference in the temperature distribution histories generated for the range of temperatures employed in this investigation.

In addition to evaluating deflections and capacity to support design loads it is also possible to calculate local stresses, internal cracking in concrete or yielding in steel reinforcement together with the redistribution of internal forces during the fire exposure. Probably the only way to assess structural performance in a fire is by computational methods since fire tests will be extremely difficult and costly to carry out.

9.3 ASSESSMENT OF THE EFFECT OF CONCRETE MATERIAL MODELS

It is generally known that in order to obtain a good correlation between test and calculated measurements, reliable material models will have to be developed that allow for the effect of degradation of the material properties as temperature increases. However, the material models developed for studying the performance of structural elements in a fire differed mainly in respect to the formulation of the mechanical properties of concrete. There is disagreement as to whether concrete exhibits transient strain in addition to classical creep strain and whether the effects of transient strain ought to be included in the concrete material model used to predict the structural response.

The analytical method reported in this thesis has clearly illustrated that a more realistic response of a reinforced concrete column exposed to fire is given by a constitutive model with transient creep or appropriate strain effect such as that due to Anderberg or Schneider. A model that does not include the transient strain such as that due to Lie gives less good results although in certain circumstances the difference may not be significant. Transient state models thus correspond largely to fire situations and bear closer relation to the conditions likely to be

encountered in an actual fire conditions as the temperature variation is progressive whilst the material is under load.

9.4 THE EFFECT OF SPALLING ON COLUMN BEHAVIOUR

The investigation reported in this thesis has described a method adopted for the computer modelling of reinforced concrete columns exposed to fire which incorporate the effect of spalling by varying the amounts of concrete lost during a specified period of exposure to fire.

The application of the method has clearly shown that the occurrence of spalling has a significant effect on the fire resistance of a reinforced concrete column in that the fire resistance decreases appreciably with any increase in spalling. However, the eventual effects were found to vary with the extent of spalling and the time of exposure at which the concrete spalls. The effect of spalling is that there is a loss of concrete which would cause more rapid temperature rises in the steel reinforcement and the unspalled concrete. The increase in temperature would have an effect of reducing the strength of the concrete and the steel reinforcement. This alone would have an effect of reducing the fire resistance without the effect of a reduced concrete cross section.

This investigation has also illustrated that the calculated severity of fire resistance loss as a result of spalling varies with the concrete model incorporated in the computer calculation. The constitutive models of Anderberg and Schneider have been shown to exhibit a similar response in most cases whilst that due to Lie gives an anomalous results. A similar conclusion can also be made for the calculated deformation at failure.

9.5 QUANTIFICATION OF THE REDUCTION IN FIRE RESISTANCE

The investigation reported in this thesis has also made an attempt to relate the extent of spalling and the time of exposure at which the concrete spalls for a reinforced concrete column where a reduction in fire resistance is quantified against the amount of spalling. The equations that have been proposed serve to provide an indication of the effect of spalling. Comparisons between the equations reveal that the change in fire resistance with respect to spalling tends to suggest that the amount of spalling is the more significant factor whilst heating pattern, loading pattern and time of spalling may be of lesser importance. However, of those three the time of spalling may be the most significant. It appears that, for all columns, the reduction in fire resistances are about 8% when spalling is around 3% and about 26% when spalling is around 10%. There is also some evidence from the investigation that the earlier spalling occurs the higher the possible decrease in fire resistance.

9.6 RECOMMENDATIONS FOR FUTURE WORK

It should be noted that the study reported in this thesis is limited in scope. In this study, an array of three columns with an additional reference column and six different percentages of spalling were considered for the first range of simulations. A two stage progressive spalling regime conducted on similar columns was used for a second range of simulations. It is suggested that a wider variety of columns and percentages of spalling should be tested to verify and augment this work and to possibly obtain design curves or equations. Further investigation may also be necessary to quantify the reduction in fire resistance

against the extent of spalling, heating and loading patterns as well as the time at which the concrete spalls.

It should be remembered that the computer calculation involves a number of simplifying assumptions which are unlikely to hold for the test column. Temperature variation along the column axis has not been considered and all the cross sections are assumed to be identical throughout the column. It has also been assumed that moisture transport has no effect on either material or thermal properties. Complete agreement therefore cannot be expected between the observed test and calculated deformations. However, it can be expected that the overall trends should exhibit agreement.

It is also possible that when a better understanding is available on the effect of moisture or moisture transport on the material properties of concrete, the current mode in which the thermal analysis and the structural analysis are completely decoupled may no longer be appropriate and that provision may have to be made for the two analyses to be run in harness with interactive feed-back on each time step, say, local moisture content. In addition, the effect of three-dimensional heat transfer analysis may also be investigated.

Further parametric study of a reinforced concrete column in fire may also be required to enable a more accurate design of structures to be constructed or maintained with compensation for faults such as the occurrence of spalling. Additional parameters for further work may include the size and shape of the column, detailing arrangements, load ratio and material strengths.

REFERENCES

Abrams, M.S. (1971), 'Compressive Strength of Concrete at Temperatures to 1600°F, Temperature and Concrete Special Publication SP-25, American Concrete Institute, Detroit.

Akhtaruzzaman, A.A. (1973), 'The Effect of Transient and Steady State Temperature on Concrete', PhD Thesis, Imperial College, London.

Akhtaruzzaman, A.A and Sullivan, P.J.E. (1970), 'Explosive Spalling of Concrete Exposed to High Temperature', Concrete Structure and Research Report, Imperial College, London.

Aldstedt, D.E. (1975), 'Non-linear Analysis of Reinforced Concrete Frames', Report No 75, Division of Structural Mechanics, Norwegian Institute of Technology, Trondheim.

Allen, D.E. and Lie, T.T. (1974), 'Further Studies of the Fire Resistance of Reinforced Concrete Columns', Technical Paper No. 416, NRCC 14047, National Research Council of Canada, Division of Building Research, Ottawa.

Anderberg, Y. (1976), 'Fire Exposed Hyperstatic Concrete Structures - An Experimental and Theoretical Study', Bulletin 55, Division of Structural Mechanics and Concrete Construction, Lund Institute of Technology, Lund, Sweden.

Anderberg, Y. (1978), 'Armeringsstahls Mekaniskan Egenskaper vid Hoga Temperaturer', Bulletin 61, Division of Structural Mechanics and Concrete Construction, Lund Institute of Technology, Lund, Sweden.

Anderberg, Y., (Ed), (1983), 'Properties of Material At High Temperatures - Steel', *RILEM Technical Committee Report*, Division of Building Fire Safety and Technology, Lund Institute of Technology, Lund, Sweden.

Anderberg, Y. and Thelandersson, S. (1976), 'Stress and Deformation Characteristics of Concrete at High Temperatures - Experimental Investigation and Material Behaviour Model', Bulletin 54, Division of Structural Mechanics and Concrete Construction, Lund Institute of Technology, Lund, Sweden.

Ashton, L.A and Bate, S.C.C. (1960), 'The Fire Resistance of Prestressed Concrete Beams', *Proceedings of the Institution of Civil Engineers*, Sept. 1960, 15 - 38.

Ashton, L.A. and Davey, N. (1953), 'Investigations on Building Fires - Part 5', *National Building Studies Research Paper 12*, H.M. Stationery Office, London.

Baldwin, R. and North, M.A. (1973), 'A Stress-strain Relationship for Concrete at High Temperatures', *Magazine of Concrete Research*, 25, No. 85, 208 - 212.

Bali, A. (1984), 'The transient Behaviour of Plain Concrete at Elevated Temperatures', PhD Thesis, University of Aston in Birmingham, UK.

Bazant, Z.P. (1982), 'Mathematical Model for Creep and Thermal Shrinkage of Concrete at High Temperatures', Report No. 82-249m, The Technical Institute, Northwestern University, Evanston.

Bazant, Z.P. and Panula, L. (1978), 'Practical Prediction of Time Dependent Deformations of Concrete', *Materiaux et Construction*, 11, No. 65, 307 - 328.

Becker, J.M., Bizri, H. and Bresler, B. (1974), 'FIRES-T: A Computer Program for the Fire Response of Structures - Thermal', Report No. UCB FRG 74 - 1, Fire Research Group, Department of Civil Engineering, University of California, Berkeley.

Becker, J.M. and Bresler, B. (1974), 'FIRES-RC: A Computer Program for the Fire Response of Structures - Reinforced Concrete Frames', Report No. UCB FRG 74 - 3, Fire Research Group, Department of Civil Engineering, University of California, Berkeley.

Becker, W. and Stanke, J. (1970), 'Brandversuche an Stahlbeton - fertigestützen', Deutscher Ausschuss für Stahlbeton, Heft 215, Berlin.

Bizri, H. (1973), 'Structural Capacity of Reinforced Concrete Columns Subject to Fire Induced Thermal Gradients', Report No. 73 - 1, Structural Engineering Laboratory, Department of Civil Engineering, University of California, Berkeley.

Bresler, B. and Iding, R (1983), 'Fire Response of Prestressed Concrete Members', in Abrams, M.S. (Ed), 'Fire Safety of Concrete Structures', Publication SP - 80, American Concrete Institute.

British Standard BS 476: Part 20 - 23, Fire Tests on Building Material and Structures, British Standard Institutions, 1987.

Christiaanse, A.E., Langhorst, A. and Gerriste, A. (1972), 'Spalling of Prestressed Concrete Beams', Dutch Society of Engineers (STUVO), Report No. 12, Holland.

Clarke, J.H. (1960), 'Method of Assessing Probable Fire Endurance of Load Bearing Columns', *Journal of the American Concrete Institute*, 31, 1223 - 1241.

Connolly, R.J. (1992), 'Report on the First Year of Research into Spalling of Concrete at Elevated Temperatures', Department of Civil Engineering, University of Aston in Birmingham, UK.

Copier, W.J. (1979), 'The Spalling of Normal Weight and Lightweight Concrete on Exposure to Fire', *Heron (Nederlands)*, Vol. 24, No. 2.

Cranston, W.B. (1967), 'A Computer Method for the Analysis of Restrained Columns', TRA Report 402, Cement and Concrete Association, London.

Cruz, C.R. (1968), 'Apparatus for Measuring Creep of Concrete at High Temperatures', PCA Research Department Bulletin 225, Skokie, Illinois.

Dougill, J.W. (1966), 'Relevance of the Established Method of Structural Fire Testing to Reinforced Concrete', *Applied Materials Research*, 5, No. 4, 235 - 240.

Dorn, J.E. (1954), 'Some Fundamental Experiments on High Temperature Creep', *Journal of the Mechanics and Physics of Solids*, 3, No. 2, 85 - 116.

Dougill, J.W. (1972a), 'Modes of Failure of Concrete Panels Exposed to High Temperatures', *Magazine of Concrete Research*, 24, No. 79, 71 - 76.

Dougill, J.W. (1972b), 'Conditions of Instability in Restrained Concrete Panels Exposed to Fire', *Magazine of Concrete Research*, 24, No. 80, 139 - 148.

Eurocode 2 (1992), 'Design of Concrete Structures Part 10: Structural Fire Design (Draft)', European Committee for Standardisation, N 232 E.

Eurocode 3 (1992), 'Design of Steel Structures Part 10: Structural Fire Design (Draft)', European Committee for Standardisation, N 232 E.

Fire Grading of Buildings Part 1 - General Principles and Structural Precautions (1946), Post War Buildings Studies No. 20, H.M. Stationery Office, London.

Forsén, N.E. (1982), 'A Theoretical Study of the Fire Resistance of Concrete Structures', N - 7034, Cement and Concrete Research Institute, The Norwegian Institute of Technology, Trondheim.

Furumura, F. (1966), 'Stress-strain Curve of Concrete at High Temperatures', Transactions of the Architectural Institute of Japan, Tokyo Institute of Technology, Abstract No. 7004.

Gary, M. (1916) 'Fire Tests on Reinforced Concrete Buildings', (In German), Verlag Wilhelm Ernst and Sohn, Heft 11, Berlin.

- Gillen, M. (1981), 'Short Term Creep of Concrete at Elevated Temperatures', *Fire and Materials*, 5, No. 4.
- Haksever, A. (1977), 'Zur Frage Des Trag - und Verformungs - verhaltens ebener Stahlbetonrahmen im Brandfall', Institute für Baustoffkunde und Stahlbetonbau der Technischen Universität Braunschweig, Heft 35, Braunschweig.
- Haksever, A. and Anderberg, Y. (1982), 'Comparison Between Measured and Computed Structural Response of Some Reinforced Concrete Columns in a Fire', *Fire Safety Journal*, 4, 293 - 397.
- Haksever, A., Haß, R. and Kordina, E.K (1982), 'Load Capacity of Columns with Simplified Stirrup Reinforcement Under Fire Conditions', (In German), Heft 332, Braunschweig, 50 - 75.
- Harmathy, T.Z. (1965), 'Effect of Moisture on the Fire Endurance of Building Elements', Special Technical Publication No. 385, American Society for Testing and Materials, Philadelphia.
- Harmathy, T.Z. (1967), 'A Comprehensive Creep Model', *Journal of Basic Engineering*, 89, Transactions of the American Society for Mechanical Engineering.
- Harmathy, T.Z. (1970), 'Thermal Properties of Concrete at Elevated Temperatures', *ASTM Journal of Materials*, 5, No. 1, 47 - 74.
- Harmathy, T.Z. (1974), 'Creep Deflection of Beams', ASCE National Structural Engineering Meeting Preprint 2216.

Harmathy, T.Z. (1988), 'How Much Fire Resistance is Really Needed', in 'Symposium on Fire Resistance of Concrete Structures', Proceedings of The American Concrete Institute, Orlando, USA.

Harmathy, T.Z. (1991), 'Design of Buildings Against Fire Spread - A Review', *Journal of Applied Fire Science*, 1, No. 1, 65 - 81.

Harmathy, T. and Stanzak, W.W. (1970), 'Elevated Temperature Tensile and Creep Properties of Some Structural and Prestressing Steels', Fire Test Performance STP - 464, American Society for Testing and Materials, Philadelphia, 186 - 208.

Hinkley, P. (1984), 'Standard Time-Temperature Curve: Its Relevance', *Fire Surveyor*, 13, No. 4.

Iding, R., Bresler, B. and Nizamuddin, Z. (1977a), 'FIRES-T3: A Computer Program For the Fire Response of Structures - Thermal 3 Dimension Version', Report No. UCB FRG 77-15, Fire Research Group, Department of Civil Engineering, University of California, Berkeley.

Iding, R., Bresler, B. and Nizamuddin, Z. (1977b), 'FIRES-RC II: A Computer Program For the Fire Response of Structures - Reinforced Concrete Frames', Report No. UCB FRG 77-8, Fire Research Group, Department of Civil Engineering, University of California, Berkeley.

ISO 834, Fire Resistance Tests - Elements of Building Construction, International Organisation of Standardisation, 1975.

Issen, L.A, Gustaffero, A.H. and Carlson, C.C. (1970), 'Fire Tests of Concrete Members - An Improved Method of Estimating Thermal Restraint Forces', Special Technical Publication No. 464, American Society for Testing and Materials, Philadelphia, 153 - 165.

Khennane, A. and Baker, G. (1993), 'Uniaxial Model for Concrete Under Variable Temperature and Stress', *Journal of Engineering Mechanics*, **119**, No. 8, August 1993.

Khoury, G.A. (1992), 'Compressive Strength of Concrete at High Temperatures: A Reassessment', *Magazine of Concrete Research*, **44**, No. 161, 291 - 309.

Khoury, G.A, Grainger, B.N. and Sullivan, P.J.E. (1986), 'Transient Thermal Strain of Concrete: Literature Review, Conditions Within Specimens and Behaviour of Individual Constituents', *Magazine of Concrete Research*, **37**, No. 132, 195 - 215.

Lie, T.T. (1983), 'A Procedure to Calculate Fire Resistance of Structural Members', *Fire Technology*, **14**, No. 1, 28 - 85.

Lie, T.T. (1992), 'Principles of Structural Fire Protection' in Lie, T.T. (Ed), 'Structural Fire Protection', ASCE Manuals and Reports on Structural Engineering Practice No. 78.

Lie, T.T. (1994), 'Fire Resistance of Circular Steel Columns Filled with Bar-Reinforced Concrete', *Journal of Structural Engineering*, **120**, No. 5.

Lie, T.T. and Allen, D.E. (1972), 'Calculation of the Fire Resistance of Reinforced Concrete Columns', Technical Paper No. 378, NRCC 12797, National Research Council of Canada, Division of Building Research, , Ottawa.

Lie, T.T. and Chabot, M. (1990), 'Fire Resistance Evaluation Using Computer Models', INTERFLAM '90, 5th International Fire Conference, 3 - 6 September 1990, Interscience Communications Limited, London, 93 - 100.

Lie, T.T. and Harmathy, T.Z. (1972), 'A Numerical Procedure to Calculate the Temperature of Protected Steel Columns Exposed to Fire', Fire Study No. 28, NRCC 12535, National Research Council of Canada, Division of Building Research, Ottawa.

Lin, F.B., Bažant, Z.P., Chern, J.C. and Marchertas, A.H. (1987), 'Concrete Model with Normality and Sequential Identification', *Comp. Struct.*, 26, No. 6, 1011 - 1025.

Malhotra, H.L. (1956), 'The Effect of Temperature on the Compressive Strength of Concrete', *Magazine of Concrete Research*, 8, No. 23, 85 - 94.

Malhotra, H.L. (1969), 'Fire Resistance of Structural Concrete Beams', Fire Research Note 741, Fire Research Station.

Malhotra, H.L. (1972), 'Spalling of Concrete - Results of Questionnaire', Fire Research Memorandum No. 70, Fire Research Station.

Malhotra, H.L. (1982), *Design of Fire Resisting Structure*, Surrey University Press, England.

Malhotra, H.L. (1984), 'Spalling of Concrete in Fires', Technical Note 118, CIRIA, London, UK.

Malhotra, H.L. (1986), 'A Survey of Fire Protection Developments for Buildings', in Anchor, R.D, Malhotra, H.L. and Purkiss, J.A. (Eds), 'Design of Structures Against Fire', Elsevier Applied Science Publishers, London, 1 - 13.

Maréchal, J.C. (1970), 'Variations in the Modulus of Elasticity and Poisson's Ratio with Temperature', American Concrete Institute - Seminar on CNR, Berlin.

Meyer-Ottens, C. (1972), 'On the Question of Spalling of Concrete Structures Made from Normal Concrete Exposed to Fire', PhD Thesis, Technischen Universität, Braunschweig, Germany.

Mooney, J. (1991), 'Surface Radiant Energy Balance for Structural Thermal Analysis', Building Research Establishment Report No. N68/91, Fire Research Station, Borehamwood, Hertfordshire, UK.

Odeen, K. (1968), 'Fire Resistance of Prestressed Concrete Double T Units', *Acta Polytechnica Scandinavia*, Civil Engineering and Building Construction Series No. 48, Stockholm, Sweden.

Pettersson, O. (1965), 'Structural Fire Engineering Research Today and Tomorrow', *Acta Polytechnica Scandinavia*, Civil Engineering and Building Construction Series No. 33, Stockholm, Sweden, 42 - 55.

Purkiss, J.A. (1972), 'A Study of the Behaviour of Concrete Heated to High Temperatures Under Restraint or Compressive Loading', PhD Thesis, University of London.

Purkiss, J.A. (1986), 'High Temperature Effects', *in* Anchor, R.D, Malhotra, H.L. and Purkiss, J.A. (Eds), 'Design of Structures Against Fire', Elsevier Applied Science Publishers, London, 41 - 51.

Purkiss, J.A. (1990), 'Computer Modelling of Concrete Structural Elements Exposed to Fires', INTERFLAM '90, 5th International Fire Conference, 3 - 6 September 1990, Interscience Communications Limited, London, 67 - 73.

Purkiss, J.A (1995), *Fire Safety Engineering Design of Structures*, Technical Communications (Publishing) Ltd and Butterworth-Heinemann. (In Course of Preparation).

Purkiss, J.A. and Weeks, N.J. (1987), 'A Computer Study of Reinforced Concrete Columns in a Fire', *Structural Engineer*, 65B, No. 1, 22 - 28.

Saito, H. (1965), 'Explosive Spalling of Prestressed Concrete in Fire', BRI Occasional Report No. 22, Building Research Institute, Ministry of Construction, Tokyo.

Schneider, U. (1976), 'Behaviour of Concrete Under Thermal Steady State and Non-Steady State Conditions', *Fire and Materials*, 1, No. 3, 103 - 115.

Schneider, U., (Ed.) (1985), 'Properties of Materials at High Temperatures - Concrete', *RILEM Technical Report 44 - PHT*, 2nd Edition, University of Kassel, Kassel.

Schneider, U. (1986), 'Modelling of Concrete Behaviour at High Temperatures', *in* Anchor, R.D, Malhotra, H.L. and Purkiss, J.A. (Eds), 'Design of Structures Against Fire', Elsevier Applied Science Publishers, London, 53 - 69.

Schneider, U. (1988), 'Concrete at High Temperatures - A General Review', *Fire Safety Journal*, 13, 55 - 68.

Sermehemetoglu, Y. (1977), 'On the Mechanism of Spalling of Concrete Under Fire Conditions', PhD Thesis, Kings College, London.

Stirland, C. (1980), 'Steel Properties at Elevated Temperatures for Use in Fire Engineering Calculations', British Steel Corporation, Teeside Laboratory, Paper for ISO KC92/Wg15 Committee.

Tassios, T.P. and Chronopoulos, M.P. (1991), 'Structural Response of RC Elements Under Fire', *Structural Engineer*, 69, No. 15, 277 - 281.

Terro, M. J. and Sullivan, P.J.E. (1992), 'Model of Reinforced Concrete Under Fire', *Journal of the Institution of Mechanical Engineers*, 438, No. 39, 39 - 46.

Thelandersson, S. (1982), 'On the Multiaxial Behaviour of Concrete Exposed to High Temperatures', *Nuclear Engineering and Design*, 75, 271 - 282.

Thomas, F.C. and Webster, C.T. (1953), 'Fire Resistance of Reinforced Concrete Columns', Paper No. 18, National Building Studies Research, H.M. Stationery Office, London.

Timoshenko, S.P. and Gere, J.M. (1961), *Theory of Elastic Stability*, Second Ed., McGraw Hill, New York.

Tomecek, D.V. and Milke, J.A. (1993), 'A Study of the Effect of Partial Loss of Protection on the Fire Resistance of Steel Columns', *Fire Technology - First Quarter*, 29, No. 9, 3 - 21.

Weeks, N.J. (1985), 'Lateral Instability of Slender Reinforced Concrete Columns in a Fire Environment', PhD Thesis, University of Aston in Birmingham, UK.

Weigler, H. and Fisher, R. (1967), 'Beton bei Temperaturen von 100 bis 750°C', *Mehmel-Festschrift*, Beton-Verlag GmbH, Dusseldorf.

Wickström, U. (1979), 'TASEF-2: A Computer Program For the Temperature Analysis of Structures Exposed to Fire', Report No. 79 - 2, Department of Structural Mechanics, Lund Institute of Technology, Lund, Sweden.

Yokel, F.Y., Mathey, R.G. and Dikkers, R.D. (1971), 'Strength of Masonry Walls Under Compressive and Traverse Loads', Building Science Series 34, National Bureau Standards, United States.

APPENDIX A

Pages removed for copyright restrictions.